Daniela Thaller

# Inter-technique combination based on homogeneous normal equation systems including station coordinates, Earth orientation and troposphere parameters

Scientific Technical Report STR08/15

Daniela Thaller

# Inter-technique combination based on homogeneous normal equation systems including station coordinates, Earth orientation and troposphere parameters

Vollständiger Abdruck der von der
Fakultät für Bauingenieur- und Vermessungswesen
der Technischen Universität München
zur Erlangung des akademischen Grades eines
Doktor-Ingenieurs (Dr.-Ing.)
genehmigten Dissertation.

Vorsitzende:             Univ.-Prof. Dr.Ing. L. Meng

Prüfer der Dissertation:  1. Univ.-Prof. Dr.phil.nat. M. Rothacher
                          2. Univ.-Prof. Dr.Ing. Dr.h.c. R. Rummel
                          3. Hon.-Prof. Dr.Ing. H. Drewes

Die Dissertation wurde am 02.01.2008 bei der Technischen Universität
München eingereicht und durch die Fakultät für Bauingenieur- und Ver-
messungswesen am 10.03.2008 angenommen.

Termin der mündlichen Prüfung: 04.04.2008

Scientific Technical Report STR08/15

# Abstract

Nowadays it is widely accepted that the space-geodetic techniques Global Positioning System (GPS), Very Long Baseline Interferometry (VLBI) and Satellite Laser Ranging (SLR) can contribute valuable information to improve the understanding of the system Earth, although the capability to contribute to the various parameters describing the system Earth varies between the techniques. Thus, the different potentials of the techniques call for a combination of all single contributions in order to fully exploit the strengths of each space-geodetic technique and to overcome the technique-specific weaknesses by a strong contribution of at least one of the other techniques. The studies described in this thesis take a closer look on the station coordinates, the troposphere parameters and on the Earth orientation parameters (EOP), i.e., polar motion, Universal time ($UT$) and nutation.

As regards the station coordinates, all three techniques contribute to their determination. It is demonstrated that mainly the VLBI and SLR sites benefit from the inter-technique combination as their single-technique solutions are weaker than a GPS-only solution. However, it is shown that weakly determined GPS sites can be stabilized, too, if there is a strong contribution from a co-located VLBI or SLR site.

Only GPS and VLBI sense the tropospheric influence in the same way, so that troposphere parameters are estimated only for the GPS and VLBI sites. The inclusion of the troposphere parameters into the combination yields time-series of zenith delay (ZD) and horizontal gradient parameters that are fully consistent with the common reference frame. For the first time, a combination of the troposphere parameters has been carried out, and the benefit of combining the troposphere ZD at co-located GPS-VLBI sites could be demonstrated. Due to the correlation of the ZD with the station height, a combination of the ZD can stabilize the determination of the height coordinates. This stabilization is most prominent if the local tie (LT) for the corresponding co-location is missing.

A stabilization of the coordinate estimates similar to the effect seen for the combination of the ZD could not be shown for the combination of the troposphere gradients. However, it is demonstrated that the common treatment of troposphere gradients together with the terrestrial reference frame can give valuable information about the discrepancy between the LT and the coordinate differences derived from the space-geodetic techniques, thus, offering an independent evaluation of the LT information.

Concerning the EOP, the capabilities of the three techniques are different: VLBI is the only technique to determine the nutation angles and $UT$ in an absolute sense, whereas the satellite-techniques have access only to the time-derivatives, i.e., the nutation rates and length of day ($LOD$). However, these time-derivatives, especially from GPS, carry valuable information that can stabilize the VLBI estimates. It is demonstrated that the combination of GPS-derived $LOD$ and VLBI-derived $UT$ and $LOD$ quantities leads to a time-series of piece-wise linear $UT$ that is clearly more stable than the VLBI-only time-series.

A similar stabilization can be shown for the time-series of the $x$-pole and $y$-pole coordinates if the contributions of all three space-geodetic techniques are homogeneously combined.

Contrary to other inter-technique combination studies, the polar motion and $UT$ parameters are set up as a piece-wise linear polygon with functional values every hour instead of only a daily resolution. However, the sub-daily resolution of polar motion induces a correlation between a retrograde diurnal term in polar motion and the nutation angles. Studies regarding the theory of this correlation and how to handle it when estimating sub-daily polar motion together with nutation are included in the thesis.

Furthermore, it is demonstrated that the common estimation of the terrestrial reference frame and EOPs can be employed to identify a mismatch between the local tie values and the estimated coordinate differences at co-located sites. Thus, the EOPs offer another independent evaluation of the LT values, as mentioned already above for the troposphere gradients.

For the studies described in this thesis, it is of vital importance that continuous observations are available for all observation techniques. Therefore, the so-called CONT campaigns of the International VLBI Service for Geodesy and Astrometry (IVS) are well-suited. Such special campaigns with continuous VLBI observations for several days are initiated from time to time in order to demonstrate the full capabilities of VLBI. The studies described in the thesis at hand are based on the two-week CONT campaign scheduled in October 2002, named CONT02.

# Zusammenfassung

Heutzutage ist es allseits anerkannt, dass die geodätischen Raumverfahren *Global Positioning System* (GPS), *Very Long Baseline Interferometry* (VLBI) und *Satellite Laser Ranging* (SLR) wertvolle Beiträge liefern, um das System Erde besser verstehen zu können. Allerdings sind die Fähigkeiten der einzelnen Verfahren hinsichtlich der Bestimmung verschiedener Parameter, die das System Erde beschreiben, unterschiedlich. Die unterschiedlichen Potentiale der einzelnen Verfahren erfordern eine Kombination aller Einzelbeiträge, um einerseits die Stärken jedes Beobachtungsverfahrens vollständig auszunutzen, und um andererseits die spezifischen Schwächen einzelner Verfahren durch einen starken Beitrag mindestens eines weiteren Beobachtungsverfahrens wett zu machen. In der vorliegenden Arbeit liegt das Augenmerk auf Analysen der Stationskoordinaten, der Troposphärenparameter und der Erdorientierungsparameter (EOP), welche die Polbewegung, *Universal Time* (*UT*) und die Nutation umfassen.

Alle drei Beobachtungsverfahren können zur Bestimmung der Stationskoordinaten beitragen. Es wird deutlich, dass hauptsächlich die VLBI- und SLR-Stationen von einer Kombination profitieren, da deren individuelle Lösungen schwächer sind als eine reine GPS-Lösung. Allerdings können auch schwach bestimmte GPS-Stationen durch einen stabilen Beitrag einer ko-lokierten VLBI- oder SLR-Station stabilisiert werden.

Nur GPS und VLBI sind von der Troposphäre in gleicher Art und Weise beeinflusst, so dass Troposphärenparameter nur für die GPS- und VLBI-Stationen geschätzt werden. Aus einer Kombination einschließlich der Troposphärenparameter resultieren Zeitreihen der troposphärischen Verzögerung in Zenitrichtung (ZD) und horizontaler Gradienten, die vollständig konsistent mit dem gemeinsamen Referenzrahmen sind. Eine Kombination der Troposphärenparameter wurde zum ersten Mal durchgeführt, und der Vorteil einer Kombination der ZD für ko-lokierte GPS-VLBI-Stationen konnte aufgezeigt werden. Aufgrund der Korrelation zwischen ZD und Stationshöhe kann die Höhenkomponente durch eine ZD-Kombination stabilisiert werden. Diese Stabilisierung ist am deutlichsten, wenn der "*Local Tie*" (LT) für diese Ko-lokation fehlt.

Für die Kombination der Troposphärengradienten ist eine Stabilisierung der geschätzten Koordinaten wie es für die ZD-Kombination der Fall ist, nicht zu erkennen. Es wird jedoch gezeigt, dass durch die gemeinsame Schätzung von Troposphärengradienten mit dem terrestrischen Referenzrahmen wertvolle Information über die Diskrepanz zwischen den LT-Werten und den Koordinatendifferenzen aus den geodätischen Raumverfahren gewonnen werden kann, so dass eine unabhängige Evaluierung der LT-Werte möglich ist.

Die Stärken der drei Beobachtungsverfahren hinsichtlich der EOP-Schätzung sind verschieden: VLBI kann als einziges Beobachtungsverfahren *UT* und die Nutation in ihrem absoluten Wert bestimmen, während die Satellitenmessverfahren nur die zeitliche Veränderung, also Nutationsraten und Tageslänge (*LOD*), bestimmen können. Allerdings sind diese zeitlichen Veränderungen, insbesondere aus GPS-Schätzungen, ein wertvoller Beitrag zur Stabilisierung der VLBI-Schätzung. Es konnte gezeigt werden, dass die Kombination von *LOD*-Beiträgen aus GPS mit *UT*- und *LOD*-Beiträgen aus VLBI zu einer kombinierten *UT*-Zeitreihe führt, die deutlich stabiler ist als eine reine VLBI-Zeitreihe. Eine ähnliche Stabilisierung konnte für die *x*-Pol- und *y*-Pol-Zeitreihen gezeigt werden, falls die Beiträge aller drei Raumverfahren homogen kombiniert werden.

Im Gegensatz zu anderen Kombinationsstudien wurden die Polkoordinaten und *UT* nicht nur mit einer täglichen Auflösung geschätzt, sondern als stückweise lineares Polygon mit Stützwerten alle Stunde. Allerdings hat die sub-tägliche Auflösung für die Polkoordinaten eine Korrelation zwischen einer retrograd-täglichen Polbewegung und den Nutationswinkeln zur Folge. Die vorliegende Arbeit beinhaltet Studien zur Theorie dieser Korrelation und Methoden, wie sie gehandhabt werden kann, wenn man sub-tägliche Polkoordinaten zusammen mit der Nutation schätzen möchte.

Außerdem wird gezeigt, dass das gemeinsame Schätzen von terrestrischem Referenzrahmen und den EOPs dazu verwendet werden kann, um eine Diskrepanz zwischen den LT-Werten und den geschätzten Koordinatendifferenzen zu identifizieren. Somit bieten die EOPs, neben den oben bereits erwähnten Troposphärengradienten, eine weitere unabhängige Evaluierungsmöglichkeit der LT-Werte.

Für die Studien, die in dieser Arbeit beschrieben werden ist es essentiell, dass kontinuierliche Beobachtungen für alle Beobachtungsverfahren verfügbar sind. Deshalb sind die sogenannten CONT-Kampagnen des *International VLBI Service for Geodesy and Astrometry* (IVS) bestens geeignet. Derartige spezielle Kampagnen mit kontinuierlichen VLBI-Beobachtungen über mehrere Tage werden von Zeit zu Zeit durchgeführt, um die maximal möglichen Fähigkeiten von VLBI aufzuzeigen. Die Studien in der vorliegenden Arbeit beruhen auf Daten der zwei-wöchigen CONT-Kampagne im Oktober 2002, genannt CONT02.

# Table of contents

# 1 Introduction

Nowadays it is widely accepted that the space-geodetic techniques Global Positioning System(GPS), Very Long Baseline Interferometry (VLBI), Satellite Laser Ranging (SLR), Lunar Laser Ranging (LLR) and Doppler Orbitography and Radiopositioning Integrated by Satellite (DORIS) can contribute valuable information to improve the understanding of the system Earth. Just to mention the most important contributions: the establishment and maintenance of a highly accurate terrestrial and celestial reference frame, the monitoring of the Earth's rotation axis w.r.t. these reference frames, the contribution to observe and study the status of the atmosphere, the determination of the low-degree spherical harmonic coefficients of the Earth's gravity field and the determination of the orbits of many satellites. The scheme in Table 1.1 summarizes those parameter groups related to the system Earth to which the space-geodetic techniques can contribute. It becomes clear from this matrix that the capability to contribute to the various parameters varies between the techniques. To give some examples, the capability of VLBI to determine a celestial reference frame (CRF) with long-term stability is unique. The same is true for monitoring the nutation (i.e., the movement of the Earth's rotation axis w.r.t. the CRF) and the daily rotation of the Earth (i.e., *UT1-UTC*) in an absolute sense and with long-term stability. In contrary, an inertial-like reference system given by the satellite orbits assures stability only for short time spans (due to deficiencies in the orbit modeling), so that the satellite techniques GPS, SLR and DORIS can only contribute the time-derivatives of the nutation angles and *UT1-UTC*. The dynamics of the orbits allow that the gravity field of the Earth can be determined from observations of the satellite techniques, although the determinability is restricted to the low-degree spherical harmonic coefficients, whereas VLBI is a purely geometrical technique and, thus, is not coupled to the Earth's gravity field. After explaining some of the differences, the attention should also be drawn to those parameter types accessible to all observation techniques, namely the terrestrial reference frame (TRF) and the polar motion (i.e., the motion of the Earth's rotation axis w.r.t. the TRF). The only differences between the techniques concerning these common parameter types must be seen in the strength and stability of their contributions.

All in all, the different potentials of the techniques call for a combination of all single contributions in order to fully exploit the strengths of each space-geodetic technique and to overcome the technique-specific weaknesses by a strong contribution of at least one of the other techniques. Unfortunately, the potential of an inter-technique combination is not yet fully exploited and several topics still have to be studied. In order to achieve a better understanding of the inter-technique combination, the studies within this thesis can be characterized by the following topics that will be explained in more detail afterwards:

- The detailed alignment of the a priori models and parameterization used in the analyses of the space-geodetic observations enables a combination based on homogeneous normal equation systems.

- The inclusion of all relevant parameters into the combination (i.e., station coordinates, Earth orientation parameters (EOP) and troposphere parameters) allows to consider the correlations between them correctly.

- A combination of the site-specific troposphere parameters is performed and its impact on the combined solution is quantified.

- The sub-daily resolution for the EOP entails a correlation between the nutation angles and a retrograde diurnal polar motion term. As the behavior concerning this correlation is different for VLBI and the satellite-techniques, theoretical considerations and simulation studies are devoted to this topic.

- As continuous VLBI observations are available for the time span of CONT02, this data set is well suited to demonstrate that the combination of GPS-derived *LOD* and VLBI-derived *UT1-UTC* and *LOD* estimates is worthwhile.

The combination studies for this thesis are restricted to GPS, VLBI and SLR. The third microwave technique, i.e., DORIS, has not been included in the studies, although it would be an additional contribution to the troposphere parameters. But the first two basic ideas mentioned above contradicted the inclusion of DORIS: The combination bases on normal equation systems (NEQ) that were generated with standardized common a priori models and the parameterization for all common parameters was unified. Those solutions (resp. NEQs) that are commonly available (e.g., via the IERS) do not fulfill all the processing standards defined for this thesis and do not include all desired parameters. Such a harmonization of the analysis requires a software

package at hand where the common processing standards can be implemented. Unfortunately, this was not the case for DORIS (and LLR, too).

One may ask, why such a high priority has been given to the harmonization of the processing standards. There is no doubt that a homogeneous processing of all data for the entire time span is indispensable if long time-series of geodetic parameters (e.g., EOP or troposphere parameters) should be analyzed. As the analysis strategies steadily improved during the years, the changes are visible in the routinely generated solutions as jumps or different levels of quality. This implies that a full re-processing of all observations using the best analysis strategy is required to get homogeneous time-series of geodetic parameters (*Steigenberger et al., 2006*). In the same way as changes in the analysis strategy are seen as discontinuities within a time-series, these discrepancies are present in the time-series of parameters derived from solutions that base on different analysis strategies. As the combination in this thesis is done on the normal equation level, all differences in the analysis of the observations related to the a priori models cannot be handled and corrected in the combination. The differences propagate into the estimated parameters and will be averaged in the combined solution, so that a rigorous combination is not possible anymore (*Drewes, 2007*). Considering this background, it is clear why we strove for consistency of the analysis of the single-technique observations to the extent possible. In principle, the same procedure is applied by *Yaya (2002)* and *Coulot et al. (2007)*, with the main difference that they analyzed all techniques with the same software package, whereas two different software packages have been used for generating the NEQs for this thesis, namely OCCAM (*Titov et al., 2001*) and the Bernese GPS Software (*Dach et al., 2007*).

**Table 1.1:** *Different characteristics of the space-geodetic techniques concerning the determination of geodetic parameters (original version by Rothacher, 2002).*

| Parameter type | | VLBI | GPS | SLR | DORIS | LLR |
|---|---|:---:|:---:|:---:|:---:|:---:|
| **CRF** | **Quasar positions** | X | | | | |
| | **Orbits (satellites, moon)** | | X | X | X | X |
| **EOP** | **Nutation** | X | | | | X |
| | **Nutation rates** | X | X | X | X | X |
| | **UT1-UTC** | X | | | | |
| | **LOD** | X | X | X | X | X |
| | **Polar motion** | X | X | X | X | X |
| **TRF** | **Station positions** | X | X | X | X | X |
| **Gravity field** | **Geocenter** | | X | X | X | |
| | **Low-degree** | | X | X | X | X |
| **Atmosphere** | **Troposphere** | X | X | | X | |
| | **Ionosphere** | X | X | | X | |

To a certain extent, an inter-technique combination is already done since several years. Within the International Earth Rotation and Reference Systems Service (IERS), the official products for the EOP result from a combination of the individual contributions by the space-geodetic techniques (*Gambis, 2004*). However, this combination is restricted to the EOP only so that the correlations with all other parameter types, especially the TRF, are ignored. For a long time, the International Terrestrial Reference Frame (ITRF) was generated as an inter-technique combination as well, but fully independent from the EOP. The separate treatment of TRF and EOP evoked steadily increasing differences in the alignment: Space-geodetic solutions for actual epochs correctly aligned to ITRF2000 (*Altamimi et al., 2002*) show a bias of about 0.2 mas in the *y*-component of polar motion compared to the official IERS EOP series (see e.g., *Dill and Rothacher, 2003*). Only since a few years, developments were initiated towards a common treatment of station positions and EOP in multi-technique solutions. A first step towards this procedure marked the IERS SINEX Combination Campaign (*Angermann et al., 2003*) where the appropriate procedures and combination methods could be developed based on a dedicated test period of one year of data. In order to carry these more experimental studies over into a routine processing, the IERS Combination Pilot Project (CPP) was initiated in 2004 (*Rothacher et al., 2005*). Results out of these two campaigns are documented in, e.g., *Thaller and Rothacher (2003)*, *Angermann et al. (2006)*. Finally, it was decided within the IERS that the ITRF computations should no longer be

restricted to the station positions but should include the EOP as well. Therefore, the latest realization, called ITRF2005[1], is the first official IERS solution where both groups of parameters have been treated together and, thus, yield a time-series of EOP that is fully consistent with the ITRF.

Unfortunately, other parameters than station positions and EOP listed in Table 1.1 (e.g., troposphere parameters, CRF, orbits, gravity field coefficients) are not yet considered within the IERS combinations. The studies within this thesis extend the groups of parameters that are treated together: Troposphere parameters determined by the microwave techniques are additionally included. Thus, the results presented hereafter are the first with consistently combined TRF, EOP and troposphere parameters. Initial results out of this kind of studies were published in *Krügel et al. (2007)*, but restricted to a combination of GPS and VLBI. The studies presented there already revealed that the solution benefits from a combination of the troposphere parameters. For the studies presented in this thesis, SLR was additionally included. Due to the fact that the influence of the troposphere on SLR observations can be modeled accurately enough, the contribution of SLR can help to decorrelate the station coordinates and the troposphere parameters determined by GPS and VLBI for sites co-located with SLR. Furthermore, the usability of the troposphere parameters to detect discrepancies between the geometrical local ties and the coordinate differences determined by the space-geodetic techniques will be demonstrated.

One further comment must be added regarding the parameters included in the combination studies for this thesis. Contrary to the standard solutions provided by the analysis centers of the space-geodetic techniques, the pole coordinates and universal time have been estimated with a high temporal resolution, i.e., one hour. The sub-daily resolution allows to validate the resulting time-series w.r.t. a model derived from satellite altimetry (i.e., the sub-daily ERP model suggested by the IERS Conventions 2003, see *McCarthy and Petit, 2004*) instead of relying only on the official time-series provided by the IERS (e.g., IERS-C04, IERS Bulletin A, see *Gambis, 2004*) that base on the same space-geodetic data and, thus, are not fully independent. The drawback of setting up the pole coordinates with a sub-daily resolution and estimating corrections to the a priori nutation model IAU2000 (*Mathews et al., 2002*) simultaneously, is the presence of a one-to-one correlation between the nutation corrections and a retrograde diurnal term in polar motion. Theoretical considerations dealing with this correlation are included in this thesis and studies based on simulated observations as well as real VLBI observations illustrate the impact of different methods to handle this singularity. In the case of the satellite techniques, three additional degrees of freedom due to a common rotation of all orbital planes are involved (*Hefty et al., 2000*). In former studies devoted to sub-daily ERP done by, e.g., *Herring and Dong (1994)* or *Watkins and Eanes (1994)*, the diurnal and sub-diurnal terms of interest were set up explicitly as unknowns so that the one-to-one correlation was avoided. However, in this case, the periods of the signals of interest have to be exactly known in advance and it is assumed that nothing else than these terms are present in the time-series of ERP. The studies presented hereafter use a different approach: Polar motion (and *UT1-UTC*) is estimated as a time-series represented by a piece-wise linear polygon and the correlation is handled by a special constraint that blocks any retrograde diurnal term in polar motion so that such a type of signal will be part of the nutation angle estimates (*Brockmann, 1997*).

Unfortunately, it is difficult and in most cases does not make sense to derive sub-daily ERP from SLR observations, but the main benefit from the inclusion of SLR into the combination is thought to be relevant for TRF-related issues rather than for Earth rotation.

In order to demonstrate the potential of VLBI to impact the combination of the techniques, the time span for CONT02 was chosen here, as continuous VLBI observations derived from a homogeneous network allow a better determination of the estimated parameters than VLBI sessions that base on changing networks and have gaps of a few days between the individual sessions. The continuous availability of VLBI is of special importance as one goal of this thesis is to demonstrate that a combination of GPS-derived *LOD* and VLBI-derived *UT1-UTC/LOD* is worthwhile and yields a time-series of piece-wise linear *UT1-UTC* values that is more stable than the VLBI-only time-series. This is in contrast to the statements by other authors, e.g., *Ray et al. (2005)* or *Gross (2000)*, that there is no method to rigorously combine the contributions of VLBI and the satellite techniques for universal time. However, as the studies presented hereafter base on datum-free normal equation systems including free satellite orbits, the *UT1-UTC* time-series derived from integrated *LOD* values delivered by GPS and SLR is free to align to the absolute value of *UT1-UTC* that is given by VLBI, and the high short-term stability of *LOD* (especially the GPS-derived values) result in a combined time-series of universal time that is more stable than the VLBI-only time-series.

---

Summarizing the main specialties of the studies presented hereafter, the combination bases on homogeneous datum-free normal equation systems, and the parameterization as well as the a priori models have been aligned for the analysis of the GPS, VLBI and SLR observations. Furthermore, troposphere parameters are consistently combined together with the TRF and EOP for the first time, and, finally, it is demonstrated that a combination of VLBI and the satellite techniques is possible for all five parameters describing the Earth's orientation and rotation.

As the combination studies base on normal equation systems, *Chapter 2* gives the mathematical background for the handling of NEQs including all manipulations that are used within the studies, e.g., transformation of a priori values and different types of constraining. The space-geodetic techniques themselves are characterized in *Chapter 3* in order to visualize the differences and similarities between the techniques that have to be considered when performing an inter-technique combination. *Chapter 4* is dedicated to the data sets that are used besides the observations of the space-geodetic techniques themselves, namely the local ties for connecting the networks and water vapor radiometer and meteorological data for validating the troposphere parameters. In addition, the characteristics of the CONT02 campaign are explained in more details. General aspects about the processing of the GPS, VLBI and SLR observations for CONT02, some aspects related to the combination and methods used for validating the resulting parameters are summarized in *Chapter 5*. The theoretical studies on the correlation between a retrograde diurnal polar motion term and the nutation angles, mentioned already before, are included in *Chapter 5.3*. Finally, *Chapter 6* summarizes the results for the estimated parameters, starting with the analysis of the single-technique solutions followed by the combined solutions. Some concluding remarks and an outlook on further studies are given in *Chapter 7*.

# 2 Least squares adjustment theory

This chapter summarizes the mathematical principles that are important for understanding the data processing algorithms used for this thesis. Starting with the well-known Gauss-Markoff model, several aspects of the parameter estimation process are introduced, e.g., parameter transformations, parameter pre-elimination, application of a priori constraints, stacking of normal equation systems and expansion of normal equations. Extensive explications of the least squares adjustment theory is given in *Koch (1988)* and *Niemeier (2002)*. For geodetic applications, especially using the Global Positioning System (GPS) and the *Bernese GPS Software* (*Dach et al., 2007*), a summary of the basic least squares adjustment formulas can be found in *Brockmann (1997)* or in *Mervart (2000)*.

## 2.1 Gauss-Markoff model

Generally speaking, a set of $u$ unknown parameters $\boldsymbol{x}$ will be estimated using a set of $n$ independent observations $\hat{\boldsymbol{o}}$. Each observation must be mathematically expressed as a function of the unknown parameters:

$$\hat{\boldsymbol{o}} \; = \; f(\boldsymbol{x}) \quad . \tag{2.1}$$

Usually the observations are derived from measurements that are influenced by various error sources so that the relationship (2.1) cannot be fulfilled exactly. If all random errors corrupting the observations are accumulated in a vector of residuals $\boldsymbol{v}$, the vector of observations $\hat{\boldsymbol{o}}$ can be separated into the original observations, denoted with $\boldsymbol{o}$, and the residuals:

$$\hat{\boldsymbol{o}} = \boldsymbol{o} + \boldsymbol{v} \quad . \tag{2.2}$$

Hence, the basic equation (2.1) is rewritten as:

$$\boldsymbol{o} + \boldsymbol{v} \; = \; f(\boldsymbol{x}) \quad . \tag{2.3}$$

This expression is known as the observation equation. In most cases the function $f(\boldsymbol{x})$ is not linear w.r.t. the parameters to be estimated. But for the Gauss-Markoff model a linear relationship is required. The linearization of (2.3) is obtained by a first-order Taylor series expansion using the a priori values $\boldsymbol{x0}$ for the unknowns and by estimating only small corrections $\Delta\boldsymbol{x}$ to these a priori values. The so-called Jacobian matrix or first design matrix $A$ is composed of all first order derivatives of the function $f(\boldsymbol{x})$ w.r.t. the estimated parameters evaluated at $\boldsymbol{x0}$:

$$\boldsymbol{o} + \boldsymbol{v} \; = \; f(\boldsymbol{x0}) + \frac{\partial f}{\partial \boldsymbol{x}}\Big|_{\boldsymbol{x}=\boldsymbol{x0}} \cdot \Delta\boldsymbol{x}$$
$$\boldsymbol{o} + \boldsymbol{v} \; = \; f(\boldsymbol{x0}) + A \cdot \Delta\boldsymbol{x} \quad . \tag{2.4}$$

Introducing the vector $\boldsymbol{l}$ as reduced observations or 'observed – computed'

$$\boldsymbol{l} \; = \; \boldsymbol{o} \; - \; f(\boldsymbol{x0}) \tag{2.5}$$

the above equation reads as

$$\boldsymbol{v} = A \cdot \Delta\boldsymbol{x} - \boldsymbol{l} \tag{2.6}$$

denoted 'equation of residuals'. To be able to solve this system, the least squares adjustment method demands the minimization of the (weighted) square sum of the residuals:

$$\boldsymbol{v}^T \, P \, \boldsymbol{v} \; \rightarrow \; min \quad . \tag{2.7}$$

The weighting of the observations and their residuals is taken into account by the matrix $\boldsymbol{P}$, which is often a diagonal matrix (i.e., if the observations are uncorrelated) using the standard deviations of the observations $\sigma_i$ and the a priori standard deviation of unit weight $\sigma_0$, so that the main diagonal elements of $\boldsymbol{P}$ are defined by

$$P(i,i) = \left(\frac{\sigma_0}{\sigma_i}\right)^2 \; . \tag{2.8}$$

The requirement for the least squares adjustment (2.7) leads to the so-called system of normal equations

$$\boldsymbol{A}^T \, \boldsymbol{P} \, \boldsymbol{A} \; \cdot \; \Delta\, \boldsymbol{x} \; = \; \boldsymbol{A}^T \, \boldsymbol{P} \, \boldsymbol{l} \tag{2.9}$$

where

$$\boldsymbol{N} \; = \; \boldsymbol{A}^T \; \boldsymbol{P} \; \boldsymbol{A} \tag{2.10}$$

denotes the normal equation matrix, and

$$\boldsymbol{b} \; = \; \boldsymbol{A}^T \; \boldsymbol{P} \; \boldsymbol{l} \tag{2.11}$$

is the vector of the right-hand side.

It can easily be seen how the unknowns are derived from the system of normal equations (2.9):

$$\Delta\, \boldsymbol{x} \; = \; \boldsymbol{N}^{-1} \; \cdot \; \boldsymbol{b} \; . \tag{2.12}$$

In the case of a linear relationship (2.3) between observations and parameters, $\Delta\, \boldsymbol{x}$ is identical to $\boldsymbol{x}$, hence, (2.12) directly gives the adjusted parameters. If a linearization (2.4) had to be performed, however, the unknowns $\Delta\, \boldsymbol{x}$ represent only an improvement for the a priori values $\boldsymbol{x0}$. Thus, the original parameters are given by

$$\boldsymbol{x} \; = \; \boldsymbol{x0} \; + \; \Delta\, \boldsymbol{x} \; . \tag{2.13}$$

After computing the residuals according to (2.6), the minimized weighted square sum can be derived and divided into two parts:

$$\boldsymbol{v}^T \; \boldsymbol{P} \; \boldsymbol{v} \; = \; (\boldsymbol{A} \cdot \Delta\, \boldsymbol{x} - \boldsymbol{l})^T \; \boldsymbol{P} \; (\boldsymbol{A} \cdot \Delta\, \boldsymbol{x} - \boldsymbol{l}) \; = \; ... \; = \; \boldsymbol{l}^T \; \boldsymbol{P} \; \boldsymbol{l} - \Delta\, \boldsymbol{x}^T \; \boldsymbol{b} \; . \tag{2.14}$$

The first part, i.e., $\boldsymbol{l}^T \, \boldsymbol{P} \, \boldsymbol{l}$, only depends on the observations, whereas the second part, i.e., $\Delta\, \boldsymbol{x}^T \, \boldsymbol{b}$, is influenced by the solution. Consequently, for computing the weighted square sum of residuals (2.14) in a combination of datum-free normal equation systems, only $\boldsymbol{l}^T \, \boldsymbol{P} \, \boldsymbol{l}$ has to be known from the single input normal equation systems, whereas the second part is derived from the combined solution itself.

The square sum of residuals leads to the a posteriori variance of unit weight:

$$\hat{\sigma}_0^{\,2} \; = \; \frac{\boldsymbol{v}^T \; \boldsymbol{P} \; \boldsymbol{v}}{n \, - \, u} \; . \tag{2.15}$$

Using the law of error propagation, the covariance matrix of the estimated parameters is

$$\boldsymbol{Q}_{xx} \; = \; \hat{\sigma}_0^{\,2} \cdot \boldsymbol{N}^{-1} \; . \tag{2.16}$$

In the case of a linearization, the a priori values $x0$ used must be good enough so that an approximation with a first order Taylor series expansion is justified. If this cannot be guaranteed, an iteration is needed using the estimated parameters as new a priori values in the subsequent step.

Starting from these basic formulas for the least squares adjustment, several manipulations of the system of normal equations can be carried out. Some operations that are important for the derivation of the results in this thesis are outlined in the following sections.

## 2.2 Scaling of normal equation systems

In principle, the scaling of a normal equation system is arbitrary, depending on the definition of the observation of unit weight. Therefore, the scaling can be changed without influencing the results. Switching from an old scaling given by the variance factor $\sigma_{old}^2$ to a new scaling $\sigma_{new}^2$, the factor for the re-scaling of the normal equation is the ratio of both variance factors:

$$s = \frac{\sigma_{new}^2}{\sigma_{old}^2} \quad . \tag{2.17}$$

Then, the re-scaled system of normal equations can be derived easily:

$$s \cdot N \cdot x = s \cdot b \quad . \tag{2.18}$$

Of course, the square sum of residuals and $l^T P l$ must be re-scaled as well by multiplying them with the scaling factor $s$.

This very simple manipulation is used in the combination process for numerical reasons. As already mentioned at the beginning, the different input normal equation systems generally do not refer to the same choice of the observation of unit weight. In order to give some examples for this degree of freedom: In the case of GPS the observation of unit weight can be either a zero difference observation or a double difference observation. For VLBI the differences result from choosing either units of length or units of time, i.e., [m] or [s], respectively. If these normal equation systems are then combined it is numerically required that they are based on reasonable scaling factors.

Additionally, the manipulation (2.18) can be applied in order to weight the different input normal equations. Multiplying one of the input normal equation systems with an additional factor corresponds to changing its weight in the combination. Therefore, the weighting method described later on in *Chapter 5.1.1* bases on formula (2.18). However, it must be kept in mind that in this special case the factor $s$ has the meaning of a weighting factor instead of a re-scaling factor.

## 2.3 Linear parameter transformation

For a linear transition from an old set of parameters $x$ to a new set $y$ the following linear relationship must be known:

$$x = C \cdot y + c \quad . \tag{2.19}$$

If (2.19) is substituted for the old parameters $x$ and for the improvements $\Delta x$ (in the case of a linearization) in the equation of residuals (2.6) and in the system of normal equations (2.9), the transformation results can be obtained after a short derivation:

$$N_{new} = C^T N_{old} C \quad , \tag{2.20}$$

$$b_{new} = C^T \cdot (b_{old} - N_{old} \cdot c) \quad , \tag{2.21}$$

$$l_{new} = l_{old} - A \cdot c \ . \tag{2.22}$$

And $l^T P l$, which is more important for the combination than $l$, is transformed according to:

$$l_{new}^T P l_{new} = l_{old}^T P l_{old} - 2 c^T b_{old} + c^T N_{old} c \ . \tag{2.23}$$

The linear parameter transformation is a convenient tool on which many other operations are based. The following subchapters describe the transformation of a priori values and the transformation from a parameter representation with offset and drift to a piece-wise linear parameterization as two examples that are important for the combination studies.

## 2.3.1 Transformation of a priori values

In general, space geodesy deals with linearized observation equations. Hence, the normal equation system refers to one special set of a priori values and the estimated improvements $\Delta x$ depend on them. If different normal equation systems are combined, they all have to refer to the same set of a priori values, because the improvements $\Delta x$ are to be estimated as one common set for all normal equation systems. As a consequence of this requirement, the normal equation systems first have to be transformed from the original a priori values $x0$ to a new set $y0$, common to all single normal equation systems and the combined system. The following linear relation between both sets of a priori values and the corresponding improvements is assumed:

$$x0 + \Delta x = y0 + \Delta y \ , \tag{2.24}$$

or written in a different way:

$$\Delta x = \Delta y + (y0 - x0) \ . \tag{2.25}$$

By comparing this expression to the general transformation equation (2.19), we readily see that the transformation matrix $C$ and the vector $c$ are given by:

$$C = I \ , \tag{2.26}$$

$$c = y0 - x0 \ . \tag{2.27}$$

$C$ as an identity matrix implies that the normal equation matrix $N$ remains unchanged, whereas the vector $b$ on the right-hand side and the reduced observations $l$ are modified by changing the a priori values (see equations (2.20)-(2.22)).

## 2.3.2 Transformation between different parameterizations

Most of the parameters estimated from space-geodetic observations are changing with time, e.g., Earth rotation parameters, troposphere parameters and station coordinates (if a longer time-span is considered). To cope with this behavior in the parameter adjustment, the whole time-span is split into sub-intervals (e.g. one hour, one day) and for each of them a parameter set is estimated. The time-dependency within one sub-interval can be expressed either by one offset at a certain epoch and an additional drift, or by functional values of a polygon at the interval boundaries assuming a linear behavior between them. Figure 2.1 visualizes both parameterizations. Two principal differences between the two methods must be mentioned: The resulting number of parameters for a certain number of intervals and the problem of continuity at the interval boundaries. To be more precise concerning the first topic, a number of $n$ sub-intervals results in $2n$ parameters in the case of a parameterization with one set of offset plus drift, whereas only $n+1$ parameters are needed for the piece-wise linear representation as a polygon. Of course, there is no difference in the case of solely one interval but the number of intervals is clearly larger for most of the parameters, thus, the number of parameters heavily increases. Furthermore, the continuity at the interval boundaries is automatically fulfilled using the polygon parameterization, contrary to the representation with offset and drift, which allows jumps to occur at the interval boundaries. In the latter case, continuity conditions have to be applied additionally to avoid jumps, altogether $n-1$ conditions. The number of conditions decreases the number of independent parameters to $n+1$, i.e., to an equal number of parameters as in the case of the polygon representation, clearly demonstrating the

over-parameterization with one set of offset plus drift per interval. In view of the arguments concerning the number of parameters and the continuity at interval boundaries, the piece-wise linear parameterization as a polygon is preferred in the *Bernese GPS Software*.
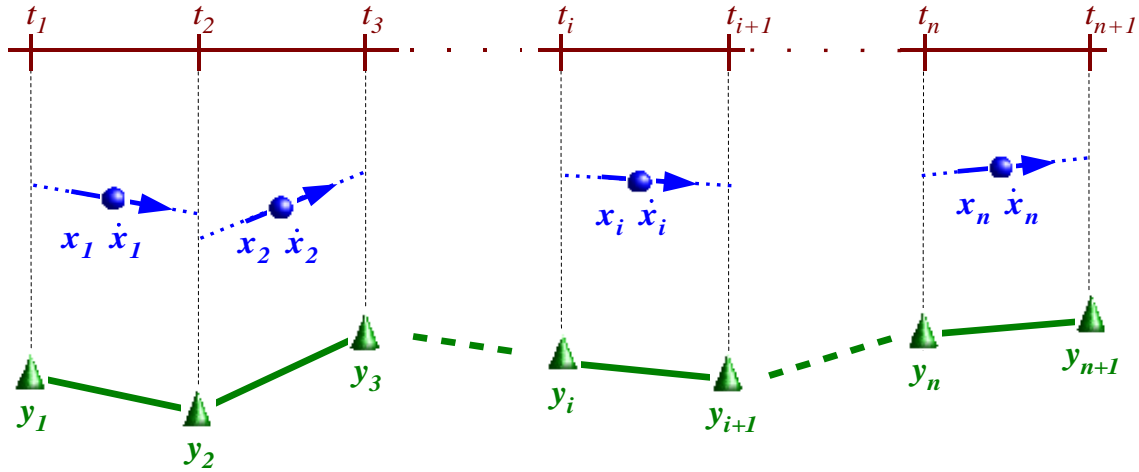


**Figure 2.1:** *Different types of parameterizations for a time-series of n intervals: **a)** offset + drift for each interval (blue), **b)** piece-wise linear polygon (green).*

If normal equation systems contain different types of parameterization, one common type must be chosen for the combination, and all normal equation systems first have to be transformed to this representation. In the following, the transformation will be given exemplarily for one interval delimited by the epochs $t_1$ and $t_2$. The corresponding two types of parameterization for this interval can be described by

$$x = \begin{pmatrix} x\,(t_i) \\ \dot{x}\,(t_i) \end{pmatrix} \quad, \quad y = \begin{pmatrix} y\,(t_1) \\ y\,(t_2) \end{pmatrix} \quad. \tag{2.28}$$

In (2.28) $x$ represents the parameterization using an offset $x\,(t_i)$ at an arbitrary epoch $t_i$ within the interval considered here, i.e., $t_i \in [t_1\ t_2]$, and a drift $\dot{x}\,(t_i)$ as second parameter. The piece-wise linear parameterization with two functional values at the interval boundaries is represented by $y$. Computing an offset at a certain epoch from an offset valid at a different epoch and a corresponding drift is basic mathematics, thus, the linear relationship between $x$ and $y$ can be given after a short derivation:

$$x = \begin{bmatrix} \dfrac{t_2 - t_i}{t_2 - t_1} & \dfrac{t_i - t_1}{t_2 - t_1} \\[2ex] \dfrac{-1}{t_2 - t_1} & \dfrac{1}{t_2 - t_1} \end{bmatrix} \cdot y \quad. \tag{2.29}$$

The transformation matrix $C$ (see (2.19)) is given by the matrix in equation (2.29) and it is clear that the vector $c$ is zero. Inserting both into the general equations for a linear parameter transformation (2.20)-(2.22) reveals the transformed normal equation system.

One comment must be added in view of the combination procedure described later on: If only an offset (instead of offset and drift) should be "transformed" to the piece-wise linear parameterization, the matrix in equation (2.29) is reduced to the first row only. Then, the single offset $x$ is portioned according to its temporal distance to both epochs of the polygon. By the way, this procedure is used as well for computing the contribution of an observation at a specific epoch to a piece-wise linear representation of any parameter.

## 2.4 Parameter pre-elimination

There are several parameter types in space geodesy that have to be estimated, but whose values are interesting only for some special studies. GPS phase ambiguities or clock parameters are examples of such parameter types. Moreover, if the user is interested only in one type of parameter, all the others can be skipped after estimating them. In order to keep the normal equation system small, it is convenient to pre-eliminate all parameters that are not interesting for the intended application. It is important to mention that the appropriate parameters are estimated implicitly although they are pre-eliminated. Therefore, this approach must be clearly distinguished from an adjustment without estimating those parameters. The pre-elimination algorithm is based on a division of the normal equation system into two parts: $x_1$ consisting of the parameters that will be retained, and $x_2$ comprising those that will be pre-eliminated. The corresponding normal equation system looks as follows:

$$\begin{bmatrix} N_{11} & N_{12} \\ N_{21} & N_{22} \end{bmatrix} \cdot \begin{bmatrix} x_1 \\ x_2 \end{bmatrix} = \begin{bmatrix} b_1 \\ b_2 \end{bmatrix} \ , \tag{2.30}$$

or, decomposed into two parts:

$$N_{11} \cdot x_1 + N_{12} \cdot x_2 = b_1 \ , \tag{2.31}$$

$$N_{21} \cdot x_1 + N_{22} \cdot x_2 = b_2 \ . \tag{2.32}$$

Solving for $x_2$ in the second equation and introducing the resulting expression into the first equation yields the normal equation system where the parameters $x_2$ are pre-eliminated:

$$(N_{11} - N_{12} \, N_{22}^{-1} \, N_{21}) \cdot x_1 = b_1 - N_{12} \, N_{22}^{-1} \cdot b_2 \ . \tag{2.33}$$

Finally, the reduced normal equation system can be characterized by the following quantities:

$$N_{reduc} = N_{11} - N_{12} \, N_{22}^{-1} \, N_{21} \ , \tag{2.34}$$

$$b_{reduc} = b_1 - N_{12} \, N_{22}^{-1} \cdot b_2 \ , \tag{2.35}$$

$$v^T \, P \, v = l^T \, P \, l - x^T \, b_{reduc} = \ldots = l^T \, P \, l - b_2^T \, N_{22}^{-1} \, b_2 - x_1^T \, b_{reduc} \ . \tag{2.36}$$

## 2.5 Stacking of normal equation systems

The basic operation in the process of combining normal equation systems is the stacking. Thereby, stacking means the correct treatment of parameters common to more than one normal equation system: one and the same parameter is contained in at least two input normal equation systems and both are merged into only one parameter in the resulting combined normal equation system. This procedure is also well known as 'Helmert blocking' (*Helmert, 1872*). It has been proven already in other publications, e.g. *Brockmann (1997)*, that a sequential least squares adjustment leads to the same result as a common adjustment in one step, provided that the different observation series are independent. Therefore, the proof of equivalence is omitted here and only the formalism necessary for combining two observation series will be outlined briefly. The generalization with more than two series can be easily verified.

Starting from two systems of observation equations of type (2.6) determining the same set of unknown parameters $x$, the Jacobian matrix $A$ and the weight matrix $P$ for the combined system - with the assumption of no correlations between the two sets of observations - would be given by:

$$A = \begin{pmatrix} A_1 \\ A_2 \end{pmatrix}, \quad P = \begin{pmatrix} P_1 & 0 \\ 0 & P_2 \end{pmatrix}.$$ (2.37)

The corresponding normal equation system is derived after a short computation:

$$(A_1^T P_1 A_1 + A_2^T P_2 A_2) \cdot x = A_1^T P_1 l_1 + A_2^T P_2 l_2.$$ (2.38)

In the case of a two-step approach, the two systems of observation equations are first converted independently into two normal equation systems:

$$A_1^T P_1 A_1 \cdot x = A_1^T P_1 \cdot l_1,$$ (2.39)

$$A_2^T P_2 A_2 \cdot x = A_2^T P_2 \cdot l_2.$$ (2.40)

Normally, in the second step, the user does not have access to the matrices $A$, $P$ and the vector $l$ any more. Instead of these quantities, only the corresponding normal equation matrices $N_1$, $N_2$ and the vectors $b_1$, $b_2$ of the right-hand side of the normal equation systems are accessible:

$$N_1 = A_1^T P_1 A_1, \qquad b_1 = A_1^T P_1 \cdot l_1,$$ (2.41)

$$N_2 = A_2^T P_2 A_2, \qquad b_2 = A_2^T P_2 \cdot l_2.$$ (2.42)

Comparing the equations (2.41) and (2.42) with (2.38) it is obvious that for a combined solution of the identical parameters $x$ only the two normal equation matrices and the vectors of the right-hand side, respectively, have to be summed up:

$$(N_1 + N_2) \cdot x = b_1 + b_2.$$ (2.43)

# 2.6 Constraining of parameters

In most cases, at least for the applications mentioned in this thesis, the observations available do not contain all the information that is needed to derive a solution. This implies that the system of normal equations (2.9) is singular or almost singular. Consequently, the normal equation matrix $N$ cannot be inverted and, therefore, the solution $x$ cannot be obtained. For solving this problem, exterior additional information about the parameters must be included, so-called constraints, that remedy the rank deficiency. The incorporation of constraints can be done in different ways. The classical way of adding constraints, named 'Gauss-Markoff model with restrictions/conditions' (see *Ebner, 1997* or *Koch, 1988*), demands the exact fulfillment of the additional conditions by the estimated parameters. In the case of geodetic applications, these strong restrictions are often undesired because there is no degree of freedom left for the parameters. In addition, in many cases it is known that the introduced additional information is not error-free, and thus, it would degrade the estimation rather than improve it. These two disadvantages are avoided if the constraining is done by pseudo-observations including an appropriate weight for these fictitious observations reflecting their accuracy. The observation equations for the fictitious observations look similar to those of the 'real' observations (2.6):

$$v_h = H \cdot x - h.$$ (2.44)

The weight matrix for the constraints is built from the known variances of the pseudo-observations, i.e., $\sigma_{h\,(i)}^2$, and is scaled the same way as the 'real' observations, i.e., with the a priori variance factor $\sigma_0^2$:

$$P_h \, (i \, , \, i) \, = \, \frac{\sigma_0{}^2}{\sigma_{h \, (i)}{}^2} \quad . \tag{2.45}$$

Of course, if the correlations between the pseudo-observations are known, more complicated constraints are possible including a fully occupied weight matrix $P_h$. The pseudo-observations yield a system of normal equations as well:

$$H^T \, P_h \, H \cdot x \, = \, H^T \, P_h \cdot h \quad . \tag{2.46}$$

Together with the original system of normal equations we obtain:

$$(A^T \, P \, A \, + \, H^T \, P_h \, H) \cdot x \, = \, A^T \, P \cdot l \, + \, H^T \, P_h \cdot h \quad . \tag{2.47}$$

In *Brockmann (1997)* it was shown that the method of introducing fictitious observations as constraints can be transformed into the strong Gauss-Markoff model with restrictions by increasing the weight for the fictitious observation, i.e., $\sigma_{h \, (i)}{}^2 \, \to \, 0$. Therefore, it is possible to pass fluently from very loose constraints to strong conditions.

The following special cases of constraints will be explained explicitly:

- Absolute constraints on parameters,
- Free-network constraints (datum definition),
- Relative constraints between parameters,
- Blocking of retrograde diurnal polar motion terms.

## 2.6.1  Absolute constraints on parameters

If 'ideal' values $w$ for the estimated parameters $x$ are known and the estimation should be constrained to these values, the appropriate equation for the pseudo-observation can be set up:

$$v_h \, = \, x \, - \, w \quad . \tag{2.48}$$

It can easily be seen that equation (2.47) is simplified to

$$(A^T \, P \, A \, + \, P_h) \cdot x \, = \, A^T \, P \cdot l \, + \, P_h \cdot w \quad . \tag{2.49}$$

A special application of (2.48) is the constraining of parameters to their a priori values, because in this case all elements of $w$ become 0, and only the weights $P_h$ must be added to the normal equation matrix.

## 2.6.2  Free-network constraints

The method of a free-network constraint offers the possibility to align the estimated network solution to an a priori reference frame. A Helmert transformation is used to describe the relation between the internal network solution derived from the observations and the coordinates of the a priori network that is used as a reference. The Helmert transformation can be formulated for each station $i$ of the network with the coordinate estimates $X_i = [X, Y, Z]$ and the coordinates $X0_i = [X0, Y0, Z0]$ used as a reference:

$$
\begin{bmatrix} X \\ Y \\ Z \end{bmatrix} = (1 + \mu) \cdot \begin{bmatrix} 1 & \gamma & -\beta \\ -\gamma & 1 & \alpha \\ \beta & -\alpha & 1 \end{bmatrix} \cdot \begin{bmatrix} X0 \\ Y0 \\ Z0 \end{bmatrix} + \begin{bmatrix} T_X \\ T_Y \\ T_Z \end{bmatrix} . \tag{2.50}
$$

Therein, the seven transformation parameters are

- $T_X$, $T_Y$, $T_Z$: Translations in $x$, $y$, $z$ direction respectively,
- $\alpha$, $\beta$, $\gamma$: Rotations around $x$, $y$, $z$ axis respectively,
- $\mu$: Scale factor.

After regrouping the variables and assuming small values for the transformation parameters (linearization), the above equation becomes

$$
\begin{bmatrix} X \\ Y \\ Z \end{bmatrix} = \begin{bmatrix} X0 \\ Y0 \\ Z0 \end{bmatrix} + \begin{bmatrix} 1 & 0 & 0 & 0 & -Z0 & Y0 & X0 \\ 0 & 1 & 0 & Z0 & 0 & -X0 & Y0 \\ 0 & 0 & 1 & -Y0 & X0 & 0 & Z0 \end{bmatrix} \cdot \begin{bmatrix} T_X \\ T_Y \\ T_Z \\ \alpha \\ \beta \\ \gamma \\ \mu \end{bmatrix} , \tag{2.51}
$$

or written in matrix notation for the station $i$:

$$
X_i = X0_i + B_i \cdot \zeta . \tag{2.52}
$$

The expressions for the vector of Helmert parameters $\zeta$ and for the matrix of coefficients for one station $B_i$ can be retrieved easily from comparing both equations. Putting together all $n_{sta}$ stations that should contribute to the free-network constraint we get:

$$
X = \begin{bmatrix} X_1 \\ X_2 \\ \vdots \\ X_{n_{sta}} \end{bmatrix} , \quad X0 = \begin{bmatrix} X0_1 \\ X0_2 \\ \vdots \\ X0_{n_{sta}} \end{bmatrix} , \quad B = \begin{bmatrix} B_1 \\ B_2 \\ \vdots \\ B_{n_{sta}} \end{bmatrix} . \tag{2.53}
$$

The basic equation of residuals for solving for the Helmert parameters $\zeta$ can then be written as

$$
v = B \cdot \zeta - (X - X0) = B \cdot \zeta - x . \tag{2.54}
$$

Thus, the Helmert parameters are determined by

$$
\zeta = (B^T B)^{-1} B^T \cdot x . \tag{2.55}
$$

The free-network restriction itself is based on the last equation (2.55) by asking for zero values for (some of) the Helmert parameters. This condition leads to the observation equation for the free-network constraint:

$$\boldsymbol{\zeta} = (\boldsymbol{B}^T \ \boldsymbol{B})^{-1} \ \boldsymbol{B}^T \cdot \boldsymbol{x} = \boldsymbol{0} \quad . \tag{2.56}$$

Comparing (2.56) with the general equation for constraints (2.44), it is obvious that $\boldsymbol{h} = \boldsymbol{0}$, and the Jacobian matrix $\boldsymbol{H}$ is

$$\boldsymbol{H} = (\boldsymbol{B}^T \ \boldsymbol{B})^{-1} \ \boldsymbol{B}^T \quad . \tag{2.57}$$

For the free-network constraints, the weight matrix $\boldsymbol{P_h}$ is compiled from the variances of the individual transformation parameters. Finally, the system of normal equations including free-network constraints has the form:

$$(\boldsymbol{A}^T \ \boldsymbol{P} \ \boldsymbol{A} + \boldsymbol{H}^T \ \boldsymbol{P}_h \ \boldsymbol{H}) \cdot \boldsymbol{x} = \boldsymbol{A}^T \ \boldsymbol{P} \cdot \boldsymbol{l} \quad . \tag{2.58}$$

Compared to absolute constraints on station coordinates (*Chapter 2.6.1*), the application of free-network constraints has the advantage that the network itself is not deformed if only datum defects (e.g. rotations, translations and scale) are constrained.

Finally, a special application of free-network constraints must be mentioned. If only those Helmert parameters are constrained that correspond to a degree of freedom of the network, the restrictions are minimum constraints. Consequently, three rotations and three translations must be constrained in the case of a global VLBI solution, whereas for a global GPS or SLR solution only three rotations need to be constrained. If only the three rotations are considered, the constraint is called no-net-rotation (NNR) condition. In the case of constraining only the three translations, the expression no-net-translation (NNT) constraint is used, and a no-net-scale (NNSc) condition constrains only the scale.

## 2.6.3  Relative constraints between parameters

In some cases the relation between two parameters $x_i$ and $x_j$ is known and it may be helpful to make use of this additional information. Such a constraint is introduced with the observation equation

$$x_i - x_j = w \quad , \tag{2.59}$$

respectively the equation of residuals:

$$v = x_i - x_j - w = \begin{bmatrix} 1 & -1 \end{bmatrix} \cdot \begin{bmatrix} x_i \\ x_j \end{bmatrix} - w \quad , \tag{2.60}$$

where $x_i$, $x_j$ represent the two relevant parameters and $w$ is the known value for the tie between them which should be realized by the solution. Let the standard deviation for keeping the value $w$ for the tie be $\sigma_w$. Then, the normal equation can be retrieved easily:

$$\left(\frac{\sigma_0}{\sigma_w}\right)^2 \cdot \begin{bmatrix} 1 & -1 \\ -1 & 1 \end{bmatrix} \cdot \begin{bmatrix} x_i \\ x_j \end{bmatrix} = \left(\frac{\sigma_0}{\sigma_w}\right)^2 \cdot \begin{bmatrix} w \\ -w \end{bmatrix} \quad . \tag{2.61}$$

Applications for constraining two parameters relative to each other are coordinate differences at co-located sites, so-called 'local ties', or differences in the troposphere zenith delays at co-located sites, named 'troposphere ties' throughout this thesis. In both cases, the value $w$ usually is not 0. The situation $w = 0$ means that the two parameters should be identical (within the strength of the constraint). An example for this particular case is the constraining of the difference between two consecutive parameters to prevent them from too large variations in time, e.g., if parameters are set up with a very high temporal resolution. Relative constraints

with $w = 0$ can also be used as an alternative to a real stacking of two parameters (see Sec. 2.5). More precisely, the two corresponding parameters are both kept in the normal equation system, but due to the relative constraint they must be identical within the limits given by the constraint.

### 2.6.4  Blocking of retrograde diurnal terms in polar motion

If polar motion is estimated with a sub-daily resolution, the nutation angles cannot be estimated simultaneously as they are one-to-one correlated with a retrograde diurnal term in polar motion. An additional correlation appears in the case of satellite techniques if orbital elements are to be estimated, because a rotation of the entire orbit system corresponds to a retrograde diurnal term in polar motion, as well. Nevertheless, it is desirable to estimate all types of parameters simultaneously in many cases, hence, an additional condition is needed to remove the singularity. For this purpose, a method to prevent a retrograde diurnal term in polar motion was developed. An elaborate derivation of the basic formulas is given in *Brockmann (1997)*. The constraint derived therein deals with the singularity between an offset for the nutation angles and a retrograde diurnal signal in polar motion with constant amplitude. The background for this constraint is given hereafter in *Section a*. However, in many cases a temporal variation of the nutation angles is considered in the parameterization as well. The presence of a linear temporal variation for the nutation angles, given either by a drift parameter or by the piece-wise linear polygon (see *Chapter 2.3.2*), gives rise to another singularity, i.e., a retrograde diurnal signal in polar motion with linearly increasing amplitude. As a consequence, the constraint was extended in order to also remove this singularity, and the mathematical expressions are given in *Section b*. More explanations on the singularity itself will be given in *Chapter 5.3.1*.

*a) Retrograde diurnal signal in polar motion with constant amplitude*

Starting from the general description of a signal with angular velocity $\omega$, phase $\phi$ and constant amplitude $A$

$$x\,(t) = A \cdot \cos\,(\omega\,t + \phi) = A \cdot \cos\,\phi \cdot \cos\,\omega\,t - A \cdot \sin\,\phi \cdot \sin\,\omega\,t \ , \qquad (2.62)$$

*Mervart (2000)* showed that in the case of a piece-wise linear representation of the signal $x(t)$ with $n$ values $x_i$ the relation (2.62) can be expressed by

$$\begin{pmatrix} x_1 \\ \vdots \\ x_n \end{pmatrix} = \begin{pmatrix} \cos\,\omega\,t_1 & \sin\,\omega\,t_1 \\ \vdots & \vdots \\ \cos\,\omega\,t_n & \sin\,\omega\,t_n \end{pmatrix} \cdot \begin{pmatrix} A \cdot \cos\,\phi \\ -A \cdot \sin\,\phi \end{pmatrix} \ . \qquad (2.63)$$

The situation becomes more complicated if the distinction has to be made between prograde and retrograde terms as it is the case for the constraint we consider here. Then, both pole coordinates have to be considered. For the purpose explained here, only a retrograde polar motion is of interest. Therefore, the subsequent derivation of formulas will be restricted to this type of signal. A retrograde polar motion term can be described by the two pole coordinates $x(t)$ and $y(t)$ in the following way:

$$x\,(t) = \quad A \cdot \cos\,\phi \cdot \cos\,\omega\,t + A \cdot \sin\,\phi \cdot \sin\,\omega\,t \ , \qquad (2.64a)$$

$$y\,(t) = -A \cdot \cos\,\phi \cdot \sin\,\omega\,t + A \cdot \sin\,\phi \cdot \cos\,\omega\,t \ . \qquad (2.64b)$$

Following (2.63) the above equations for a retrograde polar motion term described by $n$ pairs of $x_i$ and $y_i$ are summarized in matrix notation:

$$
\begin{pmatrix} x_1 \\ y_1 \\ \vdots \\ x_n \\ y_n \end{pmatrix} = \underbrace{\begin{pmatrix} \cos \omega t_1 & \sin \omega t_1 \\ -\sin \omega t_1 & \cos \omega t_1 \\ \vdots & \vdots \\ \cos \omega t_n & \sin \omega t_n \\ -\sin \omega t_n & \cos \omega t_n \end{pmatrix}}_{\boldsymbol{C}} \cdot \begin{pmatrix} A \cdot \cos \phi \\ A \cdot \sin \phi \end{pmatrix} \quad . \tag{2.65}
$$

In the case of a diurnal signal, $\omega = 2\pi / T$, with the period $T = 1$ sidereal day.
Treating (2.65) as observation equation of type (2.1) and using the denotations

$$
A_c = A \cdot \cos \phi \quad , \qquad A_s = A \cdot \sin \phi \tag{2.66}
$$

reveals the corresponding system of normal equations with the Jacobian matrix $\boldsymbol{C}$ as indicated in (2.65) and $\boldsymbol{P}_{xy}$ denoting the weight matrix of the values $x_i$ and $y_i$:

$$
\boldsymbol{C}^T \ \boldsymbol{P}_{xy} \ \boldsymbol{C} \cdot \begin{pmatrix} A_c \\ A_s \end{pmatrix} = \boldsymbol{C}^T \ \boldsymbol{P}_{xy} \cdot \begin{pmatrix} x_1 \\ y_1 \\ \vdots \\ x_n \\ y_n \end{pmatrix} \quad . \tag{2.67}
$$

Finally, the amplitudes $A_c$ and $A_s$ are obtained:

$$
\begin{pmatrix} A_c \\ A_s \end{pmatrix} = (\boldsymbol{C}^T \ \boldsymbol{P}_{xy} \ \boldsymbol{C})^{-1} \ \boldsymbol{C}^T \ \boldsymbol{P}_{xy} \cdot \begin{pmatrix} x_1 \\ \vdots \\ y_n \end{pmatrix} \quad . \tag{2.68}
$$

On the basis of equation (2.68) the blocking constraint can be derived. In order to suppress a signal with frequency $\omega$ in the polar motion time-series independently of the phase, the amplitudes $A_c$ and $A_s$ are constrained to zero using the pseudo-observation equation

$$
\begin{pmatrix} A_c \\ A_s \end{pmatrix} = (\boldsymbol{C}^T \ \boldsymbol{P}_{xy} \ \boldsymbol{C})^{-1} \ \boldsymbol{C}^T \ \boldsymbol{P}_{xy} \cdot \begin{pmatrix} x_1 \\ \vdots \\ y_n \end{pmatrix} = \boldsymbol{0} \quad . \tag{2.69}
$$

Comparing (2.69) with the general equation for constraints (2.44) reveals $\boldsymbol{h} = \boldsymbol{0}$ and the following expression for the Jacobian matrix $\boldsymbol{H}$:

$$
\boldsymbol{H} = (\boldsymbol{C}^T \ \boldsymbol{P}_{xy} \ \boldsymbol{C})^{-1} \ \boldsymbol{C}^T \ \boldsymbol{P}_{xy} \quad . \tag{2.70}
$$

Those parts of the original normal equation matrix (i.e., generated from real observations and not for the constraint) that correspond to the parameters $x_i$ and $y_i$, can be used as weight matrix $\boldsymbol{P}_{xy}$. Another possibility is to use equal weights for all pole coordinates and to assume that there are no correlations between the subsequent pole coordinates. In that case, $\boldsymbol{P}_{xy}$ becomes an identity matrix and $\boldsymbol{H}$ is simplified for the piece-wise linear representation with $n$-1 intervals to

$$
\boldsymbol{H} = \frac{1}{n} \cdot \boldsymbol{C}^T \quad . \tag{2.71}
$$

### b) Retrograde diurnal signal in polar motion with linearly increasing amplitude

For the expansion of the constraint to the more general case, the amplitude of a retrograde diurnal signal is split into two constituents: a constant part $A$, and a part $A_t$ that is linearly increasing with time starting from the epoch $t_0$:

$$x\ (t)\ =\ \left(A\ +\ A_t \cdot (t\ -\ t_0)\right)\ \cdot \cos\ (-\omega\ t\ +\ \phi)\ ,  \qquad (2.72a)$$

$$y\ (t)\ =\ \left(A\ +\ A_t \cdot (t\ -\ t_0)\right)\ \cdot \sin\ (-\omega\ t\ +\ \phi)\ .  \qquad (2.72b)$$

Similarly to (2.65), the above expressions can be summarized in matrix notation:

$$\begin{pmatrix} x_1 \\ y_1 \\ \vdots \\ x_n \\ y_n \end{pmatrix} = \begin{pmatrix} \cos\omega t_1 & \sin\omega t_1 & (t_1-t_0)\cdot\cos\omega t_1 & (t_1-t_0)\cdot\sin\omega t_1 \\ -\sin\omega t_1 & \cos\omega t_1 & -(t_1-t_0)\cdot\sin\omega t_1 & (t_1-t_0)\cdot\cos\omega t_1 \\ \vdots & \vdots & \vdots & \vdots \\ \cos\omega t_n & \sin\omega t_n & (t_n-t_0)\cdot\cos\omega t_n & (t_n-t_0)\cdot\sin\omega t_n \\ -\sin\omega t_n & \cos\omega t_n & -(t_n-t_0)\cdot\sin\omega t_n & (t_n-t_0)\cdot\cos\omega t_n \end{pmatrix} \cdot \begin{pmatrix} A\cdot\cos\phi \\ A\cdot\sin\phi \\ A_t\cdot\cos\phi \\ A_t\cdot\sin\phi \end{pmatrix} . \quad (2.73)$$

$$\underbrace{\phantom{\begin{pmatrix} \cos\omega t_1 & \sin\omega t_1 & (t_1-t_0)\cdot\cos\omega t_1 & (t_1-t_0)\cdot\sin\omega t_1 \end{pmatrix}}}_{\boldsymbol{C_t}}$$

It is obvious that considering only the first two columns of $\boldsymbol{C_t}$ in (2.73) corresponds to the situation given in (2.65) with a constant amplitude only. The pseudo-observation equation for the expanded constraint looks as follows if the weight matrix $\boldsymbol{P_{xy}}$ is set to the identity matrix:

$$\begin{pmatrix} A \cdot \cos\ \phi \\ A \cdot \sin\ \phi \\ A_t \cdot \cos\ \phi \\ A_t \cdot \sin\ \phi \end{pmatrix}\ =\ (\boldsymbol{C_t^T}\, \boldsymbol{C_t})^{-1}\, \boldsymbol{C_t^T} \cdot \begin{pmatrix} x_1 \\ \vdots \\ y_n \end{pmatrix}\ =\ \boldsymbol{0}\ ,  \qquad (2.74)$$

with

$$\boldsymbol{C_t^T}\, \boldsymbol{C_t}\ =\ \begin{bmatrix} n & 0 & \sum\limits_{i=1}^{n} t_i & 0 \\ 0 & n & 0 & \sum\limits_{i=1}^{n} t_i \\ \sum\limits_{i=1}^{n} t_i & 0 & \sum\limits_{i=1}^{n} t_i^2 & 0 \\ 0 & \sum\limits_{i=1}^{n} t_i & 0 & \sum\limits_{i=1}^{n} t_i^2 \end{bmatrix} . \qquad (2.75)$$

Tests with various epochs for $t_0$ showed that the constant part and the linearly increasing part of the amplitude can be treated independently. Therefore, the correlations in the matrix $\boldsymbol{C_t^T}\, \boldsymbol{C_t}$ can be neglected, so that all off-diagonal elements are set to zero. Then, the matrix (2.75) is simplified to a diagonal matrix and the Jacobian matrix $\boldsymbol{H}$ for the constraint can be derived according to:

$$\boldsymbol{H} \;=\; (\boldsymbol{C}_t^T \boldsymbol{C}_t)^{-1} \boldsymbol{C}_t^T \;=\; diag \left( n \quad n \quad \sum_{i=1}^{n} t_i^2 \quad \sum_{i=1}^{n} t_i^2 \right)^{-1} \cdot \boldsymbol{C}_t^T \; . \tag{2.76}$$

The vector $\boldsymbol{h}$ for the constraint according to (2.44) is 0 here as well. Comparing (2.71) and (2.76) reveals that the latter is just an expansion of the constraint derived in *Section a*.

The studies in *Chapter 5.3.1* are devoted to some special aspects of the handling of both types of constraints (i.e., the basic form and the expanded form).

# 2.7 Expansion of the normal equation system

If additional parameters have to be set up, the system of normal equations must be expanded. Three widely known situations in the combination of the space-geodetic techniques require such an expansion:

- Allowing a bias between the estimation of parameters derived from different observation types, e.g., between troposphere delays derived from GPS and VLBI;

- Estimating specific frequencies together with a time-series of parameters, e.g., a yearly signal in the motion of stations, or a daily signal in ERP time-series;

- Taking into account a similarity transformation between the networks derived from different observation types, e.g., a scale difference between the GPS and VLBI network or a different realization of the origin of the TRF by SLR and GPS.

The formulas are based on a linear parameter transformation as outlined in *Chapter 2.3*. Starting from the set of original parameters, i.e., $\boldsymbol{x}_{old}$, the expanded set of parameters including the additional parameters, i.e., $\boldsymbol{x}_{add}$, and their relationship looks as follows:

$$\boldsymbol{x}_{old} = \begin{bmatrix} \boldsymbol{I} & \boldsymbol{D} \end{bmatrix} \cdot \begin{bmatrix} \boldsymbol{x}_{old} \\ \boldsymbol{x}_{add} \end{bmatrix} \tag{2.77}$$

with the matrix $\boldsymbol{D}$ describing the dependence of the additional parameters on the original parameters. Comparing (2.77) with the general formula for a linear parameter transformation (2.19) the assignment of the transformation matrix $\boldsymbol{C}$ with $[\boldsymbol{I} \ \boldsymbol{D}]$ is obvious. Carrying out the transformation of the normal equation system according to (2.20) and (2.21) yields the expanded system

$$\begin{bmatrix} \boldsymbol{N} & \boldsymbol{N}\boldsymbol{D} \\ \boldsymbol{D}^T \boldsymbol{N} & \boldsymbol{D}^T \boldsymbol{N} \boldsymbol{D} \end{bmatrix} \cdot \begin{bmatrix} \boldsymbol{x}_{old} \\ \boldsymbol{x}_{add} \end{bmatrix} = \begin{bmatrix} \boldsymbol{b} \\ \boldsymbol{D}^T \boldsymbol{b} \end{bmatrix} . \tag{2.78}$$

The shape of the matrix $\boldsymbol{D}$ depends on the type of additional parameters to be estimated.

## 2.7.1 Helmert parameters

The motivation to set up additional Helmert parameters was already indicated in the introduction to *Chapter 2.7*. Picking up the example of the translation parameters, both, SLR and GPS, have the capability in a global solution to determine the geocenter. However, normally the two determinations differ and, hence, will cause problems in a combined solution. In order to remedy this conflict, the translational degree of freedom must be established artificially for one of the solutions by setting up three translation parameters. As SLR is more sensitive to the geocenter and as GPS geocenter estimates tend to be biased by remaining orbit modeling problems, the combined solution should adopt the geocenter estimate from SLR whereas the determination of the geocenter by GPS is neglected and three translations are introduced for it. The example of the translation parameters as well as the above mentioned example for the scale demonstrate that in most cases only a subset of Helmert parameters will have to be set up. Nevertheless, the derivation of the matrix $\boldsymbol{B}$ will be giv-

en here for the full set of seven parameters, but only those parts corresponding to parameters relevant for a specific application have to be included.

The mathematical background is similar to that of *Chapter 2.6.2*, where the Helmert transformation for the free-network restrictions was introduced. But instead of setting up the transformation between an a priori reference frame and the estimated network, equation (2.50) has to be formulated as a Helmert transformation between the combined solution and one of the input solutions:

$$
\begin{bmatrix} X \\ Y \\ Z \end{bmatrix}_{input} = (1 + \mu) \cdot \begin{bmatrix} 1 & \gamma & -\beta \\ -\gamma & 1 & \alpha \\ \beta & -\alpha & 1 \end{bmatrix} \cdot \begin{bmatrix} X \\ Y \\ Z \end{bmatrix}_{combined} + \begin{bmatrix} T_X \\ T_Y \\ T_Z \end{bmatrix} \, . \tag{2.79}
$$

The regrouping is performed similarly to *Chapter 2.6.2* with the vector $\zeta$ containing all seven Helmert parameters and with all *nsta* stations included in the transformation:

$$
\begin{bmatrix} X_1 \\ \vdots \\ X_{nsta} \end{bmatrix}_{input} = \begin{bmatrix} I & 0 & 0 & B_1 \\ 0 & \ddots & 0 & \vdots \\ 0 & 0 & I & B_{nsta} \end{bmatrix} \cdot \begin{bmatrix} X_1 \\ \vdots \\ X_{nsta} \\ \zeta \end{bmatrix} \, . \tag{2.80}
$$

The matrix **B** is compiled exemplarily for the station *i* using the station coordinates [$X_0$, $Y_0$, $Z_0$] of the a priori reference frame chosen for the combined solution:

$$
B_i = \begin{bmatrix} 1 & 0 & 0 & 0 & -Z_{0_i} & Y_{0_i} & X_{0_i} \\ 0 & 1 & 0 & Z_{0_i} & 0 & -X_{0_i} & Y_{0_i} \\ 0 & 0 & 1 & -Y_{0_i} & X_{0_i} & 0 & Z_{0_i} \end{bmatrix} \, . \tag{2.81}
$$

Comparing the expression (2.80) with the general expression (2.77) for the transformation between the original parameter set and the expanded set it becomes clear that the matrices $B_i$ according to (2.81) are simply stacked together for all stations (see as well (2.53)) in order to derive the matrix **D** in (2.77).

When estimating additional Helmert parameters it must be kept in mind that they are fully correlated with the station coordinates contributing to them. Therefore, the set-up has to be done carefully and sufficient additional information is needed to remove the artificial degree of freedom introduced by the Helmert parameters. This can be done either by a combination with another normal equation system which is able to determine these degree of freedom, or by setting up the appropriate datum constraints according to *Chapter 2.6*.

# 3 The space-geodetic techniques

The space-geodetic techniques GPS, VLBI and SLR are outlined in the following chapter. Data from these techniques build the basis for all combination studies carried out for the thesis at hand. For each of the techniques, a description of the measuring system is given at the beginning, followed by the basic observation equation explained in a simplified form according to the presentation in *Rothacher (2002)*. The major task of *Chapter 3* is to clarify and point out the common characteristics of the observation equations and to give an idea of the critical points for each of the space techniques rather than giving an elaborate derivation for the technique-specific observation equation. Such subtleties may be found in the well-established literature. The simplified observation equations given hereafter will serve in *Chapter 5.1* as the basis for explaining the processing strategy concerning identical parameters fundamental to an inter-technique combination. The introduction to each of the space-geodetic techniques is completed with an overview of the international organizations and cooperation that were built up during the past few years to enforce the development and improvement of the respective technique and to bring together the experience of different analysis groups. Finally, *Chapter 3.4* summarizes the similarities and the differences between the individual techniques.

## 3.1 Global Positioning System (GPS)

### 3.1.1 Technical description

The concrete plans for setting up the NAVSTAR GPS (= NAVigation Satellite Timing And Ranging Global Positioning System) began in 1973. The US Department of Defense wanted to establish a highly accurate system for determining position, velocity and time, originally mainly for military use. But nowadays the number of non-military users is enormous as the NAVSTAR GPS is accessible for civilian applications as well.

The nominal constellation of the GPS consists of 24 satellites evenly distributed in six orbital planes. Each orbital plane is characterized by an inclination of 55°, a semi-major axis of about 26600 km and an orbital period of exactly half a sidereal day, i.e., 11 hours 58 minutes. With this constellation it can be guaranteed that at least four satellites are visible from any location on the Earth at any time.

For all GPS signals, a fundamental frequency of 10.23 MHz is used, which is driven by the satellite clock. The two carriers are deduced from this frequency:

- frequency L1 = 154 · 10.23 MHz = 1575.42 MHz (corresponding to approximately 19 cm wavelength);

- frequency L2 = 120 · 10.23 MHz = 1227.60 MHz (corresponding to approximately 24 cm wavelength).

Both frequencies are modulated with codes, also derived from the fundamental frequency: The C/A-code (clear acquisition) is emitted with a frequency of 1.023 MHz and its chip length is about 300m. It is modulated only on L1, whereas the second code, i.e., the P-code (precision or protected), is modulated on both carriers. The P-code has a frequency of 10.23 MHz and the length of one chip corresponds to 30 m which means that the accuracy that can be achieved in the case of the P-code is roughly ten times higher than in the case of the C/A-code.

For transmitting information about the satellite itself (satellite ephemeris, satellite clock information, health status of the satellite etc.) the so-called navigation message is modulated on both carrier frequencies.

### 3.1.2 Observation equation

In principle, there exist two types of GPS measurements: The so-called pseudorange measurements using the C/A-code or the P-code and the phase measurements using the two carrier frequencies L1 and L2. The latter is the measurement type used for high-precision applications as the accuracy to be achieved with code measurements is too low. The geodetic topics like global reference frame realization, Earth rotation studies and troposphere estimation require the highest quality of observations that is possible, hence, only phase measurements come into consideration. Therefore, the code measurements are neglected here and only the obser-

vation equation for GPS phase measurements will be presented. As already indicated in the introduction to this chapter the complete derivation of the observation equation will be omitted and it is referred to, e.g., *Hofmann-Wellenhof et al. (1994)*, *Teunissen and Kleusberg (1998)* or *Leick (2004)* for the details and the theoretical background. Taking into account all corrections necessary for a phase observation $L_A^S$ at station $A$ to satellite $S$, the following observation equation expressed in meters is obtained:

$$
\begin{aligned}
L_A^S \;=\; & \left| \boldsymbol{R}_{EOP} \cdot \boldsymbol{r}_A(t_A) \;-\; \boldsymbol{r}^S(t_A - \tau_A^S) \right| \;+\; \ldots \\
& +\; \lambda \cdot N_A^S \;+\; c \cdot \delta t_A \;-\; c \cdot \delta t^S \;+\; \ldots \\
& +\; \delta \rho_{trop} \;+\; \delta \rho_{ion} \;+\; \delta \rho_{phas} \;+\; \delta \rho_{rel} \;+\; \delta \rho_{mult} \;+\; \epsilon_A^S \;.
\end{aligned}
\tag{3.1}
$$

The individual terms in equation (3.1) are:

| | |
|---|---|
| $\boldsymbol{R}_{EOP}$ | rotation matrix of Earth orientation (nutation, UT1, polar motion), |
| $\boldsymbol{r}_A(t_A)$ | 3-dimensional position of station $A$ in a terrestrial reference frame at receiving time $t_A$ of the signal, |
| $\boldsymbol{r}^S(t_A - \tau_A^S)$ | 3-dimensional position of satellite $S$ in an inertial reference frame at the epoch of signal emission, |
| $t_A$ | time of the receiver clock when the signal is received (i.e., in receiver clock time), |
| $\tau_A^S$ | signal travel time from satellite $S$ to station $A$, |
| $\delta t_A$, $\delta t^S$ | clock error of the receiver clock and the satellite clock, respectively, |
| $c$ | velocity of light, |
| $\lambda \cdot N_A^S$ | initial phase ambiguity for satellite $S$ and receiver $A$ multiplied by the wavelength $\lambda$, |
| $\delta \rho_{trop}$ | correction for troposphere delay, |
| $\delta \rho_{ion}$ | correction for ionospheric delay, |
| $\delta \rho_{phas}$ | corrections for phase center offsets and variations at satellite and receiver antennas, |
| $\delta \rho_{rel}$ | correction for relativistic effects, |
| $\delta \rho_{mult}$ | multipath effects, |
| $\epsilon_A^S$ | measurement error. |

In order to conclude the introductural part devoted to the GPS observation equation, it must be pointed out that an observation equation of type (3.1) can be formulated not only for the two basic frequencies L1 and L2 but any linear combination of both frequencies. Depending on which linear combination is used, some terms may disappear in the observation equation, e.g., the geometrical part in the case of the geometry-free linear combination or the ionospheric correction $\delta \rho_{ion}$ in the case of an ionosphere-free linear combination. Furthermore, forming differences between the basic observations of one station to one satellite is a widely-used tool in GPS processing. Thereby, original L1 and L2 observations as well as any of the linear combinations can be used to form single or double difference observations. An elaborate description of the theory and the advantages and drawbacks of using linear combinations and single or double difference observations instead

of the original GPS observables can be found in all basic GPS literature such as *Hofmann-Wellenhof et al. (1994)*, *Teunissen and Kleusberg (1998)* or *Leick (1995)*.

After introducing all terms in the phase observation equation let me pick out some aspects of those elements that are important to see the similarities and identical characteristics with other space-geodetic techniques on the one hand, and to be aware of GPS-specific problems on the other hand.

### a) Station and satellite positions

Starting with the first line in (3.1) representing the geometrical part of the observation equation, it is worthwhile to add some words concerning the two position vectors, the station position vector and the vector of the satellite position. Normally, the station positions are given in an Earth-fixed geocentric reference frame, namely the International Terrestrial Reference Frame (ITRF) provided by the IERS. This frame consists of a set of coordinates and velocities for the observing stations referring to a certain reference epoch. The ITRF is a realization of the International Terrestrial Reference System (ITRS) defined by the IERS. A new ITRF is issued by the IERS in irregular time intervals every few years. The last two realizations are called ITRF2000 (see *Altamimi et al., 2002*) and ITRF2005 (see the web-site of the *ITRF product center*[2]). The station positions given by the ITRF (using the velocities to extrapolate from the reference epoch of ITRF to the epoch of the observation) are not identical with the instantaneous position of the stations at the epoch of the observation. Several kind of displacements of the reference points have to be modeled additionally. According to the IERS Conventions 2003 (see *McCarthy and Petit, 2004*) one has to account for ocean loading effects, solid Earth tides, the effect of the permanent tide, site displacements due to pole tides and, finally, deformations due to atmospheric loading. For an elaborate characterization of these effects including a mathematical description of the correction models it is referred to the chapter "Displacement of Reference Points" of the IERS Conventions 2003 and the references given therein.

The satellite position $r^S$ completes the geometrical part of the observation equation (3.1). The basic model for describing the satellite orbit is based on the six Keplerian elements, i.e., semi-major axis $a$ of the orbital ellipse, numerical eccentricity $e$ of the ellipse, right ascension of the ascending node $\Omega$, inclination $i$ of the orbital plane w.r.t. the equator, argument of the perigee $\omega$ and the epoch of the perigee passage $T_0$. Unfortunately, several disturbing accelerations are influencing the motion of the satellite so that it deviates from the purely Keplerian model. A common classification of the accelerations is the division into gravitational and non-gravitational perturbations (see, e.g., *Hofmann-Wellenhof et al., 1994*). The influence of a non-spherical Earth and the tidal attraction of the sun and the moon have to be mentioned in connection with gravitational accelerations, whereas the non-gravitational accelerations originate, amongst others, from solar radiation pressure, air drag and relativistic effects. A description of the sophisticated methods of modeling the satellite orbits including all the disturbing accelerations is omitted here because the orbital parameters will not be treated in this thesis.

### b) Earth orientation parameters

It has been mentioned above that the station position $r_A$ is given in a terrestrial reference frame whereas the satellite positions $r^S$ are originally given in an inertial reference frame. Consequently, one of the two quantities has to be transformed into the reference frame used by the other quantity before the difference can be built. As both reference frames are linked through the Earth orientation parameters, the general transformation is carried out by several subsequent rotations considering precession, nutation, Greenwich apparent sidereal time (*GAST*) $\theta$ and polar motion ($x_P$, $y_P$), with each of the rotation matrices evaluated at the requested epoch $t$:

$$\boldsymbol{R_{EOP}}\,(t) \;=\; \underbrace{\boldsymbol{P}\,(t)}_{Precession} \;\; \underbrace{\boldsymbol{N_{IAU}}\,(t)\,\boldsymbol{N}\,(t)}_{Nutation} \;\; \underbrace{\boldsymbol{R_3}\,(-\theta)}_{GAST} \;\; \underbrace{\boldsymbol{R_1}\,(\,y_P\,(t))\,\boldsymbol{R_2}\,(x_P\,(t))}_{Polar\ motion} \;. \tag{3.2}$$

It is worthwhile to spend some more words on each part of the expression (3.2) as the Earth orientation parameters will play an important role in the analyses presented later on in this thesis (*Chapters 5* and *6*). Starting with the precession and nutation: Both together describe the motion of the Earth's rotation axis as it is seen in an inertial frame. The precession represents the motion of the rotation axis around the pole of the ecliptic like a cone of angle 23.5°, and the nutation is superimposed on the precession describing the devia-

---

2  *http://itrf.ensg.ign.fr/ITRF_solutions/2005/ITRF2005.php*

tions from the conical motion (see Fig. 3.1a). The precession is an extremely long-periodic motion of about 25800 years whereas the short-periodic terms are summarized in the nutation with an 18.6 years period of about 9.2" representing the main and longest term. *Mathews et al. (2002)* developed a model describing the precession and the major part of the nutation of a non-rigid Earth. This model has been adopted by the IAU as official "IAU2000A Precession-Nutation Model" and is used in the analyses of space-geodetic observations (corresponding to the matrices $\boldsymbol{P}(t)$ and $\boldsymbol{N}_{IAU}(t)$ in equation (3.2)). According to *McCarthy and Petit (2004)* the accuracy of IAU2000A is at the 0.2 mas level. This is mainly due to the so-called free core nutation (FCN) that has not been included in the IAU2000 model. In order to account for the deviations of the actual nutation from the model, an additional matrix is included in the transformation (3.2), i.e., $\boldsymbol{N}(t)$, containing corrections $\Delta\epsilon$ and $\Delta\psi$ for the nutation in obliquity and the nutation in longitude, respectively:

$$\boldsymbol{N}(t) = \boldsymbol{R_1}(-\epsilon_0) \cdot \boldsymbol{R_3}(\Delta\psi) \cdot \boldsymbol{R_1}(\epsilon_0 + \Delta\epsilon) , \tag{3.3}$$

with $\epsilon_0 \approx 23.5°$ being the mean obliquity of the ecliptic w.r.t. the Earth's equator.

Continuing with the third part of the transformation (3.2) from the terrestrial into the celestial reference frame, the matrix $\boldsymbol{R_3}(\theta)$ describes the daily rotation of the Earth with the Greenwich apparent sidereal time (GAST) as rotation angle. Following the IERS Conventions 2003, it is related to universal time *UT1* by

$$\theta(T_U) = 2\pi \cdot (0.7790572732640 + \rho \cdot T_U) , \tag{3.4}$$

where the epoch $T_U$ is obtained from the Julian *UT1* date (in [days]) minus 2451545.0 and the factor $\rho$ describes the ratio of universal time to sidereal time which is given in the IERS Conventions 2003 with $\rho = 1.00273781191135448$. The relationship between *UT1* and the time scale *UTC* driven by atomic clocks is known to be

$$UT1 = UTC + \Delta UT , \tag{3.5}$$

with the correction *ΔUT* either applied as provided by the IERS or set up as unknown parameter in the adjustment of geodetic parameters from the observations of the space-geodetic techniques. In the case of GPS or satellite techniques in general, the problem of a one-to-one correlation between the nutation angles and *UT1-UTC* on the one hand and the orbital elements $i$, $\Omega$ and $u_0$ on the other hand occurs. *Rothacher et al. (1999)* demonstrate this correspondence confirming that it is not possible to estimate both groups of parameters, i.e., orbital elements for the satellites together with offsets in nutation and *UT1-UTC*. Nevertheless, the authors state as well that the rates for the afore mentioned parameters are accessible by satellite techniques very well as the orbital elements can be treated as integration constants in a Keplerian approximation. This is justified even in the case of perturbing forces if the accelerations acting on the orbital elements can be modeled with sufficient accuracy within the time interval considered for one rate parameter.

Finally, the rightmost part in equation (3.2), denoted as polar motion, describes the motion of the Earth's rotation axis w.r.t. the terrestrial reference frame where $x_P$ and $y_P$ are the coordinates of the Celestial Ephemeris Pole in the terrestrial reference frame at the considered epoch $t$ (see Fig. 3.1b).

In order to summarize the remarks concerning the rotation matrix $\boldsymbol{R}_{EOP}$ contained in the observation equation (3.1), altogether five quantities contained in (3.2) are usually set up as unknown parameters in a least-squares adjustment of the space-geodetic techniques, or more precisely: the two nutation angles $\Delta\epsilon$ and $\Delta\psi$ according to (3.3) as correction to the nutation model, the deviation *ΔUT* from an exactly daily rotation of the Earth (i.e., 86400 s) given in (3.5), and the two pole coordinates $x_P$ and $y_P$. The complete set of five parameters will be denoted "Earth orientation parameters (EOP)" throughout this thesis whereas the term "Earth rotation parameters (ERP)" will be used for the subset of *ΔUT* and the pole coordinates.
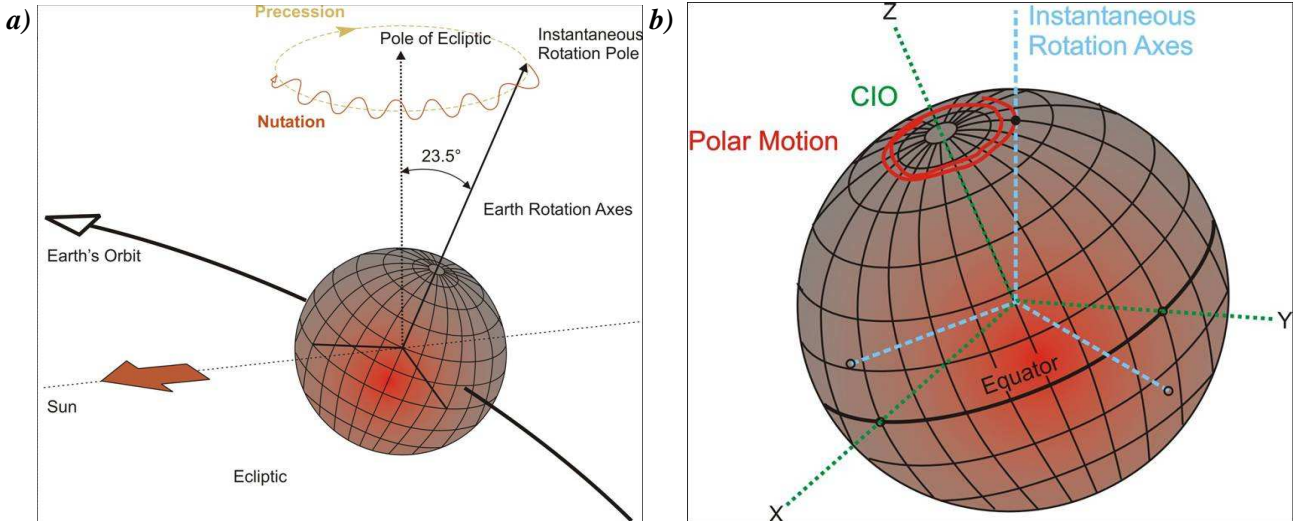
**Figure 3.1:** *Earth orientation:* **a)** *Precession and nutation,* **b)** *polar motion. (modified version of graphics created by D. Schmedt, TU Munich)*

### c) Influence of the troposphere and the ionosphere

Starting with the delay caused by the troposphere it must be mentioned that the correction term $\delta\rho_{trop}$ depends on the meteorological conditions along the signal path and, more important, on the elevation angle under which the satellite is seen from the receiving antenna. In order to give a magnitude of this influence, the delay for observing a satellite in zenith direction is about 2.3 m (~ 8 ns) whereas it can be a factor of ten larger at an elevation angle of only 5°. In principle, the troposphere delay can be modeled if meteorological measurements are available. A widely used formula for modeling the troposphere delay for microwave signals was derived by *Saastamoinen (1973)*:

$$\rho_{total}(z) = \frac{0.002277}{\cos z} \cdot \left[ p + \left( \frac{1255}{T} + 0.05 \right) \cdot e - B \cdot \tan^2 z \right] + \delta R \ , \tag{3.6}$$

with      $p$              total atmospheric pressure [mbar],

           $T$              air temperature [K],

           $e$              partial pressure of water vapor [mbar],

           $z$              zenith angle of the line of sight,

           $B, \delta R$       correction terms taking into account the height above sea level.

However, the problems with modeling the influence of the troposphere on the observations are manifold: Meteorological measurements often are not accurate enough and the values measured at the ground are not representative for the whole atmosphere along the signal path. Especially the wet part of the troposphere delay depending on the humidity is difficult to model for microwave signals although it is the minor part of the total delay with only some centimeters to decimeters. Consequently, instead of modeling the troposphere delay, the influence is determined during the parameter estimation process if high-quality results are to be achieved. For this purpose the troposphere delay is usually split into a hydrostatic part $\rho_{hydro}$ and a wet part $\rho_{wet}$ (see *Hopfield, 1969*):

$$\rho_{total} = \rho_{hydro} + \rho_{wet} \ . \tag{3.7}$$

The denotation "hydrostatic" is due to the assumption of a hydrostatic equilibrium in the atmosphere, thus it is not exactly equal to the dry delay. The hydrostatic part of the troposphere delay is proportional to the total air pressure (i.e., the first term in the square brackets in equation (3.6)). In most analyses it is used as a priori value for the estimation of the troposphere delay so that the estimated correction represents the wet delay. If troposphere parameters are estimated they are set up as a delay in zenith direction. The relationship between

the delay in the direction of the line of sight of each single observation and the zenith delay (ZD) is represented by a mapping function taking into account that a signal received at a certain elevation angle has to pass through the troposphere on a longer way than a signal received at zenith, thus, the troposphere delay will be larger:

$$\rho_{total}\,(z) = f_{hydro}\,(z) \cdot \rho_{hydro}^{zenith} + f_{wet}\,(z) \cdot \rho_{wet}^{zenith} \quad . \tag{3.8}$$

The literature provides mapping functions for the hydrostatic part and the wet part, i.e., $f_{hydro}\,(z)$ and $f_{wet}\,(z)$, respectively. The so-called "Niell Mapping Function (NMF)" derived by *Niell (1996)* is widely used in the analysis of space-geodetic techniques because solely the site coordinates and the day of the year have to be supplied as input parameter. But during the last few years, more subtle mapping functions that base on numerical weather models were developed. The "Vienna Mapping Functions (VMF)" (*Böhm and Schuh, 2004*) directly use the pressure level data from ECMWF (European Centre for Medium-Range Weather Forecasts) to derive the actual coefficients of the mapping function, whereas the "Global Mapping Function (GMF)" (*Böhm et al., 2006*) is a global spherical harmonics expansion of the VMF parameters, so that only the site coordinates and the day of the year are required as input parameters, as for the NMF.

An improved representation of the troposphere delays can be achieved if horizontal gradients are set up additionally according to the IERS Conventions 2003 (see *McCarthy and Petit, 2004*):

$$\rho\,(z\,,\,A) = f_{hydro}\,(z) \cdot \rho_{hydro}^{zenith} + f_{wet}\,(z) \cdot \rho_{wet}^{zenith} + f_{Grad}\,(z) \cdot \left[ G_N \cdot \cos A + G_E \cdot \sin A \right]. \tag{3.9}$$

The first two parts of the equation above correspond to (3.8). The third part in (3.9) contains the horizontal gradients $G_N$ and $G_E$ in north and east direction, respectively, taking into account the azimuthal asymmetry of the troposphere, whereas Eq. (3.8) only considers the elevation-dependency and is completely independent of the azimuth $A$ of the observation direction. The gradients as well need a mapping function, i.e., $f_{Grad}\,(z)$, and one option is to use the partial derivative of the mapping function with respect to the zenith angle. Further possibilities are given in the IERS Conventions 2003. An elaborate description of the estimation of troposphere parameters can be found in *Schüler (2001)* whereas the set-up for the solutions presented in the thesis at hand is explained in more details in *Chapter 5.1.2*.

Contrary to the troposphere, the ionosphere is a dispersive medium for microwave signals, hence, the ionospheric refraction $\delta \rho_{ion}$ in (3.1) is frequency-dependent. The main effect of the ionospheric influence is a scaling of the GPS baselines. The frequency-dependency of the ionospheric refraction allows to eliminate ionospheric effects by forming a special linear combination of the frequencies L1 and L2, the so-called ionosphere-free linear combination (see *Hofmann-Wellenhof et al., 1994*), resulting in an observation equation of type (3.1) but without the correction term $\delta \rho_{ion}$. Other possibilities to deal with the ionospheric influence are either estimating the correction term by using the measurements of both frequencies, or applying a correction based on a model provided by the IGS (see *Feltens, 2004*). For more details about ionospheric modeling in GPS the reader is referred to *Schaer (1999)*.

### d) Remaining correction terms

A specialty of the GPS phase observation equation is the unknown ambiguity term $N_A^S$. This value has to be determined for each satellite pass and as well after losing the phase lock to a particular satellite. This results, as one can imagine, in a huge amount of parameters for a global GPS solution. The detection and repair of so-called cycle slips and the methods for solving the unknown ambiguities are described elaborately in the GPS literature.

It is important to keep in mind that the positions of the satellite and the receiver are computed at the epoch of emission and the epoch of reception of the signal, respectively, and the time is indicated by the satellite clock and the receiver clock, respectively. Unfortunately, both clocks are deviating from GPS time, hence, the unknown clock errors $\delta t_A$ and $\delta t^S$ have to be estimated.

The correction $\delta\rho_{phas}$ takes into account the deviation of the physical point of reception of a signal from the antenna reference point in the case of the ground station antennas, and, additionally, the difference between the satellite's center of mass and the physical point of emission at the satellite antennas. For both cases, i.e., ground station and satellite antennas, a mean offset and corresponding patterns describing the dependency of the correction on the direction of the signal w.r.t. an antenna-fixed system are available. Until GPS week 1399 (November 4, 2006), one very common antenna type used in the IGS network was selected as a reference assuming no phase center variations (PCV) and all other antenna types were calibrated w.r.t. that antenna (i.e., relative antenna PCV) although there is no reason from a physical point of view why the selected reference antenna should not show any variations of the phase center depending on azimuth and elevation angle of the signal. According to *Rothacher (2000)* the neglect of any PCV of the reference antenna causes a wrong scaling of global GPS networks up to 16 ppb. Several calibration campaigns were carried out by, e.g., *Menge et al. (1998)*, with the goal to derive PCV in an absolute sense for each antenna type of the ground station network. On the contrary, the satellites are already in orbit, thus, their antennas cannot be calibrated on the ground anymore. Hence, the only possibility to get values for the phase center offsets and variations of the satellite antennas is to estimate them using observations of a global GPS network. For further details about this estimation it is referred to *Schmid and Rothacher (2003)*. The extent of the changes in the estimated parameters due to applying an absolute instead of a relative antenna phase center modeling for ground stations as well as for satellites is demonstrated in *Schmid et al. (2005)*. The studies therein base on data of the CONT02 campaign and on long, completely reprocessed GPS time-series. In the case of the GPS solution for the CONT02 campaign, used for the studies in this thesis as well (see *Chapter 5.1.2*), the change of the antenna modeling results in a mean change in station height of about 8 mm and a change in troposphere zenith delays of several millimeters depending on the station. Furthermore, the studies by *Schmid et al. (2007)* demonstrate that the influence of the phase center modeling is far from negligible, and an overall improvement of the GPS solutions is achieved if an absolute phase center modeling is applied. Fortunately, the IGS switched to an absolute phase center modeling starting with GPS week 1400 (see *IGSMAIL-5438* [3]).

The term $\delta\rho_{rel}$ summarizes all relativistic corrections concerning the behavior of the clocks and the influence of the Earth's gravity field that has to be applied in the observation equation. Following *Hofmann-Wellenhof et al. (1994)*, there are altogether four types of relativistic corrections:

 – special and general relativity affecting the satellite clocks,
 – general relativity affecting the signal propagation (Shapiro effect),
 – general relativity affecting the satellite orbit,
 – Sagnac effect.

The theory of general relativity tells us that clocks are faster if the gravity field is weaker, thus, generally speaking, the clocks at the ground stations are slower than the clocks onboard the GPS satellites. Additionally, applying the theory of special relativity, the clocks onboard the satellites are in motion and therefore they are slower compared to a static clock. Both effects are superimposed for the satellite clocks and a mean value corresponding to a circular orbit is already taken into account when generating the fundamental frequency driven by the satellite clock. According to *Hofmann-Wellenhof et al. (1994)* the mean correction of $-4.55 \cdot 10^{-3}$ Hz for the satellite clock frequency implies that the signal is received at a ground station with the nominal fundamental frequency of 10.23 MHz (see *Chapter 3.1.1*). As this correction is already applied to the satellite clock it has not to be included in the relativistic correction term in observation equation (3.1). However, this mean correction is based on the assumption of a circular orbit and a spherical Earth which is obviously not the truth. Thus, the variable part has to be corrected in the observation equation and can be as large as 10 m. The second relativistic effect is causing a delay of the signal when propagating through the Earth's gravity field. Regarding GPS signals and following *Hofmann-Wellenhof et al. (1994)*, this delay can be 18.7 mm at maximum for a zero difference observation of type (3.1), whereas the correction becomes smaller in the case of single or double difference observations because only the difference in the corrections for both stations and both satellites has to be taken into account. In the case of GPS, general relativistic corrections due to other masses than the Earth (i.e., Sun, Moon, planets) have not to be taken into account. Furthermore, the gravity field of the Earth causes relativistic perturbations on the satellite orbits, but these perturbations have to be considered already in the equation of motion of the satellite, and not in the observation equation. An extensive expression for this effect is given in the IERS Conventions 2003 (*McCarthy and Petit, 2004*)

---

[3]  *http://igscb.jpl.nasa.gov/mail/igsmail/2006/msg00161.html*

and an approximation with a numerical value of about $3 \cdot 10^{-10}$ ms$^{-2}$ can be found in *Hofmann-Wellenhof et al. (1994)*. Finally, as the satellite clock and the receiver clock are moving with respect to each other, the so-called Sagnac effect has to be considered. A mathematical expression is given by *Ashby (2003)*. Therein, further explanations including mathematical expressions for all relativistic effects influencing GPS can be found.

Finally, the last two terms in (3.1) represent those parts of a GPS observation that are difficult to model. First, multipath effects $\delta \rho_{mult}$ depend on the environment of the antenna. Thus, they differ from station to

station and a general modeling is difficult. And, not to forget, the measurement error $\epsilon_A^S$ is present in every

observation but not predictable, so that a correction term cannot be quantified.

## 3.1.3  Global GPS solutions from the IGS

For high-precision applications in geodesy and geodynamics a global network of about 350 stations can be used. This continuously measuring network is one component of the International GNSS Service (IGS) that started its routine operation on January 1, 1994. Besides the network of GPS tracking stations, ten Analysis Centers, several Associate and Regional Analysis Centers, four global Data Centers, a Central Bureau, a Governing Board and occasionally established Working Groups and Pilot Projects are forming the IGS structure. For a detailed description of the single components and their tasks it is referred to the *IGS Terms of Reference*[4].

According to the IGS Strategic Plan 2002-2007 published by the *IGS Central Bureau (2002)* all "... activities aim to advance scientific understanding of the Earth system components and their interactions, as well as to facilitate other applications benefiting society". For supporting the broad spectrum of scientific and engineering applications of GPS, the Analysis Centers generate miscellaneous products that are provided routinely to the scientific community:

  – GPS and GLONASS satellite ephemeris,

  – Earth rotation parameters,

  – IGS tracking station coordinates and velocities,

  – GPS satellite and IGS tracking station clock information,

  – station-specific troposphere estimates (zenith path delays, gradients),

  – global ionospheric maps.

Special processing strategies are required to process a global network of GPS stations and to derive high-quality products. Detailed descriptions of the different processing strategies of the IGS Analysis Centers can be found in the yearly technical reports, e.g., *Gowey et al. (eds.) (2004)* or in the regularly updated analysis center description files located on the web[5].

One of the products that should be mentioned here is the weekly solution for the positions of the IGS tracking stations together with the Earth rotation parameters (*x*-/*y*-pole and their time derivatives and *LOD*). Each solution comprises one set of station coordinates and daily sets of Earth rotation parameters derived from the observations of the week in consideration. Such a type of solution is provided by each Analysis Center using a special file format named SINEX. The abbreviation SINEX stands for "Solution/Software INdependent EXchange" and indicates already the intention of this file format. It has been initiated originally by a working group of the IGS to enable an exchange of the individual IGS Analysis Centers' solutions including the full variance-covariance information that is necessary to reconstruct the free normal equation system (see *Blewitt et al., 1994*). This implies that the a priori values of all parameters and the full matrix of constraints applied to generate the solution are stored in SINEX besides the solution itself and its variance-covariance matrix. In the meantime, the other international services dealing with the space-geodetic techniques, namely the International VLBI Service for Geodesy and Astrometry (IVS), the International Laser Ranging Service (ILRS) and the International DORIS Service (IDS), have adopted and extended the SINEX format for their special purposes so that the

---

4   *http://igscb.jpl.nasa.gov/organization/bylaws.html*
5   *ftp://igscb.jpl.nasa.gov/igscb/center/analysis/*

IERS Analysis Coordinator initiated a unified format description in order to have the basis for the combination projects within the IERS (*Rothacher et al., 2002*). The main new feature is the possibility to directly store a datum-free normal equation system if the user is not interested in a solution. Due to this possibility, the two matrix inversions for generating a solution on the one hand and re-invert the variance-covariance matrix stored in SINEX to get the normal equation matrix on the other hand, are avoided. The actual format is version 2.02 (see *IERS Message No. 103[6]*). An extensive format description can be retrieved via the web-site of the IERS Analysis Coordination[7]. As the SINEX format encourages the delivery of the complete variance-covariance information, it is possible to derive the original normal equation systems (free of constraints) for all weekly solutions of all Analysis Centers and to re-compute, respectively combine them. Such a procedure is done, e.g., at NRCan (Natural Resources Canada): Their combined solution represents the official weekly IGS product for station coordinates and ERP arising from a combination of the solutions computed by ten Analysis Centers and two Global Network Associate Analysis Centers (see *Ferland et al., 2000*). Preliminary combinations were already performed since GPS week 1000 (March 7, 1999), but starting with GPS week 1050 (February 20, 2000) the weekly combined solution became an official IGS product.

The combined troposphere parameters released by the IGS for every week are another product of interest for this thesis. The launch of weekly final troposphere products was supported by the "IGS Troposphere Working Group"[8] established in 1998. Based on the submissions of the individual IGS Analysis Centers, two-hourly combined troposphere ZD estimates are provided. According to *Gendt (2001)*, the overall agreement of the individual contributions is at the level of 3-5 mm.

## 3.2   Very Long Baseline Interferometry (VLBI)

### 3.2.1   Technical description

Very Long Baseline Interferometry (VLBI) is a purely geometrical technique. The radio waves of extragalactic radio sources, so-called quasars, are observed by large telescopes. The frequency band of the emitted radio waves covers a broad spectrum (6 – 67 cm wavelength) but for geodetic applications mainly two frequencies are used: 8.4 GHz in the X-band (corresponding to 3.5 cm wavelength) and the S-band with 2.3 GHz (corresponding to 13 cm wavelength).

According to *Campbell (1979)* a diameter of several kilometers would be needed with one single telescope to achieve an acceptable resolution, since the resolution of a telescope $\sigma_{tel}$ is given by the ratio of the observed wavelength $\lambda$ and the diameter of the telescope $D$:

$$\sigma_{tel} \approx \frac{\lambda}{D} \ .$$

(3.10)

Using two telescopes observing the same quasar simultaneously results in a better resolution because in this case the diameter of the 'telescope pair' is given by the length of the baseline between the two telescopes. This fact is the theoretical background and the motivation to use 'very long baselines' for radio source observations. The theoretical maximum baseline length for VLBI on Earth is twice the Earth's radius. The only limitation is the requirement that the quasar is simultaneously visible from both telescopes.

The precondition for such a connection of two telescopes is, that the signals are recorded together with very precise timing information, so that the signals can be correlated later on. More information about the correlation procedure can be found in *Sovers et al. (1998)*.

Hence, by observing quasars, VLBI gives access to the celestial reference system, which is realized by defining coordinates for the quasars (right ascension and declination). The motivation for using quasars instead of stars in the Milky Way Galaxy or satellite orbits for a fundamental reference frame is described in *Cannon (1999)*. The fact that the positions of the quasars can be treated as fixed makes them suitable for realizing an inertial reference system. The realization used within the IERS is named International Celestial Reference

---

6   *http://www.iers.org/products/2/10990/orig/message_103.txt*
7   *http://tau.fesg.tu-muenchen.de/~iers/web/sinex/format.php*
8   *http://www.gfz-potsdam.de/pb1/igs_trop_wg/index_IGS_TROP_WG.html*

Frame (ICRF). *Ma et al. (1998)* issued positions of 608 extragalactic radio sources and this initial ICRF was extended with 59 sources in 1999 (see *Gambis, 1999*). The new developments and studies towards future realizations of a celestial reference system were published by *Souchay and Feissel-Vernier (2006)*. It is worthwhile to mention that VLBI is the only space-geodetic technique that has the capability to establish a connection to the celestial reference system. All of the other techniques cannot provide this link. Therefore, VLBI is as well the only technique to determine the orientation of the Earth's rotation axis with respect to the celestial reference system, expressed as nutation/precession, and the daily rotation (universal time *UT*). Both quantities are part of equation (3.2) describing the relationship between terrestrial and celestial reference frames. The satellite techniques only have the possibility to monitor the time derivatives of these quantities, i.e., nutation rates and length of day (*LOD*), but not the absolute values.

### 3.2.2 Observation equation

As already mentioned, two telescopes are observing the same quasar at the same time. Since the quasars are extremely far away, plane wave fronts may be assumed for the radio signal arriving at the telescopes. Depending on the orientation of the Earth with respect to the observed quasar, the radio signal arrives at one telescope earlier than at the other one. This time delay $\Delta\tau$ directly results from the correlation of the recorded signals and is the basic observable in the VLBI analysis. Considering the pure geometry only, the relationship between the measured time delay $\Delta\tau$, the direction to the quasar $e^Q$ and the baseline $b$ of the two telescopes can be expressed following *Schuh (1987)*:

$$c \cdot \Delta\tau = -b \cdot e^Q \ . \tag{3.11}$$

As already pointed out, the relationship (3.11) results from purely geometrical considerations. Unfortunately, the time delay $\Delta\tau$ derived from cross correlation is corrupted by several effects that have to be dealt with in the VLBI modeling and parameter estimation process. *Sovers et al. (1998)* subdivide these effects into seven categories: baseline geometry (geometric delay, Earth orbital motion, gravitational delay), station positions (tectonics, tidal and non-tidal motion), Earth orientation, quasar source structure, antenna structure, instrumentation and atmosphere (troposphere, ionosphere). The authors summarize as well the maximum delay that is caused if the respective component is omitted in the model. Including the most important effects in the VLBI observation equation and expressing them symbolically as correction terms similar to the GPS observation equation (3.1) yields a simplified expression for an observation of the telescopes *A* and *B* to the quasar *Q*:

$$
\begin{aligned}
c \cdot \Delta\tau_{AB}^Q = {} & \left( -R_{EOP,A} \cdot r_A + R_{EOP,B} \cdot r_B \right) \cdot e^Q \\
& - c \cdot \delta t_A - \delta\rho_{trop,A} - \delta\rho_{ion,A} - \delta\rho_{rel,A} - \delta\rho_{ant,A} \\
& + c \cdot \delta t_B + \delta\rho_{trop,B} + \delta\rho_{ion,B} + \delta\rho_{rel,B} + \delta\rho_{ant,B} \\
& + \epsilon_{AB}^Q
\end{aligned} \tag{3.12}
$$

The first line of the expression (3.12) corresponds to the purely geometrical representation discussed before. In principle, the baseline vector $b$ can be derived from the difference between the position vectors $r_A$ and $r_B$ of the two telescopes *A* and *B*, respectively. However, normally the position vectors of observing stations are given in a terrestrial reference frame, whereas the direction to the quasar $e^Q$ is given in an inertial reference frame. For computing the inner product between the baseline vector and the direction to the quasar it is required that both vectors are expressed in the same reference frame. Consequently, one of the vectors has to be transformed. As the relationship between the terrestrial reference frame and the inertial reference frame is described by the Earth orientation parameters the transformation matrix $R_{EOP}$ is identical to that in (3.2) already given in the context of the GPS observation equation in *Chapter 3.1.2*. However, it is important to mention that the two matrices to transform the position vectors of the two stations are not identical because $R_{EOP}$ is time-dependent. Therefore, the transformation matrix has to be computed exactly for the epoch when the signal arrives at the respective telescope and, normally, these epochs differ for the two stations by

$$\Delta\tau_{AB}^Q \neq 0 \ .$$

The correction terms $\delta t_A$, $\delta t_B$ for clock errors at the stations, $\delta \rho_{trop,A}$, $\delta \rho_{trop,B}$ for the troposphere

delay, $\delta \rho_{ion,A}$, $\delta \rho_{ion,B}$ for ionospheric refraction and $\delta \rho_{rel,A}$, $\delta \rho_{rel,B}$ for the relativistic correction in

the observation equation (3.12) for VLBI are comparable to those terms given for GPS in (3.1). Therefore, it is referred to *Chapter 3.1.2* for a description of these corrections. The main difference between the two equations is that two stations have to be taken into account for VLBI, thus, only the difference between the station-specific corrections is present in the observation. This situation corresponds to GPS if single-difference observations are formed instead of using only the zero-difference observation between one station and one satellite. To further comment on the equivalence or differences between VLBI and GPS it must be stated that the troposphere influence is the same for GPS and VLBI because both techniques use microwave signals. As already explained in *Chapter 3.2.1*, geodetic VLBI observes on two frequencies, thus, similarly to GPS, the ionospheric refraction can be determined (see *Schuh, 1987*). The treatment of the relativistic corrections for VLBI is explained in *Schuh (1987)* as well. According to his work, the relativistic influence due to the gravitation of bodies in our solar system has to be applied for the moon and the planets only, if the signal path is very close to their center of mass, whereas for the sun the correction is absolutely necessary for all observations. This situation is contrary to the satellite techniques where the Earth is the only body whose gravity field causes a relativistic delay of the signal. Of course, the relativistic effects concerning satellite clocks and satellite orbits mentioned in *Chapter 3.1.2* are not relevant for the VLBI analysis.

The remaining station-specific terms $\delta \rho_{ant,A}$, $\delta \rho_{ant,B}$ include all corrections related to the antenna struc-

ture comprising temperature-depending deformation, gravitational sag and antenna axis offsets. The latter have a similar effect on VLBI solutions as the phase center variations of GPS antennas have. In most cases the manufacturer of the telescope does not provide any information about the axis offsets, thus, they must be determined either by local surveys or by estimating them using VLBI observations. *Steinforth et al. (2003)* and *Eschelbach and Haas (2003)* documented the local surveys at Ny-Alesund and Onsala, respectively, dedicated to the determination of the antenna axis offsets. Among others, the antenna axis offsets for Algonquin Park, Gilmore Creek / Fairbanks, Kokee Park and Westford were estimated by the analysis groups at Goddard Space Flight Center (GSFC) and Bundesamt für Kartographie und Geodäsie (BKG) using VLBI observations. However, the *IVS Analysis Coordinator (2005)* alerts that these estimated offsets have to be used carefully because, usually, the values differ by far from those derived by local surveys. Therefore, as the axis offsets determined by local surveys are more reliable they should be used in any case if they are available. An actual list of all antenna axis offsets is provided by the *IVS Analysis Coordinator (2005)*[9]. Regarding the thermal deformation of the VLBI antenna and the resulting displacement of the reference point, *Nothnagel et al. (1995)* carried out first studies and developed a model for the local height calibration of the reference point at the Hartebeesthoek radio telescope. Furthermore, they tried to estimate thermal parameters from VLBI data but it turned out that the quality of the data at that time was not sufficient and, moreover, the complicated structure of the telescopes inhibits a direct estimation of reliable expansion coefficients. Nevertheless, the investigations have been continued successfully so that nowadays the IERS Conventions 2003 (see *McCarthy and Petit, 2004*) provide a model for the effect of thermal deformation on the VLBI delay measurements. Quite recently, *Wresnik et al. (2007)* presented a new method to model thermal deformations of VLBI antennas.

Finally, the errors $\epsilon_{AB}^{Q}$ in the observation conclude the list of correction terms in (3.12) but, as already indi-

cated before, this list can be extended if a model or a correction value is available for other influences.

For a more elaborate description of the VLBI observation including a detailed formulation of all influences mentioned above it is referred to basic VLBI literature, e.g., *Campbell (1979)*, *Schuh (1987)*, *Sovers et al. (1998)* or *Tesmer (2004)*.

### 3.2.3 Global VLBI solutions from the IVS

By means of the observation equation (3.12), the three main parameter types that can be determined by VLBI are visible: the celestial reference frame, the terrestrial reference frame and the Earth orientation parameters as connection between both reference frames. One advantage of VLBI compared to GPS is the length of the time-series for all parameters, as the geodetic applications of radio interferometry started already in the

---

9  *http://giub.geod.uni-bonn.de/vlbi/IVS-AC/data/axis-offsets.html*

1970s. In the starting time, *Campbell (1979)* already indicated the possibility to apply geodetic VLBI experiments for geodetic as well as geodynamic studies if the accuracy is sufficient. In the meantime, the potential of VLBI has rapidly increased as it is documented in, e.g., *Schuh (1987)*, *Campbell et al. (1992)*, *Sovers et al. (1998)*, *Schuh (2000)*. Thus, VLBI can deliver long time-series for all parameters of interest in geodetic and geodynamic applications, e.g., changes in baseline lengths as an indicator for plate tectonics, or the fluctuations in EOP for a better understanding of the dynamic behavior of hydrosphere, atmosphere and the Earth's interior. Regarding the EOP, the VLBI contribution to *UT1* and the nutation angles has to be emphasized because they can be delivered, in an absolute sense, solely by VLBI. Furthermore, VLBI is the only technique to provide a stable inertial reference frame for long-term studies. And, finally, troposphere and ionosphere estimates can contribute to atmosphere studies. In order to better coordinate the activities in view of geodetic and geodynamic applications of VLBI, the International VLBI Service for Geodesy and Astrometry (IVS) was established in 1999. The organization of the IVS is similar to that of the IGS since the IGS was the first service established for the space-geodetic techniques and its success encouraged the other techniques to follow suit (see *Schlüter and Behrend, 2007*). The main products are the celestial reference frame and the monitoring of the Earth's rotation axis. Whereas the ICRF was derived from one solution, i.e., the analysis group *Ma et al. (1998)*, the official IVS time-series of EOP evolve from a combination of several analysis center solutions, performed by the IVS Analysis Coordinator. The procedure is outlined, e.g., in *Nothnagel et al. (2006)*.

The goals of the IVS concerning products and observing programs were reviewed thoroughly in 2001 by the "IVS Working Group 2 for Product Specification and Observing Programs". Its final report by *Schuh et al. (2002)* summarizes the present status of international VLBI activities including the quality of the products and compiles suggestions for future observing programs, technological improvements and further changes. From the investigations of this working group it turned out that an intensification of the observing program towards continuous observations is essential for increasing the product quality. Unfortunately, the actual observing program[10] is far from continuous observations. At the moment, regular observations for 24 hours are scheduled only twice a week, i.e., the so-called rapid-turnaround sessions R1 and R4, each session with seven participating stations at maximum. The assembly of potential stations for the two sessions is illustrated in Fig. 3.2a-b using bold lines to connect the stations that are included every week and dotted lines for those that participate only occasionally. As a consequence, the configuration of the R1 network (and the R4 network) is not the same every week. Additionally, there are only a few overlapping stations observing in the R1 as well as in the R4 sessions.

To come up to the requirement of continuous observations for most of the geodetic and geodynamic applications, the IVS is organizing special campaigns from time to time that are providing continuous observations for a time span significantly longer than 24 hours, usually lasting two weeks. This type of session is named CONT. Further details will be given in *Chapter 4.1* as the work presented here fully bases on the data of one of the CONT campaigns, namely the campaign that was scheduled for October 2002, i.e., CONT02.

Besides special sessions devoted to the CRF, regional terrestrial reference frames or technique improvement studies, there are two important sessions to monitor *UT1*, the so-called "INTENSIVES". Seven days a week, one baseline is observing for one hour. Two different baselines are selected, one is Wettzell – Kokee Park (observing five times a week), and the other one is Wettzell – Tsukuba (observing twice a week). Both baselines have in common a large east-west extension and therefore they are well-suited for monitoring the rotation of the Earth. The results of both baselines fit quite well as it was pointed out in *Fischer et al. (2003)*.

---

10 *http://ivscc.gsfc.nasa.gov/program/index.html*

*a)*                                                 *b)*
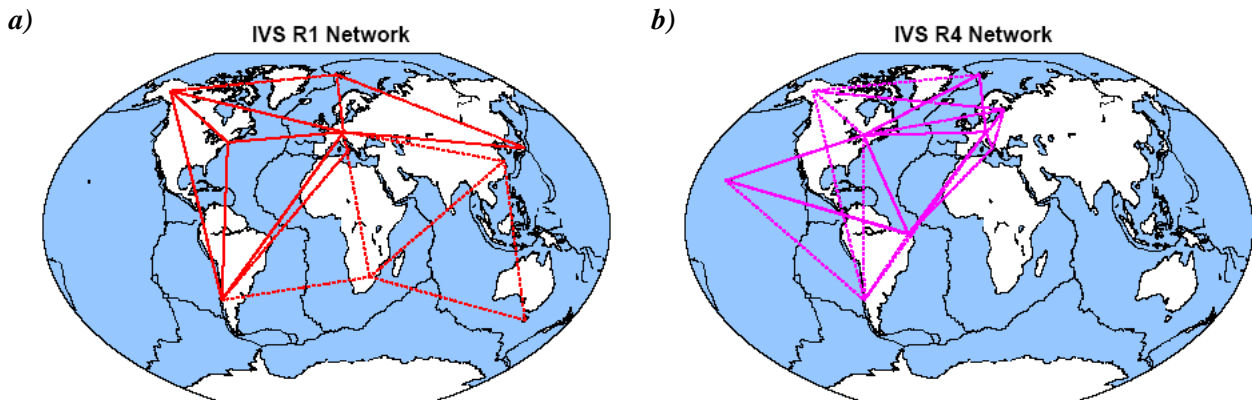


**Figure 3.2:** *Networks of the IVS rapid turnaround sessions:* **a)** *R1 session,* **b)** *R4 session. (provided by A. Nothnagel, GIUB)*

As already mentioned above, the troposphere influences the VLBI measurements and must be treated in the analysis, e.g., by mapping all troposphere delays gathered from observations at different elevation angles to the zenith and estimate troposphere zenith delays plus gradients. The "IVS Pilot Project - Troposphere Parameters" was set up to compare and combine troposphere estimates from different Analysis Centers. Since the Pilot Project proved to be successful, it was decided to release combined troposphere parameters (hourly zenith delays and daily gradients) as an operational IVS product, starting July 2003. For more details it is referred to *Schuh and Böhm (2003)*. Furthermore, *Heinkelmann et al. (2007)* provide a long time-series of combined troposphere zenith delays covering the time-span 1984 to 2004.

Preparing for the future, the IVS established the working group "VLBI2010" to examine the current and upcoming requirements for geodetic VLBI systems. The recommendations made in the working group report by *Niell et al. (2005)* embrace improvements concerning construction of antennas, network design, observing strategy, assessment of the error budget, correlation process, and analysis. All recommendations aim at the three major goals that turned out from the report of the IVS Working Group 2 and that are put in the game by the IAG project GGOS, i.e., a 1 mm long-term accuracy, continuous measurements and rapid product generation.

# 3.3 Satellite Laser Ranging (SLR)

## 3.3.1 Technical description

The basic principle of laser ranging in general is very simple. Short laser pulses are emitted in direction to a target equipped with retro-reflectors, the signal is reflected back to the laser telescope and detected there. At the time the laser pulse is emitted, a timer starts until the reflected signal is detected at the laser telescope so that the elapsed time is the traveling time of the laser pulse from the telescope to the reflection target and back again to the telescope. Two different types of reflecting targets are used in space-geodesy: On the one hand, artificial satellites are equipped with retro-reflectors and, on the other hand, several reflector arrays have been positioned on the surface of the Moon. Hence, the laser ranging technique for geodetic applications is divided into Satellite Laser Ranging (SLR) and Lunar Laser Ranging (LLR). The latter does not play an important role for the presented work, thus, the following descriptions will be restricted to SLR but many facts apply to LLR as well, of course. For more details about LLR, its specialties in the analysis and the main contributions to space-geodetic applications it is referred to *Müller (1991)*.

Regarding SLR, the satellites are either developed solely for laser ranging duties or their primary task is another scientific topic but they are equipped with retro-reflectors and SLR is used as instrument for the orbit determination. Concerning this second group of satellites, the gravity missions "Challenging Minisatellite Payload" (CHAMP) and "Gravity Recovery and Climate Experiment" (GRACE, consisting of two satellites, i.e., GRACE-A and GRACE-B following each other) as well as the altimetry satellites TOPEX, Jason-1 and Envisat-1 must be mentioned. However, only the passive geodetic satellites launched solely as a target for SLR play an important role in the framework of this thesis. Here, the two LAser GEOdynamics Satellites

(LAGEOS) have to be mentioned. *Cohen and Smith (1985)* give a characterization of both satellites. The spherical satellites with a diameter of only 60 cm were developed exclusively for laser ranging and are equipped with 422 corner cube reflectors. The altitude of about 6000 km is one of the characteristics important to be mentioned here, because this altitude was chosen to reduce the atmospheric drag in order to get a stable orbit modeling. LAGEOS1 and LAGEOS2 are in orbit since 1976 and 1992, respectively. The only difference between both satellites is the inclination: LAGEOS1 has an inclination of 109.84° whereas the inclination of LAGEOS2 is significantly smaller with 52.64°. Since 1964 when the first satellite equipped with retro-reflectors was tracked by an SLR station, about 60 different satellites have been tracked in total until now.

In order to distinguish SLR from the other techniques described before, the laser technique is working in the optical frequency band whereas VLBI and GPS (and DORIS, too) are using microwave signals. The wavelength used by most of the SLR observing stations is 532 nm (see *Otsubo and Appleby, 2003*). The drawback of employing optical signals is that an inter-visibility between the emitting and the reflecting unit is required. Hence, clouds above an SLR station disables observations to satellites.

An elaborate review of the developments regarding SLR including detailed background information about the laser technique itself is given in *Seeber (1993)* or by *Degnan (1993)*.

## 3.3.2  Observation equation

The basic observable of SLR is the measured time difference $\tau_A^S$ between the emission of a laser pulse and

its reception at the station *A* after the reflection at the satellite *S*. Multiplying this time interval with the speed of light *c* yields the two-way distance between the station and the satellite. However, the obtained distance cannot be considered equal to the purely geometrical distance derived from the positions of the station and the satellite, but some correction terms have to be taken into account comparable to the other space techniques:

$$\frac{1}{2} \cdot c \cdot \tau_A^S = \left| \boldsymbol{R}_{EOP} \cdot \boldsymbol{r}_A(t^S) - \boldsymbol{r}^S(t^S) \right|$$
$$+ \delta\rho_{rel} + \delta\rho_{trop} + \delta\rho_{bias} + \delta\rho_{CoM} + \epsilon_A^S . \tag{3.13}$$

The first line in (3.13) represents the purely geometrical part with station position and satellite position in the same way as already explained for GPS in equation (3.1). The only difference is that the station position in (3.13) is computed for the same time as the satellite position, i.e., the time of reflection of the laser pulse at the satellite. In an ideal case, the epoch of reflection is in the middle between the emission and detection of the laser pulse at the station. The terms listed in the second line contain all correction terms that are relevant

for an SLR observation including the measurement errors $\epsilon_A^S$. The relativistic corrections $\delta\rho_{rel}$ are simi-

lar to those of GPS so that it is referred to *Chapter 3.1.2* for an explanation, but with one exception: the corrections concerning satellite clocks are not relevant for SLR.

Similar to GPS and VLBI, an SLR observation has to be corrected for troposphere disturbances as well but

the correction $\delta\rho_{trop}$ in (3.13) is different from that for GPS and VLBI contained in (3.1) and (3.12), re-

spectively. As SLR bases upon optical instead of microwave signals the troposphere delay has to be modeled in a different way. *Marini and Murray (1973)* developed a model that is commonly used in the SLR analysis to correct for the troposphere disturbances. However, its zenith delay and mapping function do not apply to all wavelengths used in modern SLR, and, additionally, the model is valid only for elevations above 10°. A first improvement has been achieved with a new mapping function provided by *Mendes et al. (2002)* that is valid for elevation angles down to 3° and can be used in combination with any model for the zenith delay. As a next step, *Mendes and Pavlis (2004)* suggest the development of more accurate models for the zenith delay that are applicable to the full range of wavelengths used in modern SLR systems. Since the troposphere refraction is dispersive at optical wavelengths, SLR observations at two different wavelengths allow for the determination of its influence. The procedure is comparable to the determination of the ionospheric influence for microwave techniques (see *Chapter 3.1.2*). The derivation of the dispersive delay of two-color laser range observations is given by, e.g., *Riepl and Schlüter (2001)* or *Hulley et al. (2004)*. However, routine two-

color laser observations are carried out at the moment only at the stations Matera (Italy), Zimmerwald (Switzerland) and TIGO/Concepcion (Chile) (see *Mendes et al., 2003*).

Station-specific range biases $\delta\rho_{bias}$ are set up in the SLR analysis to account for a constant offset between the theoretical and the measured distance from the station to the satellite. Following *Schillak (2004a)* the systematic effects that can be compensated by estimating a range bias are manifold if they are not corrected separately. Just to mention the grouping for such kind of effects and give some keywords that are explained at length by *Schillak (2004a)*: environmental effects (e.g., atmospherical model, meteorological measurements), systematic errors within the SLR system (e.g., calibration with ground targets, signal strength variations, mount eccentricities, time interval counter) and systematic errors in the timing unit (e.g., frequency standard, connection to the UTC system) can cause biases. The author gives more detailed information about the characteristics of the systematic effects, their order of magnitude and how they are handled at the station Borowiec. According to his studies, the most important systematic deviations are due to deficiencies in the atmospheric model Marini-Murray (see above) and the uncertainty in the location of the reflectors w.r.t. the satellite's center of mass.

The latter effect is similar to GPS: The reflection point of the signal at the satellite is not identical to the center of mass (CoM) where the satellite position vector $r^S$ refers to. Thus, the correction $\delta\rho_{CoM}$ is accounting for this difference. However, *Otsubo and Appleby (2003)* demonstrate that a constant value, as it has been used since the very beginning of SLR observations, is not acceptable anymore if millimeter accuracy is desired. In fact, the CoM correction strongly depends on the laser ranging system and the detection energy level. For more details it is referred to the studies of *Otsubo and Appleby (2003)* where they determined CoM corrections for the three satellite types LAGEOS, ETALON and AJISAI distinguishing between three types of SLR systems. According to their studies, the correction varies by about 1 cm for the LAGEOS satellites and 5 cm for AJISAI and the ETALON satellites, clearly demonstrating the error that will be introduced into the solution if a constant value is used.

As for the other techniques presented in *Chapter 3.1* and *3.2*, the above descriptions should only introduce the SLR technique in view of an inter-technique combination, whereas further information about the technique itself, the mathematical model and the analysis process can be found in, e.g., *Seeber (1993)*, *Degnan (1993)*, *Schillak (2004a)* and *Schillak (2004b)*.

### 3.3.3 Global SLR solutions from the ILRS

The International Laser Ranging Service (ILRS) was established in 1998 as the second technique-specific international service following the IGS. The organization is similar to that of the IGS and the IVS and is outlined in, e.g., *Pearlman et al. (2002)*. According to the authors, the data sets of SLR and LLR observations provided by the ILRS are the basis for generating a number of fundamental data products important for a wide range of scientific, engineering and operational applications and experiments:

- highly accurate satellite ephemerides,
- polar motion and length of day,
- 3D coordinates and velocities of the ILRS tracking stations,
- time-varying geocenter coordinates,
- static and time-varying coefficients of the Earth's gravity field,
- fundamental physical constants (GM),
- lunar ephemerides, libration and lunar orientation parameters.

The primary target for the ILRS and the most interesting satellites for geodetic applications in view of reference frame, Earth rotation and combination with other space-geodetic techniques are the two LAGEOS and ETALON satellites. But, although they have the highest priority for the 40 currently observing stations, *Noomen and Shelus (2005)* emphasize that nearly 30 satellites equipped with retroreflectors are actually tracked. Besides the passive geodetic satellites (LAGEOS, ETALON), Earth sensing satellites and navigation satellites are supported as well by the ILRS. Some examples were already given in *Chapter 3.3.1*, and the

ILRS website[11] provides further information about the various satellite missions supported by SLR measurements so far.

LAGEOS1/2 and ETALON1/2 data are regularly processed by the ILRS Analysis Centers to derive station coordinates and Earth rotation parameters on a weekly basis. As the ILRS is the Technique Center responsible for the SLR contributions within the IERS, the "ILRS Analysis Working Group" under the coordination of *Noomen and Shelus (2005)* has been working towards an official ILRS solution including station coordinates and ERP that are combined from various input solutions delivered by altogether five Analysis Centers. Time-series of such weekly solutions were issued for the first time in 2003 and now cover the entire time span since 1992. After finalizing a benchmarking, the ILRS has decided that, starting at mid-2004, Agenzia Spaziale Italiana (ASI) delivers the official combined ILRS solution and Deutsches Geodätisches Forschungsinstitut (DGFI) acts as backup combination center (*Noomen and Shelus, 2005*).

The ILRS Central Bureau maintains a website with general information about laser ranging including the most actual information about the tracking network, the analysis of the data and the satellite missions currently supported. Therefore, it is referred to the ILRS website[12] for more details about the ILRS and its activities.

# 3.4   Differences and similarities between the space techniques

In view of a combination of the space-geodetic techniques it is worthwhile to add some remarks on the similarities as well as on the differences between the individual techniques. Several common features are already visible from the symbolic observation equations (3.1), (3.12), and (3.13) for GPS, VLBI and SLR, respectively. For the terms present in the observation equations, Table 3.1 distinguish whether they are handled in a typical analysis by an a priori model, by setting up an unknown parameter, or both (i.e., apply an a priori model and estimate corrections to this model). Crosses enclosed in brackets indicate that an estimation of the corresponding parameter type by the space-geodetic technique is possible but does not belong to a "standard" solution.

The columns for the parameters that are normally estimated are similar to the overview given in Table 1.1.

The inertial reference frame is given either by the positions of the quasars or by the satellite orbits, but only the quasars allow a long-term stability. Therefore, VLBI is the only technique that can provide a stable CRF, and, thus, has access to the nutation and universal time in an absolute sense, so that corrections to the a priori model are normally estimated. Contrary to this, the satellite techniques can contribute only short-term information, i.e., the nutation rates and *LOD*, whereas the nutation and *UT* have to be modeled.

Besides the time-derivatives of the nutation angles and *UT*, the pole coordinates are the only EOP that can be estimated by all three techniques. The same holds for the position of the observing stations.

The atmospheric properties are common to GPS and VLBI as both techniques use microwave signals. Concerning the troposphere, an a priori model is normally applied for the hydrostatic part and corrections are estimated to scope with the wet part of the troposphere delay which is more variable and hardly predictable. The influence of the ionosphere can be handled because observations for two wavelengths are available, as already explained in *Chapter 3.1.2*. In the case of optical observations by SLR, the impact of the troposphere can be modeled quite well, so that no parameters need to be estimated. The ionosphere plays no role for SLR observations.

Common properties of GPS and SLR are related to the satellite orbits. The satellite orbits themselves are normally handled by an a priori model and corrections estimated additionally to the orbital parameters. And, due to the dynamics of the orbits, the gravity field of the Earth has to be considered in the SLR and GPS analysis. This is normally done by an a priori model only, but the estimation of low-degree spherical harmonic coefficients is possible.

Finally, the relativistic corrections as well as those terms related to the behavior of the antennas (ground antenna and satellite antenna or reflectors) have to be modeled for all three techniques, and the behavior of the clocks belongs to the parameter estimation for all techniques.

---

11 *http://ilrs.gsfc.nasa.gov/satellite_missions/index.html*
12 *http://ilrs.gsfc.nasa.gov*

***Table 3.1:*** *Differences and similarities between the space-geodetic techniques concerning the a priori modeling and the estimation of parameters in the analysis of the observations.*

| Parameters and correction terms in the observation equations | | VLBI Model | VLBI Estimate | GPS Model | GPS Estimate | SLR Model | SLR Estimate |
|---|---|---|---|---|---|---|---|
| **Quasar positions** | $e^Q$ | **X** | **(X)** | | | | |
| **Nutation** | $\Delta\varepsilon, \Delta\psi$ | **X** | **X** | **X** | | **X** | |
| **Nutation rates** | | | **X** | | **X** | | **X** |
| **UT1-UTC** | | **X** | **X** | **X** | | **X** | |
| **LOD** | | **X** | **X** | **X** | **X** | **X** | **X** |
| **Polar motion** | $x_P, y_P$ | **X** | **X** | **X** | **X** | **X** | **X** |
| **Station positions** | $r_A, r_B$ | **X** | **X** | **X** | **X** | **X** | **X** |
| **Gravity field** | | | | **X** | **(X)** | **X** | **(X)** |
| **Troposphere** | $\rho_{trop}$ | **X** | **X** | **X** | **X** | **X** | |
| **Ionosphere** | $\rho_{ion}$ | **X** | | **X** | **(X)** | | |
| **Satellite orbits** | $r^S$ | | | **X** | **X** | **X** | **X** |
| **Antenna / reflector** | $\rho_{phas}$ $\rho_{ant}$ $\rho_{CoM}$ | **X** | | **X** | | **X** | |
| **Clocks** | $\delta t, \rho_{bias}$ | | **X** | | **X** | | **X** |
| **Relativity** | $\rho_{rel}$ | **X** | | **X** | | **X** | |

# 4 Description of the data

The following section will describe the data sets that have been used in the combination studies. At the beginning it is worthwhile to address the CONT02 campaign itself in order to emphasize its uniqueness and importance. The goal of this introduction is to give an explanation why this time period was chosen for the analysis. The remaining two sections characterize the data sets necessary to combine station coordinates and to validate the estimated troposphere parameters, i.e., local ties and data from water vapor radiometers including meteorological measurements, respectively.

## 4.1 The VLBI campaign CONT02

The observing program of the IVS has been outlined already in *Chapter 3.2.3*. Summarizing the major disadvantages, the changing network and non-continuous observing sessions cause a sub-optimal situation for combination studies using VLBI together with other space-geodetic techniques. In order to avoid this problem and to demonstrate the remarkable capability of VLBI of determining geodetic parameters, especially EOP, the IVS organized a special campaign in 2002, named CONT02, with continuous observations for a period of 15 days. The campaign started on October 16, 2002 at 18:00 UTC and lasted till October 31, 2002 at 18:00 UTC, separated into 15 sessions each lasting 24 hours. The participating stations were carefully selected and, altogether, the resulting network consists of eight stations, namely Algonquin Park, Fairbanks, Hartebeesthoek, Kokee Park, Ny-Alesund, Onsala, Westford and Wettzell. Unfortunately, the global distribution of these stations cannot be regarded perfect as it can be seen easily on the map in Fig. 4.1. Regarding the east-west direction only half of the globe is covered and in terms of the north-south distribution the major part of the stations is located on the northern hemisphere, more precisely, Hartebeesthoek is the only station on the southern hemisphere. As baselines with a large extension in north-south direction are especially important for a good determination of polar motion (see *Nothnagel, 1991*), it is expected that the polar motion results for CONT02 will suffer from this deficiency in the network configuration.

Compared to the disadvantage concerning the distribution of the stations the list of advantages of the CONT02 campaign is much longer: Besides the continuous observing network without changes in the configuration, CONT02 provides a co-location with GPS at all sites, a co-location with SLR at two sites (Hartebeesthoek, Wettzell), a co-location with DORIS at four sites (Fairbanks, Hartebeesthoek, Kokee Park, Ny-Alesund) and, in addition, a co-location with water vapor radiometers (WVR) at Onsala, Wettzell, Kokee Park and Westford (see *Chapter 4.3*).
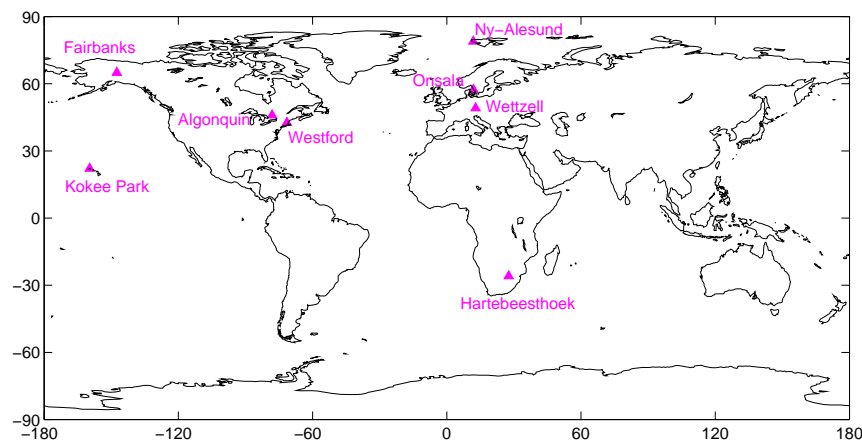


*Figure 4.1: VLBI network used for CONT02.*

CONT02 was neither the first nor the last campaign providing continuous VLBI observations for such a long period. The other CONT campaigns took place in January 1994 (CONT94), August 1995 (CONT95), fall 1996 (CONT96) and September 2005 (CONT05). Thus, the first three campaigns provide comparably old data sets and do not reflect the quality achievable today, whereas the observations of CONT05 came too late to be included in the studies described in this thesis. However, the CONT05 data are of high interest to continue and extend these studies, of course. Especially because the network could be extended compared to CONT02 with three stations (see the IVS website[13] for more information): The Russian station Svetloe, the station Tsukuba (Japan) fills the gap in the Asian region, and the station TIGO/Concepcion (Chile) is a second station located in the southern hemisphere and, furthermore, provides an additional co-location with SLR and DORIS. Especially the contributions of Tsukuba and TIGO are highly important to get a more stable global network, which stabilizes the solution for the EOP as well.

Summarizing the considerations and taking into account all the points mentioned above, the VLBI data of the CONT02 campaign are well suited for studies in view of a rigorous combination of the space-geodetic techniques.

# 4.2   Local ties

An essential part in combining different techniques is the identification of parameters that can either be stacked or combined by using additional information (see *Chapter 5.1.1* for more details). One important example for the latter situation is the combination of station coordinates at co-located sites. Normally, the different techniques do not refer to the same reference point and, therefore, the coordinates themselves cannot be stacked directly. As a way out, known values for the three-dimensional coordinate differences between the reference points, so-called local ties (LT), are introduced into the combination. The procedure is based on the mathematical principle of relative constraints described in *Chapter 2.6.3*. In most cases, the LT have been derived from local terrestrial surveys carried out at the stations. Examples including a detailed description of the planning, the measurements and the analysis can be found in, e.g., *Sarti et al. (2004)* for the station Medicina, *Schlüter et al. (2005)* for Wettzell, *Eschelbach and Haas (2003)* for Onsala, *Steinforth et al. (2003)* for Ny-Alesund and documentations for the Australian stations Yarragadee, Mount Pleasant and Mount Stromlo are available online[14] (e.g., *Johnston and Dawson, 2004* for Yarragadee). However, the problems concerning LT are manifold. The most important ones, affecting the major part of the co-location sites, are:

– For many co-locations, the LT values are missing.

– Some values are very dubious and do not fit to the space-geodetic results by far.

– Statistical information, particularly the variance-covariance matrix or at least the standard deviation, is not available.

– A detailed documentation is missing.

– There is no central archive where all actual LT including their documentation are available and accessible to all users.

For further details it is referred to, e.g., *Angermann et al. (2004)* for an overall analysis of co-locations, or to *Ray and Altamimi (2005)*, who evaluated especially the VLBI-GPS LT. Altogether, the problems mentioned above reduce the potential of a multi-technique combination because normally the station coordinates are a central part of the combination. In order to stress the importance of the LT, the IERS postulates to give the local survey measurements the same status as the space-geodetic techniques' observations themselves. The first time this goal was thoroughly discussed was the "IERS Workshop on Site Co-Location", held in Matera/Italy in October 2003, which was the first workshop devoted solely to this topic. On the one hand, the actual situation was demonstrated by means of several analyses, and, on the other hand, some groups that are responsible for co-location sites presented their experience with local surveys and generating LT. The outcome and the presentations during this workshop are published in *Richter et al. (2005)*. The necessity to build a working group to cope with all the recommendations resulting from the workshop became clear. In the mean time, the "IERS Working Group on Site Survey and Co-location" has been established and it pushes and coordinates activities related to local surveys at co-location sites including guidelines for the analysis and the disposability of the appropriate information (see *Dawson, 2005*).

---

13  *http://ivscc.gsfc.nasa.gov/program/cont05/*
14  *ftp://ftp.auslig.gov.au/sgac/sinex/ties/*

Concerning the CONT02 stations, the basic local tie information was taken from a list compiled for the ITRF computations available at the IERS ITRF Product Center at the Institut Géographique National (IGN)[15]. The latest compilation includes LT for all GPS-VLBI co-locations relevant for CONT02. One special comment must be added concerning the local tie for Kokee Park: The value from the ITRF list was corrected by $\Delta N =$ 27 mm, $\Delta E = 24$ mm and $\Delta U = 11$ mm for the north, east and height component, respectively. The corrections were taken from *IGSMAIL-4151*[16] announcing that a jump of the afore mentioned size has been recognized in the IGS long time-series. The jump occured after a change of the GPS antenna and the removal of the radome in September 2002 just before CONT02. As a re-analysis using the corrected site eccentricities for the new GPS antenna without radome is not available, the correction of the old local tie values by the "known" jump seemed to be the best method to retrieve a usable value for the combination although the jump belongs to the eccentricity vector between the marker and the antenna reference point rather than to the LT, of course.

All co-locations for the CONT02 analyses and the appropriate local tie values are summarized in Table 4.1. The numerical values are given in a geocentric system *x*, *y*, *z*. Additionally, the summary includes the corresponding height difference because this is relevant if the troposphere zenith delays derived from VLBI and GPS are combined. The theory for this task is comparable to those of the LT (see *Chapter 2.6.3*). A detailed description of the handling of troposphere ties is given in *Chapter 5.1.1* followed by various examples of combination results in *Chapter 6*. Finally, the last column in Table 4.1 shows the three-dimensional distance between the reference points to give an idea how far the two instruments are separated.

Unfortunately, there are only two stations amongst the eight GPS-VLBI co-locations that assemble all three techniques, namely Wettzell and Hartebeesthoek. However, there are additionally eleven GPS-SLR co-locations within the networks chosen for the analyses: Borowiec, Fort Davis, Grasse (two SLR sites), Graz, Herstmonceux, Monument Peak, Potsdam, Shanghai, Tahiti, Washington and Yarragadee. Fortunately, the LT values are available at the ITRF web-site for all co-locations with SLR mentioned above. Hence, altogether 14 GPS-SLR co-locations can contribute to the combination as a link between the networks of these two techniques whereas VLBI and SLR are tied together mainly via GPS. However, contrary to the GPS-VLBI co-locations for CONT02, the network of GPS-SLR co-locations strongly varies from day to day and the maximum number of 14 co-locations is not available for any day (see Table 4.2). In view of combining SLR with the other techniques on a daily basis, this situation may cause problems because the network of co-locations that transfers the datum information between the techniques is not homogeneous. Thus, the stabilization of the combined solutions concerning the datum parameters (translations and scale) due to including SLR is attenuated for daily solutions. Fortunately, the situation is much improved if weekly solutions are considered as Borowiec, Shanghai and Tahiti are the only co-locations that are not common to both weeks. Shanghai can be employed as co-location only in the 14-day solution.

---

15 *http://itrf.ensg.ign.fr/local_surveys.php*
16 *http://igscb.jpl.nasa.gov/mail/igsmail/2002/msg00490.html*

***Table 4.1:*** *Co-locations and the corresponding geocentric LT information used in the analyses (values are given in [m]).*

| Station name + GPS-ID | DOMES | Techniques | Local tie (geocentric) | | | dH | Distance |
|---|---|---|---|---|---|---|---|
| | | | dX | dY | dZ | | |
| Algonquin Park ALGO | 40104M002 S001 | GPS - VLBI (7282) | 94.756 | 61.021 | 6.665 | -23.100 | 112.901 |
| Borowiec BOR1 | 12205M002 S001 | GPS - SLR (7811) | 25.767 | -72.908 | -0.324 | 1.717 | 77.328 |
| Fairbanks FAIR | 40408M001 S002 | GPS - VLBI (7225) | -74.1410 | 49.2757 | -31.2367 | -13.0558 | 94.3436 |
| Fort Davis MDO1 | 40442M012 M006 | GPS - SLR (7080) | 22.3935 | 8.4672 | 23.4078 | 0.2145 | 33.4826 |
| Grasse GRAS | 10002M006 S001 | GPS - SLR (7835) | -0.632 | -44.858 | 1.199 | -3.528 | 44.878 |
| Grasse GRAS | 10002S001 S002 | SLR (7835) - SLR (7845) | -0.542 | -36.489 | 4.421 | -0.507 | 36.760 |
| Graz GRAZ | 11001M002 S002 | GPS - SLR (7839) | -2.558 | 8.516 | -1.321 | -1.097 | 8.989 |
| Hartebeesthoek HRAO | 30302M004 S001 | GPS - VLBI (7232) | -90.2996 | 132.1881 | -34.6542 | -1.5478 | 163.7945 |
| Hartebeesthoek HRAO | 30302M004 M003 | GPS - SLR (7501) | -48.6253 | 65.5918 | -42.7992 | 7.3698 | 92.1872 |
| Herstmonceux HERS | 13212M007 S001 | GPS - SLR (7840) | 6.505 | 10.278 | -3.945 | 1.083 | 12.787 |
| Kokee Park KOKB | 40424M004 S007 | GPS - VLBI (7298) | -0.5043 | -19.3777 | -42.2654 | -9.2431 | 46.4985 |
| Monument Peak MONP | 40497M004 M001 | GPS - SLR (7110) | 31.3649 | -5.4557 | 20.5255 | 3.5295 | 37.8790 |
| Ny-Alesund NYA1 | 10317M003 S003 | GPS - VLBI (7331) | -28.797 | -102.167 | 6.464 | -3.101 | 106.344 |
| Onsala ONSA | 10402M004 S002 | GPS - VLBI (7213) | 52.631 | -40.464 | -43.865 | -13.710 | 79.571 |
| Potsdam POTS | 14106M003 S009 | GPS - SLR (7836) | 50.091 | 95.219 | -40.438 | 10.896 | 114.939 |
| Shanghai SHAO | 21605M002 S001 | GPS - SLR (7837) | -645.1758 | -537.3040 | 196.6938 | -5.7491 | 862.3432 |
| Tahiti THTI | 92201M009 M007 | GPS - SLR (7124) | -8.4555 | 24.5510 | -28.2988 | 3.6575 | 38.4066 |
| Washington GODE | 40451M123 M105 | GPS - SLR (7105) | 54.230 | 97.009 | 93.863 | -4.685 | 145.471 |
| Westford WES2 | 40440S020 S003 | GPS - VLBI (7209) | 26.796 | 41.022 | 30.476 | -1.735 | 57.703 |
| Wettzell WTZR | 14201M010 S004 | GPS - VLBI (7224) | 40.7973 | 118.3964 | -61.3207 | -3.1011 | 139.4359 |
| Wettzell WTZR | 14201M010 S018 | GPS - SLR (8834) | 3.8238 | 68.2017 | -15.5177 | 0.6457 | 70.0492 |
| Yarragadee YAR2 | 50107M004 M001 | GPS - SLR (7090) | -18.6149 | -12.4650 | -5.8451 | -0.0435 | 23.1529 |

**Table 4.2:** *GPS-SLR co-locations available for daily and weekly solutions. "G" and "S" means that only the GPS site or the SLR site, respectively, is available for that day.*

| Station | Day of the year | | | | | | | | | | | | | | Week | |
| --- | 290 | 291 | 292 | 293 | 294 | 295 | 296 | 297 | 298 | 299 | 300 | 301 | 302 | 303 | W1 | W2 |
| **BOR1** | | | | | | | | | | X | | | | | | X |
| **MDO1** | X | | X | | X | X | X | X | | | | X | X | X | X | X |
| **GRAS** | | | | | | X | X | X | | | X | X | X | X | X | X |
| **GRAS-L** | | | | | | | X | | | | | X | X | | X | X |
| **GRAZ** | X | X | X | X | X | X | X | X | X | X | X | X | X | | X | X |
| **HRAO** | | X | X | X | X | | X | X | X | X | X | | | | X | X |
| **HERS** | X | X | X | | | | X | X | | X | X | X | | | X | X |
| **MONP** | X | X | X | X | X | X | X | X | X | | | X | X | X | X | X |
| **POTS** | X | X | | X | | | X | X | | | | X | | | X | X |
| **SHAO** | G | G | G | | | | | | S | S | S | | | | | |
| **THTI** | | | | | | | | | | | | | | X | | X |
| **GODE** | X | X | X | | X | X | X | X | | X | X | | | | X | X |
| **WTZR** | | | X | X | X | | | | | | | X | X | | X | X |
| **YAR2** | X | X | X | X | X | X | X | X | X | | | X | X | X | X | X |

# 4.3   Water vapor radiometers and meteorological data

The space-geodetic techniques VLBI, GPS and DORIS are not the only techniques to yield information about the water vapor content in the troposphere. Other techniques like water vapor radiometers (WVR) or radiosondes can deliver similar information but only a few of these instruments are available. The Onsala Space Observatory in Sweden is one station that operates a WVR and, additionally, has access to radiosonde measurements. The comparisons between the different instruments (space-geodetic techniques, WVR and radiosondes) carried out by *Gradinarsky (2002)* show a rather good agreement so that each of the techniques can be used to control and validate the others. Similar studies were done by *Niell et al. (2001)* for the station Westford. The possibility of validating the troposphere estimates from VLBI and GPS with independent techniques was used for the CONT02 analyses as well (see *Chapter 5.2.2*). Albeit radiosonde measurements were not available for the studies, several WVR were placed on selected stations during CONT02. Altogether four stations were equipped with a WVR: Onsala, Wettzell, Kokee Park and Westford (see Table 4.3).

## 4.3.1   WVR measurements and their pre-processing

A WVR measures the sky brightness temperature at different frequencies. The three major constituents of the atmosphere (i.e., oxygen, water vapor and liquid water) have a unique and distinguishable frequency-dependency resulting in a different sky brightness temperature. Thus, each contribution to the total sky brightness temperature measured by the WVR can be separated from the others if measurements at different frequencies are carried out (see *Elgered et al., 1991*). *Gradinarsky (2002)* gives the two frequencies for the WVR operating at Onsala with about 21 GHz and 31 GHz. The latter corresponds to the frequency that is more sensitive to the radiation emitted by the liquid water whereas the former frequency is more sensitive to the radiation emitted by water vapor. The approach to convert the sky brightness temperature into the wet delay is not unique according to *Elgered et al. (1991)* and has to be optimized for each particular site by determining the retrieval coefficients empirically, e.g., relying on radiosonde measurements.

Unfortunately, the retrieval coefficients for the WVR operating at Westford are missing so that the wet delay cannot be computed out of the original WVR measurements and a comparison with GPS and VLBI is not possible. The availability of WVR data at Kokee Park is another limiting factor for validating the space tech-

niques by using WVR data: The WVR data start only on October 21 at 23:00 UTC (= day of the year 294), so that about five days of the CONT02 campaign are missing.

One general comment about the WVR measurements must be added. The WVR determines the wet delay in the direction where the instrument is pointing to (azimuth, elevation). To compare these slant delays with the results of GPS or VLBI whose troposphere delays are expressed as zenith delays, the WVR measurements have to be mapped to the zenith first. The same mapping function can be used as in the case of computing the troposphere influence on space technique observations given in Eq. (3.8), but using the relationship for the wet part only:

$$\rho_{wet}^{zenith} = f_{wet}^{-1}(z) \cdot \rho_{wet}(z) \; , \tag{4.1}$$

with $\rho_{wet}(z)$ denoting the wet troposphere slant delay at zenith angle $z$ that is originally derived from the WVR measurements, $\rho_{wet}^{zenith}$ denoting the corresponding wet troposphere delay in zenith direction, and $f_{wet}(z)$ is the mapping function for the wet part of the troposphere delay. Many mapping functions are available but, to be consistent with the space-geodetic techniques, it is reasonable to use that applied in the GPS and VLBI analysis for the WVR measurements as well. Thus, the mapping function described by *Niell (1996)* is employed for the analyses presented in this thesis. The conversion from slant delays to zenith delays using the given elevation angles had to be done for the WVR at Wettzell and Kokee Park whereas the WVR data provided by the Onsala Space Observatory (*Elgered and Haas, 2003*) has been pre-processed so that the wet delays were already given for the zenith.

It is commented in Table 4.3 that additional rain sensors are available for the station Wettzell. As the name already indicates, rain sensors detect rainfall. This information is useful for the application of WVR data because the wet delay measured by the WVR is reasonable only if it is not raining and no water is accumulated on the optics of the instrument (see *Elgered et al., 1991*). Thus, the WVR data were ignored in the comparisons with the space-geodetic techniques if at least one of the two sensors indicated rainfall. Unfortunately, a comparable external rain sensor was not available for the station Kokee Park, but the radiometer itself has an internal sensor. Thus, this information was used to detect and eliminate measurement epochs deteriorated by rain. Figures 4.2a-b visualize the raw measurements of the WVR at Wettzell and Kokee Park, respectively, and the epochs influenced by rain are indicated. As already mentioned above, the WVR measurements at Onsala had been pre-processed so that a data screening concerning rain epochs was not necessary any more.
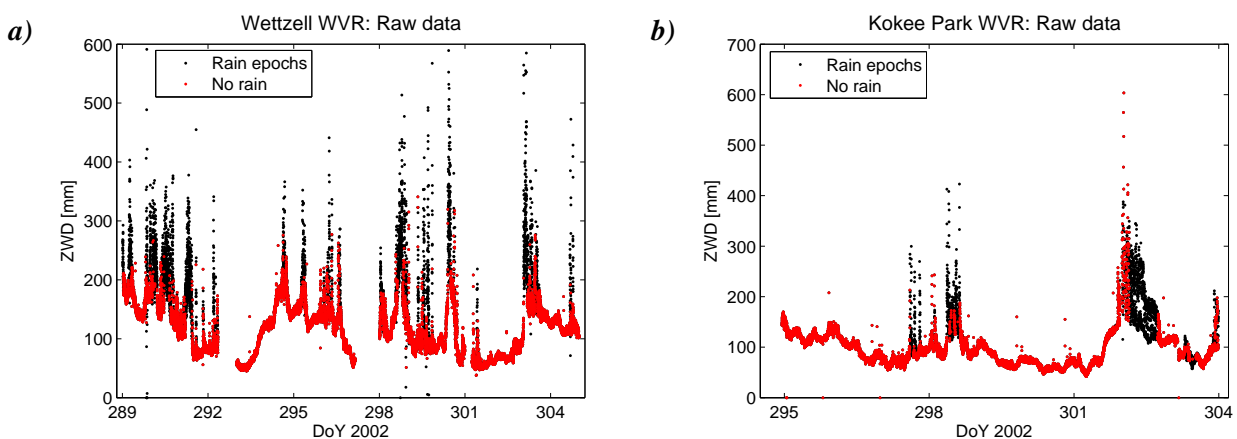


***Figure 4.2:*** *Raw WVR measurements with rain-free epochs distinguished from rain epochs: a) Wettzell, b) Kokee Park.*

After eliminating the data corresponding to rain epochs, a second step in preparing the WVR data for a comparison with the space-geodetic techniques is the averaging to hourly mean values to be in accordance with the temporal resolution of the GPS and VLBI estimates (see *Chapter 5.1.2*). In order to give an impression

how the mean values and the raw data fit together, Fig. 4.3a-c display both time-series for all three stations occupied with a WVR. Regarding Onsala, the sampling to hourly values does not induce a big change due to the original resolution of 30 minutes whereas the raw data for Wettzell and Kokee Park are originally given with a roughly one-minute spacing. Another important feature of the Onsala time-series is that the half-hourly values have been provided including standard deviations. Hence, the hourly mean values displayed in Fig. 4.3a are weighted mean values and their resulting standard deviations were added to the plot. Unfortunately, there are no standard deviations available for the other two WVR measurements. However, for the derivation of a comparable quality assessment for the hourly mean values, every original measurement was assigned with the weight 1 for the averaging process, i.e., corresponding to a standard deviation of 1 m. Thus, the "standard deviations" shown in Fig. 4.3b-c for the hourly mean values of Wettzell and Kokee Park reflect the number of single measurements contributing to the mean value. Such a procedure seems to be reasonable in the case of a WVR as the scatter from one minute to the next is quite large so that a mean value out of more data points is thought to be more reliable, especially when it is compared to the estimates of the space-geodetic techniques later on, although these standard deviations should not be interpreted in an absolute sense.



*a)* Onsala WVR: Hourly weighted mean
*b)* Wettzell WVR: Hourly mean
*c)* Kokee Park WVR: Hourly mean
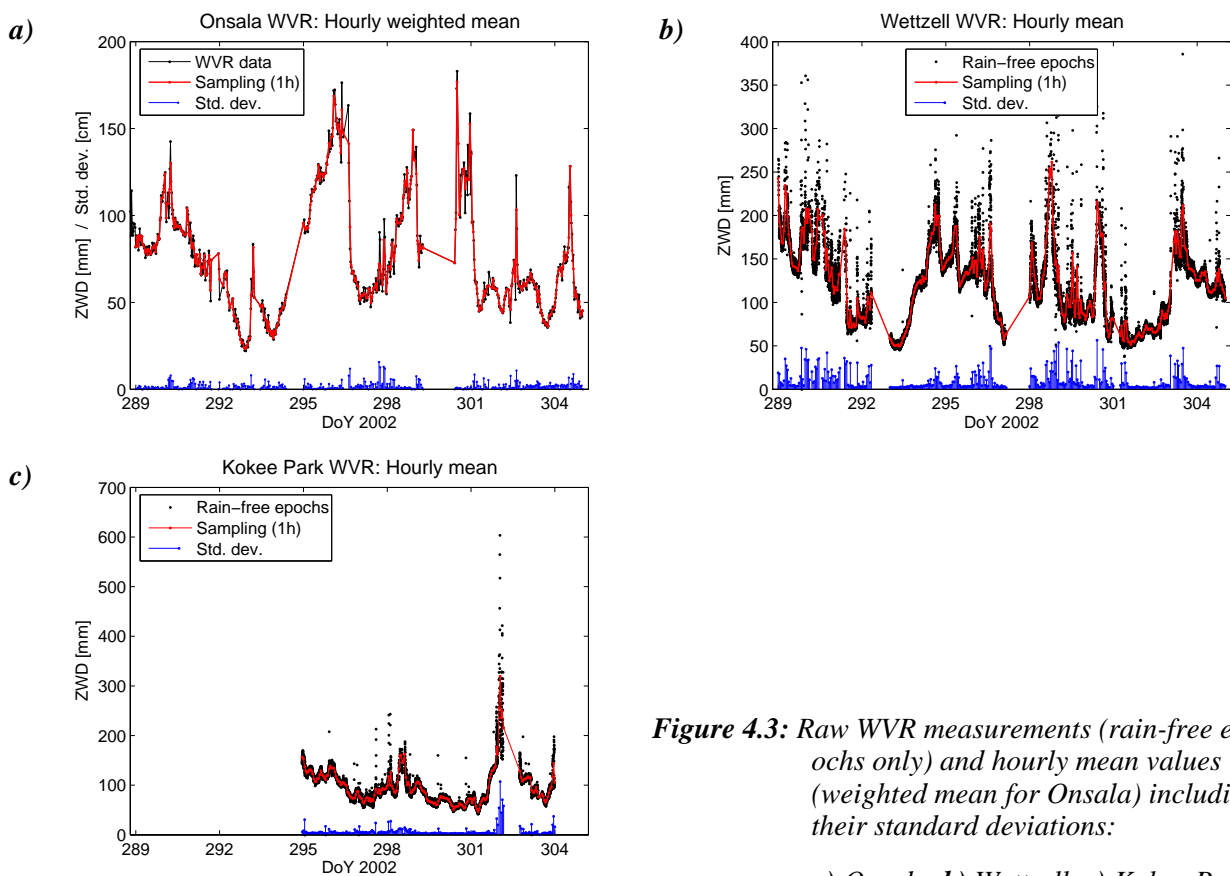
**Figure 4.3:** *Raw WVR measurements (rain-free epochs only) and hourly mean values (weighted mean for Onsala) including their standard deviations:*

*a) Onsala, b) Wettzell, c) Kokee Park.*

## 4.3.2 Special aspects concerning the usability of WVR and meteorology data

In contrast to the space-geodetic techniques that measure the total amount of the troposphere delay, the WVR is determining only the delay caused by the wet part of the troposphere. In order to use these values for comparisons, the wet part of the total troposphere zenith delay $\rho_{total}^{zenith}$ estimated by VLBI or GPS must be derived first. Equation (3.7) gives the separation into a hydrostatic and a wet part. The wet part depends on the temperature and the partial pressure of water vapor. Especially the partial pressure of water vapor shows a high variability in space as well as in time, thus, the wet delay is difficult to model using meteorological measurements. If GPS or VLBI estimates are to be compared to WVR data, the wet part of the troposphere delay is obtained by computing the hydrostatic part and subtracting it from the total delay estimated by GPS or VLBI. The hydrostatic delay is proportional to the total pressure and can be modeled rather well, e.g., using the expression given by *Elgered (1992)* or *Davis et al. (1985)* (in millimeters):

$$\rho_{hydro}^{zenith} = \frac{2.2768 \cdot p}{1 - 0.00266 \cdot \cos{(2 \cdot B)} - 0.00028 \cdot h} \quad , \tag{4.2}$$

where $p$ denotes the total atmospheric pressure at the ground in [mbar], $B$ is the latitude of the station and $h$ is the station height above the ellipsoid in [km]. Subtracting (4.2) from the total delay, the remaining part corresponds to the troposphere delay caused by the water vapor in the atmosphere and can be compared to the values derived from WVR measurements. Admittedly, two facts have to be considered:

– Using meteorological measurements like pressure, temperature and relative humidity or partial pressure of water vapor for computing the troposphere delay (total delay or one of the two constituents) it must be considered that all meteorological quantities are height-dependent. Therefore, introducing the measurements directly into Eq. (4.2) gives the hydrostatic delay at the height of the pressure sensor, but in general this is not identical to the reference height of the VLBI or GPS point the hydrostatic part of which should be computed.

– When subtracting the hydrostatic delay from the GPS- and/or VLBI-derived total delay, the remaining wet delay is identical to the WVR values only if both refer to the same height.

Concerning the first point, i.e., the meteorology sensor having another reference height than the GPS or VLBI reference point, the measured pressure and temperature must be extrapolated to the desired height $h$ and only the relative humidity $H$ can be assumed to be constant close to the ground. Under the precondition of a hydrostatic equilibrium the meteorological quantities at the height of GPS/VLBI are derived from the measured values (index '$m$') according to *Brunner (2004)*:

$$p\,(h) = p_m - 0.03416 \, \frac{p_m}{T_m} \, (h - h_m) \quad , \tag{4.3a}$$

$$T\,(h) = T_m - \Gamma \cdot (h - h_m) \quad , \tag{4.3b}$$

$$e\,(h) = \frac{H}{100} \cdot e_{sat}\,(T) \quad , \tag{4.3c}$$

with $p$ denoting the total atmospheric pressure in [mbar], $T$ the temperature in [K] and $\Gamma$ is the vertical temperature gradient with $\Gamma = 0.00977$ °C/m. As already mentioned, the relative humidity $H$ is assumed to be constant but the partial pressure of water vapor $e$ (in millibar) is not, as it depends also on the saturated vapor pressure $e_{sat}$ which is on its part influenced by the temperature according to the formula of Magnus-Tetens:

$$e_{sat}\,(T) = e^{2.3026 \cdot \left( 0.7858 + \frac{7.5 \cdot T}{T + 237.3} \right)} \quad . \tag{4.4}$$

As regards the second remark mentioned above, i.e., the WVR and the space-geodetic techniques referring to different heights, the additional troposphere wet delay in the layer between the two reference heights must be accounted for in the comparison. *Brunner (2004)* gave a formula valid for this purpose based on the theory derived by *Saastamoinen (1973)*:

$$\Delta \, \rho_{wet} = \rho_{wet_2}^{zenith} - \rho_{wet_1}^{zenith} = -2.789 \, \frac{e_1}{T_1^2} \cdot \left[ \frac{5383}{T_1} - 0.7803 \right] \cdot \Gamma \cdot (h_2 - h_1) \quad . \tag{4.5}$$

The indices 1 and 2 stand for values referred to either the WVR or the space-geodetic reference point. Therefore, the temperature and the partial pressure of water vapor first must be extrapolated to the appropriate height of instrument '1' using the Eq. (4.3a-c).

Summarizing the information necessary for comparing the troposphere estimates derived by water vapor radiometers and the space-geodetic techniques, three topics have to be considered:

– Measurements of the total atmospheric pressure are needed for computing the hydrostatic delay (Eq. (4.2)).

    –  Measurements of temperature and relative humidity (or partial pressure of water vapor) are necessary if differences in the reference heights of WVR and GPS/VLBI must be taken into account (Eq. (4.5)).

    –  The reference heights for all instruments (GPS/VLBI, WVR and pressure sensor) must be known, or at least the corresponding height differences, to be able to correct the influence of different heights on meteorological values (Eq. (4.3a-c)) and troposphere delays (Eq. (4.5)) if necessary.

Unfortunately, the above demands were not fulfilled for all stations participating in the CONT02 campaign. Meteorological files with pressure, temperature and relative humidity stored every few minutes (not in regular steps) are available for all VLBI sites. But in some cases the values stored in the files are dubious or even missing. The pressure measurements seem to be all right whereas the humidity and the temperature for Kokee Park, Hartebeesthoek and Westford must be treated carefully (see *IVS Analysis Mail No. 00991, 00992, 00994, 01000, 01002*). Additionally, the pressure records for Ny-Alesund show constant values for roughly two sessions which is a questionable behavior (see *IVS Analysis Mail No. 00994*).

As Hartebeesthoek and Ny-Alesund had no WVR running during CONT02, the wrong temperature and humidity values and the questionable pressure values, respectively, do not matter in this case. However, it is a disadvantage when testing different combination methods for the troposphere delays as it will be described later in *Chapter 5.1.1*.

For the station Kokee Park the situation is more problematical because comparisons with WVR data are possible. Thus, the hydrostatic delay (4.2) has to be calculated so that pressure measurements extrapolated to the appropriate height are needed. For this extrapolation, in turn, the measured temperature is needed in Eq. (4.3a). Furthermore, as the reference height of the WVR differs from that for GPS and VLBI, the differential wet delay must be computed according to (4.5) requiring correct temperature and humidity values. One way out of this dilemma might be the usage of the meteorological values stored in the WVR observation files. The WVR itself measures temperature, pressure and humidity and stores them in the output file together with the other measurements. The only question mark behind this procedure is the quality of the meteorological values provided by the WVR.

A similar situation exists for the station Westford: There are two different sources for meteorological data, one file stemming from the IVS CONT02 data archive and another set of files has been delivered with the WVR data. Unfortunately, they are not consistent, and according to the *IVS Analysis Mail No. 01000* the meteo file from the CONT02 data archive should be used carefully. Unlike this data source, the content of the meteo files delivered with the WVR data seems to be usable. However, for both the same problem exists: The reference height is not delivered together with the data and other sources like the IGS sitelog files or the RINEX meteo files contain inconsistent values. Nevertheless, the controversial height information differs by about 10 m and tests showed that the subsequent influence on the differential troposphere wet delay according to (4.5) is clearly below 0.01 mm. Therefore, it was decided to simplify matters and assume the same height for the meteorological data sensor as for the GPS antenna.

The remaining two stations equipped with a WVR during CONT02 (Onsala, Wettzell) fulfill the criteria mentioned above: The meteorology files are okay and the demanded height differences are available. Onsala was one of the stations that answered the IVS initiative to collect information about the meteorology equipment at each VLBI station (see *IVS-met mail* from January 14, 2004[17] and the corresponding IVS website[18]). All data and their sources together with the additional information necessary for comparisons of troposphere estimates described above are summarized in Table 4.3.

In order to give an idea about the size of the differential wet delay according to Eq. (4.5) that should be applied when comparing space-geodetic techniques with WVR data, Fig. 4.4 displays the time-series of the correction for the relevant stations. The values given in Fig. 4.4 are valid for a comparison between VLBI and WVR, however, they look quite similar in the case of comparing GPS and WVR. In the case of Kokee Park, the meteorological values stored by the WVR itself have been used due to the problems with the CONT02 meteo files mentioned above. Therefore, the data start only at DoY 295, though the very large variations during the first two days are unrealistic and cast doubt on the quality of the measurements, too. The mean corrections for VLBI over the CONT02 time span are 1.0 mm, 0.7 mm and 0.6 mm for Kokee Park, Onsala and Wettzell, respectively. Thus, the corrections are not really large but they have an order of magnitude that is not negligible if meaningful comparisons should be carried out. Due to the smaller height differences between GPS and WVR the mean corrections for GPS are also smaller than for VLBI: 0.1 mm for Ko-

---

17 *http://ivscc.gsfc.nasa.gov/pipermail/ivs-met/2004-January/000007.html*
18 *http://mars.hg.tuwien.ac.at/~ivstrop/ivsmet.html*

kee Park and 0.4 mm for Wettzell. The WVR data provided by the Onsala Space Observatory refer to the same height as GPS so that a correction is obsolete in this case.

Finally, a further aspect concerning the usage of meteorological data in the analyses presented in the following chapters should be addressed. As already mentioned before, a combination of the troposphere parameters from GPS and VLBI is intended in the framework of this thesis. In analogy to the comparison with WVR, the height difference between the GPS and VLBI reference points and the resulting difference in the troposphere delay estimated by both techniques must be taken into account. This is not only the case if the troposphere delays are combined but also if they are "simply" compared. For computing these additional troposphere delays, so-called troposphere ties, a standard atmosphere or real meteorological data can be used. Therefore, the GPS-VLBI co-locations without a WVR running during CONT02 are listed in Table 4.3 as well, because the meteorological data is used when troposphere zenith delays from VLBI and GPS are combined. Further details about the computation of the troposphere ties, their application in the combination and comparisons and the results for the CONT02 stations will be explained elaborately in Chapter 5.1.1 and Chapter 6.
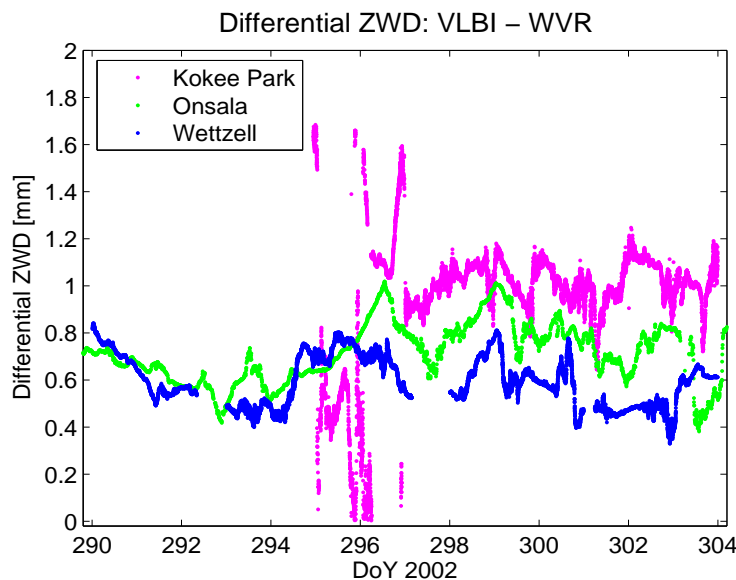


**Figure 4.4:** *Differential wet zenith delay (ZWD) necessary to correct the VLBI-derived wet delay in order to compare it with WVR data.*

***Table 4.3:*** *Data from WVR, meteorology sensors and related information. Indicators for sources of height information:*

*[1] IVS-met mails: <http://ivscc.gsfc.nasa.gov/pipermail/ivs-met/2004-January/>*
*[2] Summary at TU Vienna: <http://mars.hg.tuwien.ac.at/~ivstrop/ivsmet.html>*
*[3] WAVEFRONT project*
*[4] IGS site log files*
*[5] RINEX meteo files*
*[6] Personal communication with staff at Kokee Park observatory*
*[7] RadCalWet observation campaign (Pottiaux et al., 2003)*

| *Station* | *Source for meteorological data* | *Height diff. to meteorological sensor* | *Height diff. to WVR* | *Comments* |
|---|---|---|---|---|
| Algonquin Park | IVS-CONT02 | *[4]* Meteo = GPS | - | DoY 300 is missing |
| Fairbanks | IVS-CONT02 | Not available | - | |
| Hartebeesthoek | IVS-CONT02 | Not available | - | IVS-CONT02 file with artificial values for relative humidity |
| Kokee Park | IVS-CONT02 and WVR | *[2]* Meteo – VLBI = -18 m | *[6]* GPS – WVR = 1.28 m | IVS-CONT02 file only with good pressure data; WVR data starts on 21-10-2002; WVR-internal rain sensor only |
| Ny-Alesund | IVS-CONT02 | *[1], [2]* Meteo – VLBI = -5.102 m | - | Two sessions with constant pressure values |
| Onsala | IVS-CONT02 | *[1], [2], [3]* Meteo = GPS | *[3]* WVR = GPS | WVR data including standard deviations |
| Westford | IVS-CONT02 and WVR | *[5]* Meteo – GPS = -10.22 m *[4]* Meteo – GPS = -1.1 m | Not available | CONT02 file only with good pressure; DoY 297 is missing; Ambiguous height information for meteorological sensor; Retrieval coefficients for WVR are missing |
| Wettzell | IVS-CONT02 | *[2], [3]* Meteo – GPS = -10.5 m | *[7]* GPS – WVR = 6.584 m | Two additional rain sensors available |

# 5 Processing and validation strategies

It is worthwhile to address several general aspects about the processing and validation strategy applied for the combination studies prior to the presentation and discussion of the results in the subsequent chapter. The background for the combination on the normal equation level including a short overview about the realization of all relevant topics in the software that was used should ease the understanding of the analyses steps carried out later on. The afore mentioned aspects are outlined in *Chapter 5.1.1* succeeded by a more detailed explanation of the daily normal equation systems especially generated for the studies presented in this thesis (*Chapter 5.1.2*). *Chapter 5.2* concentrates on the methods for validating the results obtained in the studies. Three different types of validation criteria are mentioned: a solution-internal criterion for the station coordinates (*Chapter 5.2.1*), the possibility of comparing all parameter types with external data sets (*Chapter 5.2.2*), and the comparison of the combined solution with the single-technique solutions (*Chapter 5.2.3*). The section about the processing and validation strategy is finished with some theoretical considerations in *Chapter 5.3* concerning correlations between the parameter types included in the solution, as the understanding of these correlations is indispensable for interpreting the results.

## 5.1 Processing

The explanation of the processing strategy starts with some general aspects related to the inter-technique combination (*Chapter 5.1.1*) followed by a description of the daily single-technique normal equation systems for VLBI, GPS and SLR that build the basis for the combination studies (*Chapter 5.1.2*).

### 5.1.1 Combination aspects

*a) Level of combination*

In principle, three different combination methods are possible: the combination on the parameter level, the combination on the normal equation level and the combination on the observation level. The methods are ordered according to the augmenting degree of consistency that can be achieved solely by the method of combination. The last combination type guarantees the highest consistency because the analysis of all observations is done together with one software package, so that all parameters of interest result directly from the analysis process and all correlation are taken into account (*Drewes and Angermann, 2002*).

Contrary to the combination on the observation level, the other two methods always consist of at least two steps. In a first step the observations are analyzed separately, e.g., one analysis per technique or a separation into different geographical regions. After these primary analyses the different parts are brought together in a second step, the combination itself. Generally, the analyses of the first step can be done with different software packages and, if no special care is taken, this fact can lead to inconsistencies regarding the a priori models, the parameterization and the processing methods. These inconsistencies are passed then to the estimated parameters and will be "averaged" in the combination step as they cannot be eliminated any more.

Two fundamental differences between a combination on the normal equation level and a combination on the parameter level are other possible sources for inconsistencies: the parameter types included in the combination and the datum definition. The combination on the parameter level implies that only one parameter type is considered. Thus, each parameter type is combined independently from the others so that the correlations between different parameter types (e.g., station coordinates and EOP) are lost. On the contrary, if all relevant parameters are included in all single normal equation systems, inconsistencies are avoided for the combination based on normal equation systems. As regards the second source of inconsistencies mentioned above, only datum-free normal equation systems resulting from the first step of separated analyses are used, if the combination is done on the normal equation level. The common parameters are stacked and all additional information (mainly datum definition) is added to the combined normal equation system whereas the datum definition has been added for each part separately already in the first step if the combination is carried out on the parameter level. In the latter case, the parameters including their variance-covariance matrix result from a specific datum definition that is not necessarily consistent for all analyses parts. If these different systems are subsequently combined some tensions will be induced in the combined solution.

Consequently, from the point of view of consistency, the combination on the observation level is the optimal and most flexible method to use. The remaining methods allow a rigorous combination solely under some preconditions: All relevant parameters must be included, common processing standards concerning a priori models have to be applied, the set-up of the common parameters has to be done identically, parameters that are not included in the normal equation system (e.g., orbital parameters in the case of the satellite techniques) should not be fixed. In general, these preconditions are not fulfilled for solutions (SINEX files) provided by the international services IGS, IVS and ILRS so that a rigorous combination based on these data set is not possible. However, the combination on the observation level implies that a software package is needed that can deal with all space-geodetic techniques on a very high level of quality which is comparable to any existing software package specifically developed and used for one of the techniques. This is the crucial point why a combination on the observation level is problematical at the moment, albeit several developments are on the way, e.g., by *Andersen (2000)*, *Yaya (2002)*, and *Coulot et al. (2007)*. Therefore, the method of combination commonly used nowadays is the combination on the normal equation level. If detailed agreements about the processing standards are made for generating the normal equation systems and if all parameters of interest are contained in the single normal equation systems, the results can approach a combination on the observation level. The work for the thesis at hand bases upon this idea of a thorough standardization of the a priori models and the parameterization used in the separated analyses of the single-techniques' observations. Thus, the technique-specific normal equation systems are as homogeneous as possible and a rigorous combination becomes possible (*Drewes, 2006*). The specific details about these normal equation systems are described in *Chapter 5.1.2*.

### *a) Combination of estimated parameters*

Regardless of the type of combination chosen for the work, one essential part is the identification of common parameters. *Rothacher (2002)* gives an overview of the parameter space for a rigorous combination of the space-geodetic techniques VLBI, GPS/GLONASS, SLR, LLR, DORIS/PRARE and altimetry subdivided into the parameter groups celestial reference frame, terrestrial reference frame, Earth orientation, atmosphere, gravity field and time transfer. This compilation results in a large amount of parameters. However, normally not all of the parameters listed there are included in combination studies. Furthermore, not all of the techniques listed above contribute to the standard combinations that are carried out at the moment by several institutions within the IERS. Most of the studies are dedicated only to the terrestrial reference frame and the Earth orientation parameters. The work described hereafter is restricted to the three techniques VLBI, GPS and SLR. Looking into their observation equations given in *Chapter 3*, i.e., Eq. (3.1), (3.12) and (3.13) for GPS, VLBI and SLR, respectively, the common parameters can easily be recognized. Although some other common parameter groups are present in more than one technique (e.g., clocks, satellite orbits), the combination studies here will focus on the following parameters:

- terrestrial reference frame: station coordinates, geocenter;
- Earth orientation: polar motion ($x$- and $y$-pole), *UT1-UTC*, nutation (in longitude and obliquity); all parameters including their time derivatives;
- atmosphere: station-specific troposphere ZD and horizontal gradients (only for microwave techniques).

After finding the common parameters, one must think about how they can be combined. Some of them can be stacked directly (assuming the same reference epoch), e.g., geocenter, Earth orientation parameters and horizontal troposphere gradients (for identical stations) by applying the algorithm given in *Chapter 2.5*. But the station coordinates and the troposphere ZD normally refer to different points. Therefore, they cannot be stacked directly although the potential of co-located sites should be exploited. In this case, the difference caused by non-identical reference points has to be taken into account. For the combination studies described in the following, the difference between the corresponding parameters is constrained to a known value according to the formulas derived in *Chapter 2.6.3* and all corresponding parameters are kept in the normal equation system as unknowns. This method was already addressed in *Chapter 4.2*, where the so-called local ties were introduced as nominal values for the difference between station coordinates at co-locations. Additionally, it has already been indicated in *Chapter 4.2* and *4.3* that a similar procedure is applied for combining the troposphere ZD at co-located VLBI-GPS sites. For this purpose four different methods of computing the nominal value for each co-location will be tested in *Chapter 6.2*:

1) "rule of thumb": A 10 m height difference corresponds to about 3 mm difference in the troposphere ZD (hydrostatic delay);

2) dry part according to the Saastamoinen model using a standard atmosphere ("standard");

3) Saastamoinen model using true meteorological data ("meteo");

4) mean differential troposphere ZD derived from the space-geodetic solutions ("solution").

The rule of thumb mentioned in item 1) is based on the Saastamoinen model for the troposphere delay caused only by the hydrostatic part, i.e., depending solely on the pressure $p$:

$$\rho_{hydro}^{zenith} = 2.277 \cdot 10^{-3} \cdot p \quad . \tag{5.1}$$

The second method ("standard") directly uses Eq. (5.1) with values for the pressure $p$ that are extrapolated to the respective heights of the two reference points, i.e., VLBI and GPS. Then, the difference between the two hydrostatic ZD resulting from (5.1) is taken as nominal value for the combination. The extrapolation of the pressure to the desired reference heights $h$ is done using a standard atmosphere according to *Berg (1948)* with the index $r$ indicating the reference values of the standard atmosphere for height and pressure, i.e., $h_r = 0$ m and $p_r = 1013.25$ mbar, respectively:

$$p\,(h) = p_r \cdot (1 - 0.0000226 \cdot (h - h_r))^{5.225} \quad . \tag{5.2}$$

The third method ("meteo") is the most sophisticated one. It takes into account not only the hydrostatic part of the troposphere delay but also the wet part, and, additionally, the derived nominal value for the troposphere tie is based on true meteorological measurements instead of a standard atmosphere. Formulas for the differential zenith wet delay $\Delta\rho_{wet}^{zenith}$ have been given already in *Chapter 4.3* in view of comparing VLBI or GPS with WVR-derived wet delays, but the differential wet delay between the VLBI and GPS reference points can be derived applying Eq. (4.5) in the same way, of course. Additionally, the hydrostatic part is needed for the purpose of troposphere ties and *Brunner (2004)* gave a formula for this part, too:

$$\Delta\,\rho_{hydro}^{zenith} = \rho_{hydro_2}^{zenith} - \rho_{hydro_1}^{zenith} = -2.277 \cdot 10^{-3} \cdot 0.03416 \cdot \frac{p_1}{T_1} \cdot (h_2 - h_1) \quad . \tag{5.3}$$

Needless to say that the meteorological values first have to be extrapolated to the height $h_1$ of GPS or VLBI employing the equations given in (4.3). The sum of the differential hydrostatic delay according to (5.3) and the differential wet delay according to (4.5) is used as nominal value for combining troposphere ZD.

The meteorological data needed for the computations above and the problems related to them were already described in *Chapter 4.3* in view of using them for comparisons between the space techniques and water vapor radiometers. The problems summarized in Table 4.3 occur similarly in the computation of the troposphere ties: Dubious meteorological values and missing height information for the sensors render the derivation of "true" values impossible. Nevertheless, for some of the eight CONT02 co-locations the data are usable so that the differential troposphere delay caused by the height difference between the VLBI and GPS reference points can be computed: Algonquin Park, Ny-Alesund, Onsala and Wettzell. As already indicated in Table 4.3, the meteorological files for Kokee Park should not be used due to wrong temperature and humidity values. But the WVR running there recorded the meteorological conditions as well and these data can be used instead, although they do not cover the whole time span of CONT02.

For the other stations, some assumptions or restrictions had to be made in order to derive values for the differential troposphere delay. The meteorological files for Westford contain only good pressure measurements (see Table 4.3) so that they are not usable whereas the meteorological records of the WVR seem to be alright. Unfortunately, the height of the WVR relative to the other instruments is missing so that the meteorological measurements cannot be extrapolated to the exact heights. However, tests using varying heights for the WVR showed that the influence of the height uncertainty on the troposphere tie can be neglected. The reference height of the WVR at Westford can vary more than 200 m without having a significant effect – larger than 0.01 mm – on the differential troposphere ZD between VLBI and GPS. Such a height difference between the WVR and the GPS or VLBI antenna seems to be unrealistic, hence, the reference height for the WVR was set equally to that of GPS.

Similar tests were done for the station Fairbanks as well, as the reference height of the meteorology sensor is not available there, but the data themselves seem to be usable. Unfortunately, the level of 0.01 mm for

changes in the troposphere tie is already exceeded for variations in the reference height of the meteorological sensor of about 20 m. This range allowed for the reference height is quite small compared to Westford, but this must be explained by the larger height difference between GPS and VLBI (about 13 m for Fairbanks compared to only 1.7 m for Westford). Nevertheless, there is no other possibility than making an assumption about the reference height of the meteorology sensor if the data should be used. Therefore, the height of GPS was taken as reference height, though the uncertainty of this setting should be kept in mind.

Finally, the humidity values for the station Hartebeesthoek are artificial values (i.e. constant) for the first three days (October 16-18) according to *IVS Analysis Mail No. 1005*, and, additionally, the height information is missing. Neglecting the wrong humidity values from the first days, the test with a varying reference height for the meteorology sensor described above was carried out for Hartebeesthoek as well, revealing that a height difference of more than +/- 100 m w.r.t. GPS has no influence on the troposphere tie. Due to this behavior it was decided to proceed in the same way as for the other stations and assume identical heights for GPS and the meteorology sensor.

All in all, with the assumptions described above it is possible to derive troposphere ties for all eight co-locations. The time-series of troposphere ties computed for each epoch of meteorological records are displayed in Fig. 5.1. The resulting mean values over 14 days together with their standard deviation and the corresponding height difference are listed in Table 5.1.

Finally, the fourth method of computing troposphere ties – called "solution" – bases on the troposphere estimates derived from the space-geodetic techniques themselves. In a first step, either single-technique solutions are computed, or a multi-technique solution is computed but without combining the troposphere ZD (i.e., only station coordinates and EOP are combined). Then, the weighted mean biases between the GPS- and VLBI-derived time-series are derived for each co-location, and these values will be applied as troposphere ties in a subsequent combination. The advantage of this method must be seen in the fact that the troposphere ties neither rely on a standard atmosphere, that might be inadequate for the stations, nor on meteorological data that are often dubious, as explained before. However, any systematic bias between the space-geodetic techniques that shows up in the troposphere ZD but does not belong to real meteorology will stay in the troposphere estimates. Of course, values for this method cannot be given in advance of analyzing the space-geodetic solutions. Thus, it is referred to *Chapter 6*.
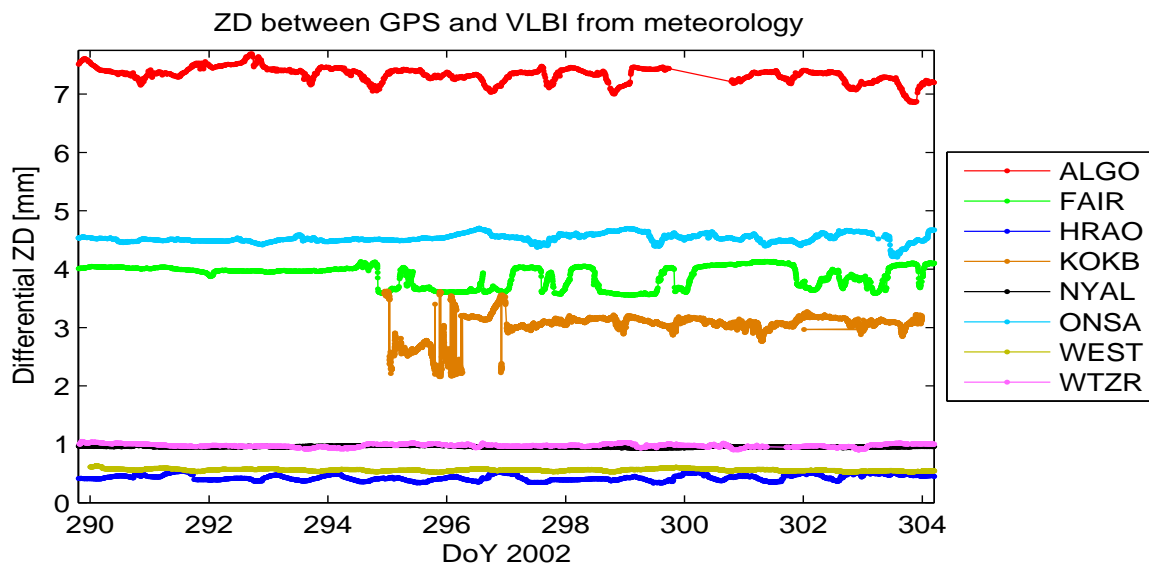


*Figure 5.1: Troposphere ties for the difference GPS – VLBI computed with meteorological data.*

An alternative option might be to set up a bias parameter between the GPS- and VLBI-derived troposphere ZD, so that only the temporal behavior of both time-series is tied together but the absolute value of the difference is determined by the space techniques instead of introducing a "known" value. But this method of combination was not tested for this thesis. Similar to the fourth method described above ("solution"), the estimated bias does not necessarily contain only meteorological information, but systematic effects might be contained therein, too.

Considering the temporal variations of the troposphere ties derived from meteorological data, the question arises whether it will be sufficient to use a mean value over 14 days or whether it is necessary to compute the instantaneous value for each epoch of the comparison or combination. Looking at the variation of the values in Fig. 5.1 and taking into account the standard deviations listed in Table 5.1 there exist probably no general answer to this question. For the stations Ny-Alesund, Westford, Wettzell and Hartebeesthoek it should be definitely sufficient to use a mean value whereas for Algonquin, Fairbanks and Kokee Park it seems to be worthwhile to test whether epoch-wise values should be used. Although only the first two days are responsible for the comparatively large standard deviation for Kokee Park. Assuming a malfunctioning of the WVR at the beginning and considering only the values starting with DoY 297, the corresponding differential zenith total delay is 3.09 mm with a standard deviation of only 0.07 mm. This situation is comparable to Onsala where the variations become larger only during the last days. Thus, both stations probably mark an edge case concerning the necessity of epoch-specific troposphere ties or a mean value. The effect of averaging the troposphere ties over 14 days instead of using epoch-wise values will be discussed in *Chapter 6*.

Summarizing the processing strategy in terms of troposphere ties, the values derived with the first three methods described above are listed in Table 5.2. It is astonishing that the rule of thumb is quite close to the true meteorological conditions (as a mean value), at least if the height difference is not too large. More precisely, if the height difference is clearly below ten meters (so for Hartebeesthoek, Ny-Alesund, Westford and Wettzell) it might be sufficient to apply only the rule of thumb instead of reverting to the meteorological measurements and their complex handling. A final statement about the necessity of meteorological data for troposphere ties will be given after analyzing the VLBI and GPS combination results in *Chapter 6*.

**Table 5.1:** *Differential troposphere ZD between GPS and VLBI reference points using true meteorological data (given as GPS – VLBI in [mm]). The last column indicates how much the real reference height of the meteo sensor can vary without changing the troposphere tie by more than 0.01 mm.*

|          | *Height diff. VLBI – GPS [m]* | *Mean total ZD* | *Mean ZD dry part* | *Mean ZD wet part* | *Assumption* | *Scope for height* |
|----------|-------------------------------|-----------------|--------------------|--------------------|--------------|--------------------|
| *ALGO*   | 23.100                        | $7.33 \pm 0.13$ | $6.52 \pm 0.11$    | $0.81 \pm 0.19$    |              |                    |
| *FAIR*   | 13.056                        | $3.90 \pm 0.18$ | $3.60 \pm 0.07$    | $0.30 \pm 0.13$    | $h_{Meteo} = h_{GPS}$ | 20 m          |
| *HRAO*   | 1.527                         | $0.43 \pm 0.05$ | $0.35 \pm 0.01$    | $0.08 \pm 0.05$    | $h_{Meteo} = h_{GPS}$ | 100 m         |
| *KOKB*   | 9.243                         | $3.04 \pm 0.21$ | $2.20 \pm 0.02$    | $0.84 \pm 0.21$    |              |                    |
| *NYAL*   | 3.101                         | $0.96 \pm 0.01$ | $0.91 \pm 0.01$    | $0.05 \pm 0.01$    |              |                    |
| *ONSA*   | 13.710                        | $4.53 \pm 0.08$ | $3.82 \pm 0.07$    | $0.71 \pm 0.13$    |              |                    |
| *WEST*   | 1.735                         | $0.56 \pm 0.02$ | $0.49 \pm 0.01$    | $0.06 \pm 0.02$    | $h_{WVR} = h_{GPS}$ | > 200 m        |
| *WTZR*   | 3.101                         | $0.98 \pm 0.03$ | $0.81 \pm 0.01$    | $0.17 \pm 0.03$    |              |                    |

**Table 5.2:** *Differential troposphere ZD between GPS and VLBI reference points computed with different methods (given as GPS – VLBI in [mm]).*

|        | Height diff. VLBI – GPS [m] | Rule of thumb | Saastamoinen dry part + standard atmosphere | Saastamoinen + meteorological data (mean value) |
|--------|-----------------------------|---------------|---------------------------------------------|-------------------------------------------------|
| **ALGO** | 23.100 | 6.93 | 6.17 | 7.33 |
| **FAIR** | 13.056 | 3.92 | 3.46 | 3.90 |
| **HRAO** | 1.527  | 0.46 | 0.37 | 0.43 |
| **KOKB** | 9.243  | 2.77 | 2.24 | 3.04 |
| **NYAL** | 3.101  | 0.93 | 0.84 | 0.96 |
| **ONSA** | 13.710 | 4.11 | 3.72 | 4.53 |
| **WEST** | 1.735  | 0.52 | 0.47 | 0.56 |
| **WTZR** | 3.101  | 0.93 | 0.79 | 0.98 |

### b) Relative weighting of normal equation systems

A further aspect in the combination is the weighting of different input normal equation systems as, normally, it is not reasonable to stack them as they are. The weighting is done by analyzing the main-diagonal of the normal equation matrix together with the repeatability of the station coordinates. Although this method is not as sophisticated as a variance component estimation, it works quite well. It was already applied for the studies related to the "IERS SINEX Combination Campaign" done by *Thaller and Rothacher (2003)* and bases on two ideas: First, the repeatability of station coordinates can be used as an indicator for the quality of a solution series, and, the second idea is that the size of the main-diagonal element of the normal equation matrix is correlated with the weight of the corresponding parameter in the solution. *Chapter 5.2.1* will give the details how the coordinate repeatability is computed. Now, for the purpose of deriving weighting factors, the repeatabilities are assumed to be already known for all solution series subdivided into values $r_{North}$, $r_{East}$, $r_{Height}$ for the components north, east and height, respectively. Then, the quadratic mean value of the three components

$$r^2 = \frac{r_{North}^2 + r_{East}^2 + r_{Height}^2}{3} \tag{5.4}$$

is computed for each solution series. Applying the principle that a solution series with a better repeatability (i.e., a smaller value $r$) should have a larger influence on the combined solution, a factor $w_{rep\,ij}$ for weighting the system of normal equations $j$ w.r.t. the system $i$ according to their coordinate repeatabilities can be derived:

$$w_{rep_{ij}} = \frac{r_i^2}{r_j^2} \; . \tag{5.5}$$

The main-diagonal elements of the normal equation matrix $N$ are still missing in the weighting factor (5.5). For this part, only the station coordinates are taken into account, as they are those parameters with the closest connection to the observations, e.g., the Earth orientation parameters are derived by a kind of summation over all observing stations and therefore the number of observations (i.e., the number of stations) highly influences the size of the corresponding main-diagonal elements of $N$. The mean value $N_{mean}$ of all main-diagonal elements of $N$ corresponding to station coordinate parameters is computed for each normal equation system ($n_{crd}$ denoting the number of contributing parameters):

$$N_{mean} = \frac{\sum\limits_{i\,=\,1}^{n_{crd}} N_{ii}}{n_{crd}} \quad . \tag{5.6}$$

Finally, together with (5.5), the complete factor for weighting a system of normal equations *j* w.r.t. the system *i* is given by:

$$w_{ij} = \frac{N_{mean_i}}{N_{mean_j}} \cdot w_{rep_{ij}} \quad . \tag{5.7}$$

The values for the weighting factors (5.7) applied in the work presented here are given in *Chapter 6.1* after analyzing the coordinate repeatability of the single-technique solutions (see Table 6.4).

### c) Datum information delivered by the space techniques

It has been already mentioned that the space techniques have different strengths in view of determining geodetic parameters. Concerning the definition of the terrestrial reference frame (TRF) none of the techniques can contribute to the orientation of the TRF so that the degrees of freedom of the normal equation system always contain three rotations. In order to remove this degree of freedom, so-called no-net-rotation conditions (NNR) are applied to the normal equation system for all the solutions computed hereafter. NNR conditions are free-network restrictions described in *Chapter 2.6.2* using only the rotational part. Normally, the free-network conditions are based on a subset of stations instead of the whole network because only good stations should be used for the reference frame. About 90 stations are used for NNR in case of a GPS-only solution, 14 stations for an SLR-only solution and all eight available stations for a VLBI-only solution. In order to get the most stable datum definition for the combined solution, the NNR condition is set up only for the 90 GPS stations, whereas the VLBI and SLR networks are attached by the LT.

The different potential of the techniques in view of defining the geodetic datum becomes visible in the translational part and in the definition of the scale. VLBI, as a purely geometric technique, has no access to the geocenter and therefore the translations are arbitrary and are handled by a no-net-translation condition (NNT) using all eight VLBI stations. The satellite techniques are coupled with the gravity field (including the geocenter) by the orbits. However, the higher the satellite the smaller is its sensitivity to the gravity field of the Earth. Hence, SLR measurements to LAGEOS1 and -2 have a better capability of determining the geocenter than GPS. In case of a combination of both techniques this implies that two independent determinations of the geocenter are present, one from SLR and one weaker estimation from GPS, and both are competing for the definition of the common reference frame. Generally speaking, the geocenter seen by SLR should be more accurate due to the reason mentioned above. Thus, it is often desired to define the origin of the TRF solely by SLR as it is done for the realizations of the International Terrestrial Reference System (ITRS) by, e.g., *Boucher et al. (2004)*. In order to eliminate the contribution of GPS to the combined geocenter solution its translational degrees of freedom have to be fully opened. This is done by introducing three translation parameters for the GPS normal equation system w.r.t. the combined solution. A similar method is applied concerning the scale of the combined network as all techniques contribute to the scale but with different values and different quality. Either the scale of the combined network is a kind of weighted mean or one technique is selected as reference and a scale parameter is estimated for each of the other contributions. Often, SLR or VLBI or the sum of both is selected as reference, as the scale derived from GPS is affected by wrong phase center values for satellite and ground station antennas. In the ITRF2000 solution, a weighted mean scale from selected VLBI and SLR solutions was chosen as reference, whereas a scale parameter was estimated for the other techniques, i.e., GPS and DORIS (see *Altamimi et al., 2002*). Fortunately, the usage of absolutely calibrated phase centers and their variation for ground station and satellite antennas significantly reduces the scale difference of GPS solutions compared to other techniques (see *Chapter 5.1.2*).

The general theory for expanding the normal equation system with Helmert parameters has been given in *Chapter 2.7.1*. In the special cases described above, the Helmert parameters are estimated as technique-specific parameters and only those related to the regained degrees of freedom are set up instead of all seven pa-

rameters contained in the formulas. The impact of estimating a scale parameter or translations for GPS on the combined solution is studied in *Chapter 6.2.3*.
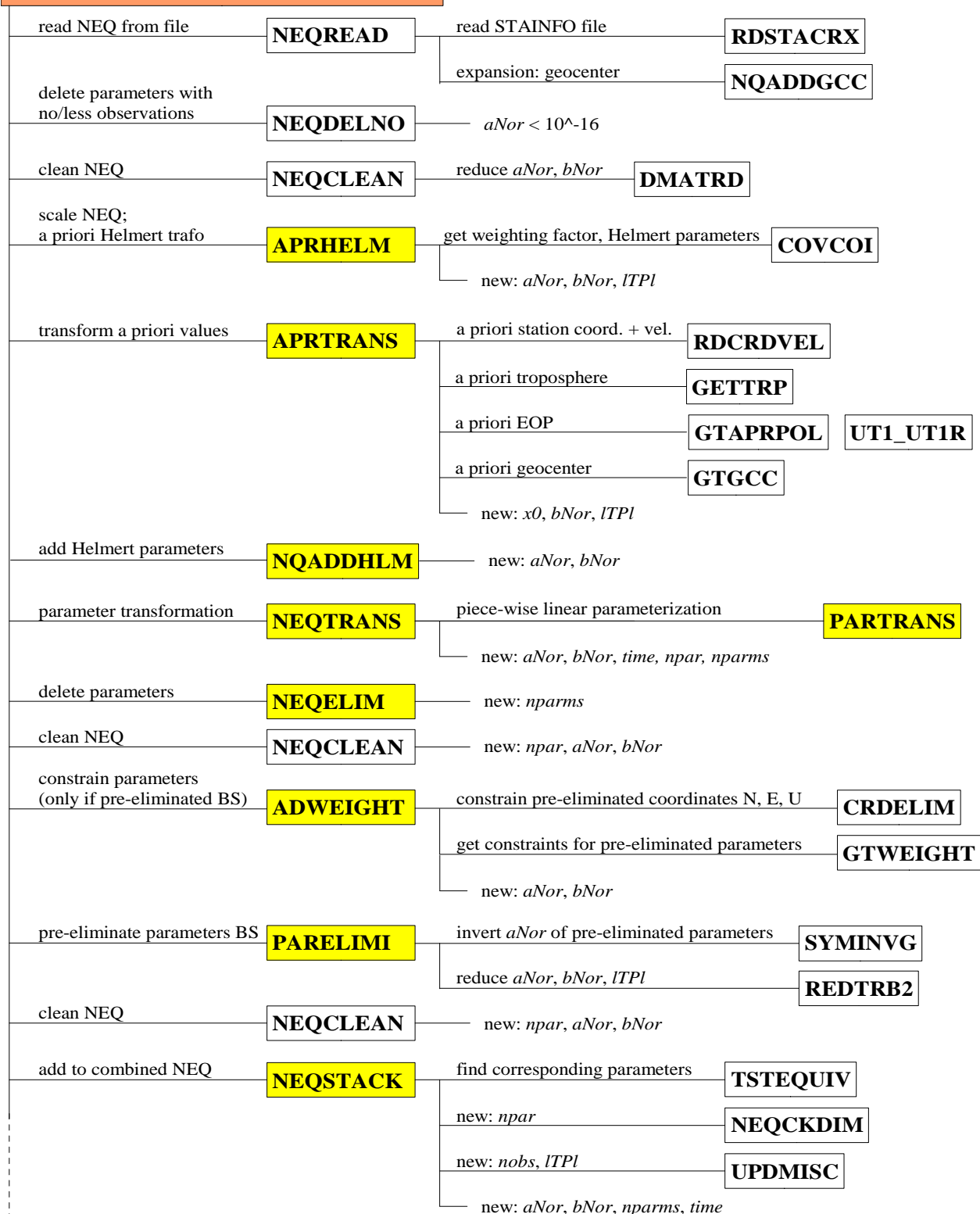
### d) Combination program ADDNEQ2

Finally, it is worthwhile to give an overview of the program used for the combination studies and address some special aspects. The program ADDNEQ2 is included in the Bernese GPS Software (*Dach et al., 2007*) and is described in detail by *Mervart (2000)*. Roughly speaking, the program is subdivided into three major parts:

  – part 1: operations with the individual input normal equation systems (NEQ) and stacking them into one combined NEQ;
  – part 2: operations with the combined NEQ;
  – part 3: comparison of the combined solution with solutions derived for each individual NEQ.

A flowchart for the first two parts of ADDNEQ2 is displayed in Fig. 5.2 and Fig. 5.3 and the shaded subroutines will be discussed in the following as they cover the main topics of the combination process. The other subroutines deal mainly with book-keeping, mathematical operations, reading information from files and storing information into files. The short notices included in the flowcharts should indicate which parts of the normal equation system and its related information are affected by the operations carried out by the appropriate subroutine: *aNor* and *bNor* stand for the matrix and the vector of the right-hand side of the normal equation system, respectively, *lTPl* is the weighted square sum of "observed–computed", *x0* contains the a priori values of the parameters, *npar* is the number of parameters actually contained in the NEQ whereas *nparms* is the total number of parameters (i.e., including all pre-eliminated parameters), *nobs* is the number of original observations and *time* contains the validity epochs of the estimated parameters.

Starting with the first part of ADDNEQ2, each individual input normal equation system is treated one by one and all operations that have to be done before the stacking of the input NEQs are carried out. The application of the weighting factor according to (5.7) (*Chapter 2.2*, APRHELM) belongs to this part as well as the transformation from NEQ-specific a priori values to unified a priori values for the estimated parameters (*Chapter 2.3.1*, APRTRANS). If Helmert parameters for the appropriate normal equation system have to be set up due to any reason described in the previous *Chapter 5.1.1d* the normal equation system is expanded with the required translations, rotations or scale parameters (*Chapter 2.7.2*, NQADDHLM). The subroutines named NEQTRANS and PARTRANS perform the change in the representation of the parameters from one offset plus drift per epoch to a piece-wise linear polygon parameterization according to the formulas given in *Chapter 2.3.2*. Furthermore, a reduction of the temporal resolution of parameter types, e.g., from hourly values to daily values, is done by this subroutine as well. Parameters to be deleted are handled in NEQELIM by canceling the corresponding rows and columns of the normal equation system so that the parameters are implicitly fixed on their a priori values. Concerning the pre-elimination of parameters (*Chapter 2.4*, PARELIMI) the user has the choice whether the parameter should be pre-eliminated before stacking, i.e., for each normal equation system separately, or if the parameter should be stacked with those of other normal equation systems first, and then the combined parameter is pre-eliminated (i.e., pre-eliminated after stacking). Therefore, the subroutine PARELIMI is called in both parts of ADDNEQ2 but it is executed in each case only for those parameters that have to be pre-eliminated before (BS) respectively after (AS) the stacking of all input NEQs. Before the parameters are pre-eliminated it is checked in ADWEIGHT, whether a constraint should be added to them. After all these operations mentioned above have been carried out, the single input normal equation system is added to the combined NEQ and identical parameters are stacked according to the algorithm given in *Chapter 2.5* (NEQSTACK).

**ADDNEQ2:** Part 1 (individual NEQs)

| | | | | |
|---|---|---|---|---|
| read NEQ from file | **NEQREAD** | read STAINFO file | **RDSTACRX** | |
| | | expansion: geocenter | **NQADDGCC** | |
| delete parameters with no/less observations | **NEQDELNO** | *aNor* < 10^-16 | | |
| clean NEQ | **NEQCLEAN** | reduce *aNor*, *bNor* | **DMATRD** | |
| scale NEQ; a priori Helmert trafo | **APRHELM** | get weighting factor, Helmert parameters | **COVCOI** | |
| | | new: *aNor*, *bNor*, *lTPl* | | |
| transform a priori values | **APRTRANS** | a priori station coord. + vel. | **RDCRDVEL** | |
| | | a priori troposphere | **GETTRP** | |
| | | a priori EOP | **GTAPRPOL** | **UT1_UT1R** |
| | | a priori geocenter | **GTGCC** | |
| | | new: *x0*, *bNor*, *lTPl* | | |
| add Helmert parameters | **NQADDHLM** | new: *aNor*, *bNor* | | |
| parameter transformation | **NEQTRANS** | piece-wise linear parameterization | **PARTRANS** | |
| | | new: *aNor*, *bNor*, *time*, *npar*, *nparms* | | |
| delete parameters | **NEQELIM** | new: *nparms* | | |
| clean NEQ | **NEQCLEAN** | new: *npar*, *aNor*, *bNor* | | |
| constrain parameters (only if pre-eliminated BS) | **ADWEIGHT** | constrain pre-eliminated coordinates N, E, U | **CRDELIM** | |
| | | get constraints for pre-eliminated parameters | **GTWEIGHT** | |
| | | new: *aNor*, *bNor* | | |
| pre-eliminate parameters BS | **PARELIMI** | invert *aNor* of pre-eliminated parameters | **SYMINVG** | |
| | | reduce *aNor*, *bNor*, *lTPl* | **REDTRB2** | |
| clean NEQ | **NEQCLEAN** | new: *npar*, *aNor*, *bNor* | | |
| add to combined NEQ | **NEQSTACK** | find corresponding parameters | **TSTEQUIV** | |
| | | new: *npar* | **NEQCKDIM** | |
| | | new: *nobs*, *lTPl* | **UPDMISC** | |
| | | new: *aNor*, *bNor*, *nparms*, *time* | | |

**ADDNEQ2:** Part 2 (combined NEQ)

***Figure 5.2:*** *Flowchart of the first part of ADDNEQ2 (shaded elements are mentioned in the text).*

**ADDNEQ2:** Part 2 (combined NEQ)

transform a priori values   **APRTRANS**

a priori station coordinates and velocities   **RDCRDVEL**

a priori troposphere   **GETTRP**

a priori EOPs   **GTAPRPOL**   **UT1_UT1R**

a priori geocenter   **GTGCC**

new: *x0*, *bNor*, *lTPl*

constrain parameters (only if pre-eliminated AS)   **ADWEIGHT**

constrain pre-eliminated coordinates N, E, U   **CRDELIM**

get constraints for pre-eliminated parameters   **GTWEIGHT**

new: *aNor*, *bNor*

pre-eliminate parameters AS   **PARELIMI**

invert aNor of pre-eliminated parameters   **SYMINVG**

reduce *aNor*, *bNor*, *lTPl*   **REDTRB2**

clean NEQ   **NEQCLEAN**   new: *npar*, *aNor*, *bNor*

sort parameters within NEQ   **NEQSORT**   new: *aNor*, *bNor*, *x0*

save NEQ in file   **NEQSTORE**

save general information   **NQWTHEAD**

save: *aNor*, *bNor*, *x0*, *name*, *time*

constrain parameters   **ADWEIGHT**

suppress retrograde diurnal polar motion   **BLOCKRET**

free network restrictions (coord. + vel.)   **FREENET**

constrain coordinates N, E, U   **CRDELIM**

absolute + relative constraints   **GTWEIGHT**

introduce ties (coord. + trop.)   **ADDTIE**

new: *aNor*, *bNor*

compute solution   **NEQSOLVE**   invert *aNor* and solve NEQ   **SYMINVG**   **SOLVE**

print results for output   **NEQPRT**

save parameters in files   **CRDSTORE**   **TRPSTORE**   **POLSTORE**

**ADDNEQ2:** Part 3 (comparison)

***Figure 5.3:*** *Flowchart of the second part of ADDNEQ2 (shaded elements are mentioned in the text).*

The second part of ADDNEQ2 is dealing only with the combined normal equation system. The parameter pre-elimination after the stacking of all input NEQs was already mentioned above and here as well, constraints are added if the pre-eliminated parameters are included in any of the constraining options. After the pre-elimination step in the second part, the free normal equation system including all parameters that should be solved for is prepared so that the datum definition and all other constraints can be applied. The following methods are possible: an absolute constraining of the parameters w.r.t. their a priori values (*2.6.1*, GT-WEIGHT), the application of free-network restrictions to the TRF (*2.6.2*, FREENET), the suppression of a retrograde diurnal polar motion term if sub-daily pole coordinates are estimated together with nutation (*2.6.4*, BLOCKRET), and the introduction of local ties and troposphere ties for the combination of station coordinates and troposphere parameters, respectively (*2.6.3*, ADDTIE). The combined normal equation system including all constraints should no longer contain any rank deficiency. Hence, it should be solvable and the parameters including their variance-covariance matrix are computed (*2.1*, NEQSOLVE).

The third part is optional and executed only if the single solutions, that can be derived for each input normal equation system separately, should be compared to the combined solution computed in part two. In that case, all options concerning parameter pre-elimination, parameterization and constraining are applied to each individual NEQ in the same way as it was done for the combined NEQ in the first two parts. Afterwards, a seven-parameter Helmert transformation between each single solution and the combined solution is performed and the resulting coordinate residuals of all single solutions are used to compute the repeatabilities of station coordinates (see *Chapter 5.2.1*).

## 5.1.2  Generation of daily single-technique normal equation systems

At the beginning of this chapter some general remarks on the generation of the normal equation systems for CONT02 will be given before some special topics related to each of the three techniques VLBI, GPS and SLR will be explained.

*a) General remarks on the alignment of the analyses*

As described in *Chapter 5.1.1*, a combination based on normal equation systems can be rigorous only if the a priori models and the parameterization of all parameters common to at least two techniques are unified in all software packages used for generating the single-technique normal equation systems. This adaptation was done thoroughly with the models listed in Table 5.3. Therefore, a combination on the normal equation level using these NEQs approaches a combination on the observation level. The estimated parameters, their parameterization and temporal resolution are summarized in detail in Table 5.4. The distinction between the original daily NEQs and the 14-day NEQs concerning the temporal resolution is necessary, because later on all 14 daily normal equation systems will be stacked together to obtain a more stable reference frame and then the temporal resolution of some parameter types is changed: Only one set of station coordinates is estimated over the whole time span and the nutation is parameterized as only one straight line over 14 days with two offsets, i.e., one at the beginning epoch and one at the ending epoch. Looking at the nutation in Table 5.4, one of the two remaining differences between the parameterization used for the normal equation systems becomes visible notwithstanding the adaptations of the software packages. However, both differences are not thought to be critical. Normally, the changes in the nutation corrections $\Delta\varepsilon$ and $\Delta\psi$ over one day are very small so that the difference between one constant value and a linear function is negligible. In case of the 14-day NEQs, the daily nutation offsets can easily be transformed into the fortnightly polygon.

The troposphere horizontal gradients in north and east direction are represented in the VLBI normal equation systems as one constant offset over the whole day, hence inducing a jump at the day boundaries. In contrary, the GPS normal equation systems contain two offsets per day (0:00 and 24:00) with a linear connection of both so that the offset at 24:00 of one day can be stacked with that at 0:00 of the following day if all 14 NEQs are stringed together. The combination of VLBI- and GPS-derived gradients with such different representations is thought to cause no large problems because the VLBI offset at the middle of the day can be "woven" into the GPS-derived polygon if the matrix given in Eq. (2.29) is restricted to the first row.

One part in the analysis models that was not unified is the mapping function applied for the troposphere gradient estimation. In the case of GPS, the partial derivative of the ZD mapping function w.r.t. the zenith angle is applied to the gradients (which is approximately "tan $z$ / cos $z$"), whereas the mapping function itself multiplied by "tan $z$" is used in the VLBI analysis (see *MacMillan, 1995*). The difference between both representations is extremely small in its influence on the estimated parameters. From analyzing a global GPS network

with both methods of mapping the gradients it turned out that the station coordinates differ by less than 1 mm: 0.71 mm in north, 0.05 mm in east and 0.29 mm in height as a mean value over all stations (*P. Steigenberger, personal communication*).

Another aspect that should be mentioned in the context of troposphere ZD is the usage of identical a priori values for the VLBI and the GPS analyses although the different reference heights would lead to slightly different a priori values using the Saastamoinen model for the hydrostatic delay. However, as the height differences are not so big (see Table 5.1) and the combination of the ZD is more straight forward if the a priori values are identical, it was decided to use the Saastamoinen value corresponding to the GPS reference height for the co-located VLBI station as well. Consequently, the troposphere estimates from VLBI contain not only the wet delay and a correction for the hydrostatic delay deviating from the a priori model, but the total troposphere delay due to the atmospheric layer between the GPS and VLBI reference height is additionally included in the estimates. However, the delay caused by different reference heights has to be taken into account in comparisons with the GPS estimates anyway.

Concluding the general remarks on the daily single-technique normal equation systems for CONT02, a statistical summary is compiled in Table 5.5 to give an idea about the average dimension of a daily normal equation system due to the settings described above. It must be pointed out that, indeed, the number of GPS observations exceeds that of the other techniques by orders of magnitude. However, the number of parameters, that have to be estimated, does as well. The original set-up of unknown parameters includes, amongst others, orbit parameters in the case of GPS and SLR, phase ambiguities in the case of GPS and all troposphere parameters for the GPS stations not co-located with VLBI.

*Table 5.3: List of adapted a priori models for the software packages used.*

|  | ***A priori model*** |
| --- | --- |
| ***Solid Earth tides*** | Subroutine provided by V. Dehant |
| ***Pole tide*** | Mean pole values |
| ***Ocean loading*** | Files *.BLQ provided by H.-G. Scherneck[19] |
| ***ERP and interpolation*** | IERS C04 (*Gambis, 2004*) with linear interpolation |
| ***Sub-daily Earth rotation*** | IERS Conventions 2003 (*McCarthy and Petit, 2004*) |
| ***Nutation*** | IAU2000 (*Mathews et al., 2002*); parameters $\Delta\varepsilon$, $\Delta\psi$ |
| ***Troposphere delays*** | Hydrostatic part of the model developed by *Saastamoinen (1973)* with a standard atmosphere according to *Berg (1948)* for the GPS height |
| ***Troposphere mapping function*** | Niell mapping function (*Niell, 1996*); dry part for a priori values, wet part for estimated corrections |

*Table 5.4: Parameterization and temporal resolution of common parameters.*

|  | ***Temporal resolution in daily NEQs*** | ***Temporal resolution in 14-day NEQ*** | ***Parameterization*** |
| --- | --- | --- | --- |
| ***Station coordinates*** | daily | fortnightly | constant offset |
| ***Polar motion, UT1-UTC*** | 1 hour | 1 hour | piece-wise linear polygon |
| ***Nutation $\Delta\varepsilon$, $\Delta\psi$ (daily VLBI / others)*** | daily | fortnightly | constant offset / piece-wise linear polygon |
| ***Troposphere ZD*** | 1 hour | 1 hour | piece-wise linear polygon |
| ***Troposphere gradients (GPS-only / VLBI-only / combination)*** | daily | daily | piece-wise linear polygon / constant offset / piece-wise linear polygon |

---

19 *http://www.oso.chalmers.se/~loading*

## b) VLBI analysis

Starting with the observations contributing to one normal equation system, it was already indicated before that daily NEQs build the basis for this work. More precisely, daily means a time span starting at 0:00 UTC and ending at 24:00 UTC. Looking at the VLBI contribution this definition of "daily" requires that the VLBI data are concatenated and regrouped because the original boundary for the sessions was 18:00 UTC. In order to include only days with 24 hours of VLBI observations, the normal equation systems for the combination studies were generated only for October 17 until October 30, i.e., altogether 14 days.

The analysis of the VLBI observations was carried out with the OCCAM software version 5.0 (*Titov et al., 2001*) at DGFI (Deutsches Geodätisches Forschungsinstitut). Using improved values for the antenna axis offsets provided by the *IVS Analysis Coordinator (2005)* led to a higher consistency with other space techniques. The eight participating VLBI stations are already displayed in Fig. 4.1. Unfortunately, there is some outage at Algonquin Park for the session 300, i.e., October 26, 18:00 until October 27, 18:00. Additionally, Wettzell and Kokee Park are missing for about one hour for several days due to the intensive sessions (see *Chapter 3.2.3*).

As an output, datum-free daily normal equation systems were stored in SINEX files to enable an exchange with the Bernese GPS Software that was used for the subsequent combination studies.

*Table 5.5:* *Statistical summary for daily NEQs (average over all 14 daily NEQs).*

|                                              | *VLBI* | *GPS*  | *SLR* |
|----------------------------------------------|--------|--------|-------|
| *# Observations*                             | 3334   | 423983 | 363   |
| *# Stations*                                 | 8      | 153    | 22    |
| *# ERP (pole coordinates, UT1-UTC)*          | 75     | 75     | 75    |
| *# Nutation ($\Delta\varepsilon, \Delta\psi$)* | 2      | 4      | 4     |
| *# Troposphere ZD (8 co-locations)*          | 200    | 200    | -     |
| *# Troposphere gradients (8 co-locations)*   | 16     | 32     | -     |

## c) GPS analysis

The situation concerning the exchange of the unconstrained daily normal equation systems is simplified in the case of GPS as the analysis as well as the combination have been done using the Bernese GPS Software Version 5.0 (see *Dach et al., 2007*). Thus, the normal equation systems including the whole information are already available in the software internal file format so that the way via SINEX can be skipped. Altogether 153 globally distributed stations, including the eight co-locations with VLBI (see Fig. 5.4), contributed to the GPS network used for the studies of this thesis.

A very important topic about the GPS processing is the usage of absolute phase center calibration values for the ground station antennas as well as for the satellite antennas. The details were already given in *Chapter 3.1.2*. In view of the combination with other space-geodetic techniques, the benefit of using absolute PCV must be seen in an overall improvement of the GPS solution (see *Schmid et al., 2007*), and especially in a clear reduction of the scale difference between the networks. As the scale of a network is correlated with station heights and troposphere ZD it is essential for the work presented here. As already mentioned in *Chapter 3.1.2* and published by *Schmid et al. (2005)*, the station heights changed by about 8 mm at mean and the troposphere ZD by several millimeters due to applying an absolute instead of a relative antenna phase center modeling. Thus, the influence of the phase center modeling is not negligible.

In view of a successful combination of *UT1-UTC / LOD* with VLBI, it is important to mention that constraints have not been applied to the GPS orbits. The arc length for the GPS orbits is one day.

## d) SLR analysis

The detour via SINEX files can be avoided not only for the GPS normal equations but also for the SLR normal equations, because they were also generated with the Bernese GPS Software. At a first glance, this pro-

cedure seems to be astonishing as it is not yet confirmed that this SLR-only solution can reach the quality of any solution provided by the ILRS Analysis Centers. However, one focal point of this thesis is the usage of highly consistent normal equation systems for the combination and it was not possible to get normal equation systems for SLR that were derived with one of the software packages used by the ILRS Analysis Centers but adopting all the pre-defined common a priori models and parameterizations listed in *Section a* of this chapter. In contrast, using the Bernese GPS Software for the SLR analysis guarantees that the SLR normal equation systems are consistent with the GPS normal equation systems. Thus, after balancing the pros and cons of using Bernese-derived SLR normal equation systems for the combination studies instead of reverting to official SLR solutions it was decided that the arguments in favor prevail for these special studies.

It must be clarified that, of course, the SLR-only solution generated here for the CONT02 campaign cannot be used to derive general statements about the quality of SLR. Especially when choosing the high temporal resolution for ERP listed in Table 5.4 it is clear that SLR has not the capability to do this on its own. Therefore, we will switched to daily values when ERP estimated solely by SLR are analyzed in *Chapter 6.1*. But even the official ILRS solutions containing daily ERP show that SLR cannot deliver strong contributions to the estimation of ERP anyway, as it has been demonstrated amongst others in the IERS SINEX Combination Campaign (e.g. *Thaller and Rothacher, 2003*). Thus, SLR will easily adapt to the ERP given by GPS and VLBI in a combination, independent whether a sub-daily or daily resolution was chosen. The benefit from SLR must be seen in a more stable definition of the geocenter and scale of the network as it has been already indicated in *Chapter 5.1.1*. Furthermore, SLR can probably help to decorrelate station coordinates and troposphere parameters derived from the microwave techniques if a co-location with SLR is available. For more details about this topic it is referred to *Chapter 5.3*.

A total number of 22 globally distributed SLR stations were selected for the SLR solutions generated for the CONT02 period as displayed in Fig. 5.4 and observations to the satellites LAGEOS1 and LAGEOS2 were analyzed. Here as well, it must be emphasized that the orbital elements contained in the NEQs are free, i.e., without any constraint. Contrary to the GPS orbits, the orbits of both LAGEOS satellites were compiled for one week in order to get more stable orbits and, thus, a more stable reference frame.
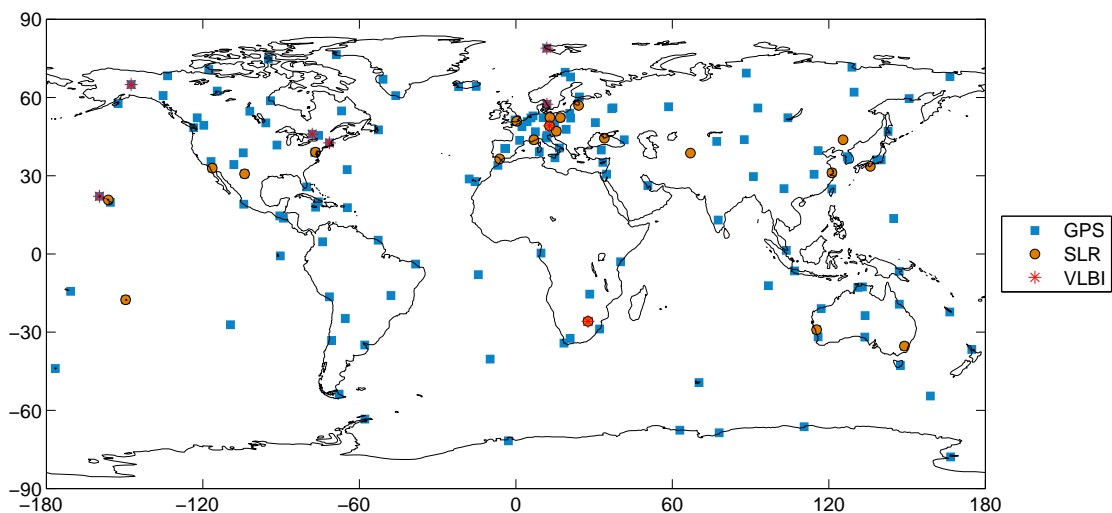


**Figure 5.4:** *Map of VLBI, GPS and SLR stations for the analysis of CONT02.*

# 5.2 Validation criteria

An important step in the analyses of solutions is the validation of the results. For this purpose objective criteria are necessary for all parameter types estimated in the solutions. In order to give the background of the validation criteria before the analyses of the solutions are done, the following sub-chapters will explain those

criteria that have been applied in the CONT02 studies starting with a special criterion dedicated to the terrestrial reference frame (*Chapter 5.2.1*). The other two chapters describe criteria for all parameter types using external data sets (*Chapter 5.2.2*) and a sort of internal validation, namely the comparison with the single-technique solutions (*Chapter 5.2.3*).

## 5.2.1  Repeatability of station coordinates

The stability of the reference frame can be expressed by means of the repeatability of the station coordinates. Repeatability in this context is the measure to which extent the terrestrial reference frame can be reproduced with another set of data, i.e., observations of another day but applying the identical datum definition. In the case of CONT02 the consistency of all single-day solutions with the 14-day combined solution gives the background for the repeatabilities. The only difference that is allowed between the solutions is a seven-parameter Helmert transformation. Therefore, every daily solution is transformed onto the two-week solution using all stations. The resulting coordinate residuals $v$ from all 14 transformations build the basis for computing the station-specific repeatability:

$$r_{ista} = \sqrt{\frac{\sum_{i=1}^{nsol} v_i^2}{nsol - 1}} \tag{5.8}$$

with *nsol* being the number of solutions where the considered station *ista* is included, i.e., for the major part of the stations this will be equal to 14 in case of the CONT02 analyses. It must be mentioned that the residuals $v$ and the repeatabilities $r_{ista}$ are separated into the three coordinate components of a topocentric system. Therefore, altogether three values for the station-specific repeatability are computed according to (5.8): $r_{ista, North}$, $r_{ista, East}$, $r_{ista, Height}$. On the basis of the repeatability values it becomes obvious how well each station fits into the datum definition. Furthermore, daily solutions with a notably bad determination of the station coordinates can be detected by looking at the residuals of each single solution. It is clear that a sufficient number of single solutions *nsol* is necessary to derive significant values for the repeatability. The number of 14 single solutions in case of the CONT02 studies certainly is large enough, although some stations are not available at all days. This is especially a problem in the SLR solution whereas there are nearly no outages regarding the eight VLBI-GPS co-locations (see *Chapter 5.1.2*).

In addition to the station-specific repeatability $r_{ista}$, a solution-specific repeatability $r_{sol}$ for each coordinate component is computed. This quantity is a sort of a weighted average of the station-specific repeatabilities of all *nsta* stations taking into account the number of single solutions $n_{ista}$ where each station is contained. Exemplarily for the three components, the solution-specific repeatability in north direction is derived as follows:

$$r_{sol, North} = \sqrt{\frac{\sum_{ista=1}^{nsta} n_{ista} \cdot r_{ista, North}^2}{\sum_{ista=1}^{nsta} n_{ista}}} \; . \tag{5.9}$$

Besides the validation of the solutions, the solution-specific repeatability (5.9) is employed for the derivation of weighting factors described in *Chapter 5.1.1* using the expressions (5.4) and (5.7).

Another output of the Helmert transformations between the daily solutions and the 14-day combination are, of course, the estimated seven Helmert parameters. They should not be ignored in the evaluation of the reference frame as they deliver valuable information about its stability. In view of the stability of the geocenter estimation, the daily translations are of interest for the evaluation. Especially the differences between a GPS-

only, an SLR-only and a combined solution are to be investigated in order to asses, whether the inclusion of SLR improves the stability of the geocenter determination. As the rotations belong to the degrees of freedom for all techniques, they are not studied in more detail. Contrary the scale, it is given implicitly for every technique, and looking at the daily scale parameters reveals the stability of its technique-internal precision.

## 5.2.2 Comparison with external data sets

Independent data sets for the estimated parameters are needed for an external validation of the solutions. Subdivided according to the parameter types the following comparisons are done in order to evaluate the analysis results in *Chapter 6*:

- terrestrial reference frame: ITRF2000;
- troposphere: water vapor radiometer, IVS and IGS combined troposphere products;
- polar motion (daily values): IERS C04, weekly IGS reference frame product, IVS combined EOP results;
- *UT1-UTC* (daily values): IERS C04, IVS combined EOP results;
- sub-daily ERP: model IERS2003;
- nutation: IERS C04.

Using the ITRF2000 for evaluating the terrestrial reference frame of the computed solutions the validation will concentrate on a Helmert transformation. The estimated transformation parameters including their standard deviations, the RMS of the transformation and the coordinate residuals can be analyzed. The transformation parameters give information about the general agreement with the ITRF2000 which was used as a priori reference frame for the datum definition. Hence, the transformation parameters are an indicator for the quality of the alignment regarding translation, rotation and scale, although a Helmert transformation need not to be carried out necessarily by setting up all seven parameters.

The possibilities for validating the troposphere parameters were already indicated in *Chapter 4.3*. Regarding the analyses presented in *Chapter 6*, WVR measurements represent the only really independent data set that will be used to validate the troposphere ZD, although the possibility to validate the estimates with WVR data is given for only three stations, namely, Onsala, Wettzell and Kokee Park. The problems related to these data sets and their usage for comparing with the estimates derived from the space-geodetic techniques have been already outlined in *Chapter 4.3*. For the remaining five stations with no WVR running during CONT02 only the combined troposphere products from the IGS[20] and IVS[21] are used for comparisons although these time-series cannot be considered as fully independent because they originate from the same GPS and VLBI data, respectively, that were used in the studies for this thesis. Moreover, it must be kept in mind that the IGS products for the CONT02 time span still represent solutions based on a relative PCV model for the GPS antennas. The problems related to this type of antenna phase center models were already outlined in *Chapter 3*, thus, it is clear that the comparison with the IGS troposphere products have to be treated carefully. Finally, it must be emphasized that already the comparison of the VLBI- and GPS-derived time-series estimated independently from each other should be a quite good reliability check.

Concerning the validation of the Earth orientation parameters it must be distinguished between daily values for polar motion and *UT1-UTC*, sub-daily ERP estimates and the nutation parameters. In the case of a daily resolution several official IERS products are available: C04 series, Bulletin A, Bulletin B. For more details about the differences between the afore mentioned series it is referred to the dedicated website[22]. In the studies carried out for this thesis the C04 series (*Gambis, 2004*) was used as a priori values and for the comparison with daily ERP estimates. Since the "IERS Analysis Campaign to Align EOPs to ITRF2000/ICRF" (see *IERS Message No. 19*[23]) and the "IERS SINEX Combination Campaign" (see *IERS Message No. 27*[24]) it is well known that the actually provided C04 polar motion series is not consistent anymore with ITRF2000, so that space technique solutions aligned to ITRF2000 will show an offset in the pole coordinates w.r.t. C04, especially for the *y*-pole. All analyses in the framework of these two IERS campaigns consistently revealed a bias in the *y*-pole of about 0.2 mas (see e.g. *Dill and Rothacher, 2003*). Fortunately, the IERS Product Cen-

---

20 *ftp://ftp.gfz-potsdam.de/pub/igstrop/prod/wWWWW/xxxxWWWW.zpd (WWWW = GPS week, xxxx = GPS site code)*

21 *http://mars.hg.tuwien.ac.at/~ivstrop/cont02/cont02xx.zpd (xx = abbreviation for the VLBI site)*

22 *http://www.iers.org/iers/products/eop/*

23 *http://www.iers.org/products/2/1034/orig/message_019.txt*

24 *http://www.iers.org/products/2/1042/orig/message_027.txt*

ter for EOP recently revised the combination strategy for generating the C04 series (see *Bizouard and Gambis, 2007*). One of the major improvements is the alignment to the latest ITRF, so that the clear bias in the *y*-pole vanished. However, as the revised solution (called "EOP05C04") still has to undergo some validation processes within the IERS, it is not yet the official product so that we revert to the old C04 series for comparing the EOP estimates – in spite of the bias. In order to allow a bias-free validation of the estimated polar motion series (daily values) the official weekly IGS reference frame products[25] and the combined EOP results provided by the IVS[26] (*Nothnagel et al., 2006*) are additionally used for comparisons.

All official EOP series mentioned above have in common that they are derived from observations of the space-geodetic techniques. As a consequence, these series cannot be considered as a completely independent validation for the time-series resulting from the studies presented here because the same observation techniques with the identical drawbacks built the basis, although the analyses were done at different analysis centers using different strategies. Unlike the daily ERP products, the sub-daily ERP model according to the IERS Conventions 2003 (see *McCarthy and Petit, 2004*) was derived from satellite altimetry, hence, it can be regarded as completely independent from VLBI, GPS, SLR and DORIS. This model will be denoted as IERS2003 throughout this thesis. Totally 71 constituents for diurnal and sub-diurnal variations in polar motion and *UT1* are included.

Finally, the nutation estimates are validated using the IERS C04 series mentioned already above. Unfortunately, the nutation corrections provided in the IVS combined EOP product refer to the old nutation model IAU80 so that they were not used here.

## 5.2.3  Comparison with single-technique solutions

One intention of the comparison with the single-technique solutions is to carry out a consistency check as it does not seem to be reasonable that the time-series of EOP or troposphere parameters show a completely different behavior in the combination than in the single-technique solutions. Otherwise there must be an explanation for these differences.

Moreover, comparing the combined results with those of the single-techniques answers the question whether a multi-technique combination yields any improvements and quantifies such an improvement. For this purpose, the comparison is not limited to solely opposing the different time-series but all validation criteria mentioned in *Chapter 5.2.1* and *5.2.2* can be consulted. The corresponding results for the combined solution and the single-technique solutions can be analyzed and decided whether there is an improvement or not, e.g., whether the repeatability of station coordinates becomes better or whether the agreement of the ERP time-series with an independent sub-daily model increases. Out of these comparisons it is possible to assess which technique benefits most of the combination, respectively, how large the influence of each of the techniques on the different parameter types is in the combination.

# 5.3  Correlations between parameter types

Preliminary investigations dealing with correlations between parameter types that are included in the CONT02 solution comprise two topics:

  – the singularity between a retrograde diurnal polar motion and the nutation angles (offsets and linear drifts);
  – the correlation between troposphere parameters and station coordinates.

## 5.3.1  Nutation and retrograde diurnal polar motion

*a) Theoretical considerations*

The first type of correlation has to be considered every time when sub-daily polar motion is estimated together with nutation since an exactly retrograde diurnal term in polar motion can also be expressed as a constant offset in the nutation angles (see *Moritz and Mueller, 1987*).

---

25 *ftp://cddis.gsfc.nasa.gov/pub/gps/products/wwww/igs02Pwwww.erp.Z (with wwww for the GPS weeks 1188-1190)*
26 *ftp://cddis.gsfc.nasa.gov/pub/vlbi/ivsproducts/eops/ivs06q1e.eops.gz*

In order to explain the theory behind this one-to-one correspondence we start with the matrix $\boldsymbol{R}_{EOP}(t)$ given in equation (3.2) to describe the rotation between an inertial and a terrestrial reference frame for the epoch $t$. If the model part is neglected therein (i.e. precession and a priori nutation model), and the mean obliquity $\epsilon_0$ is considered as a given value, altogether five quantities remain that are estimated from the space-geodetic observations: the two pole coordinates ($x_P$, $y_P$), the Greenwich true sidereal time ($\theta$, connected with the quantity *UT1-UTC* that is normally estimated as a parameter) and the two nutation angles ($\Delta\varepsilon$, $\Delta\psi$ as corrections to the a priori model). The presence of five parameters in a three-dimensional rotation means that the parameters cannot be fully independent from each other. Thus, the reduction to only three independent rotation angles for the epoch considered is arbitrary. Since a relationship between polar motion and nutation should be derived, two types of reduced rotation matrices are built: $\boldsymbol{R}_{PM}(t)$ only contains the rotations of polar motion and $\theta$, whereas $\boldsymbol{R}_N(t)$ only contains $\theta$ and the nutation angles:

$$\boldsymbol{R}_{PM}(t) = \boldsymbol{R}_3(-\theta) \cdot \boldsymbol{R}_1(y_P(t)) \cdot \boldsymbol{R}_2(x_P(t)) \ , \tag{5.10a}$$

$$\boldsymbol{R}_N(t) = \boldsymbol{R}_1(-\epsilon_0) \cdot \boldsymbol{R}_3(\Delta\psi(t)) \cdot \boldsymbol{R}_1(\epsilon_0 + \Delta\epsilon(t)) \cdot \boldsymbol{R}_3(-\theta) \ . \tag{5.10b}$$

Both matrices describe a three-dimensional similarity transformation for the epoch $t$ unambiguously. Equating them and assuming small angles for all quantities (except for $\epsilon_0$ and $\theta$) yields the relationship between nutation offsets and polar motion we are looking for:

$$x_P(t) = -\Delta\psi(t) \cdot \sin\epsilon_0 \cdot \cos\theta \ - \ \Delta\epsilon(t) \cdot \sin\theta \ , \tag{5.11a}$$

$$y_P(t) = -\Delta\psi(t) \cdot \sin\epsilon_0 \cdot \sin\theta \ + \ \Delta\epsilon(t) \cdot \cos\theta \ . \tag{5.11b}$$

Due to the angle $\theta$ in (5.11), the polar motion signal is diurnal. Therefore, the correlation will only cause problems if polar motion is estimated with a high temporal resolution (i.e., sub-daily), whereas choosing a daily resolution overcomes the singularity. As the *x*-component precedes the *y*-component by 90°, the polar motion given in (5.11) is a retrograde signal. Following the general relationship

$$A \cdot \cos\omega t \ + \ B \cdot \sin\omega t \ = \ C \cdot \sin(\omega t + \varphi) \ , \tag{5.12}$$

with
$$C = \sqrt{A^2 + B^2} \ , \quad \tan\varphi = \frac{A}{B} \ , \tag{5.13}$$

it becomes clear that the polar motion signal corresponding to constant nutation offsets given by $\Delta\epsilon$ and $\Delta\psi$ as described by (5.11) has an amplitude of

$$C_{xy} = \sqrt{\Delta\epsilon^2 + \Delta\psi^2 \cdot \sin^2\epsilon_0} \ . \tag{5.14}$$

Going one step further and estimating nutation offsets and drifts or use the equivalent piece-wise linear parameterization (see *Chapter 2.3.2*), there are two contributions to the singularity superimposed: the mean nutation offset and the linear trend. The first contribution is similar to the case described in (5.11), whereas linear drifts in the nutation angles, i.e., $\Delta\dot{\psi}$ and $\Delta\dot{\epsilon}$, correspond to a signal in polar motion of the following form:

$$x_P(\Delta t) = -\Delta\dot{\psi} \cdot \sin\epsilon_0 \cdot \Delta t \cdot \cos\theta \ - \ \Delta\dot{\epsilon} \cdot \Delta t \cdot \sin\theta \ , \tag{5.15a}$$

$$y_P(\Delta t) = -\Delta\dot{\psi} \cdot \sin\epsilon_0 \cdot \Delta t \cdot \sin\theta \ + \ \Delta\dot{\epsilon} \cdot \Delta t \cdot \cos\theta \ . \tag{5.13b}$$

It becomes evident that a nutation rate is identical to a retrograde diurnal signal in polar motion with an amplitude linearly increasing with time:

$$ C_{xy}(\Delta t) \; = \; \Delta t \; \cdot \; \sqrt{\Delta\dot{\epsilon}^2 \; + \; \Delta\dot{\psi}^2 \cdot \sin^2\epsilon_0} \; . \tag{5.16} $$

*b) The constraint for a retrograde diurnal polar motion term with constant amplitude*

In order to remedy the singularity between nutation offsets and a retrograde diurnal signal in polar motion with constant amplitude, the constraint described in *Chapter 2.6.4* is applied in the program ADDNEQ2. Two aspects concerning the application of this constraint will be addressed in the following:

– In practice, the constraint does not only affect the exactly diurnal retrograde term but also adjacent retrograde terms that are, theoretically, not involved in the singularity.

– The singularity involving linear drifts in the nutation angles can be handled by this constraint under special conditions as well.

The first limitation is a consequence of the requirement that two signals can only be fully decorrelated if their phases differ by at least $2\pi$ at the end of the time interval considered. The bandwidth $\Delta T$ of polar motion terms influenced by the blocking constraint depends on the length of the time-series $T_S$ and the period $T_0$ of the reference signal ($T_0 = 23.934$ h in the case of the constraint). The difference in the period $\Delta T$ that is necessary to decorrelate a signal present in the data set from the diurnal signal involved in the singularity is then given by:

$$ \Delta T \geq \frac{T_0^2}{T_S + T_0} \; . \tag{5.17} $$

The values for $\Delta T$ together with the resulting periods of signals that can be distinguished unambiguously from a diurnal signal are summarized in Table 5.6 for different lengths of time-series. From this theoretical consideration, periods from diurnal down to half a day are affected by the constraint if a daily solution is computed, and periods larger than 22.3 h are affected for the CONT02 time span of 14 days. The dependency on the length of the data set considered for the constraint was investigated by *Thaller et al. (2007)* using simulated GPS observations. Additionally, the simulation studies described therein revealed that the temporal resolution of the polar motion estimates has no influence on the constraint.

If linear drifts for the nutation angles are present in the normal equation system, the constraint only suppresses a retrograde polar motion term with a mean amplitude that corresponds to the mean nutation offset over the time span considered. Thus, the polar motion estimates remaining after applying the constraint are equal to the difference between a retrograde diurnal signal with linearly increasing amplitude corresponding to a nutation rate and a retrograde diurnal signal with constant amplitude corresponding to a mean nutation offset. Figure 5.5 illustrates this relationship exemplarily for the *x*-pole assuming a rate of 1 mas per 14 days for $\Delta\dot{\psi}$ and $\Delta\dot{\epsilon}$. Applying equation (5.16), these rates lead to an offset $C_{xy}$ of 1.077 mas after 14 days.

**Table 5.6:** *Periods that can be fully decorrelated from a diurnal signal depending on the length of the time-series.*

| Length of data set $T_S$ | $\Delta T$ | $T_0 - \Delta T$ |
|:---:|:---:|:---:|
| 1 day | 11.9505 h | 11.9835 h |
| 3 days | 5.9712 h | 17.9628 h |
| 7 days | 2.9845 h | 20.9495 h |
| 14 days | 1.5915 h | 22.3425 h |
| 28 days | 0.8231 h | 23.1109 h |
| 365 days | 3.91 min | 23.8688 h |

In the case of using the VLBI normal equation systems of CONT02 described in *Chapter 5.1.2*, the consequences and possible handling of the singularity involving nutation offsets and rates can easily be demonstrated, because there is no further singularity with orbital parameters as it would be the case for GPS. In a first step, the singularity involving nutation offsets will be demonstrated. To do so, two types of VLBI solutions were computed: In the first solution, the retrograde diurnal constraint was not applied although the correlated parameter types were both estimated. The second solution was derived by applying the retrograde diurnal constraint on the 14-day normal equation system. The singularity is fully present in the first solution, thus, the main signal contained in the resulting pole coordinates is a daily signal with more or less constant amplitude. Figure 5.6a shows this behavior exemplarily for the *x*-component (*y*-component looks similar). The results for the nutation angles confirm that the polar motion estimates mainly suffer from an offset in the nutation angles due to the correlation: $\Delta\varepsilon$ is shifted by about 2.776 mas and $\Delta\psi \cdot \sin\varepsilon_0$ is shifted by 4.932 mas compared to the second solution where the constraint has been applied (see Fig. 5.6b, exemplarily for the nutation in longitude). Applying Eq. (5.14), this shift results in an amplitude of 5.660 mas which is in good agreement with the results for the polar motion displayed in Fig. 5.6a. It becomes thus obvious that the singularity causing the large retrograde diurnal term in the pole coordinates and the corresponding nutation offsets is remedied by the constraint. However, a signal with varying amplitude is still present in the pole coordinates and the size of the amplitude at the beginning and the end is in quite good agreement with the nutation rates estimated in this solution. Together with the theoretical considerations above this leads to the conclusion that the retrograde constraint applied to the 14-day normal equation system removes the singularity caused by the estimation of mean nutation offsets but not the singularity involving a linear drift in the nutation.
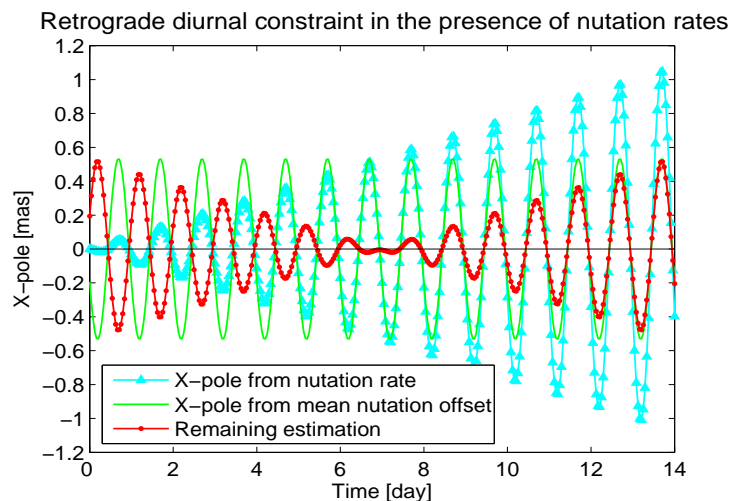


***Figure 5.5:*** *Simulated hourly x-pole estimates if nutation rates are present (1.0 mas per 14 days for both nutation angles) and the retrograde diurnal constraint is applied on the 14-day normal equation system.*

The question whether the singularity involving nutation rates can be remedied by the available constraint as well is answered by investigating further types of VLBI solutions. All tests base on the idea that VLBI is capable to correctly determine the mean nutation offset for exactly the time span considered for the retrograde diurnal constraint. Moreover, if the nutation angles are estimated as only one offset plus linear drift (or as polygon with only one interval) for the whole 14 days, solely two offsets are necessary to determine this parameterization unambiguously. This implies that splitting the entire time span into at least two parts for the constraint delivers two offsets (i.e., one for each partial interval of the constraint) which allows to represent the nutation angles with one offset and linear drift for the whole time span without any singularity left. The way of splitting the interval should have a secondary role thereby, but one must be aware that the mean offsets of the sub-intervals will force the nutation rate to fit exactly to these values. The following methods are tested:

– using the first and second week for the constraint ("weekly");

  – using the first day and the remaining 13 days for the constraint ("1 + 13 days");
  – constraining only the first and the last day ("first + last day");
  – applying the constraint on every day separately ("daily").

a)



b)
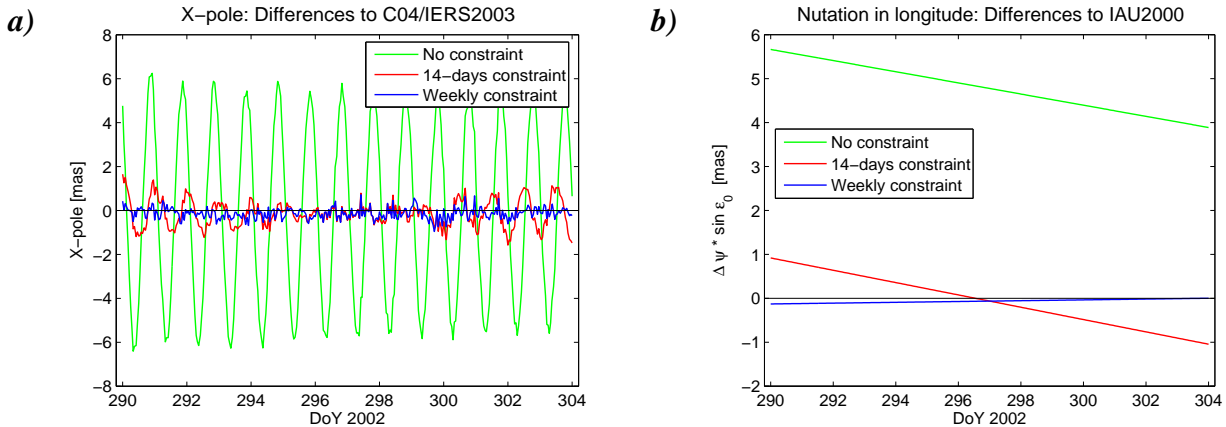
**Figure 5.6:** *The effect of the singularity between polar motion and nutation offsets and rates on the VLBI estimates with different handling of the retrograde diurnal constraint blocking a mean nutation offset for each time interval: **a)** hourly x-pole estimates compared to IERS C04 / IERS2003, **b)** nutation in longitude as correction to IAU2000.*

The first method halves the time span so that the constraint is applied once taking into account the polar motion estimates of the first week only and once taking into account the second week only. Splitting the time span into one day and 13 days (i.e., second method) bases on the idea to choose at least one of the intervals for the constraint as long as possible, following the theoretical consideration in Table 5.6 concerning the detectable periods in dependence on the interval length. A third option is to constrain only two days out of 14 (e.g., the first and the last day) so that the nutation rate over the entire time span will be determined only by the mean offsets of these two days whereas the remaining days have no influence.

The polar motion series in Fig. 5.6a resulting from the solution with "weekly constraint" exemplarily shows that, obviously, the singularity involving nutation rates is removed. The quite large nutation rate present before is reduced as well (see Fig. 5.6b). All the first three methods of interval splitting mentioned above yield similar results with an overall agreement of the polar motion estimates on the level of about 0.1 mas. Taking the solution with the retrograde diurnal constraint applied on a weekly basis as reference and looking at the differences compared to the other solution types, Fig. 5.7a visualizes that the only differences in the polar motion time-series result from slightly different nutation estimates (see Fig. 5.7b) given by the mean offsets of the intervals considered for the constraint. The differences themselves are, again, a retrograde diurnal polar motion term.

An extreme case of splitting the entire time span is the fourth solution tested here: The retrograde diurnal constraint was applied on a daily basis for each day. Consequently, VLBI can determine the mean nutation offset correctly for each day, and the estimated offset and drift for the entire time span results from a fitting to all the 14 daily offsets. The nutation in longitude fits rather well to the other solutions (see Fig. 5.7b) and the same holds for the nutation in obliquity which is not shown here. However, the comparison of the polar motion estimates in Fig. 5.7a clearly demonstrates that this solution is over-constrained as higher-frequent differences to the minimum constraint solution exist.

Finally, Fig. 5.7b additionally shows the nutation in longitude resulting from a solution with daily polar motion estimates so that there is no singularity present and the retrograde diurnal constraint is not needed. The comparison demonstrates that all solution types with interval splitting for the constraint seem to be reasonable although it is difficult to decide which one would be the best choice.

In order to summarize the analyses above, the retrograde constraint blocking a constant diurnal amplitude in polar motion removes the singularity between a nutation offset and a retrograde diurnal term in polar motion. Additionally, the constraint is capable to remove as well the singularity involving nutation rates if it is ap-

plied for at least two sub-intervals of the nutation interval. The type of division into sub-intervals has no re-markable influence in the case of analyzing a time-series of 14 days.
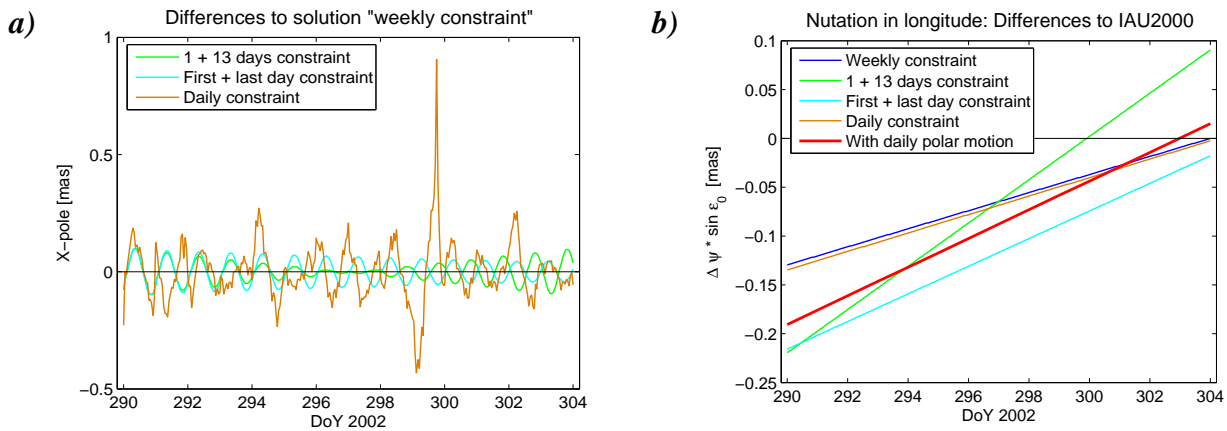


***Figure 5.7:*** *Handling of the singularity involving nutation rates by applying the retrograde diurnal con-straint blocking a mean nutation offset in different ways for VLBI solutions: **a)** hourly x-pole estimates compared to the solution where the retrograde diurnal constraint is applied on a weekly basis, **b)** nutation in longitude as correction to IAU2000 (the nutation estimates from a solution with daily polar motion serve as reference).*

### c) The constraint for a retrograde diurnal polar motion term with linearly increasing amplitude

The analyses hereafter deal with the extended retrograde diurnal constraint that blocks an amplitude linearly increasing with time in the polar motion series (see *Chapter 2.6.4*) in addition to the blocking of a retrograde diurnal signal with constant amplitude. Contrary to the methods described above, the extended constraint di-rectly removes the singularity between nutation rates and retrograde diurnal polar motion with linearly in-creasing amplitude. Therefore, the question arises: How well do the results of both methods fit together? The results from a VLBI-only solution using the extended constraint are compared to the over-constrained solu-tion from above with the constraint for constant amplitude / nutation offsets applied for each day ("daily con-straint") and the solution, where the time span for the constraint was split into two weeks ("weekly con-straint"). The latter should represent the group of solutions with minimum number of constrained intervals. Figure 5.8 displays the pole coordinates and Fig. 5.9 shows the two nutation angles. Obviously, the method of dividing the time span into two weeks and applying the constraint for a constant amplitude in polar motion on a weekly basis can realize the partitioning between a polar motion signal and nutation offset and rate very well as there are nearly no differences to the solution where both types of singularities (i.e., involving nuta-tion offsets and rates) are handled directly by the extended constraint. Contrary to this, the solution with dai-ly blocking of a constant amplitude in polar motion delivers noticeably different results, not only a quite dif-ferent rate for the nutation in obliquity (even with opposite sign). More important are the differences in the pole coordinates that are quite large and do not result only from the different nutation rate, but demonstrate that higher frequent changes in polar motion (different from the exactly diurnal term) are blocked as well.

a)



b)
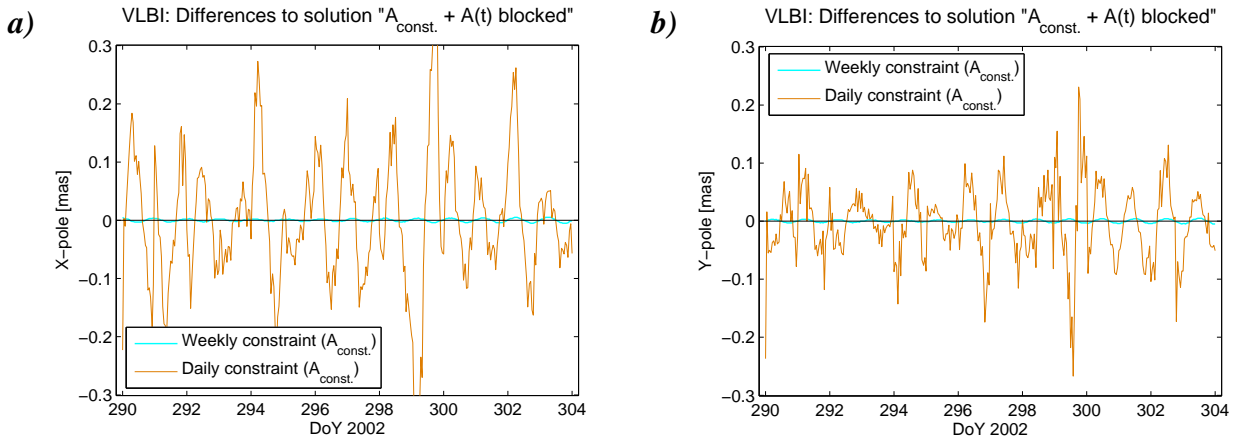
**Figure 5.8:** *Hourly polar motion estimates from VLBI as difference to a solution where the retrograde di-urnal constraint is applied for a constant amplitude ($A_{const.}$) as well as for a linearly increasing amplitude ($A(t)$) in polar motion: **a)** x-pole, **b)** y-pole.*

a)



b)
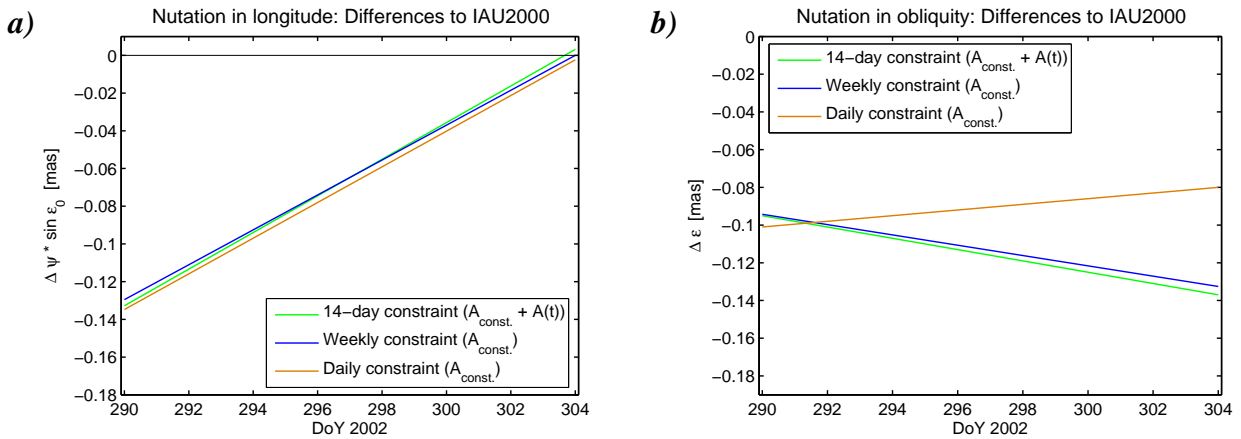
**Figure 5.9:** *Nutation estimates from VLBI (correction to IAU2000) for solutions with the retrograde diur-nal constraint blocking only a constant amplitude ($A_{const.}$) in polar motion but handling the singularity with nutation rates as well, and for a solution with a linearly increasing amplitude ($A(t)$) blocked additionally: **a)** nutation in longitude, **b)** nutation in obliquity.*

Finally, it must be mentioned that the situation is more complicated for satellite techniques because, additionally, orbital parameters are involved in the singularity, the nutation offset cannot be determined and only the nutation rate is accessible. The *x*-pole coordinates estimated by GPS shown in Fig. 5.10 demonstrate the similarities with the VLBI-only solution as well as the important differences. If only the constraint handling the correlation between nutation offsets and a constant amplitude for the retrograde diurnal polar motion is applied for the whole time span, it is obvious that the singularity with nutation rates is still present in the polar motion results (as it is the case for VLBI). Applying this constraint for each day seems to remove the remaining singularity, similarly to VLBI as well. However, the difference between the two techniques becomes obvious regarding the third solution type in Fig. 5.10. Whereas in the case of VLBI, the application of the extended constraint handling directly the singularity with nutation offsets and rates allows to estimate polar motion without any singularity left, this procedure cannot totally remove all singularities in the case of GPS. The remaining signal visible in the pole coordinates has neither the structure of a signal correlated with an offset in the nutation angles nor a nutation rate, but it must be explained by the correlation with the orbital elements: Due to an arc length of only one day for the GPS orbits, there is no continuity at the day boundaries, whereas the 14-day constraint implies linearity over 14 days. Thus, the differences of each daily orbit compared to the mean and linear orbit for 14 days cause the irregular structure seen in Fig. 5.10.

As the orbital elements are unconstrained in order to allow a combination of *UT*/*LOD* and the nutation rates with VLBI, it was decided to apply the retrograde diurnal constraint on a daily basis in the case of a GPS-only solution. Hence, the impact of the remaining singularity on the GPS solution will be noticeable only for the time span of one day assuming that this effect is quite small.
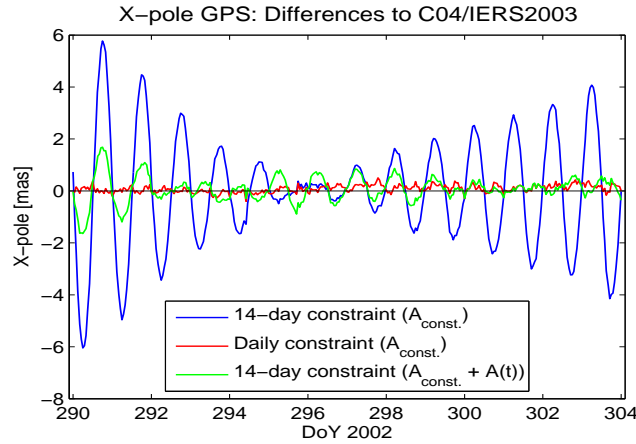


**Figure 5.10:** *Hourly x-pole estimates from GPS for different strategies concerning the application of the retrograde diurnal constraint for a constant amplitude only ($A_{const.}$) or for a linearly increasing amplitude (A(t)) additionally.*

## 5.3.2 Station coordinates and troposphere parameters

The second type of correlation mentioned at the beginning is not a singularity. However, the correlation between troposphere ZD and the height of a station is very strong for microwave techniques such as VLBI and GPS. The question to be answered in this context deals with the potential of SLR to reduce this correlation, as the troposphere influence on optical techniques like SLR can be modeled with sufficient accuracy and no troposphere parameters have to be estimated (see *Chapter 3.3.2*). It is clear that SLR can reduce the correlation only at stations, where GPS or VLBI is co-located with SLR and that the SLR influence is only indirect via the height component of the LT. Therefore, all problems related to LT mentioned in *Chapter 4.2* are important for these considerations, too. The theoretical considerations start with the generalized interrelationship between a troposphere ZD parameter and the station height expressed in the corresponding elements of the normal equation matrix as integrals over the zenith angles $z$ of all observations uniformly distributed between the minimum zenith angle $z_0$ and a maximum zenith angle $z_{max}$ (see *Rothacher and Beutler, 1998*):

$$N = \begin{bmatrix} N_{height} & N_{height\,,\,trop} \\ N_{height\,,\,trop} & N_{trop} \end{bmatrix} = \begin{bmatrix} \int_{z_0}^{z_{max}} \sin^2 z \, \cos^2 z \, dz & -\int_{z_0}^{z_{max}} \sin^2 z \, dz \\ -\int_{z_0}^{z_{max}} \sin^2 z \, dz & \int_{z_0}^{z_{max}} \sin^2 z \, \cos^{-2} z \, dz \end{bmatrix}. \quad (5.18)$$

The expression (5.18) represents a normal equation matrix of a GPS or VLBI analysis. Combining it with SLR means nothing than adding information on the main-diagonal element corresponding to the height component, i.e., $N_{height}$. In order to simulate this situation, the size of the value added to $N_{height}$ was varied and the matrix was inverted. The resulting correlation coefficients are displayed in Fig. 5.11 visualizing that the correlation can be halved from 0.4 to 0.2 if the additional information has about three times the weight of the original element $N_{height}$. This order of magnitude has to be kept in mind when the actual stabilization due to the integration of SLR is analyzed in *Chapter 6*.
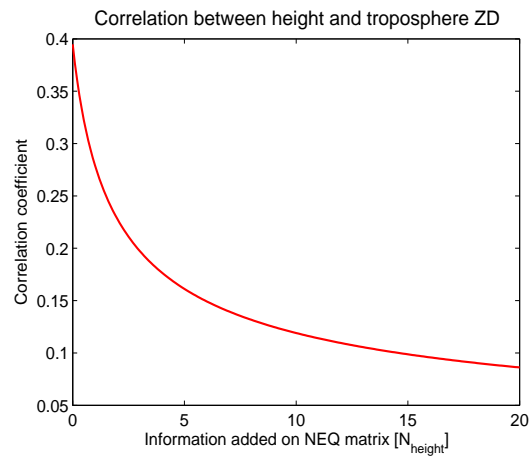
***Figure 5.11:*** *Resulting correlation coefficient if additional information is put on the height element of the normal equation matrix (corresponding to an SLR contribution at a co-location site).*

# 6 Analyses results

Although the main topic of this thesis is the combination of space-geodetic techniques, the analysis of each single-technique contributing to the combination should precede the combination itself for several reasons:

- The analysis of the single-technique solutions is the only way to assess the potential of each technique regarding the determination of the parameters of interest. Thus, the contribution to the combination can only be evaluated realistically by analyzing each technique separately.

- In the combination approach used here, the relative weighting factors applied to the single-technique normal equation systems are derived from the coordinate repeatability delivered by each technique.

- The comparison with the single-technique solutions is an important criterion for validating the combined solution and investigating the benefit of the combination.

## 6.1 Single-technique solutions

In order to be able to assess the potential of each technique realistically, it is important that no unnecessary constraints are applied to any of the parameters. This is in many cases contrary to the philosophy applied if the best time-series of parameters derived from only one technique is of interest (as it is the case for the technique-specific analysis centers of the IGS, IVS and ILRS). But the deficiencies and strengths of each technique can be clearly distinguished only if the parameters are determined solely by the observations, i.e., without any stabilization.

### 6.1.1 Station coordinates

The main criteria for validating the estimated station coordinates is their daily repeatability. The station-specific and the solution-specific repeatabilities were computed for the three single-technique solutions according to the theory given in *Chapter 5.2.1*. As SLR does not have the capability to deliver stable daily solutions with all parameters estimated including free orbits, it was decided to fix the orbital parameters for the repeatability studies. Additionally, the NNR condition on a daily basis seems to be too weak to get a stable daily SLR solution so that the coordinates of all SLR stations were constrained absolutely with 1 cm. But it must be emphasized that both exceptions (i.e., fixed orbits and constrained coordinates instead of NNR conditions) are made solely for the SLR-only solution and only for the repeatability studies. The daily instead of hourly resolution for the ERP marks the third exception that is necessary for an SLR-only solution. In order to have comparable single-technique solutions, Table 6.1 summarizes not only the repeatabilities for GPS and VLBI with sub-daily ERP, but gives the corresponding values for a daily resolution in addition. The comparison of these two solution types demonstrates that, obviously, the high temporal resolution for polar motion and *UT1-UTC* does not degrade the solution of these two techniques very much, and for GPS it is even more or less identical. Furthermore, GPS and VLBI have a comparable repeatability on the millimeter-level whereas SLR is one order of magnitude worse with repeatabilities of about 1 cm for all three components. The advantage of SLR must be seen in the equal quality of all components which is in contrast to the typical difference of a factor of three between the height and the horizontal components in the case of the microwave techniques. The correlation of the height component with the troposphere delay and the differential receiver clock corrections is responsible for this behavior seen in GPS and VLBI solutions. At a first glance it is striking that the north component of the VLBI solution is clearly worse than the east component, but this can be explained by the network configuration of CONT02 with a bad distribution in the north-south direction, as it has been already mentioned in *Chapter 4.1* (see Fig. 4.1).

Beside the solution-specific repeatability for an overall validation of the solution, it is interesting to look at the station-specific repeatabilities of the co-located sites to be able to evaluate the effect of the combination more distinctively later on. The repeatabilities for the eight GPS-VLBI co-locations are given in Table 6.2, and Table 6.3 lists the corresponding values for the 14 GPS-SLR co-locations. The general order of magnitude is similar to that of the solution-specific repeatabilities in Table 6.1, of course, but there are remarkable variations between the stations, especially for SLR, which must be explained by the network configuration

that is changing very strongly from day to day (see Table 4.2 in *Chapter 4.2*). Thus, the positive effect of the combination should become visible especially for those stations that cannot be determined stable enough within the single-technique solution, e.g., the GPS site Fairbanks, the VLBI sites Hartebeesthoek and Wett-zell, and nearly all SLR sites.

***Table 6.1:*** *Daily repeatabilities of station coordinates for solutions with hourly and daily ERP (the satellite orbits were fixed for the SLR-only solution).*

| Component | Daily repeatability (1-h ERP) [mm] | | Daily repeatability (24-h ERP) [mm] | | |
|---|---|---|---|---|---|
| | GPS | VLBI | GPS | VLBI | SLR |
| North | 1.97 | 3.72 | 1.94 | 3.29 | 11.11 |
| East | 1.95 | 1.97 | 1.96 | 1.97 | 11.84 |
| Up | 5.93 | 7.67 | 5.92 | 7.01 | 13.32 |

***Table 6.2:*** *Station-specific daily repeatabilities for the VLBI-GPS co-locations (hourly ERP).*

| Station | Repeatability for GPS site [mm] | | | Repeatability for VLBI site [mm] | | |
|---|---|---|---|---|---|---|
| | North | East | Up | North | East | Up |
| Algonquin Park | 2.45 | 1.51 | 4.76 | 2.34 | 1.03 | 5.26 |
| Fairbanks | 2.41 | 2.06 | 10.51 | 2.91 | 1.40 | 6.47 |
| Hartebeesthoek | 1.94 | 3.24 | 5.17 | 5.53 | 2.64 | 10.68 |
| Kokee Park | 2.14 | 1.80 | 7.34 | 6.43 | 2.92 | 6.91 |
| Ny-Alesund | 0.76 | 1.12 | 5.45 | 1.39 | 2.25 | 5.05 |
| Onsala | 0.96 | 1.43 | 6.27 | 3.10 | 1.56 | 8.85 |
| Westford | 1.68 | 1.27 | 4.41 | 2.11 | 1.92 | 4.88 |
| Wettzell | 0.97 | 0.96 | 4.33 | 2.91 | 1.12 | 10.55 |

***Table 6.3:*** *Station-specific daily repeatabilities for the GPS-SLR co-locations (hourly ERP for GPS, daily ERP and fixed orbits for SLR).*

| Station | Repeatability for GPS site [mm] | | | Repeatability for SLR site [mm] | | |
|---|---|---|---|---|---|---|
| | North | East | Up | North | East | Up |
| Borowiec | 1.09 | 1.06 | 4.11 | 1.56 | 0.09 | 5.79 |
| Fort Davis | 1.90 | 1.92 | 6.96 | 12.95 | 3.86 | 8.29 |
| Grasse (7835) | 1.85 | 1.21 | 4.69 | 8.27 | 8.98 | 7.21 |
| Grasse (7845) | 1.85 | 1.21 | 4.69 | 14.48 | 9.01 | 7.14 |
| Graz | 1.56 | 1.27 | 3.29 | 7.77 | 9.34 | 8.32 |
| Hartebeesthoek | 1.94 | 3.24 | 5.17 | 9.57 | 15.36 | 9.33 |
| Herstmonceux | 1.72 | 1.46 | 4.02 | 8.20 | 11.48 | 8.72 |
| Monument Peak | 1.22 | 1.76 | 4.75 | 6.09 | 8.25 | 8.97 |
| Potsdam | 0.72 | 0.99 | 4.61 | 5.75 | 8.97 | 15.13 |
| Shanghai | 2.58 | 0.89 | 4.17 | 13.91 | 12.08 | 6.23 |
| Tahiti | 2.75 | 1.97 | 6.85 | 0.34 | 7.20 | 2.80 |
| Washington | 1.50 | 1.98 | 7.13 | 7.75 | 10.83 | 8.73 |
| Wettzell | 0.97 | 0.96 | 4.33 | 5.47 | 12.77 | 15.45 |
| Yarragadee | 1.55 | 1.60 | 3.72 | 14.28 | 8.36 | 5.77 |

After analyzing the repeatabilities of the single-technique solutions it is possible to derive the weighting fac-tors described in *Chapter 5.1.1c* as the major input parameter representing the quality of each technique is its

solution-specific repeatability listed in Table 6.1. Consequently, the contribution of SLR is down-weighted by a factor of about ten compared to GPS whereas the weight of the VLBI contribution is only slightly smaller than that for GPS. For a summary of all values important for the computation of the weighting factors it is referred to Table 6.4. One may argue that these weighting factors probably do not reflect the real proportion of the three techniques due to the short time span and the exceptions made for SLR. However, if the weekly repeatabilities determined within the IERS SINEX Combination Campaign by *Thaller and Rothacher (2003)* are taken into account, the appropriate weighting factors would be 5.132058e-6 and 1.271317e-1 for VLBI and SLR, respectively. Thus, these values derived from one year of weekly solutions agree very well with the weighting factors for the daily CONT02 solutions listed in Table 6.4, so that the latter seem to be reasonable.

***Table 6.4:*** *Weighting factors using daily repeatabilities of station coordinates and the mean main-diagonal of the normal equation matrix (NEQ) according to the formulas given in Chapter 5.1.1 (the references to the relevant formulas are indicated in brackets).*

|  | **GPS** | **VLBI** | **SLR** |
|---|---|---|---|
| ***Mean repeatability for 3 components [mm]*** | 3.77 | 4.61 | 12.12 |
| ***Quadratic mean repeatability (5.4) [mm²]*** | 14.2172 | 21.2131 | 147.0134 |
| ***Mean NEQ element for coordinates (5.6)*** | 9.414865 | 1676565.915949 | 5.331945 |
| ***Weighting factor (5.7)*** | 1.0 | 3.763600 e-6 | 1.707598 e-1 |

Another study that can be done using the station coordinates is a comparison of the coordinate differences between the co-located sites and the corresponding LT. However, it must be kept in mind that the geodetic datum of the single-technique solutions is not unified although all solutions are aligned to ITRF2000. Thus, the differences listed in Table 6.5 may partly stem from slightly different underlying reference frames. For the major part of the co-locations the differences are on the level of some millimeters up to a few centimeters. The apparently better agreement for the GPS-VLBI co-locations can probably be explained by a better stability of the GPS and VLBI solutions than that of the SLR solution. The extremely large discrepancies for Borowiec and Tahiti should not be taken too seriously as these SLR stations are available only for one day (see Table 4.2) so that their coordinates are determined very weakly. In order to judge the size of the differences, the corresponding values from comparing the ITRF2000 coordinates with the official LT are additionally given in Table 6.5. As the discrepancies for the ITRF2000 coordinates are as well at the level of several millimeters up to a few centimeters, the results from the single-technique solutions seem to be reasonable. The agreement between the single-technique solutions for CONT02 and ITRF2000 is quite good regarding the GPS-VLBI co-locations because those components with large discrepancies to the LT are common to both comparisons, e.g., the north and height component of Fairbanks, the height component of Ny-Alesund or the east component of Westford. The larger discrepancy for the CONT02 solutions for the north component of Hartebeesthoek might be explained by the poor north-south distribution of the VLBI network with Hartebeesthoek as the only station on the southern hemisphere so that its north component is weakly determined. The large deviation of the ITRF2000 coordinate differences compared to the LT of Kokee Park is not astonishing, as the GPS coordinates in ITRF2000 refer to the site point before the jump in September 2002 and the LT value used here in the comparison had been corrected for the observed coordinate differences (see *Chapter 4.2*).

***Table 6.5:*** *Comparison of the LT values from Table 4.1 with the coordinate differences determined by the single-technique solutions and derived from the ITRF2000 coordinates.*

| | Co-location | Technique solutions – LT [mm] | | | ITRF2000 coordinates – LT [mm] | | |
|---|---|---|---|---|---|---|---|
| | | *North* | *East* | *Up* | *North* | *East* | *Up* |
| GPS–VLBI co-locations | **Algonquin Park** | -1.99 | 4.29 | -5.95 | -6.76 | 0.90 | 12.02 |
| | **Fairbanks** | -12.23 | 1.37 | 17.96 | -14.96 | 9.02 | 20.49 |
| | **Hartebeesthoek** | 15.57 | 9.07 | -5.38 | 4.47 | 7.82 | -2.11 |
| | **Kokee Park** | 6.91 | 2.05 | -10.91 | -31.80 | -23.31 | -11.68 |
| | **Ny-Alesund** | -6.28 | 2.01 | -13.23 | -3.71 | -3.41 | -14.11 |
| | **Onsala** | -2.34 | 2.51 | -7.21 | -1.77 | -4.28 | 2.96 |
| | **Westford** | 0.64 | 17.77 | 2.33 | -11.41 | 14.42 | 17.48 |
| | **Wettzell** | -2.99 | 1.88 | 0.32 | -3.83 | -3.54 | -6.31 |
| GPS-SLR co-locations | **Borowiec** | 2699.08 | 1207.18 | -1432.99 | -6.79 | -3.50 | -6.58 |
| | **Fort Davis** | -4.14 | -8.20 | 33.61 | 5.62 | -0.32 | 3.73 |
| | **Grasse (7835)** | -22.21 | -23.31 | 17.77 | -2.55 | -3.36 | 6.63 |
| | **Grasse (7845)** | -22.21 | -23.31 | 17.80 | -6.80 | -0.13 | 7.01 |
| | **Graz** | -10.16 | -22.01 | 0.70 | -6.02 | -2.82 | 0.47 |
| | **Hartebeesthoek** | -8.60 | -27.05 | 17.28 | -1.40 | -22.19 | 0.68 |
| | **Herstmonceux** | -8.26 | -20.34 | -0.39 | -5.11 | -6.30 | 5.88 |
| | **Monument Peak** | -7.74 | -0.36 | -8.08 | -3.42 | 4.29 | -5.88 |
| | **Potsdam** | -13.90 | -24.38 | -23.97 | -5.88 | -3.63 | 0.92 |
| | **Shanghai** | -46.19 | 73.04 | 61.83 | 1.93 | -0.72 | 21.47 |
| | **Tahiti** | 2450.35 | -4337.05 | -2435.34 | -6.69 | 6.53 | 0.29 |
| | **Washington** | -25.41 | -2.82 | -2.41 | -8.18 | 5.31 | 16.19 |
| | **Wettzell** | -13.40 | -17.75 | -17.79 | -5.03 | -2.92 | 17.49 |
| | **Yarragadee** | -27.70 | 2.51 | 1.37 | -4.36 | -3.24 | -1.55 |

## 6.1.2 Earth orientation parameters

As already mentioned before, SLR has too few observations to determine ERP with a sub-daily resolution, thus, we have to change to daily ERP if an SLR-only solution is analyzed. Therefore, the pole coordinates and *UT1-UTC* with a daily resolution are analyzed in a first step, and the results for the GPS and VLBI solutions with a sub-daily resolution are discussed afterwards. Comparing the estimated daily pole coordinates with the IERS C04 series reveals significant biases especially for the *y*-pole (see Fig. 6.1a+b). It has been outlined in *Chapter 5.2.2* that the *y*-pole of C04 is shifted by about 0.2 mas compared to space-geodetic solutions aligned to ITRF2000 so that the mean biases of the GPS and SLR solutions listed in Table 6.6 are in quite good agreement with the offset that is already known. However, it has to be taken into account that the SLR-derived estimates at the orbit boundaries (DoY 290, 297/298, 304) are significantly less well-determined, so that the weighted mean bias compared to C04 increases to 0.305 mas for the *y*-pole. In general, the discrepancy in the *y*-pole is reduced by about 0.15 mas if the weekly IGS products are used for the comparison so that the GPS and SLR solutions agree with an official unbiased time-series within some tens of µas (see Fig. 6.2a+b and Table 6.6) which is the level of agreement that is actually reached between different analysis centers (see the website of IGS Analysis Center Coordination[27]). Furthermore, the fact that the IGS is still using antenna phase centers from a relative modeling instead of absolute calibrations can evoke differences in the polar motion estimates of several tens of µas as well (*P. Steigenberger, personal communication*). Against this background, the *x*- and *y*-pole coordinates estimated by GPS and SLR agree rather well with the official time-series. Solely the significantly larger offset of the VLBI solution cannot be explained by the mis-alignment of the C04 series to ITRF2000. In order to evaluate whether the remaining differences

---

are technique-specific features or whether they are present only in the VLBI solution used for the studies here, the VLBI estimates are additionally compared to the official IVS combined EOP series. The comparisons with all three official series are displayed in Fig. 6.3a+b so that it becomes obvious that the remaining offset in the *y*-pole of about 0.2 mas is a technique-specific feature caused by the sub-optimal network configuration for CONT02. Analyses presented in *Thaller et al. (2007)* additionally proved this statement by tightly constraining all eight stations to the coordinates of the GPS reference points corrected with the corresponding LT values instead of directly using the VLBI coordinates. This kind of solution yields a polar motion time-series that agrees much better with the GPS-only solution. Looking at the *x*-pole, it seems to suffer from the poor station distribution as well, resulting in a mean bias of about 0.1 mas according to Table 6.6. By the way, the long-term agreement (2000 up to now) between the official time-series provided by the IVS and the IGS confirms the differences visible for the CONT02 solutions here: According to the web-site of the IVS Analysis Coordination[28], the mean biases are 0.1283 mas and -0.1491 mas for the *x*- and *y*-pole, respectively. As a last aspect it has to be mentioned that the small peak in the *x*-pole time-series at DoY 300 must be credited to the VLBI solution used for the analyses here because the IVS series as well as the C04 and the IGS series do not show this behavior.

In order to conclude the analyses of the daily polar motion estimates, Table 6.7 summarizes the RMS (unweighted and weighted) of the unbiased residuals for all comparisons carried out and described above. The GPS and VLBI solutions are on the level of 0.1 mas for both pole components whereas the SLR solution is clearly worse. However, the major contributions to the large RMS obviously stem from the interval boundaries of the weekly satellite orbits (i.e., DoY 290, 297, 304) if the time-series in Fig. 6.1a+b are considered.

***Table 6.6:*** *Comparison of daily and hourly ERP estimates of the single-technique solutions with official series from the IERS, the IGS and the IVS: mean biases.*

| Solution type | | X-pole [mas] | | | Y-pole [mas] | | | UT1-UTC [ms] | |
|---|---|---|---|---|---|---|---|---|---|
| | | C04 | IGS | IVS | C04 | IGS | IVS | C04 | IVS |
| **Daily** | **GPS** | 0.092 | 0.111 | | 0.193 | 0.041 | | - | - |
| | **VLBI** | -0.127 | -0.108 | -0.008 | 0.361 | 0.209 | 0.004 | 0.0016 | -0.0016 |
| | **SLR** | 0.018 | 0.037 | | 0.194 | 0.042 | | - | - |
| **Hourly** | **GPS** | 0.083 | 0.086 | | 0.149 | 0.006 | | - | - |
| | **VLBI** | -0.136 | -0.133 | -0.015 | 0.350 | 0.207 | -0.004 | 0.0014 | -0.0018 |

***Table 6.7:*** *Comparison of daily and hourly ERP estimates of the single-technique solutions with official series from the IERS, the IGS and the IVS: RMS of residuals (mean bias removed; a linear drift was removed additionally from the UT1-UTC time-series in the case of GPS and SLR (= det)). Values in brackets are WRMS values.*

| Solution type | | X-pole [mas] | | | Y-pole [mas] | | | UT1-UTC [ms] | |
|---|---|---|---|---|---|---|---|---|---|
| | | C04 | IGS | IVS | C04 | IGS | IVS | C04 | IVS |
| **Daily** | **GPS** | 0.101 (0.096) | 0.130 (0.126) | | 0.092 (0.082) | 0.077 (0.072) | | det 0.0395 | - |
| | **VLBI** | 0.123 (0.109) | 0.168 (0.155) | 0.118 (0.109) | 0.099 (0.098) | 0.098 (0.096) | 0.077 (0.075) | 0.0076 (0.0066) | 0.0047 (0.0043) |
| | **SLR** | 0.507 (0.439) | 0.519 (0.431) | | 0.439 (0.312) | 0.456 (0.310) | | det 0.1998 | - |
| **Hourly** | **GPS** | 0.143 | 0.142 | | 0.143 | 0.138 | | det 0.0211 | - |
| | **VLBI** | 0.237 | 0.244 | 0.234 | 0.244 | 0.244 | 0.241 | 0.0146 | 0.0140 |

Regarding the comparison of the *UT1-UTC* results with the C04 series in Fig. 6.1c, it is not astonishing that the satellite techniques show large systematic discrepancies as they are not capable to realize an inertial reference system that is stable enough for a good determination of the daily rotation of the Earth over longer

---

28 *http://vlbi.geod.uni-bonn.de/IVS-AC/combi-all/HTML/start_q.html*

time-spans. Solely VLBI has this capability and the agreement with the C04 series as well as with the IVS combined series is quite good, as it can be seen in Fig. 6.3c. The mean bias compared to both series is only 2 µs (see Table 6.6) with a scattering of only a few microseconds (see Table 6.7). It does not make sense to give an RMS for the time-series determined by the satellite techniques, but the attempt to describe the systematics in the time-series with a linear trend revealed at least for GPS that the scattering of 0.039 ms apart from the systematic drift is not too bad. However, the RMS of the detrended SLR series given in Table 6.7 reveals that a linear drift is not a good approximation for the systematics, as it would be already expected from Fig. 6.1c.
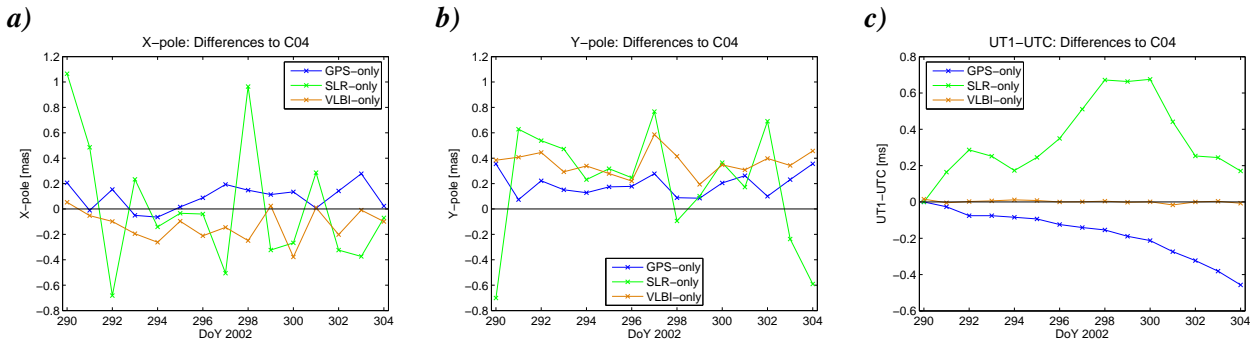


**Figure 6.1:** *Comparison of daily ERP estimates from single-technique solutions with the IERS C04 series: **a)** x-pole, **b)** y-pole, **c)** UT1-UTC.*
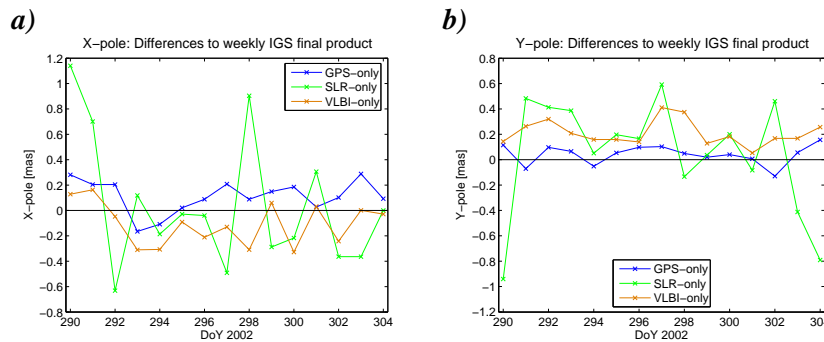


**Figure 6.2:** *Comparison of daily ERP estimates from single-technique solutions with the weekly IGS polar motion series: **a)** x-pole, **b)** y-pole.*
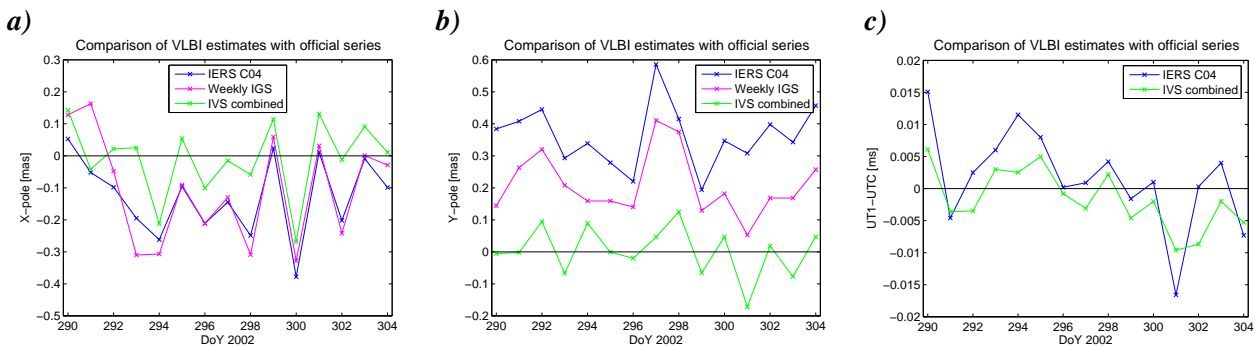


**Figure 6.3:** *Comparison of daily ERP estimates from VLBI with IERS C04, the weekly IGS products and the official IVS combined series: **a)** x-pole, **b)** y-pole, **c)** UT1-UTC.*

Changing to the original sub-daily resolution for the ERP, only the results of GPS and VLBI can be analyzed. The polar motion estimates of both techniques have already been studied in *Chapter 5.3.1* concerning the correlation with the nutation angles handled by the retrograde diurnal constraint (BLOCKRET) in the

program ADDNEQ2. Figures 6.4a+b show the polar motion time-series of both techniques displayed as differences to IERS C04 and the sub-daily model IERS2003. It is not astonishing that the mean offsets of both time-series are similar to those solutions with a daily resolution of ERP (see Table 6.6), as the comparison bases on the same time-series regarding the daily values and only the sub-daily part is added. Regarding the VLBI solution, the time period around DoY 299 and 300 is striking: Both pole coordinates seem to be shifted for this period. An explanation might be that the station Algonquin Park was missing for the respective session (see *Chapter 4.1*), although one would expect that the IVS combined time-series would be shifted then as well. But from the comparison of the daily polar motion series in Fig. 6.3 it is visible that only the VLBI solution used here shows a small shift. Nevertheless, there seems to be no other systematic difference besides this shift in the comparison of the single-technique solutions with the IERS2003 model. The scatter of the differences to the independent sub-daily model is only slightly worse than for the daily polar motion estimates in the case of GPS (see Table 6.7). And even for VLBI the RMS of the unbiased residuals increases only by a factor of about two. Thus, it can be stated that VLBI as well is capable to determine the pole coordinates quite well with a very high temporal resolution, although only eight stations participated. The same is true for the sub-daily estimates of *UT1-UTC*, as can be seen from Fig. 6.4c and Table 6.7. In order to display the sub-daily *UT1-UTC* values integrated from *LOD* estimated by GPS in a reasonable way, a mean linear trend was removed from the original values. The detrended time-series shown in Fig. 6.4c confirms that a linear trend is a rather good approximation for the systematic drift of the GPS-derived *UT1-UTC* time-series, at least for this short time interval of 14 days. Furthermore, the RMS of the detrended residuals of 0.0211 ms (Table 6.7) is in the same order of magnitude as for the VLBI-derived time-series.
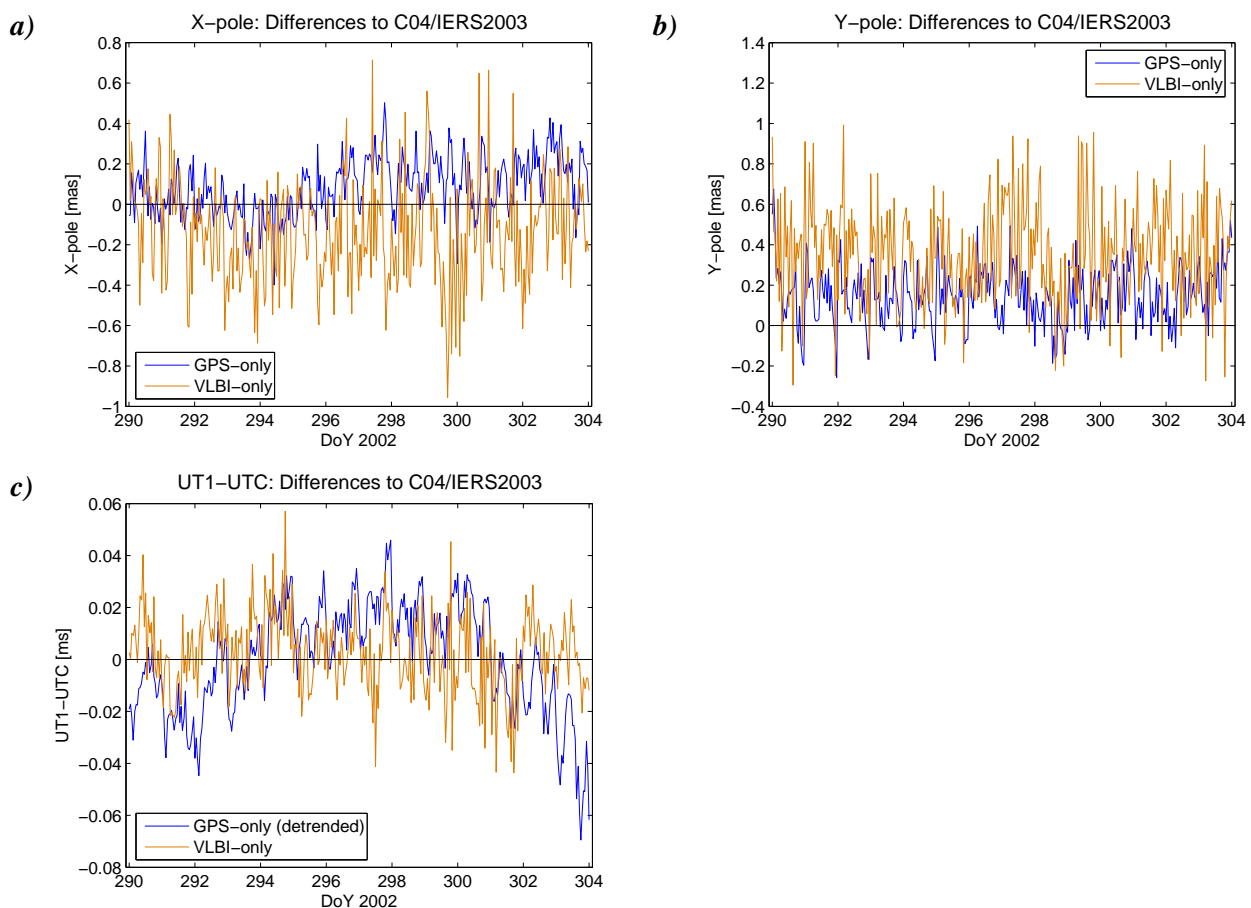
***Figure 6.4:*** *Comparison of hourly ERP estimates from GPS and VLBI with IERS C04 / IERS2003:* ***a)*** *x-pole,* ***b)*** *y-pole,* ***c)*** *UT1-UTC (a linear trend was removed in the GPS series).*

In spite of the systematic drift in the GPS-derived *UT1-UTC* time-series, a combination with VLBI should be possible as the corresponding formal errors rapidly increase with time, whereas the VLBI estimates have stable formal errors during the whole time span (see Fig. 6.5c). Thus, the influence of the GPS contribution on

the combined estimates decreases in the same way as its formal errors increase so that the VLBI contribution should not be destroyed. The situation is different for the polar motion estimates. From Fig. 6.5a+b it becomes visible that both techniques determine the pole coordinates with constant quality over the whole time span. The absolute size of the formal errors in Fig. 6.5a+b has no meaning concerning the level of quality as the values are solution-internal formal errors that strongly depend on the number of observations, that is by far larger for GPS than for VLBI (see Table 5.5). An additional remark should be made concerning the pattern of the formal errors. In the case of GPS, one nicely sees a daily structure in all three ERP with the smallest formal errors in the middle of the day. This pattern is due to the set up of new orbital arcs every day, and the parameters are best determined in the middle of the orbital arcs. The steps at the day boundaries that are present in the formal errors of the *UT1-UTC* estimates of GPS but not in the polar motion estimates can be explained by the fact that the GPS-derived *UT* values are integrated from *LOD* estimates whereas the pole coordinates are estimated directly. As VLBI does not have daily orbits, the pattern of the formal errors of all ERP are expected to show one arch for the entire time-span, with the smallest formal errors in the middle of the interval. However, all three time-series in Fig. 6.5 are split into two arcs around the day 300. This behavior must be explained by the fact that the station Algonquin is missing for the session 300 (see *Chapter 5.1.2b*), and the VLBI estimates and their formal errors are very sensitive to changes in the network geometry.

**a)**                                  **b)**                                  **c)**
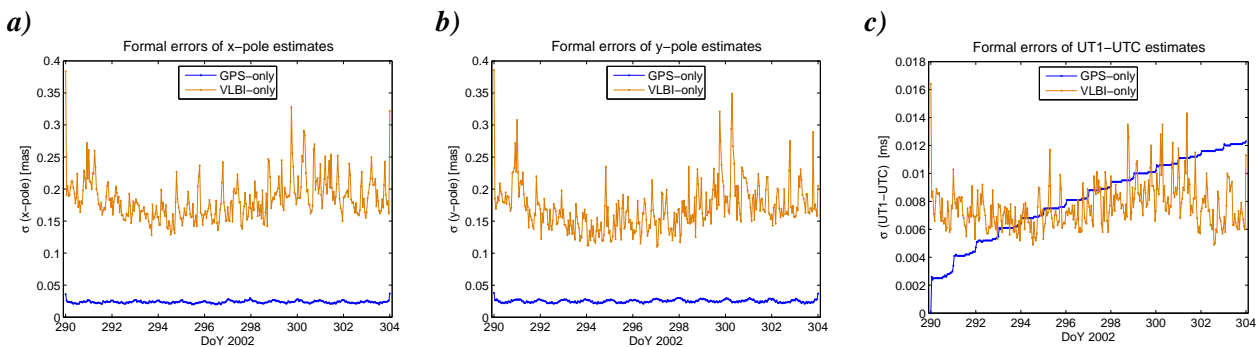


***Figure 6.5:*** *Formal errors of hourly ERP estimates from GPS and VLBI: **a)** x-pole, **b)** y-pole, **c)** UT1-UTC.*

The situation for estimating the nutation angles is similar to the *UT1-UTC* estimates: The satellite techniques are not capable to determine the nutation corrections in an absolute sense due to correlations with the orbital elements. The results for the fortnightly piece-wise linear nutation estimates in Fig. 6.6 reveal large drifts for the satellite techniques compared to the VLBI solution. The options for generating the SLR-only solution had to be modified compared to the other techniques regarding two aspects in order to be able to estimate nutation corrections from SLR, too: First, the temporal resolution of the pole coordinates is 24 h (as already mentioned at the beginning), and, second, a small constraint of 1 mas had to be put on all nutation parameters in addition to the first value that must be fixed for satellite techniques anyway. The latter analysis option explains why the SLR estimates show clearly smaller drifts than the GPS time-series that was estimated without any constraint (beside fixing the first values).

The nutation corrections to IAU2000 provided by the IERS are additionally given in Fig. 6.6 for an external validation, but such a comparison is reasonable only for the VLBI solution in view of the known drifts for the satellite techniques. Therefore, Fig. 6.7 zooms into the VLBI results derived by applying different strategies. The solution with hourly polar motion and fortnightly piece-wise linear nutation angles was already displayed in Fig. 6.6. If it is switched to daily offsets for the nutation angles (constant, not piece-wise linear; see Table 5.4) the results for $\Delta\varepsilon$ agree rather well with the IERS C04 series whereas the nutation in longitude differs significantly. The main difference is a clear drift of about 0.15 mas over 14 days that is seen as well for the fortnightly resolution. But the behavior from day to day differs as well, especially for the middle of the time span. One may argue that there still might be a singularity left for solutions with a sub-daily resolution for the pole coordinates or the retrograde diurnal constraints do not work properly so that such differences would be the consequence. However, the solutions with daily pole coordinates additionally shown in Fig. 6.7 are closer to those with sub-daily resolution than to the IERS C04 series so that the correlation cannot be the explanation for the differences to the IERS C04 series.
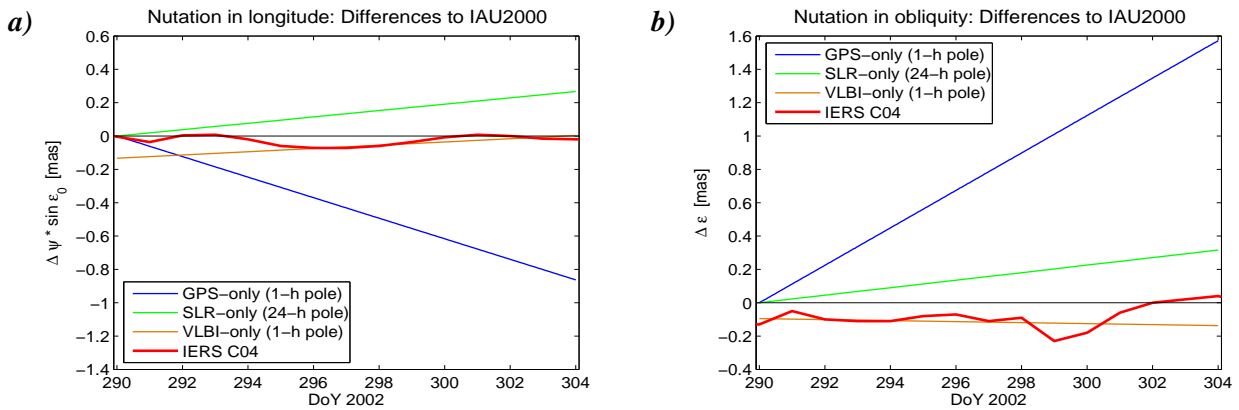
**Figure 6.6:** *Comparison of nutation estimates (fortnightly polygon) determined by the single-technique solutions. The daily values provided by the IERS are shown for comparison. **a)** Nutation in longitude, **b)** nutation in obliquity (both as corrections to the IAU2000 model).*
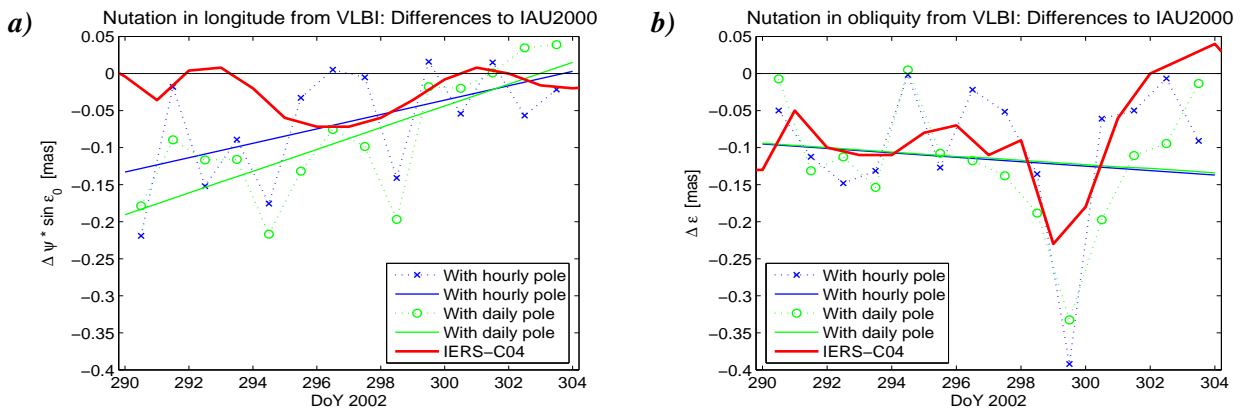


**Figure 6.7:** *Nutation estimates from VLBI for different solution types: sub-daily or daily polar motion estimates and daily or fortnightly nutation estimates (constant offsets in the case of daily nutation and piece-wise linear polygon for fortnightly nutation estimates). The daily values provided by the IERS are shown for comparison. **a)** Nutation in longitude, **b)** nutation in obliquity (both as corrections to the IAU2000 model).*

### 6.1.3 Troposphere parameters

Troposphere parameters were set up for both microwave techniques and the estimated ZD and horizontal gradients can be compared at the eight co-located sites. The ZD are shown in Fig. 6.8 as the estimated corrections to the a priori values. It has been outlined in *Chapter 5.1.2* that the a priori values for the troposphere ZD for both techniques are computed from the hydrostatic part of the Saastamoinen model using a standard atmosphere referred to the height of the GPS reference point. Consequently, the GPS time-series shown in Fig. 6.8 mainly consists of the wet part of the troposphere delay with small corrections due to deviations of the true meteorological conditions (especially the pressure) from the standard atmosphere. The VLBI time-series additionally contains the total troposphere delay caused by the atmospheric layer between the reference heights of GPS and VLBI. It is visible from Fig. 6.8 that both time-series agree very well regarding the temporal behavior as the long-term variations (e.g. Ny-Alesund, Kokee Park) as well as the short-term variations are estimated similarly by both techniques. This is confirmed by the correlation coefficients listed in Table 6.8. They are clearly better than 0.9 for all stations.

In view of combining the troposphere parameters, the ZD difference between the time-series of both techniques is of special interest. The mean differences for 14 days are listed in Table 6.8 for all eight co-locations. Additionally, a weighted mean value was computed based on the formal errors of the ZD estimates because most of the outliers visible in Fig. 6.8 have large standard deviations and the differential ZD for these

epochs should not destroy the mean value. It has to be kept in mind that the differential ZD, i.e., $\Delta ZD_{GPS\text{-}VLBI}$, listed in Table 6.8 still contains the effect of the different reference heights of GPS and VLBI. Thus, the absolute values are not so important but their agreement with the theoretical differences in Table 5.2 is of special interest, because the theoretical troposphere ties will be introduced when the ZD are combined. Three methods for computing the troposphere ties have been presented in *Chapter 5.1.1b* and the agreement of the weighted mean differential ZD estimates for each of these strategies can be seen in Fig. 6.10a. We see that not all stations agree very well with the theoretical values and the differences between the three types of troposphere ties are small compared to the discrepancy itself. The agreement for Algonquin, Wettzell and Hartebeesthoek is excellent. Even the differences for Ny-Alesund are only about 1.5 mm although a radome covers the GPS antenna and it is well known that the troposphere estimates are falsified by a non-calibrated radome. This fact might be the reason for the large discrepancies for Fairbanks, Onsala and Westford as well, because the GPS antenna and/or the VLBI antenna there are covered by a radome whose phase center variations are not yet calibrated. However, the largest discrepancy of 5-6 mm appears for the station Kokee Park but there was no radome installed during this period so that the reason is not clear at the moment. Beside the largest difference, the variability of the differential ZD is largest for Kokee Park, too, as it can be seen from the RMS values listed in Table 6.8. As already mentioned above, some outliers mainly in the VLBI solution are destroying the mean ZD differences so that it is reasonable to take into account the formal errors and look at the WRMS. However, even the WRMS for Kokee Park is almost 9 mm whereas the differential ZD of the other stations is nearly a factor two more stable, except for Fairbanks and Hartebeesthoek. The explanation for the comparably large RMS and WRMS values for Fairbanks might be the large variations visible in the second half of the GPS time-series that are not seen by VLBI (see Fig. 6.8). As the formal errors of the GPS estimates in general are very small (and too optimistic), peaks in the GPS time-series are not identified as weak data points as clear as peaks in the VLBI time-series (e.g. Kokee Park). The large WRMS of 7.5 mm for Hartebeesthoek might be explained by the isolated location of the VLBI site within the network, that decreases the stability for the VLBI-derived time-series of ZD (see Fig. 6.8). Furthermore, there is a general correlation between the WRMS of the differential ZD and the size of the ZD estimates: Figure 6.9 shows that the larger the wet ZD is, the larger is the scatter in the ZD differences between the GPS and VLBI estimates. A possible reason why Fairbanks does not fit into this scheme was already given above.

***Table 6.8:*** *Comparison of the ZD estimated independently by GPS and VLBI. The effect of different reference heights ΔH is not yet corrected in the mean differences ΔZD. A mean bias was removed for the RMS computation. ZD differences and RMS values are given in [mm].*

|  | **ALGO** | **FAIR** | **HRAO** | **KOKB** | **NYA1** | **ONSA** | **WES2** | **WTZR** |
|---|---|---|---|---|---|---|---|---|
| **$\Delta H_{VLBI\text{-}GPS}$ [m]** | 23.100 | 13.056 | 1.527 | 9.243 | 3.101 | 13.710 | 1.735 | 3.101 |
| **Mean $\Delta ZD_{GPS\text{-}VLBI}$** | 7.26 | 0.86 | -0.33 | 7.60 | -0.46 | 1.17 | 4.38 | 1.25 |
| **Weighted mean $\Delta ZD_{GPS\text{-}VLBI}$** | 6.84 | 0.85 | -0.71 | 8.26 | -0.57 | 0.99 | 4.18 | 0.86 |
| **RMS of $\Delta ZD_{GPS\text{-}VLBI}$** | 5.63 | 7.08 | 8.66 | 13.00 | 3.35 | 4.79 | 5.50 | 6.94 |
| **WRMS of $\Delta ZD_{GPS\text{-}VLBI}$** | 4.18 | 5.87 | 7.54 | 8.86 | 3.11 | 3.98 | 5.08 | 5.49 |
| **Correlation coefficient** | 0.931 | 0.939 | 0.975 | 0.969 | 0.994 | 0.971 | 0.978 | 0.957 |
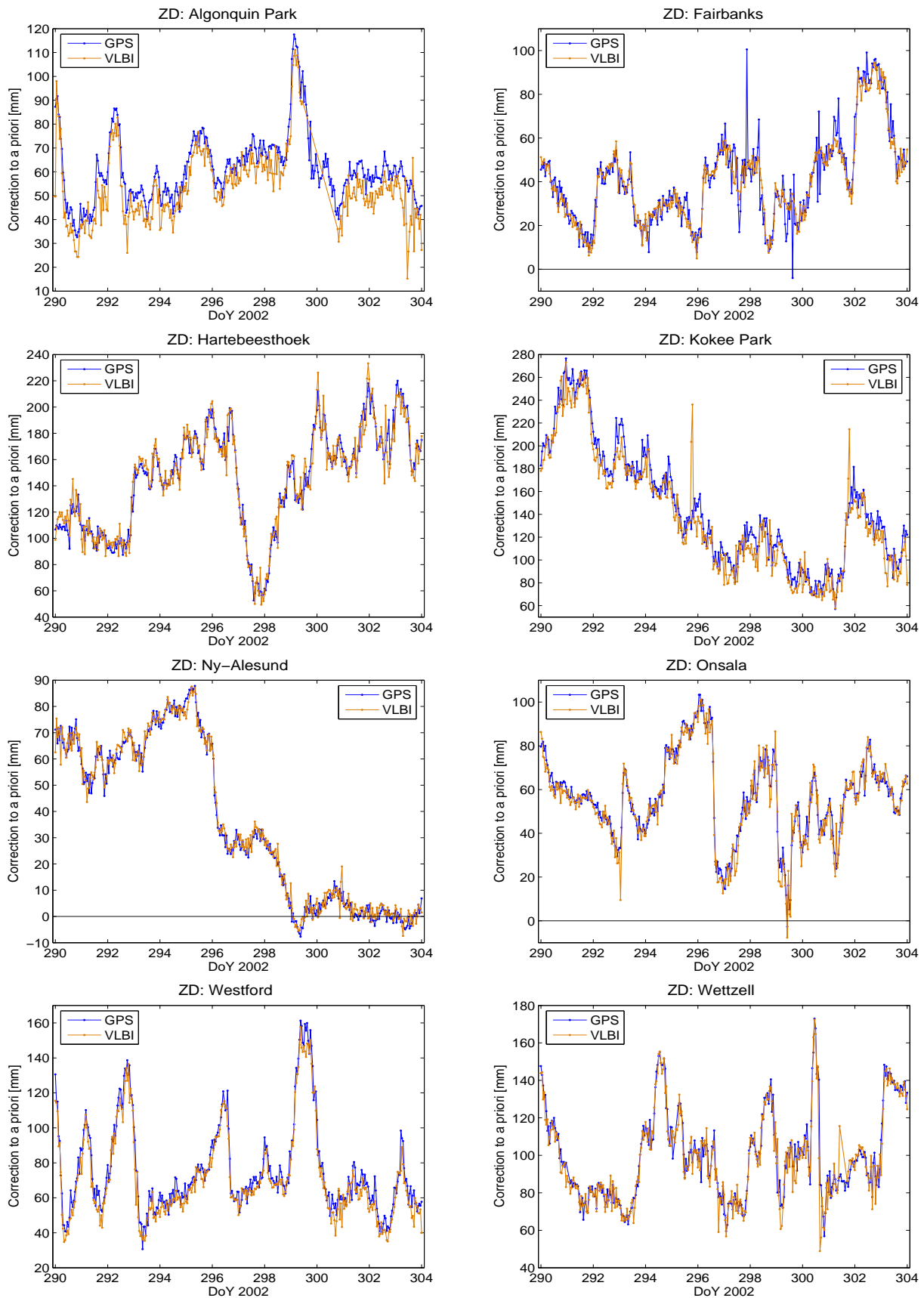
***Figure 6.8:*** *Comparison of the hourly troposphere ZD estimated independently by GPS and VLBI for the co-located sites. The plotted values are the differences to the a priori Saastamoinen dry delay referring to the GPS height.*

RMS of ZD differences depending on the ZD estimates
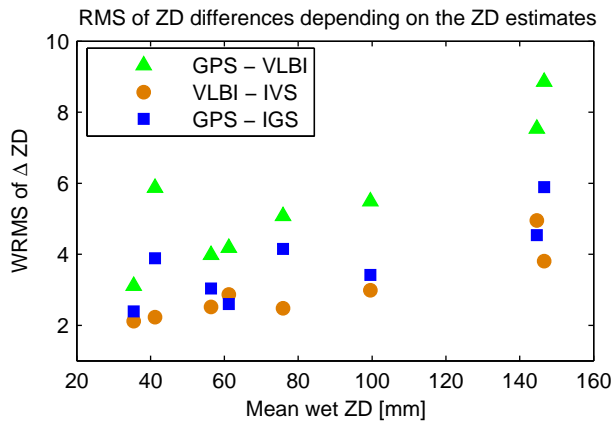
***Figure 6.9:*** *WRMS of the ZD differences depending on the size of the estimated ZD (mean values of the GPS estimates shown in Fig. 6.8).*

In order to validate the ZD time-series, both techniques are compared to the official products of the IVS and IGS. Table 6.9 summarizes the comparison of the VLBI estimates with the ZD provided by the IVS. In general, the mean biases are very small, the correlation between the time-series is better than 0.98 for all stations (except Algonquin Park), and the scattering of the ZD differences is well within the analysis noise between the individual Analysis Centers contributing to the IVS combined product[29]. As already explained for the ZD differences between GPS and VLBI, the scatter of the ZD differences increases with larger ZD estimates (see Fig. 6.9). The very good agreement is shown in Fig. 6.11a exemplarily for Fairbanks. The worst agreement in terms of WRMS is present for Hartebeesthoek, and Fig. 6.11b visualizes that the IVS time-series is clearly more stable than the VLBI solution generated within this study. Two important differences between the IVS product and the VLBI solution used here are responsible for this behavior: First, the IVS product is a combination of up to eight individual contributions by different analysis centers. As the uncertainty in the time-series due to the so-called "analysis noise" is reduced in the combination, the combined time-series is smoother than the individual contributions (see the station-specific plots on the IVS website[30]). The second reason is the application of constraints by the analysis centers in the generation of the IVS time-series in order to stabilize those epochs that are weakly determined, whereas the VLBI solution generated for the studies within this thesis does not contain any constraint for smoothing the time-series. Due to these reasons it is not astonishing that the comparison of the GPS time-series with the IVS products reveals more stable differential ZD and a better correlation of both time-series than for the VLBI solution used within this thesis (see Table 6.10). However, for all stations except for Onsala, the mean ZD biases between GPS and VLBI derived from the comparison with the IVS products deviate more from the theoretical troposphere ties than those mean ZD biases derived by using the VLBI solution of this thesis (see Fig. 6.10b compared to Fig. 6.10a). This fact indicates that the careful adaptation of the a priori models used for the GPS and VLBI analysis (see *Chapter 5.1.2*) is worthwhile in order to get better and more consistent results.

***Table 6.9:*** *Comparison of the ZD for the VLBI sites with the IVS combined troposphere product. The mean bias was removed for the RMS computation.*

|  | **ALGO** | **FAIR** | **HRAO** | **KOKB** | **NYA1** | **ONSA** | **WES2** | **WTZR** |
|---|---|---|---|---|---|---|---|---|
| ***Weighted mean*** $\Delta ZD_{VLBI-IVS}$ ***[mm]*** | -1.64 | -0.44 | 2.04 | -0.09 | 0.09 | -1.79 | -0.35 | 1.17 |
| ***RMS of*** $\Delta ZD_{VLBI-IVS}$ ***[mm]*** | 4.47 | 2.79 | 5.97 | 9.11 | 2.41 | 3.21 | 3.23 | 4.36 |
| ***WRMS of*** $\Delta ZD_{VLBI-IVS}$ ***[mm]*** | 2.87 | 2.23 | 4.95 | 3.81 | 2.12 | 2.52 | 2.48 | 2.99 |
| ***Correlation coefficient*** | 0.959 | 0.990 | 0.988 | 0.985 | 0.998 | 0.987 | 0.992 | 0.983 |

---

29 *http://mars.hg.tuwien.ac.at/~ivstrop/info/reportWWWW_new.dat (with WWWW for GPS week)*
30 *http://mars.hg.tuwien.ac.at/~ivstrop/statistics2/XXXXtzd.eps (with XXXX for the station)*

**Table 6.10:** *Comparison of the ZD estimated by GPS with the IVS combined troposphere product. The effect of different reference heights ΔH is not yet corrected in the mean differences ΔZD. The mean bias was removed for the RMS computation.*

| | ALGO | FAIR | HRAO | KOKB | NYA1 | ONSA | WES2 | WTZR |
|---|---|---|---|---|---|---|---|---|
| *Weighted mean ΔZD$_{GPS-IVS}$ [mm]* | 8.16 | 1.22 | -2.70 | 8.10 | -0.61 | 3.10 | 4.67 | -0.59 |
| *WRMS of ΔZD$_{GPS-IVS}$ [mm]* | 4.81 | 5.85 | 6.75 | 8.04 | 3.16 | 4.20 | 4.99 | 4.27 |
| *Correlation coefficient* | 0.952 | 0.939 | 0.981 | 0.985 | 0.994 | 0.973 | 0.979 | 0.973 |

Comparing the GPS estimates with the IGS combined troposphere products clearly points out the influence of applying a relative model for the antenna phase center variations (as it is the case for the IGS solutions) compared to a model with absolutely calibrated phase center variations for ground and satellite antennas (as it is the case for the GPS solutions studied in the thesis at hand). This difference in the a priori models causes large biases in the troposphere estimates of several millimeters (see Table 6.11). The time-series for two sites are shown exemplarily in Fig. 6.12. Similar to the VLBI estimates, the larger temporal variations in the GPS time-series compared to the IGS product must be explained by the smoothing effect of the combination carried out for deriving the IGS time-series. Additionally, the temporal resolution of the IGS time-series is only two hours whereas the GPS solution generated for this thesis contains hourly values. Thus, another part of the increased scatter must be dedicated to the doubling of the temporal resolution. Consequently, it is not astonishing that the RMS and WRMS values of the ZD differences given in Table 6.11 are larger than the analysis noise usually reported for the IGS combination (i.e., 1-3 mm)[31]. Figure 6.9 shows that the WRMS of the ZD differences depends on the size of the ZD estimates themselves, as it was already mentioned for the comparisons between the GPS and VLBI estimates and for the comparison of the VLBI estimates with the IVS time-series.

**Table 6.11:** *Comparison of the ZD estimated by GPS with the IGS combined troposphere product. The IGS time-series were interpolated to hourly values. The mean bias was removed for the RMS computation.*

| | ALGO | FAIR | HRAO | KOKB | NYA1 | ONSA | WES2 | WTZR |
|---|---|---|---|---|---|---|---|---|
| *Weighted mean ΔZD$_{GPS-IGS}$ [mm]* | 4.99 | 6.75 | 7.15 | 2.90 | 3.55 | 4.54 | 4.20 | 4.42 |
| *RMS of ΔZD$_{GPS-IGS}$ [mm]* | 2.75 | 6.00 | 5.34 | 5.92 | 2.54 | 3.32 | 4.45 | 4.21 |
| *WRMS of ΔZD$_{GPS-IGS}$ [mm]* | 2.60 | 3.89 | 4.54 | 5.89 | 2.39 | 3.04 | 4.15 | 3.42 |
| *Correlation coefficient* | 0.982 | 0.957 | 0.991 | 0.994 | 0.997 | 0.985 | 0.985 | 0.984 |

Finally, as there are noticeable biases in the troposphere ZD estimates between the IGS combined product and the GPS solution used within this thesis, the question arises, which type of solution fits better to the VLBI-derived troposphere estimates and the theoretical values for the troposphere ties. According to Fig. 6.10 it can be stated that the agreement with the theoretical troposphere ties is clearly better for the GPS solution generated for this thesis. Except for Onsala, the discrepancies are larger for the IGS solution. As the size of the discrepancies agree very well with the studies concerning relative vs. absolute modeling of antenna phase center variations documented in *Schmid et al. (2005)*, the large deviations for the IGS products must be dedicated to the usage of a relative antenna model. Furthermore, these results show that the application of an a priori model with absolutely calibrated antennas in the GPS analysis is indispensable if meaningful comparisons and combinations should be done with VLBI-derived troposphere parameters.

---

31 *ftp://ftp.gfz-potsdam.de/pub/igstrop/prod/wWWWW/TROPWWWW.sum (with WWWW for the GPS week)*
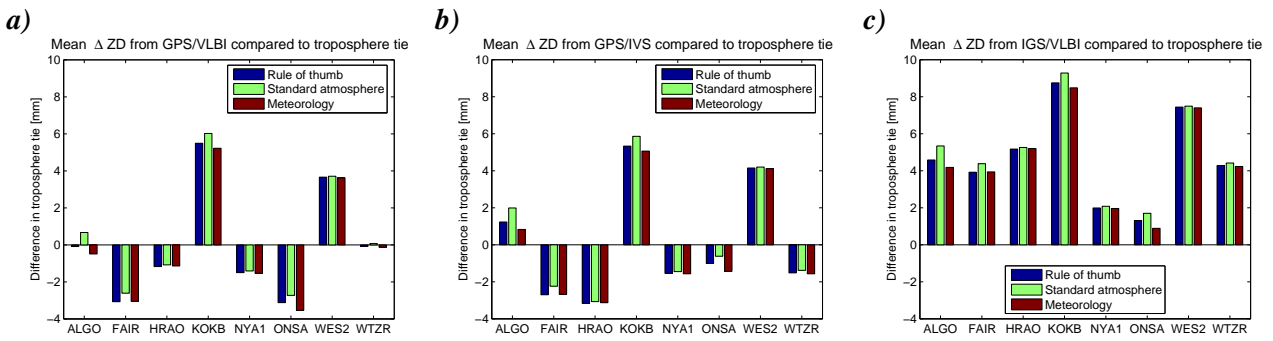
**Figure 6.10:** *Comparison of the differential troposphere ZD GPS-VLBI with the troposphere ties computed using three different methods listed in Table 5.2:* ***a)*** *for the GPS and VLBI estimates (weighted mean ΔZD_GPS-VLBI given in Table 6.8),* ***b)*** *for the GPS estimates and the IVS combined troposphere product (given in Table 6.10),* ***c)*** *for the IGS combined troposphere product and the VLBI estimates.*
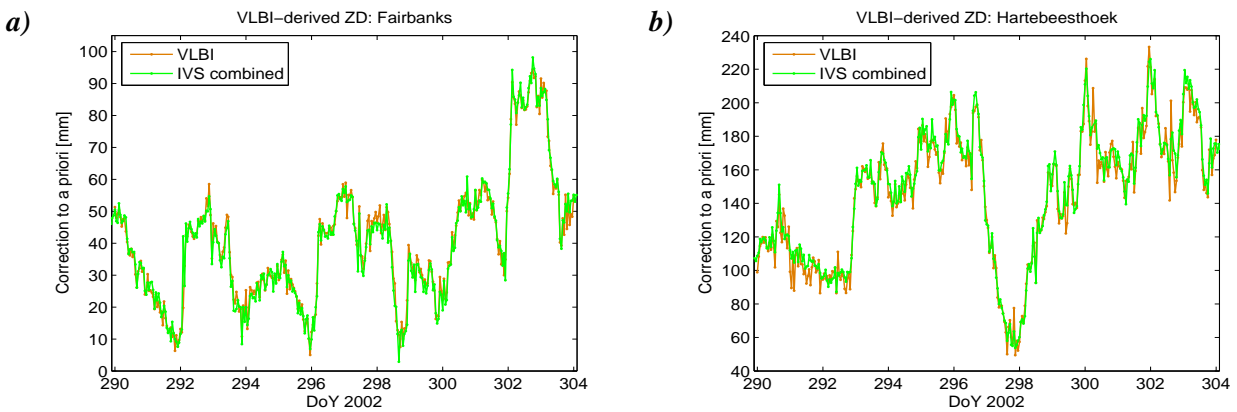


**Figure 6.11:** *Comparison of the VLBI ZD estimates with the IVS combined product for two sites:* ***a)*** *Fairbanks,* ***b)*** *Hartebeesthoek.*
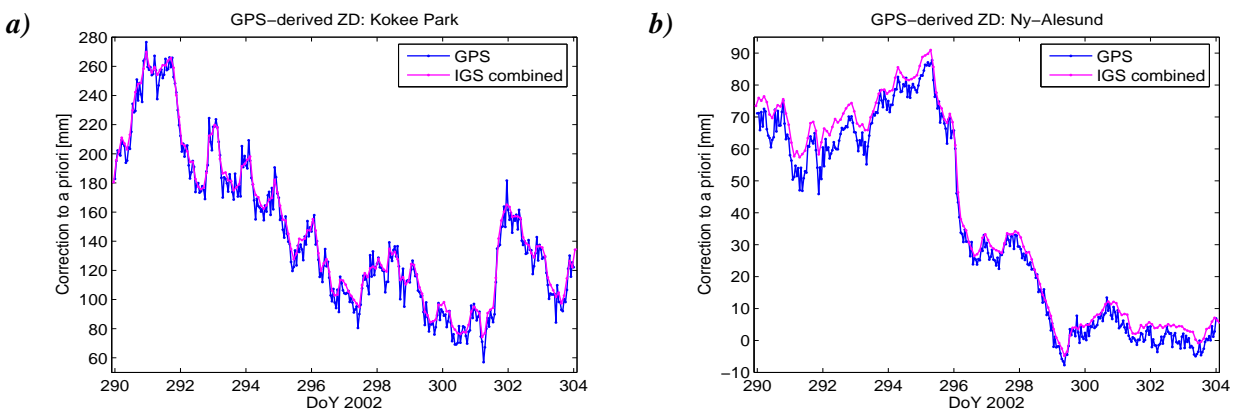


**Figure 6.12:** *Comparison of the GPS ZD estimates with the IGS combined product for two sites:* ***a)*** *Kokee Park,* ***b)*** *Ny-Alesund.*

The question whether the differential ZDs show any systematics that can probably be explained by using only a mean value for the troposphere tie in the comparison can be answered by Fig. 6.13. The time-series of

the epoch-wise troposphere ties already shown in Fig. 5.1 are displayed together with the differential ZD derived from the GPS and VLBI estimates for those stations that reveal remarkable variations in the time-series of troposphere ties computed from meteorological data (see Fig. 5.1). It becomes clear from this comparison that the temporal variations in the troposphere ties are negligible compared to the variations in the estimated ZD differences. Therefore, the usage of a mean value for the troposphere ties (see Table 5.2) will be sufficient for further comparisons as well as for the combination.
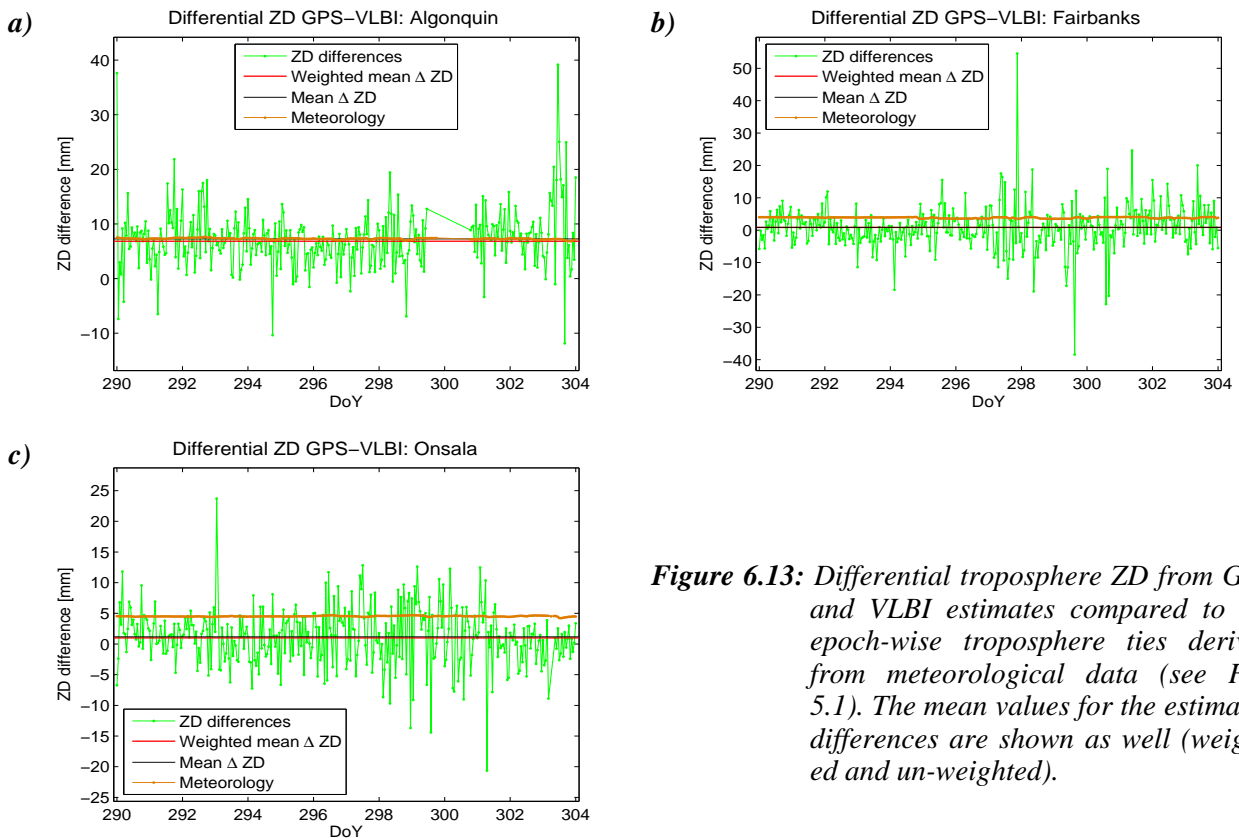


***Figure 6.13:*** *Differential troposphere ZD from GPS and VLBI estimates compared to the epoch-wise troposphere ties derived from meteorological data (see Fig. 5.1). The mean values for the estimated differences are shown as well (weighted and un-weighted).*

The second possibility for validating the ZD estimates mentioned in *Chapter 5.2.2* is the comparison with WVR data for Kokee Park, Onsala and Wettzell. The procedure for deriving the wet part (ZWD) from the total troposphere delay estimated by GPS and VLBI was outlined in *Chapter 4.3*. Figures 6.14a-c display the ZWD estimates and the WVR observations for the three stations (hourly mean values of rain-free epochs, see Fig. 4.3). Except for some peaks in the WVR time-series, the temporal behavior agrees quite well with the GPS- and VLBI-derived ZWD, which is confirmed by the correlation coefficients given in Table 6.12. At a first glance, the agreement for Kokee Park seems to be clearly worse, but this must be dedicated to the large peaks in the WVR time-series around DoY 302. The WVR-internal rain sensors do not indicate rainfall for all epochs of the original measurements (see Fig. 4.2) although their data are questionable, too. Thus, a few epochs remained for computing hourly mean values and large formal errors are assigned to them (see Fig. 4.3). However, contrary to the weighted mean bias and the WRMS of the differences, the formal errors are not taken into account when computing the correlation coefficient, so that all epochs are treated equally. Omitting the questionable epochs around DoY 302 in the WVR time-series, the correlation coefficients clearly improve to 0.921 and 0.802 for the comparison with GPS and VLBI, respectively. Besides the peaks in the WVR time-series, the bias compared to GPS and VLBI for Wettzell is striking. The weighted mean bias over 14 days is about 12 mm for both, GPS and VLBI (see Table 6.12). For the values given in Table 6.12, the corrections due to the height differences are taken into account according to the description given in *Chapter 4.3*.

Although the scatter of the residuals is quite different for the three stations, the WRMS of the wet ZD residuals of the comparison with WVR (Table 6.12) is larger than for the total ZD residuals between GPS and VLBI (Table 6.8) in all cases. Looking at the short-term temporal behavior of the time-series opposed in Fig.

6.14 it becomes obvious that the increased WRMS values are caused by the WVR estimates which show larger variations than the GPS and VLBI estimates. It must be pointed out again, that the WRMS of the wet ZD residuals is correlated to the size of the ZWD itself.

*a)*



*b)*



*c)*
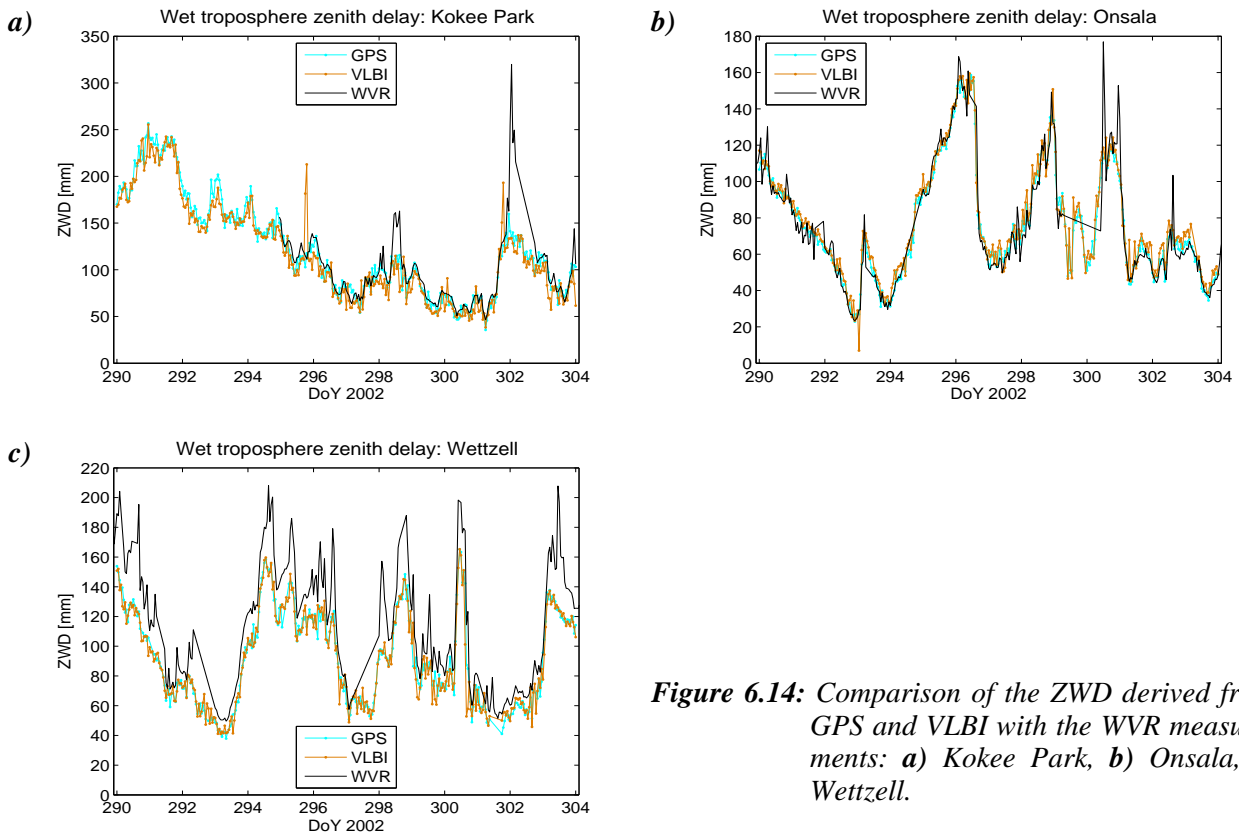


**Figure 6.14:** *Comparison of the ZWD derived from GPS and VLBI with the WVR measurements:* **a)** *Kokee Park,* **b)** *Onsala,* **c)** *Wettzell.*

**Table 6.12:** *Comparison of the ZWD derived from GPS and VLBI (GV) with the WVR measurements. The differential ZWD due to height differences is already taken into account. The mean bias was removed for the RMS computation.*

|  | **KOKB** | | **ONSA** | | **WTZR** | |
|---|---|---|---|---|---|---|
|  | **GPS** | **VLBI** | **GPS** | **VLBI** | **GPS** | **VLBI** |
| *# common epochs* | 203 | 203 | 277 | 273 | 258 | 273 |
| *Weighted mean $\Delta ZWD_{GV-WVR}$ [mm]* | -8.35 | -7.87 | 0.51 | 4.97 | -12.63 | -12.02 |
| *WRMS of $\Delta ZWD_{GV-WVR}$ [mm]* | 10.11 | 12.40 | 4.06 | 5.30 | 8.70 | 9.40 |
| *Correlation coefficient* | 0.836 | 0.732 | 0.967 | 0.958 | 0.962 | 0.949 |

In addition to the troposphere ZD, horizontal gradients were estimated for GPS and VLBI. Figure 6.15 shows the estimated north gradients (first row) and east gradients (second row) for some selected stations that are representative for the others. It has to be kept in mind that the parameterization for the troposphere gradients was not unified in the single-technique solutions (see *Chapter 5.1.2*): The GPS solution contains a daily polygon indicated by a straight line in Fig. 6.15, whereas daily constant offsets were set up in the VLBI solution. The agreement of both techniques differs strongly between the stations and can be grouped into three types: The north gradient for Wettzell and the east gradient for Ny-Alesund (first column in Fig. 6.15) represent the major part of station-specific gradients with a quite good agreement of both techniques. For the two stations shown in the middle column the temporal behavior of both techniques matches well but the time-series are biased. Finally, the examples for Hartebeesthoek and Kokee Park displayed in the last column represent those gradient estimates with a comparably bad agreement of the temporal behavior. In order to con-

clude the analysis of the troposphere gradients, the good agreement for most of the time-series is very promising in view of a combination that is envisaged for the troposphere gradients as well.
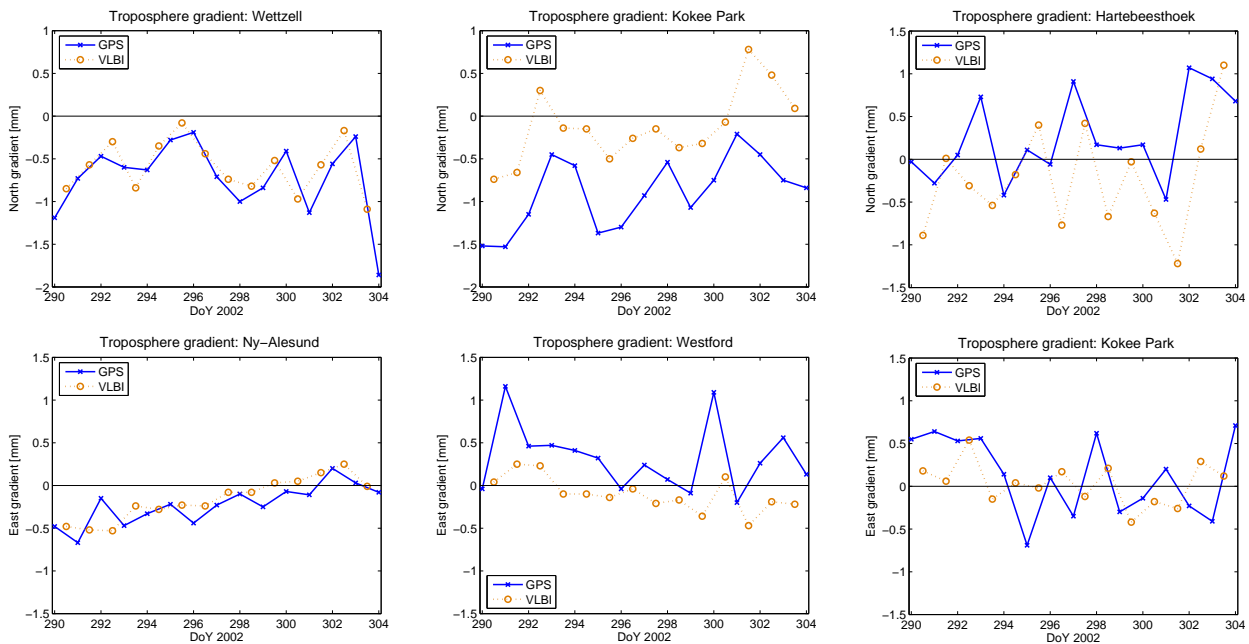


**Figure 6.15:** *Comparison of horizontal troposphere gradients. The straight line for GPS indicates a parameterization as polygon in contrast to the dotted line for VLBI connecting the constant offsets at the middle of the day.*

## 6.1.4 Datum parameters: translations and scale

As regards the determination of the geocenter, only the satellite techniques can be compared, whereas all three techniques can be analyzed regarding their contribution to the global scale. In a first step, the quality of the techniques is analyzed on a weekly basis as SLR is too weak if daily solutions are considered. However, it must be emphasized that a meaningful statement about the potential of weekly solutions cannot be made by analyzing only two weeks of data (as in the case of the CONT02 campaign). It is clear that a longer time-span is needed for this. But the two weekly solutions for the CONT02 time-span can give a first idea whether the combined solution can benefit from the contribution of SLR. For this purpose, two seven-day solutions were computed for each single-technique and then compared to the 14-day solution of the appropriate technique via a seven-parameter Helmert transformation. The resulting translation parameters listed in Table 6.13 indicate the strength of SLR. As expected, the *z*-component is clearly better determined by SLR with variations of only some millimeters compared to about 2 cm for GPS. The other two components are of similar quality for both techniques. However, looking at the scale parameters in Table 6.13 reveals that the contribution of SLR to this datum parameter is very weak as the determination of the weekly global scale by GPS and VLBI is about one order of magnitude more stable. Finally, the RMS of the Helmert transformation indicates the overall stability of the weekly single-technique solutions (Table 6.13). Again, we can see about one order of magnitude difference between the GPS and VLBI solutions on the one hand, and the SLR solution on the other hand.

Similar analyses can be done for GPS and VLBI on the basis of daily instead of weekly solutions. As expected, the variations for the scale and the translation parameters (only GPS) become larger than for the weekly comparison and the RMS of the Helmert transformations increases (see Fig. 6.16 and 6.17). Nevertheless, the scale variations from day to day are in the range of ±0.3 ppb and ±0.4 ppb for GPS and VLBI, respectively, if the obviously bad days with 1.0 ppb or even 2.0 ppb are neglected in the case of VLBI. Regarding the translation parameters in Fig. 6.17, GPS shows variations of about 1 cm for the *x*- and *y*-component and about 2 cm for the *z*-component. In view of the combination it is expected that SLR can stabilize the *z*-component, although the SLR network probably might be too weak on a daily basis to see this stabilization.

a)



b)
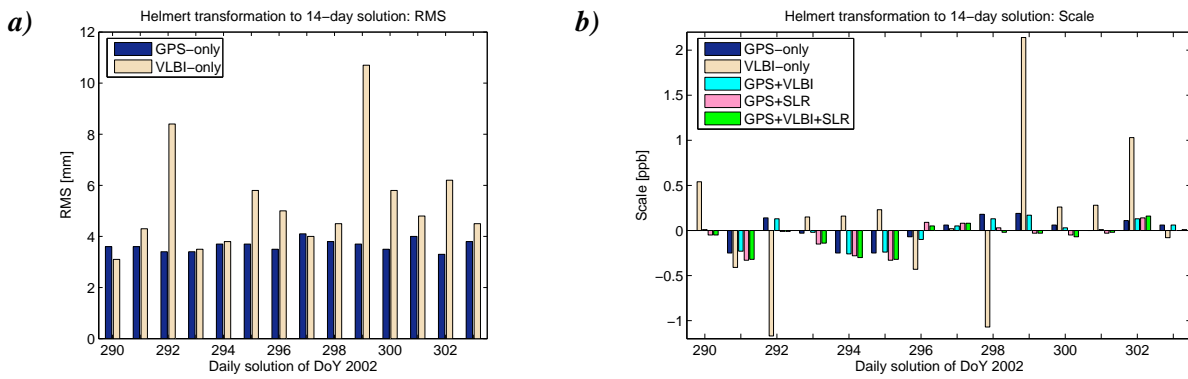
*Figure 6.16:* *Comparing the daily solutions with the corresponding 14-day solution via a seven-parameter Helmert transformation:* ***a)*** *RMS,* ***b)*** *scale. The combined solutions will be addressed in Chapter 6.2.1e.*
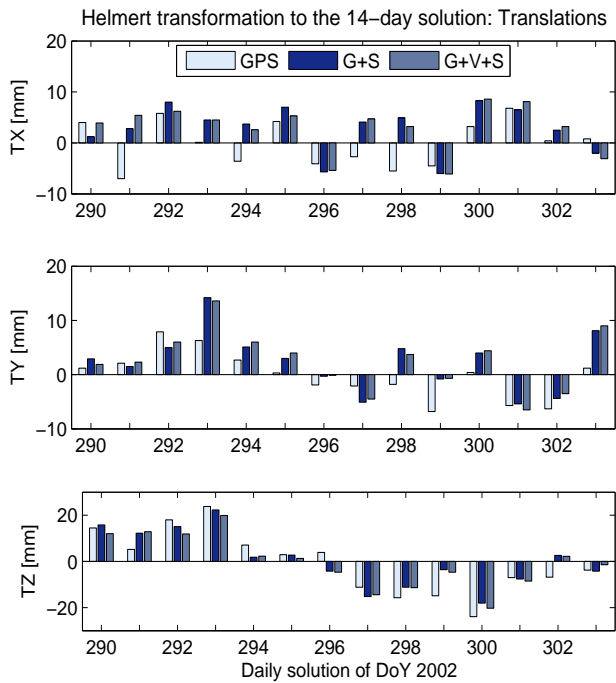


*Figure 6.17:* *Comparing the daily solutions with the corresponding 14-day solution via a seven-parameter Helmert transformation: translations. The combined solutions will be addressed in Chapter 6.2.1e.*

*Table 6.13:* *Comparing both weekly solutions with the 14-day solution (single-techniques) using a seven-parameter Helmert transformation.*

| Tech-nique | Translations [mm] | | | | | | Scale [ppb] | | RMS [mm] | |
|---|---|---|---|---|---|---|---|---|---|---|
| | 1st week | | | 2nd week | | | 1st week | 2nd week | 1st week | 2nd week |
| | Tx | Ty | Tz | Tx | Ty | Tz | | | | |
| **GPS** | 0.5 | 2.5 | 9.8 | -0.2 | -2.8 | -12.9 | -0.08 | 0.08 | 1.24 | 1.25 |
| **SLR** | 2.1 | -4.7 | -2.3 | 1.3 | -1.3 | -5.0 | 0.68 | -0.26 | 15.86 | 8.25 |
| **VLBI** | - | - | - | - | - | - | -0.09 | 0.15 | 1.56 | 2.06 |

# 6.2   Combination studies

In order to better assess the impact of combining the different parameter types, the combination studies are sub-divided into several steps. We start with a consistent combination of the TRF and the EOP (*Chapter 6.2.1*). The troposphere parameters are included in the solution so that they can adapt to the common reference frame, but apart from this, the troposphere parameters for the GPS and VLBI sites are still estimated independently. Based on this type of solution, the analysis of the LT is carried out in order to identify those LT that fit well to the space-geodetic solutions and that should be introduced in all further combined solutions. The combination of the EOP itself is sub-divided as well: First, only the pole coordinates are combined as all techniques are capable to determine them. The capability of the satellite techniques to contribute to *UT1-UTC* and the nutation angles is studied afterwards. On the basis of a solution with combined TRF and EOP, the benefit of allowing for Helmert parameters will be addressed in *Chapter 6.2.2. Chapter 6.2.3* is devoted to the combination of the troposphere parameters at co-located GPS-VLBI sites. Finally, a fully combined solution is computed by taking into account the outcome of the studies presented in the previous chapters. All parameters resulting from this final solution are presented in *Chapter 6.2.4*.

For some studies the combination is done step-by-step not only concerning the parameters but also concerning the techniques involved in the combination. In this context, solutions denoted with "G+V" and "G+S" are two-technique combinations restricted to GPS and VLBI only or GPS and SLR only, respectively. The combined solution including all three techniques is denoted "G+V+S". The relative weighting for the GPS, VLBI and SLR normal equation systems is done according to Table 6.4 for all combined solutions presented hereafter.

## 6.2.1   Combining TRF and EOP consistently

*a) Repeatabilities of station coordinates*

It can be expected from the coordinate repeatabilities of the single-technique solutions (Tables 6.1-6.3) that mainly SLR and VLBI will benefit from a combination with GPS because the latter gives the most stable single-technique reference frame. Figure 6.18 and Tables  and 6.15 confirm this expectation. Three types of solutions are compared: single-technique solutions, two-technique combinations (i.e., GPS is combined with only one of the other techniques), and, finally, a full combination including all three techniques. In the case of VLBI, the embedding of the eight-site network into the dense GPS network leads to an improvement of the repeatability for nearly all sites, with a mean improvement over all sites of about 1.6 mm for the north and height component, and 0.2 mm for the east component. These values reflect well the difference in the coordinate repeatability present between both single-technique solutions (see Table 6.1) so that the combination results fulfill the expectations. Compared to the repeatabilities for the VLBI-only solution, the north component benefits most, as the decrease of 1.6 mm corresponds to a mean improvement of about 42%, whereas the improvements for the east and height components are only about 5% and 14%, respectively. However, this behavior was expected, as the network configuration of the VLBI-only solution is limiting the stability of the north component. The additional inclusion of SLR into the combination does not have any large impact on the VLBI sites, but this must be attributed to the fact that only two VLBI-SLR co-locations are present in the network, i.e., Hartebeesthoek and Wettzell.

The analysis of the results for SLR is more difficult because the sites must be grouped into those that are co-located with GPS and those that are SLR-only sites. The co-located sites are directly linked to the GPS network by the LT, whereas the others can benefit only indirectly from the stable GPS network, so that the improvement in the repeatability is expected to be smaller. Furthermore, the station Shanghai (7837, SHAO) marks a special case because it can be employed as GPS-SLR co-location only in the full 14-day solution but not in the daily solutions (see Table 4.2, *Chapter 4.2*). Consequently, Shanghai should not be treated as a co-located site in repeatability studies as long as the repeatabilities are computed by comparing daily solutions with the 14-day solution (see *Chapter 5.2.1*). Thus, Table  gives the changes in repeatability additionally if Shanghai is neglected for the co-located sites, and Shanghai is omitted for the mean repeatabilities listed in Table 6.15, too. From these values and Fig. 6.18b it can be clearly seen that the stability of the horizontal components of the SLR sites co-located with GPS increases by about 6 to 7 mm, thus demonstrating the benefit of the combination that was expected from Tables 6.1 and 6.3. The mean improvement for the height component is only about 1.3 mm but this is not astonishing as the height component for GPS is less stable

than the horizontal components (see Tables 6.1-6.3) and the mean value for the co-located GPS sites of 8.07 mm is even slightly worse than for the co-located SLR sites, i.e. 7.39 mm (see Table 6.15). The strongly degraded repeatabilities for the non-co-located SLR sites by more than 1 cm must be dedicated to two facts: First, all SLR sites are used for the datum conditions in the SLR-only solution if daily repeatabilities are computed (see *Chapter 6.1.1*), whereas some of them (i.e., sites 1884-7824 in Fig. 6.18b) are neither included in the datum definition of the combined solution nor directly attached to GPS by the LT. And, second, the SLR-only solution was computed with fixed satellite orbits for LAGEOS (see *Chapter 6.1.1*) whereas the combined solutions are computed without any constraints on orbit parameters so that this additional stabilization is missing in the combination.

The repeatabilities for the GPS sites co-located with VLBI do not change significantly in the combination, as it should be the case (see Table ). Unfortunately, the inclusion of SLR degrades the height component of those GPS sites co-located with SLR by about 2 mm, although the comparison in Table 6.3 showed that both techniques have a similar level of stability respectively the GPS heights are even slightly better. Compared to the size of the height repeatability for the GPS-only solution, this change is a degradation of about 41%, whereas the change in the north and east component is only about 8% and 24%, respectively. Thus, as the horizontal components are nearly unaffected and the height component is correlated to the scale, one reason for this behavior might be some discrepancies in the scale of the GPS and SLR networks that are not handled in the solutions computed here. This topic will be studied in *Chapter 6.2.2*.

Finally, it is clear that those LT that are introduced into the combination but do not fit to the space-geodetic solutions can countervail the stabilization of the coordinate repeatabilities by a combination. The methods of identifying good LT (out of the full set of eight GPS-VLBI and 14 GPS-SLR LT) and the effect on the results is described subsequently.

*a)*                               *b)*
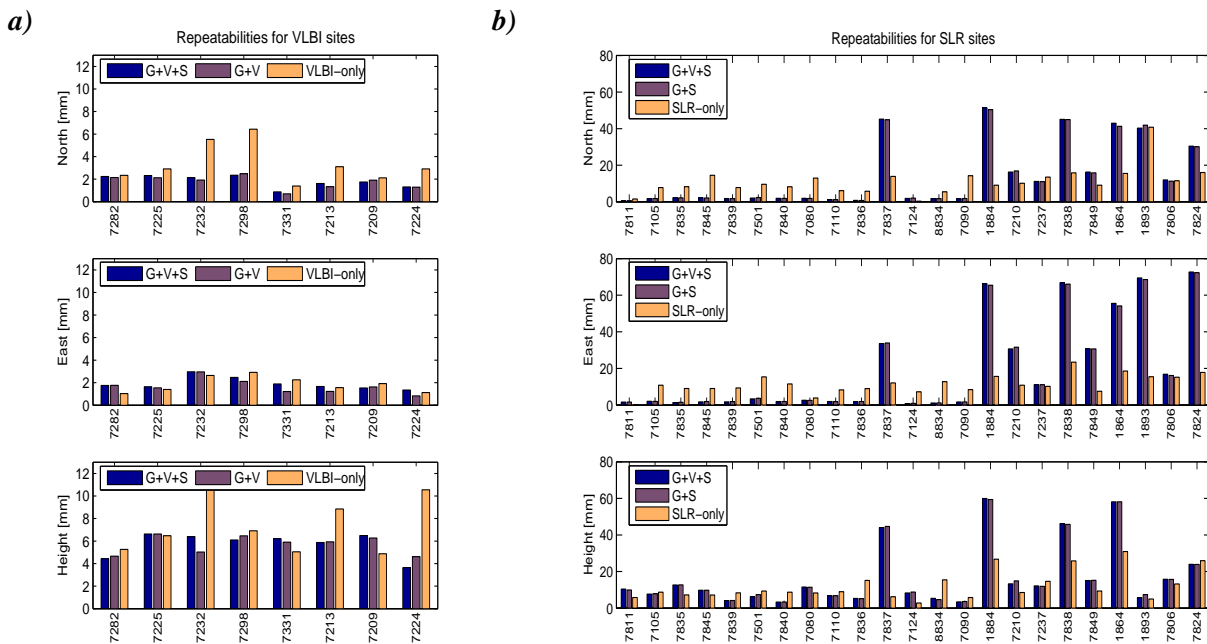


***Figure 6.18:*** *Daily coordinate repeatabilities of the single-technique and combined solutions:* ***a)*** *VLBI sites,* ***b)*** *SLR sites (7811-7090: Co-locations with GPS, 1884-7849: used for reference frame definition in SLR-only solution but no co-location with GPS, 1864-7824: neither used for reference frame definition nor a co-location with GPS).*

***Table 6.14:*** *Change of daily coordinate repeatabilities in the combined solutions compared to the single-technique solutions, given as a mean value over the selected sub-set of sites (in [mm]). Negative values indicate an improvement due to the combination. The values given in brackets are by neglecting the co-location SHAO-7837.*

| Sub-set of sites | GPS + VLBI | | | GPS + SLR | | | GPS + VLBI + SLR | | |
|---|---|---|---|---|---|---|---|---|---|
| | *ΔN* | *ΔE* | *ΔU* | *ΔN* | *ΔE* | *ΔU* | *ΔN* | *ΔE* | *ΔU* |
| *All VLBI* | -1.60 | -0.20 | -1.64 | - | - | - | -1.52 | 0.05 | -1.61 |
| *GPS co-loc. with VLBI* | -0.04 | -0.07 | -0.07 | - | - | - | 0.03 | 0.14 | -0.06 |
| *GPS co-loc. with SLR* | - | - | - | 0.21 (0.10) | 0.53 (0.37) | 6.10 (2.28) | 0.18 (0.09) | 0.46 (0.30) | 5.97 (2.17) |
| *SLR co-loc. with GPS* | - | - | - | -3.56 (-6.21) | -4.88 (-6.93) | 1.57 (-1.26) | -3.55 (-6.23) | -4.97 (-7.01) | 1.49 (-1.31) |
| *SLR not co-located* | - | - | - | 13.58 | 31.25 | 10.24 | 13.82 | 31.72 | 10.01 |

***Table 6.15:*** *Daily repeatability of station coordinates for different types of combined solutions and a sub-set of stations considered. "6 LT" in the case of the G+V solution means that the LT for Fairbanks and Westford are omitted. Although the LT for Shanghai is introduced, the GPS and SLR sites are omitted for the computation of the repeatabilities. The solution types A-D will be addressed in Chapter 6.2.2.*

| Solution type | Sub-set of stations | Repeatability [mm] | | | |
|---|---|---|---|---|---|
| | | *North* | *East* | *Up* | *3D* |
| *G+V, all LT* | All VLBI | 1.93 | 1.91 | 5.48 | 3.53 |
| *G+V, all LT* | GPS co-located with VLBI | 1.87 | 1.67 | 5.50 | 3.49 |
| *G+V, 6 LT* | All VLBI | 1.82 | 1.77 | 5.74 | 3.62 |
| *G+V, 6 LT* | GPS co-located with VLBI | 1.71 | 1.71 | 6.24 | 3.86 |
| *G+S, 14 LT* | SLR co-located with GPS (w/o 7837) | 1.78 | 2.09 | 7.39 | 4.55 |
| *G+S, 14 LT* | GPS co-located with SLR (w/o SHAO) | 1.73 | 1.98 | 8.07 | 4.90 |
| *G+V+S* | All VLBI | 1.89 | 1.97 | 5.81 | 3.71 |
| *G+V+S* | SLR co-located with GPS (w/o 7837) | 1.75 | 2.02 | 7.31 | 4.49 |
| *G+V+S* | GPS co-located with VLBI | 1.75 | 1.87 | 6.30 | 3.93 |
| *G+V+S* | GPS co-located with SLR (w/o SHAO) | 1.73 | 1.98 | 8.07 | 4.90 |
| *G+V+S type A* | GPS co-located with SLR (w/o SHAO) | 1.73 | 2.03 | 7.87 | 4.80 |
| *G+V+S type B* | GPS co-located with SLR (w/o SHAO) | 1.74 | 2.09 | 8.20 | 4.99 |
| *G+V+S type C* | GPS co-located with SLR (w/o SHAO) | 1.74 | 2.12 | 8.10 | 4.94 |
| *G+V+S type D* | GPS co-located with SLR (w/o SHAO) | 1.71 | 2.04 | 7.90 | 4.81 |
| *G+V+S type A* | SLR co-located with GPS (w/o 7837) | 1.78 | 2.05 | 7.32 | 4.51 |
| *G+V+S type B* | SLR co-located with GPS (w/o 7837) | 1.79 | 2.03 | 7.69 | 4.71 |
| *G+V+S type C* | SLR co-located with GPS (w/o 7837) | 1.82 | 2.06 | 7.92 | 4.84 |
| *G+V+S type D* | SLR co-located with GPS (w/o 7837) | 1.75 | 2.05 | 7.24 | 4.46 |

### b) Selection of local ties

A careful selection of good LT is essential for high-quality combined solutions, as mismatching LT values will destroy the estimated parameters. In order to allow for a better analysis of the impact of the LT on all estimated parameters, the selection of good LT is done on the basis of two-technique combinations instead of analyzing a full GPS-VLBI-SLR combination. This procedure is reasonable as one LT connects the coordinates of only two techniques. Additionally, only two VLBI-SLR co-locations are present for CONT02, and both are co-located with GPS as well, so that it was decided to use the LT to the GPS site and omit the VLBI-SLR LT. Consequently, a direct link between VLBI and SLR on the level of the networks is not applied in the combination.

The parameters directly influenced by the LT are, of course, the station coordinates. However, to assess the quality of the LT, the impact on the other parameters is studied as well.

The general goal of the combination concerning the station coordinates is considered in all LT studies: the alignment of the coordinate repeatability of all co-located sites to that of the best single-technique solution, i.e., the GPS solution. Additionally, polar motion and the Helmert parameters are considered in the case of analyzing the GPS-SLR LT. In the case of VLBI, *UT1-UTC* and the troposphere gradients are taken into account. Analyzing the polar motion time-series did not give any information about mismatching GPS-VLBI LT, so that these analyses are omitted here. It is clear that analyzing UT gives only information about the geocentric *x*- and *y*-component, but as the troposphere gradients are considered as well, discrepancies in the *z*-component should be detectable, too.

Starting with the VLBI-GPS LT, Fig. 6.19 summarizes the results of the LT studies concerning two of the criteria mentioned above: the mean repeatability of the VLBI sites and the mean bias of the *UT1-UTC* time-series compared of the IERS-C04 series. Ideally, the mean repeatability of the VLBI sites should be equal to or better than that of the GPS sites, and, additionally, the mean bias of the *UT1-UTC* time-series should be zero or at least not larger than for the VLBI-only solution. For all combined solutions shown here, *UT1-UTC* is derived solely from VLBI, which means that only the station coordinates and polar motion are combined but the GPS contribution to universal time is omitted. It is clearly visible that the second criteria mentioned above is not fulfilled for the solution using all eight LT (triangle) as the bias in *UT* increases to 0.0143 ms. In order to find out whether this bias can be attributed to a specific LT, each LT was tested individually by computing a combined solution without one of the LT and applying only the seven remaining LT (i.e., solutions marked with stars). From these tests it becomes obvious that omitting the LT for Fairbanks or Westford are the only solutions where the bias in *UT* can be reduced without degrading the mean repeatability significantly. Therefore, a solution without these two LT was computed subsequently (diamond). Fortunately, the bias in *UT* can be further reduced to 0.0043 ms, whereas at the same time the mean repeatability of all VLBI sites is not heavily degraded. Table 6.15 shows that only the height component suffers from the reduced number of LT whereas the horizontal components are even improved. This is in line with the results given in Table 6.5 for the comparison between the theoretical LT values and the coordinates determined by the space-techniques, where the north component for Fairbanks and the east component for Westford show a comparably large disagreement. Omitting a third LT in the combination (i.e., solutions marked with circles in Fig. 6.19) does not allow a further reduction of the bias in *UT* without a clear degradation of the coordinate repeatability.

In the context of LT analysis, it can be shown that looking at the troposphere gradients can give an idea which theoretical LT values disagree with the space-geodetic techniques. Figure 6.20 shows the troposphere gradients estimated by GPS and VLBI for the single-technique solutions, a combined solution introducing all LT ("8 LT"), and a second combined solution where the LT of one co-location has not been used ("7 LT"). The gradient estimates in the combination with all LT applied are biased compared to the single-technique solutions for all four co-locations shown in Fig. 6.20. The mean biases expressed as the sum of the VLBI and GPS biases are 0.98 mm for Fairbanks, 0.47 mm for Westford, 0.38 mm for Algonquin and 0.48 mm for Kokee Park. Omitting the corresponding LT in the combination ("7 LT") shifts the estimates back to those of the single-technique solutions. This behavior indicates that solely the application of the LT is responsible for the bias instead of differences in the underlying reference frame of the combination and the VLBI-only solution. Moreover, as the GPS estimates are biased as well and the datum definition of the combination is done in the same way as for the GPS-only solution, the reference frame cannot be the reason for the bias. For all other gradients not shown in Fig. 6.20 no significant bias is visible.
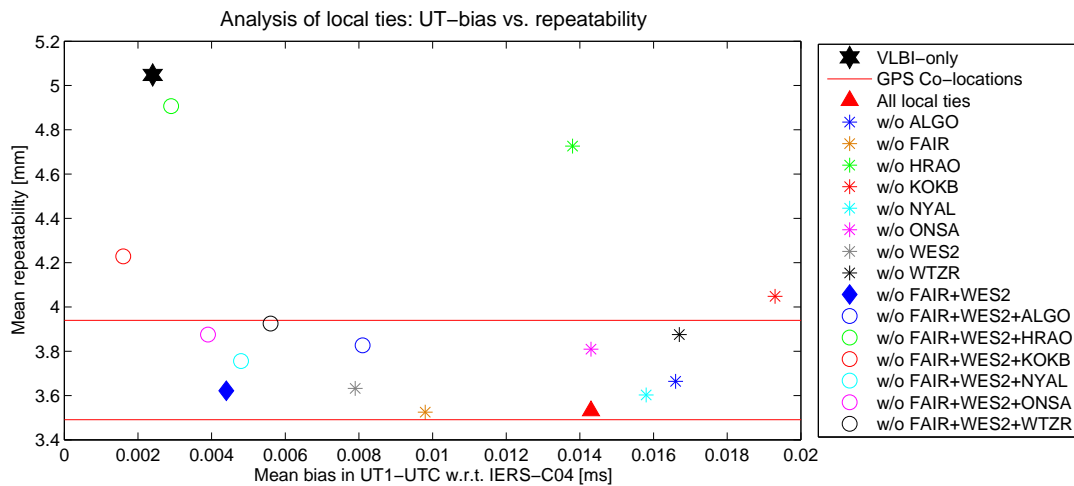
***Figure 6.19:*** *Analysis of the GPS-VLBI LT concerning their effect on the repeatabilities of station coordinates and the bias in the time-series of UT1-UTC. The mean repeatability is computed for the eight VLBI sites according to Eq. (5.9). In the case of GPS (red lines), only the eight co-locations with VLBI are taken into account: The upper line represents the GPS-only solution, the lower line represents the combined solution using all eight LT.*
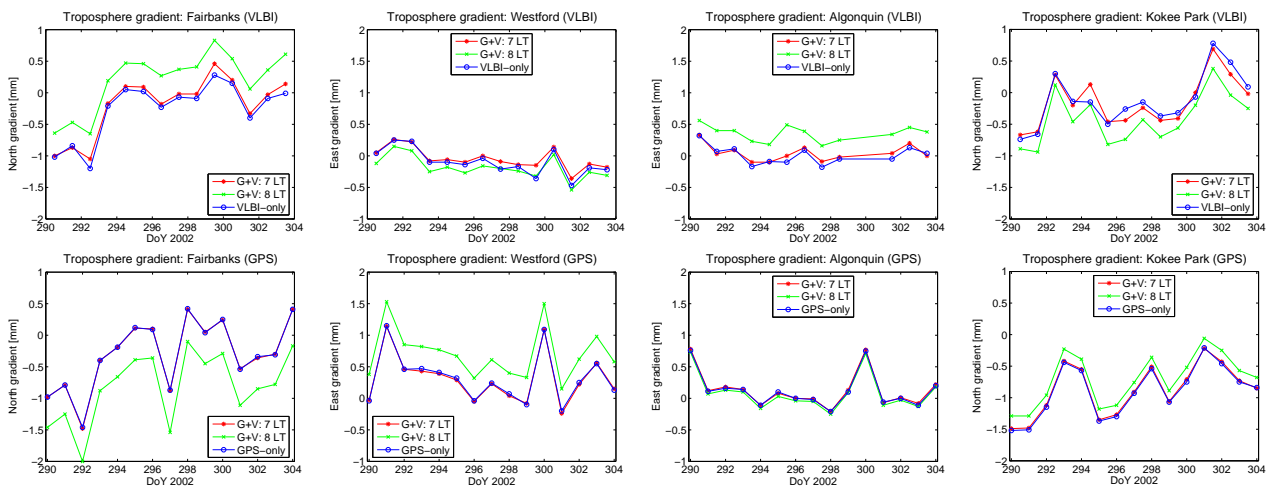


***Figure 6.20:*** *Analysis of GPS-VLBI LT concerning their effect on the troposphere gradients. Combined solutions of GPS and VLBI are either with all eight LT introduced, or the LT of one station was omitted (i.e, "7 LT").*

In order to summarize the LT studies for VLBI-GPS co-locations, it must be stated that the disagreement for the Fairbanks and Westford LT propagates into the troposphere gradients as well as into the time series of *UT1-UTC*. Additionally, biases in the troposphere gradients for Algonquin and Kokee Park indicate disagreements in the LT for these stations as well. However, as the omission of these two LT either degrades the coordinate repeatability (Kokee Park, see Fig. 6.19) or increases the bias in *UT* (Algonquin, see Fig. 6.19), it was decided to omit only the LT for Fairbanks and Westford, thus, using a sub-set of six LT for all further combinations.

The LT studies concerning the GPS-SLR co-locations are more complicated than for GPS-VLBI LT because there is no parameter that is "unique" for SLR, as *UT1-UTC* is in the case of VLBI. A first attempt to assess the agreement of the GPS-SLR LT is the analysis of the polar motion estimates. Similarly to the LT analyses described above, each LT is tested individually so that altogether 15 combinations are computed: one combination using all available 14 LT, and 14 combinations omitting one of the available LT at a time. Figure 6.21

shows the daily polar motion estimates for all combined solutions (without markers) and for both single-technique solutions (with markers). It becomes visible that the *y*-pole of all combined solutions is shifted by about 0.06 mas w.r.t. the GPS-only time-series (corresponding to about 1.8 mm on the Earth's surface), but this bias cannot be denoted to one single LT. It was decided that the visible bias is well within the range of acceptable changes, as a limit of even 3 mm for the impact of a GPS-SLR LT on polar motion was used for the TRF computations done at DGFI in order to be able to select a reasonable number of LT (*M. Krügel, personal communication*). Consequently, no GPS-SLR LT will be excluded due to these results for polar motion.

In a second step, the scatter in the daily Helmert parameters (translation and scale) are considered. Since the analyses shown in Table 6.20 suggest that only the *z*-translation can expect a stabilization due to the inclusion of SLR, the studies devoted to the LT selection concentrate on this component. However, it is clear that only one component of the LT can be tested by this approach. Figure 6.22 summarizes the results of all test solutions (see above) concerning the three criteria, i.e., the scatter in the daily *z*-translations, the scatter in the daily scale parameters and the mean coordinate repeatability of the co-located sites. It can be concluded from these results that the LT for GODE, WTZR, YARR, GRAZ and HERS are essential for the combination. Furthermore, there is no obvious outlier in the official LT values that degrades the combined solution, confirming the analyses of the polar motion estimates (Fig. 6.21). Consequently, the usage of all available LT for the GPS-SLR co-locations is the final outcome of the LT studies.
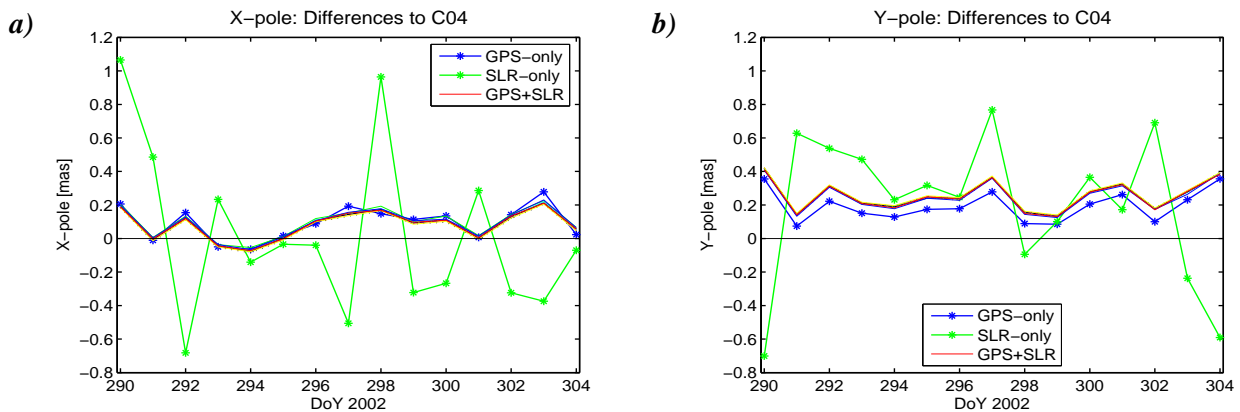


**Figure 6.21:** *Analysis of GPS-SLR LT concerning their effect on the combined polar motion estimates. The red line in the legends stands symbolically for all lines without a marker representing the combined solutions, i.e., one solution using all LT, and the 14 remaining solutions by omitting one of the LT at a time: **a)** x-pole, **b)** y-pole.*
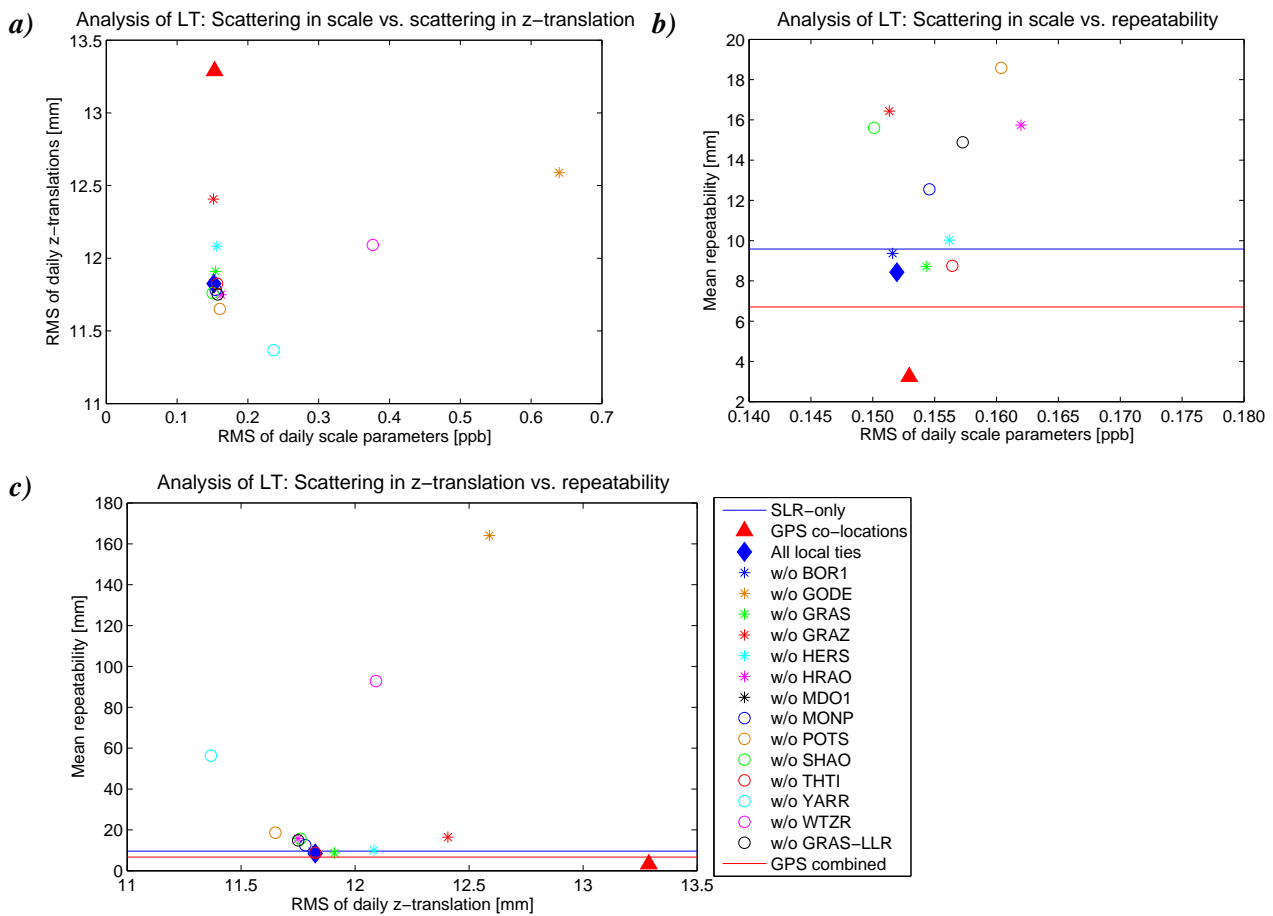
***Figure 6.22:*** *Analysis of GPS-SLR LT: **a)** the stability of the daily scale vs. the daily center-of-network, **b)** the stability of the daily scale vs. the daily coordinate repeatability (zoomed), **c)** the stability of the daily center-of-network vs. the daily coordinate repeatability. The mean repeatability is computed according to eq. (5.9) by taking into account only the co-located sites.*

## c) Earth orientation parameters

In order to assess the effect of the combination on the sub-daily EOP, the combination of common parameters is done step-by-step: In the first step, only the station coordinates are combined, then the pole coordinates are additionally combined in the second step, and, finally, station coordinates and all five EOP are combined. The troposphere parameters are not combined in all solutions. As SLR cannot contribute to sub-daily EOP the studies here concentrate on a GPS-VLBI combination. Consequently, the solution of the first step includes one time-series of all five EOP based on the GPS network and a second time-series based on the VLBI network. The solution out of step two contains only one time-series for polar motion (i.e., the combined time-series) but *UT* and nutation are still separated for the contributions of GPS and VLBI. Solely the third solution contains only one time-series for all EOP. Figure 6.23 displays the differences of the ERP resulting from the three combined solutions described above compared to the VLBI-only solution. In the case that the parameter considered was not combined, the VLBI-derived time-series is shown. Thus, the comparison demonstrates the impact of the GPS contribution, but the scatter is not a measure for improved or degraded quality of the time-series. For this purpose, the WRMS values of the unbiased differences w.r.t. the official IERS-C04 series including the sub-daily model IERS2003 are listed in Table 6.16. The differences themselves are displayed in Fig. 6.24 for the fully combined solution (step 3) and the best non-combined time-series.

The comparison shown in Fig. 6.23 for the first-step-solution ("Crd") shows that the influence of a different underlying reference frame on the VLBI-derived ERP is mainly a bias. The question whether the embedding of the VLBI network into the large GPS network stabilizes the ERP time-series cannot be demonstrated by Table 6.16 as the WRMS values are more or less similar to those of the VLBI-only solution. On the other

hand, this fact underlines that the homogeneous and large VLBI network for CONT02 is already well suited to derive high-quality ERP with a sub-daily resolution, whereas a stabilization effect due to a combined network might be visible if normal VLBI sessions with changing network configurations were used.
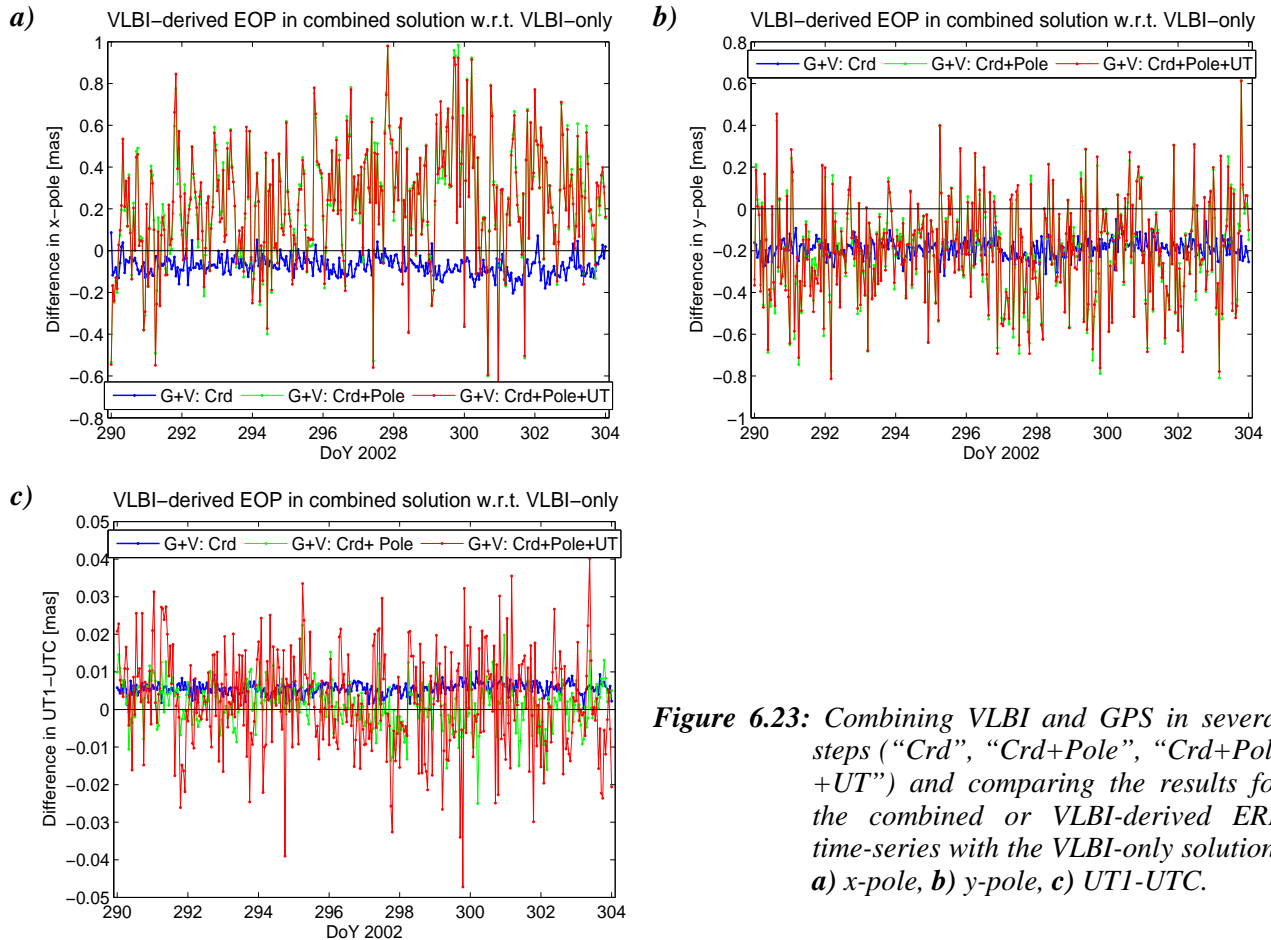


***Figure 6.23:*** *Combining VLBI and GPS in several steps ("Crd", "Crd+Pole", "Crd+Pole+UT") and comparing the results for the combined or VLBI-derived ERP time-series with the VLBI-only solution: **a)** x-pole, **b)** y-pole, **c)** UT1-UTC.*

Combining the pole coordinates ("Crd+Pole") results in noticeable differences compared to the VLBI-only solution (Fig. 6.23a,b), but this is not astonishing if we remember the bias between the single-technique solutions in Fig. 6.4. The additional combination of *UT* and the nutation angles ("Crd+Pole+UT") has nearly no influence on the combined pole coordinates (Fig. 6.23, Table 6.16). At a first glance the combined polar motion time-series looks slightly worse than the GPS-only time-series (Table 6.16). However, taking into account that the constraint for blocking the retrograde diurnal term in polar motion ("BLOCKRET") has to be applied on a daily basis in the case of a GPS-only solution (see *Chapter 5.3.1*) it is remarkable that the combination with VLBI results in a polar motion time-series nearly as stable as that derived from GPS, although the combined time-series is less constrained (Fig. 6.24, Table 6.16). In order to demonstrate the pure effect of combining GPS with VLBI, another fully combined solution was computed but with the BLOCKRET-constraint applied on a daily basis (instead of 14 days), as it is done in the case of GPS. The WRMS decreases by about 0.02 mas (Table 6.16) clearly demonstrating the benefit of the combination.

Combining the pole coordinates evokes already clearly more changes in the *UT* time-series compared to the VLBI-only solution than combining solely the station coordinates (Fig. 6.23c). However, obviously the combined pole coordinates do not allow a stabilization of the *UT* time-series w.r.t. the official IERS-C04 series, i.e., only a change of 0.4 µs in terms of WRMS (Table 6.16). The inclusion of the GPS-derived *UT* quantity changes the time-series significantly (Fig. 6.23c). In fact, the change points towards a higher stability (Table 6.16, Fig. 6.24c) as the WRMS of the differences to the official time-series decreases by 2.9 µs (corresponding to about 1.3 mm on the Earth's surface). These results clearly demonstrate the benefit that can be gained by including the GPS contribution into the time-series of *UT* despite of the bad long-term stability due to problems in the orbit modeling.

*a)*



*b)*



*c)*
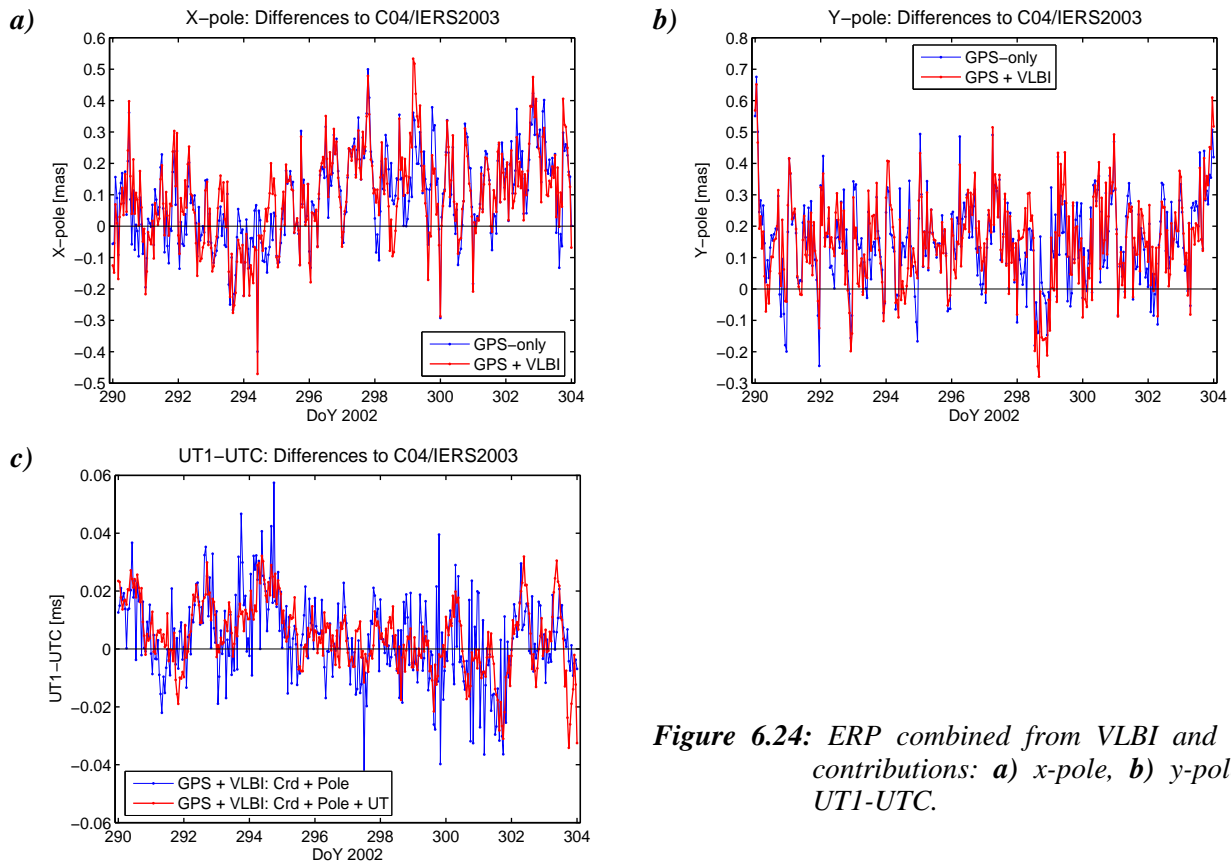


**Figure 6.24:** *ERP combined from VLBI and GPS contributions: **a)** x-pole, **b)** y-pole, **c)** UT1-UTC.*

**Table 6.16:** *Comparison of hourly ERP from different types of GPS, VLBI and combined solutions with the IERS-C04 series including the sub-daily model IERS2003: RMS of residuals (mean bias removed). In solutions where the GPS and VLBI contributions are not combined, the VLBI-derived time-series is analyzed. The final solution will be addressed in Chapter 6.3.*

| Solution | Combined parameters | BLOCKRET | X-pole [mas] | Y-pole [mas] | UT1-UTC [ms] |
|----------|---------------------|----------|--------------|--------------|--------------|
| VLBI | - | 14 days | 0.2549 | 0.2486 | 0.0151 |
| G+V | TRF | 14 days | 0.2581 | 0.2516 | 0.0152 |
| G+V | TRF, Pole | 14 days | 0.1533 | 0.1482 | 0.0148 |
| G+V | TRF, Pole, UT/LOD | 14 days | 0.1498 | 0.1479 | 0.0119 |
| G+V | TRF, Pole, UT/LOD | daily | 0.1283 | 0.1248 | 0.0118 |
| GPS | - | daily | 0.1430 | 0.1426 | - |
| "Final" | TRF, Pole, UT/LOD, Trop. | 14 days | 0.1499 | 0.1479 | 0.0116 |

*d) Troposphere parameters*

Although the troposphere parameters were not yet combined in this first part of the studies, it is worthwhile to take a look at them because the combined TRF might cause changes in the troposphere estimates due to the correlation described in *Chapter 5.3.2*. The impact of the LT on the troposphere gradients have already been discussed in section *b)* of the current chapter, but, apart from the effects shown in Fig. 6.20, the gradients do not change significantly compared to the single-technique solutions. As the troposphere parameters are common to GPS and VLBI only, their combined solution is studied first, whereas the impact of SLR is studied afterwards.

The mean changes of the ZD estimates due to combining the station coordinates and EOP from GPS and VLBI are listed in Table 6.17. Generally speaking, the mean change is below or around 1 mm for most of the eight co-located sites. However, the scatter of the differences for the VLBI sites is quite large so that only the mean change for Onsala is significant (if the 2σ-criterion is applied). As regards the GPS sites, only the mean

biases for HRAO, NYA1 and ONSA are significant. It is remarkable that all three sites also showed large discrepancies between the official LT values and the coordinates determined by the single-technique solutions regarding the height component (see Table 6.5). Generally speaking, forcing the coordinate difference to the nominal LT value entails changes in the ZD estimates due to the correlation of both parameter types. In order to give one example, the height of the GPS site for Ny-Alesund (which had the largest discrepancy) changed by -5.8 mm, that of the VLBI site by +4.6 mm, so that the ZD had to change accordingly. Of course, we would hope that the differential ZD between GPS and VLBI now agrees better with the theoretical troposphere ties derived from meteorological data. In order to answer this question, Fig. 6.25 summarizes the differences between the meteorological troposphere ties and the mean differential troposphere ZD derived from GPS and VLBI estimates for different solution types. In the case of NYA1 and ONSA, the first two solutions in Fig. 6.25 (i.e., "single-techniques" and "G+V") show that the change in the ZD estimates points into the right direction as the agreement with the theoretical troposphere ties clearly improves. Unfortunately, this is not the case for HRAO. One reason might be that HRAO is a rather isolated station especially in the VLBI network, thus, the site-specific parameters are weaker than for other sites, so that inconsistencies in other parameters (for other sites) may be absorbed by the HRAO site. Especially the nearly antipodal location of HRAO and KOKB allows that discrepancies in the height or ZD estimates for KOKB propagate into the height or ZD estimates for HRAO. Finally, regarding the other co-locations, the mean changes in the ZD estimates are small, thus, the agreement with the troposphere ties changes only slightly due to the combined network (Fig. 6.25).

In general, the inclusion of SLR into the combination evokes only small changes in the ZD estimates (see Table 6.18), but this is not astonishing as only two sites among the eight GPS-VLBI co-locations are additionally equipped with SLR. For both sites, i.e., HRAO and WTZR, the GPS-derived ZD changes significantly, whereas the mean change for the VLBI-derived ZD is only significant for HRAO. Unfortunately, the ZD for both techniques change into the same direction for HRAO, so that the discrepancy with the theoretical troposphere tie is not reduced (solution "G+V+S" in Fig. 6.25). A better agreement with the troposphere ties due to the contribution of SLR can only be achieved for WES2 and WTZR. The GPS-derived ZD for WES2 changes significantly by almost the same value as for WTZR although there is no co-location with SLR. This behavior nicely demonstrates that all parameters in a full combination are correlated and, thus, influence each other. All weighted mean values for the differential ZD between the GPS and VLBI estimates are listed in Table 6.19. These values will be used as one alternative for the troposphere tie when the combination of the ZD parameters is studied (*Chapter 6.2.3*).

**Table 6.17:** *Change of the ZD estimates in a combined GPS-VLBI solution ("GV") compared to the ZD estimated independently in the single-technique solutions. A mean bias was removed for the RMS computation. All values are given in [mm].*

|  | *ALGO* | *FAIR* | *HRAO* | *KOKB* | *NYA1* | *ONSA* | *WES2* | *WTZR* |
|---|---|---|---|---|---|---|---|---|
| *Weighted mean ΔZD$_{GV-GPS}$* | 0.08 | -0.02 | 0.73 | 0.66 | 1.49 | 1.05 | -0.07 | -0.04 |
| *WRMS of ΔZD$_{GV-GPS}$* | 0.10 | 0.11 | 0.22 | 0.38 | 0.24 | 0.18 | 0.14 | 0.07 |
| *Weighted mean ΔZD$_{GV-VLBI}$* | -0.96 | -0.20 | -3.37 | 0.86 | -0.83 | -1.33 | -0.22 | -0.40 |
| *WRMS of ΔZD$_{GV-VLBI}$* | 1.34 | 0.75 | 3.23 | 1.62 | 0.52 | 0.65 | 0.86 | 0.71 |

**Table 6.18:** *Change of the ZD estimates for the GPS and VLBI sites due to the inclusion of SLR into the combination. The values are given as 'GPS+VLBI' – 'GPS+VLBI+SLR'. A mean bias was removed for the RMS computation. All values are given in [mm].*

|  | *ALGO* | *FAIR* | *HRAO* | *KOKB* | *NYA1* | *ONSA* | *WES2* | *WTZR* |
|---|---|---|---|---|---|---|---|---|
| *Weighted mean ΔZD$_{GPS\ site}$* | 0.09 | 0.12 | -1.60 | -0.02 | 0.00 | -0.01 | 0.40 | 0.41 |
| *WRMS of ΔZD$_{GPS\ site}$* | 0.07 | 0.10 | 0.33 | 0.21 | 0.10 | 0.06 | 0.12 | 0.11 |
| *Weighted mean ΔZD$_{VLBI\ site}$* | 0.22 | -0.02 | -1.38 | 0.13 | -0.06 | -0.11 | 0.00 | 0.11 |
| *WRMS of ΔZD$_{VLBI\ site}$* | 0.22 | 0.12 | 0.65 | 0.25 | 0.08 | 0.12 | 0.15 | 0.15 |

***Table 6.19:*** *Differential ZD GPS-VLBI for the three-technique combination. A mean bias was removed for the RMS computation. All values are given in [mm].*

|  | *ALGO* | *FAIR* | *HRAO* | *KOKB* | *NYA1* | *ONSA* | *WES2* | *WTZR* |
|---|---|---|---|---|---|---|---|---|
| ***Weighted mean** $\Delta ZD_{GPS\text{-}VLBI}$* | 8.05 | 0.93 | 3.84 | 8.37 | 1.75 | 3.43 | 3.92 | 0.99 |
| ***WRMS of** $\Delta ZD_{GPS\text{-}VLBI}$* | 4.15 | 5.65 | 7.69 | 8.94 | 3.18 | 4.10 | 5.08 | 5.65 |
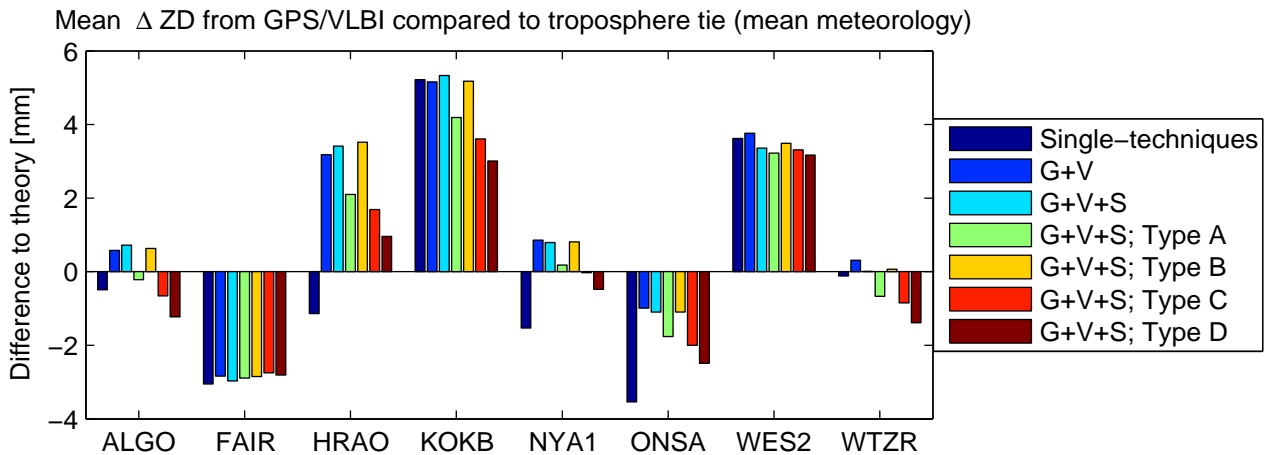


***Figure 6.25:*** *Comparison of the mean differential troposphere ZD GPS-VLBI with the theoretical troposphere ties computed using meteorological data. The solution types A-D are explained in Chapter 6.2.2.*

Regarding the correlation between the VLBI- and GPS-derived time-series of ZD estimates, the combination of the reference frame as well as the inclusion of SLR does not evoke large changes, i.e., the maximum change of the correlation coefficient is 0.003 compared to the values listed in Table 6.8. This might be due to the fact that the VLBI network for CONT02 is very homogeneous and stable, whereas a time-series of ZD based on inhomogeneous session-wise VLBI networks would probably benefit much more from the embedding into a larger and more stable network.

### e) Datum parameters: translations and scale

According to the time-series shown in Fig. 6.16b, the stability of the daily scale of any combined solution (two-techniques or all three techniques) does not improve compared to the GPS single-technique solution. Although the daily scale parameters themselves slightly varies, the scatter over 14 days remains at the same level (see Table 6.20). This behavior is not astonishing as Fig. 6.16b already revealed that the VLBI-derived daily scale is clearly more weakly determined than the GPS-derived scale, and for SLR it is even not possible to derive a reasonable daily time-series. Additionally, due to the weakness of daily SLR solutions manifested in worse station coordinate repeatabilities, the contribution of SLR is down-weighted in the combination by a factor of about ten (see Table 6.4). For the same reasons, the daily translations in *x* and *y* cannot be stabilized by the inclusion of SLR (see Fig. 6.17, Table 6.20). Nevertheless, a small improvement is achieved for the *z*-component: In spite of the weakness of SLR for daily solutions, the scatter of the daily *z*-translations decreases from 13.29 mm for a GPS-only solution to 11.73 mm for the combined solution including SLR (see Table 6.20).

Similarly to the single-techniques, weekly solutions are analyzed for the combined solutions as well in order to have a stronger contribution of SLR. Although a comparison based on only two weeks is not significant (as already mentioned in *Chapter 6.1.4*), Table 6.21 gives an idea that the datum parameters of the combination can benefit from an SLR contribution if weekly solutions are considered. Contrary to daily solutions, all three translations as well as the scale seem to be improved on a weekly basis. However, it should be mentioned again that, of course, two weeks are not enough to derive a meaningful general statement about the strength of an SLR contribution to the the datum parameters.

*Table 6.20: Comparing daily solutions with the corresponding 14-day solution via a seven-parameter Helmert transformation using all sites: Scatter of the daily transformation parameters. The solution types A-D and the final solution will be explained in Chapter 6.2.2 and 6.3.4, respectively.*

| Solution | RMS of daily translation parameters [mm] | | | RMS of daily scale parameters [ppb] |
|---|---|---|---|---|
| | Tx | Ty | Tz | |
| G | 4.32 | 4.19 | 13.29 | 0.15 |
| G+V | 4.25 | 3.98 | 12.62 | 0.15 |
| G+S | 4.42 | 5.18 | 11.73 | 0.15 |
| G+V+S | 4.44 | 5.21 | 11.11 | 0.15 |
| G+V+S: Type A | 4.29 | 5.29 | 11.07 | 0.50 |
| G+V+S: Type B | 10.80 | 6.28 | 15.85 | 0.16 |
| G+V+S: Type C | 10.76 | 5.76 | 15.67 | 0.45 |
| G+V+S: Type D | 4.56 | 5.30 | 11.26 | 0.34 |
| Final solution | 10.49 | 5.50 | 15.74 | 0.32 |

*Table 6.21: Comparing both weekly solutions with the 14-day solution via a seven-parameter Helmert transformation using the GPS sites only. The solution types A-D and the final solution will be explained in Chapter 6.2.2 and 6.3.4, respectively.*

| Solution | Translations [mm] | | | | | | Scale [ppb] | | RMS [mm] | |
|---|---|---|---|---|---|---|---|---|---|---|
| | Tx | | Ty | | Tz | | | | | |
| | 1st week | 2nd week | 1st week | 2nd week | 1st week | 2nd week | 1st week | 2nd week | 1st week | 2nd week |
| G | 2.7 | -3.8 | 2.4 | -2.5 | 9.7 | -11.4 | -0.08 | 0.08 | 1.21 | 1.20 |
| G+V | 2.2 | -3.3 | 2.4 | -2.6 | 8.8 | -10.2 | -0.08 | 0.08 | 1.21 | 1.24 |
| G+S | 1.4 | -4.3 | 1.0 | -1.4 | 6.5 | -6.6 | -0.06 | 0.05 | 1.23 | 1.17 |
| G+V+S | 1.3 | -4.2 | 1.0 | -1.8 | 6.2 | -6.5 | -0.07 | 0.06 | 1.23 | 1.18 |
| G+V+S: Type A | 1.3 | -4.5 | 1.2 | -1.8 | 6.0 | -6.4 | -0.23 | -0.05 | 1.22 | 1.18 |
| G+V+S: Type B | -0.8 | -5.0 | -0.1 | -1.4 | 2.4 | -5.0 | -0.08 | 0.07 | 1.24 | 1.18 |
| G+V+S: Type C | -0.4 | -5.4 | 0.3 | -1.8 | 2.9 | -4.3 | -0.22 | -0.15 | 1.24 | 1.20 |
| G+V+S: Type D | 1.1 | -4.5 | 1.0 | -1.7 | 6.9 | -5.8 | 0.03 | 0.19 | 1.23 | 1.18 |
| Final | -0.3 | -5.5 | 0.2 | -1.8 | 3.0 | -4.7 | -0.24 | 0.00 | 1.24 | 1.18 |

## 6.2.2  Estimating additional Helmert parameters

The following four solution types are tested:

- – Solution A: Estimating a scale parameter for GPS;
- – Solution B: Estimating three translations for GPS;
- – Solution C: Estimating a scale parameter and three translations for GPS;
- – Solution D: Estimating a scale parameter for all three space-techniques and applying a NNSc condition using a sub-set of GPS sites (the same sites as for the NNR condition).

All solutions were set up as 14-day solutions with one set of Helmert parameters for the entire interval. The resulting Helmert parameters are summarized in Table 6.22. It is interesting to see that mainly the scale and the *z*-translation change if translations and scale are estimated together (type C) compared to the solutions with either the scale or the translations set up (type A, B). This correlation appears due to the fact that the major part of the GPS sites is located in the northern hemisphere, whereas the translations and scale should be de-correlated in an ideally homogeneous network. In the case of setting up a scale parameter for GPS (i.e.,

solution type A), a weighted mean of the contributions by VLBI and SLR defines the scale of the combined network that is transported to the GPS network via the LT. The estimated scale of 0.75 ppb w.r.t. the a priori set of coordinates (Table 6.22) corresponds to about 4.8 mm on the Earth's surface. This change is in good agreement with smaller station heights of 4.1 mm (as a mean value for all GPS sites). At the same time, the mean change of the station heights for the VLBI and SLR sites is 1.6 mm in the other direction, i.e., the heights are getting larger. As a consequence of this opposite development of the station heights, the scale parameters estimated in solution type D for VLBI and SLR have negative signs if the scale of the GPS network is constrained to the a priori network (due to the NNSc condition).

Due to correlations between the station heights, the scale of the network and the troposphere ZD, the ZD estimates change if a scale parameter is set up in the combination. Table 6.23 summarizes the mean change of the GPS and VLBI-derived ZD for solution type A compared to a combination without setting up any Helmert parameter. Applying the $2\sigma$-criteria, the changes are significant for all sites except for FAIR (GPS and VLBI), HRAO (VLBI) and WES2 (VLBI). The size of the changes varies between the sites and can reach values up to about 0.8 mm. The ZD estimates for the GPS sites become smaller whereas the VLBI-derived ZD increase (considering only the significant values $\Delta ZD$). This behavior in turn influences the troposphere tie. The discrepancies with the theoretical values for all solution types A-D have already been included in Fig. 6.25. According to the results shown there, the question whether the agreement with the theory improves if Helmert parameters are set up cannot be answered generally for all sites. Regarding FAIR and WES2, the scale information cannot be transformed directly from VLBI to GPS as the LT is omitted for these two sites. Therefore, the influence of estimating Helmert parameters on the differential ZD is very small. Looking at the remaining co-locations, the agreement with theory improves for solution type A, except for ONSA and WTZR. As expected, setting up translations for GPS (type B) has nearly no influence on the differential ZD, so that the differences between the solution types C and A must be dedicated to the fact that the estimated scale parameters are slightly different (see Table 6.22) due to correlations with the *z*-translation, as explained already above. Finally, allowing for a scale parameter for all three techniques and fixing the scale of the solution to the a priori network (type D) results in better differential ZD solely for the co-locations HRAO and KOKB compared to allowing a scale only for GPS (type A). As both sites are heavily correlated due to the nearly antipoded location, they probably benefit from the more stable scale definition via a NNSc condition for 90 GPS sites (compared to transferring the mean scale of VLBI and SLR only via the co-located sites, that are not homogeneously distributed over the globe). Based on the more stable scale, the de-correlation of the height and the ZD for HRAO on the one hand and the height and the ZD for KOKB on the other hand is obviously improved.

Although the time-series of ZD change compared to a solution without setting up Helmert parameters, the correlation between the GPS- and VLBI-derived time-series does not change strongly, i.e., 0.002 at maximum. The same holds for the scatter of the differential ZD between GPS and VLBI estimates: The reduction of the WRMS due to estimating a scale parameter for GPS (type A) or for all techniques (type D) ranges from 0.0 up to 0.05 mm for the eight co-locations. Thus, one can conclude that the changes in the ZD estimates evoked by the estimation of Helmert parameters can be described mainly by a bias, but they do not implicate a significantly better alignment of the GPS- and VLBI-derived time-series.

**Table 6.22:** *Estimated Helmert parameters and their formal errors (14-day solutions). The final solution will be addressed in Chapter 6.3*

| *Solution* | *Scale [ppb]* | | | *Translations [mm]* | | |
|---|---|---|---|---|---|---|
| | *GPS* | *VLBI* | *SLR* | *Tx* | *Ty* | *Tz* |
| *Type A* | $0.75 \pm 0.03$ | - | - | - | - | - |
| *Type B* | - | - | - | $-3.88 \pm 0.35$ | $-11.72 \pm 0.35$ | $-8.82 \pm 0.59$ |
| *Type C* | $1.04 \pm 0.03$ | - | - | $-5.76 \pm 0.35$ | $-12.14 \pm 0.35$ | $-14.53 \pm 0.61$ |
| *Type D* | $0.06 \pm 0.02$ | $-0.38 \pm 0.04$ | $-1.50 \pm 0.06$ | - | - | - |
| *Final* | $1.12 \pm 0.02$ | - | - | $-5.65 \pm 0.28$ | $-12.66 \pm 0.28$ | $-15.22 \pm 0.49$ |

***Table 6.23:*** *Mean change of ZD estimates for the GPS and VLBI sites in a combined GPS-VLBI-SLR solution due to estimating a scale parameter for GPS (solution type A). The values are given as difference 'solution with scale estimation' – 'solution without scale'. A mean bias was removed for the RMS computation.*

| | ***ALGO*** | ***FAIR*** | ***HRAO*** | ***KOKB*** | ***NYA1*** | ***ONSA*** | ***WES2*** | ***WTZR*** |
|---|---|---|---|---|---|---|---|---|
| ***Weighted mean $\Delta ZD_{GPS}$ [mm]*** | -0.15 | 0.01 | -0.83 | -0.44 | -0.38 | -0.29 | -0.09 | -0.29 |
| ***WRMS of $\Delta ZD_{GPS}$ [mm]*** | 0.03 | 0.01 | 0.18 | 0.09 | 0.06 | 0.05 | 0.03 | 0.06 |
| ***Weighted mean $\Delta ZD_{VLBI}$ [mm]*** | 0.76 | -0.07 | 0.44 | 0.66 | 0.21 | 0.34 | 0.04 | 0.35 |
| ***WRMS of $\Delta ZD_{VLBI}$ [mm]*** | 0.30 | 0.05 | 0.26 | 0.22 | 0.07 | 0.11 | 0.05 | 0.14 |

In *Chapter 6.2.1a* it has been assumed that discrepancies in the network scales of GPS and SLR may be the reason for the degraded height repeatability compared to the GPS-only solution. If this guess was true, setting up a scale parameter for GPS should help. Table 6.15 shows that, in fact, the height repeatability for the GPS sites is improved. But the improvement is solely about 0.2 mm so that the original level of the single-technique solution is not reached, neither by estimating a scale for GPS only (type A) nor by estimating scale parameters for all techniques (type D). Taking into account SLR leads to only a slight improvement of about 0.07 mm for the height repeatability, but only for solution type D, i.e., if the scale is fixed to the a priori network. As regards the solution types B and C, the degraded repeatabilities in Table 6.15 demonstrate that the SLR network, and especially the co-located sites, changes too much from day to day (see Table 4.2) so that the information about the origin cannot be transferred from SLR to the other techniques in an adequate way.

For the same reason, the scatter of the daily translations w.r.t. the 14-day solution heavily increases if translation parameters are set up for GPS (type B and C in Table 6.20). Furthermore, the same holds for the stability of the daily scale w.r.t. the 14-day solution if GPS does not contribute to the global scale of the combined network (type A and C in Table 6.20 and Fig. 6.26). Finally, if we switch to weekly solutions instead of daily, Table 6.21 indicates that defining the origin of the combined network solely by SLR (type B) could stabilize its determination, especially for the *z*-component which is highly desirable. Unfortunately, the weekly comparisons regarding the scale of the network are not encouraging for setting up a scale parameter for GPS. However, as already stated before, for a reliable statement the analyses must be definitely based on longer time-series of weekly solutions.
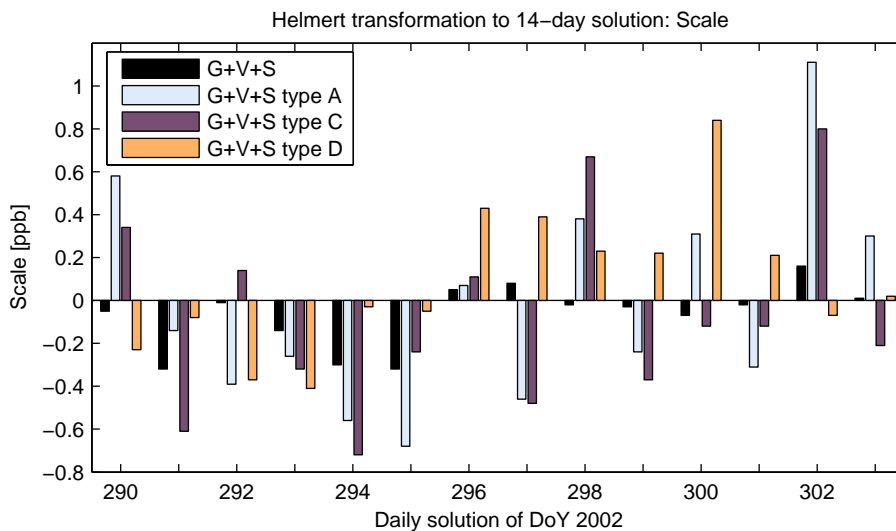


***Figure 6.26:*** *Comparing the daily solutions with the corresponding 14-day solution via a seven-parameter Helmert transformation: scale.*

In order to summarize the studies devoted to the estimation of additional Helmert parameters, the GPS contribution to the translations is needed for a good stability as long as daily solutions are considered, although there might be some discrepancies to the SLR contribution. If the origin of the combined network should be determined solely by SLR, weekly solutions are needed for a stable determination, but the size of the improvement still has to be confirmed using longer time-series. The situation is slightly different regarding the

scale, because VLBI contributes information in addition to SLR. As the VLBI network for CONT02 is homogeneous for all days, the combined solution benefits from a scale estimation for GPS.

## 6.2.3  Combining troposphere parameters

The combination of the troposphere parameters is divided into two parts: First, the potential of combining the ZD estimates is examined (*Section a*), and afterwards the combination of the gradients is analyzed (*Section b*). For both parts, the analysis starts with site-specific investigations before solutions with combined troposphere parameters for all eight co-locations are discussed. As the troposphere estimates do not change dramatically due to the inclusion of SLR (see Table 6.18), the analyses are done only for a full three-technique combination. Similar analyses using a GPS-VLBI combination without SLR are documented in *Krügel et al. (2007)*.

### *a) Combining troposphere zenith delays*

As regards the ZD, the discrepancies between the meteorological values and the GPS- and VLBI-derived ZD visible for some co-locations in Fig. 6.25 (solution "G+V+S") evoke the question whether the introduction of the meteorological values as constraints can really improve the combined solution. An improvement, if present, is expected for two types of parameters, both correlated with the ZD: the height component of the station coordinates and the scale of the network. Thus, the height repeatability and the time-series of daily scale parameters w.r.t. the 14-day solution are chosen as validation criteria for the ZD combination.

As the agreement or disagreement of the space-techniques' ZD differences with theory depends on the co-location considered (Fig. 6.25), the first tests for combining the ZD are carried out station-wise. For this purpose, eight different solutions are computed, each with combined ZD for only one co-location at a time. The theoretical values derived from true meteorological data (see Table 5.2) are used as troposphere ties, and the LT are introduced for the six selected co-locations (see *Chapter 6.2.1b*). Figure 6.27a displays the change of the height repeatability for that site with combined ZD compared to a solution with independently estimated ZD. The changes in the repeatability are plotted against the discrepancy between the theoretical troposphere tie and the ZD estimates that is present for the corresponding site in a solution with combined TRF and EOP only. Generally speaking, the improvement or degradation of the repeatability seems to be independent of the mismatch in the troposphere tie. It is clear that always one circle and one triangle belong to one co-location, i.e., the corresponding GPS and VLBI sites. Therefore, it becomes obvious from Fig. 6.27a that combining the ZD changes the repeatability for the corresponding GPS and VLBI sites nearly identically, with mean changes of -0.09 mm and +0.24 mm, respectively. The two exceptions belong to Fairbanks and Westford where the LT are not applied in the combination so that the co-located sites are not directly linked to each other. In order to evaluate the benefit of a ZD combination independently of the LT for the remaining stations as well, a second test series consists of solutions with combined ZD for one co-location at a time but the corresponding LT has not been introduced. A solution with neither introducing the corresponding LT nor combining the ZD estimates serves as reference for the change of the repeatabilities displayed in Fig. 6.27b. If the LT was not introduced, the station coordinates of the co-location in consideration can change independently for GPS and VLBI. However, similar to Fig. 6.27a, a dependence on the discrepancy of the solution-derived ZD differences w.r.t. the theoretical values introduced as constraints cannot be identified. As negative values for the change in the repeatability represent an improvement, it can be concluded from Fig. 6.27b that the combination of the ZD stabilizes the height component of the VLBI site in absence of the LT, with a mean improvement of -1.94 mm for all VLBI sites. The fact that the VLBI sites Kokee Park and Hartebeesthoek benefit so much from combining the ZD if the LT is missing can be explained by their isolated location within the VLBI network: They are very weakly determined if no LT is applied, so that the combination of the ZD can already give a large stabilization. We have already seen in Fig. 6.19 that the overall repeatability of the solution heavily degrades if one of these two LT was not introduced. Looking at Fig. 6.19, one can see as well that the LT for Wettzell plays an important role, which can explain the large improvement for the VLBI repeatability seen in Fig. 6.27b.

The mean change for the GPS sites is -0.12 mm, so that on average only a slight improvement is visible. But contrary to the VLBI sites, the GPS sites do not solely depend on the LT because they are already included in the datum definition. Therefore, the combined ZD are only an additional stabilization that acts only indirectly on the height.

According to Fig. 6.27, the benefit for the coordinate repeatability due to the combination of the ZD obviously does not depend on the agreement of the theoretical troposphere tie with the differential ZD between the GPS and VLBI estimates. Therefore, it was decided to switch from the site-specific ZD combination to a combination of ZD for all co-locations in one solution. Two further questions will be addressed in the following:

1) To what extent can the combination of the ZD stabilize the solution or even replace missing or questionable LT (height component)?

2) Does the application of different troposphere ties change the results? If there are differences, which theoretical value is the best?

In order to answer the above questions, two different solutions were computed for each of the four types of theoretical troposphere ties ( see Table 5.2 for "rule of thumb", "standard" and "meteo"; for "solution" see Table 6.19): one solution with the LT applied in three components ("3D"), and a second solution where the GPS-VLBI LT are introduced only for the horizontal components but not for the height ("Horizontal"). In the latter solution type, the combination of the ZD can be investigated independently of the combination of the coordinates, except for the fact, that the height component of one station corresponds, to a minor part, to horizontal components of the remaining co-locations whose coordinates were combined by introducing the horizontal LT.
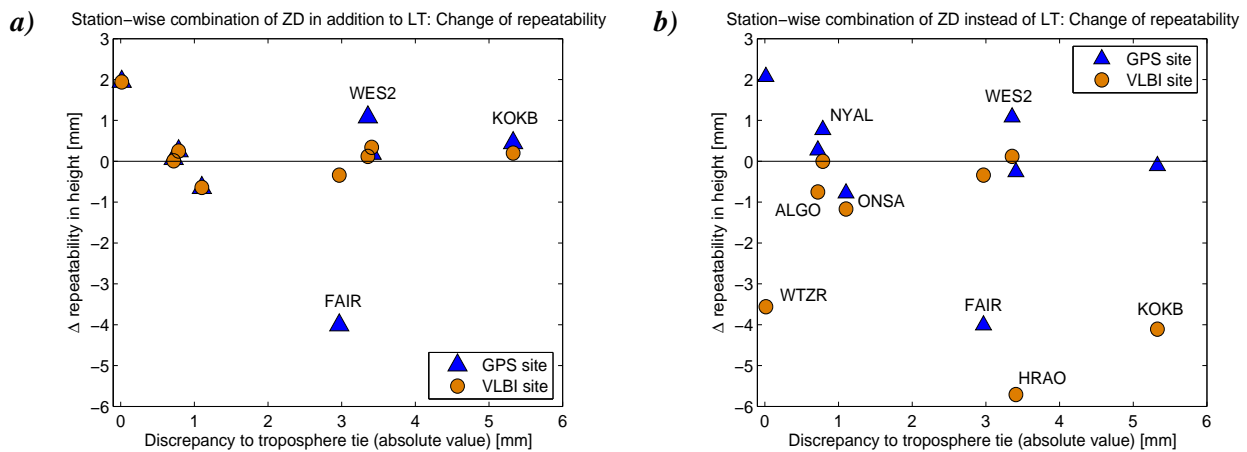


**Figure 6.27:** *Change of the height repeatability due to a station-wise combination of the ZD (negative values indicate an improvement). The reference solution for the repeatabilities and the discrepancies in the troposphere tie is computed with combined TRF and EOP only. **a)** The LT for the station in consideration is applied (except for FAIR and WES2); **b)** the LT for the station in consideration is not applied.*

The resulting height repeatabilities for all test solutions are given in Table 6.24 as a mean value for all sites and for different sub-sets of sites that are of interest: only the eight GPS sites co-located with VLBI, only the eight VLBI sites, or the GPS and VLBI sites of the co-locations together. For comparison, the mean repeatabilities are given additionally for solutions without combining the ZD (first two rows). These solutions serve as reference for the site-specific changes of the height repeatabilities displayed in Fig. 6.28. In the case that the ZD are combined additionally to the coordinates ("3D"), the mean repeatability for all GPS-VLBI co-locations (last column in Table 6.24) improves only slightly by 0.01 mm at maximum. It is interesting to see that the mean stability of the GPS sites improves by about 0.4 mm whereas the VLBI sites obviously degrade by about 0.2 mm. Looking at the site-specific behavior in Fig. 6.28a it becomes clear that the strong improvement for the GPS site FAIR of almost 4 mm is the major contributor. In view of the comparably large scatter in the GPS-derived ZD time-series for FAIR seen in Fig. 6.8 and the bad height repeatability of about 10 mm (see Table 6.2), it is clear that the GPS site FAIR benefits so much from combining the ZD. Apart from the site FAIR and both sites at Onsala (7213 and ONSA), the combination of the ZD tends to slightly degrade the repeatability instead of stabilize it (Fig. 6.28a). As already seen in the station-wise ZD combination described before (Fig. 6.27), the improvement or degradation of the repeatability cannot be attributed to a good agreement or large discrepancies in the LT, respectively, because the height component of

the geometric LT for Wettzell showed the smallest discrepancy with the estimates of the space techniques (see Table 6.5) but the height repeatability degrades most when the ZD are combined.

Analyzing the solutions with combined ZD but the LT applied only for the horizontal components, the benefit for the height repeatability is more pronounced than for solutions with the LT applied in 3D (Table 6.24). The mean improvement for the VLBI sites is about 1.4 mm. It can be seen from Fig. 6.28b that most of the sites show an increased stability. Again, especially those sites that are weakly determined within the VLBI network (i.e., Hartebeesthoek and Kokee Park) or whose LT is essential (i.e., Wettzell) benefit most when the ZD is combined. Thus, it can be concluded, that the combination of the ZD can stabilize the height component if the corresponding LT is missing. However, the ZD combination cannot fully replace the LT as the mean height repeatability for the VLBI sites is still about 1 mm worse than for solutions with three-dimensional LT applied (Table 6.24). Regarding the GPS sites, the results are similar to those described before (i.e., with three-dimensional LT). This is not astonishing because the GPS sites do not suffer so much from the missing height LT as they are already included in the datum conditions. Nevertheless, again Fairbanks and Onsala are those sites that benefit from the combination of the ZD (see Fig. 6.28b) leading to a mean improvement of about 0.5 mm.

Concerning the question which type of theoretical troposphere tie delivers the best solution, it must be concluded from Table 6.24 and Fig. 6.28 that the differences between the four tested methods in view of the height repeatability are very small (i.e., below 0.04 mm), independent of the handling of the LT.

Finally, one comment must be spent on the scale parameter. Independent of whether the LT are introduced in three dimensions or only for the horizontal components, and independent of which troposphere tie values are applied, the combination of the ZD does not show any significant stabilization for the daily scale parameters. Their scatter remains at 0.15 ppb, as it was the case for the combined solution described in *Chapter 6.2.1* (see solution "G+V+S" in Table 6.20).
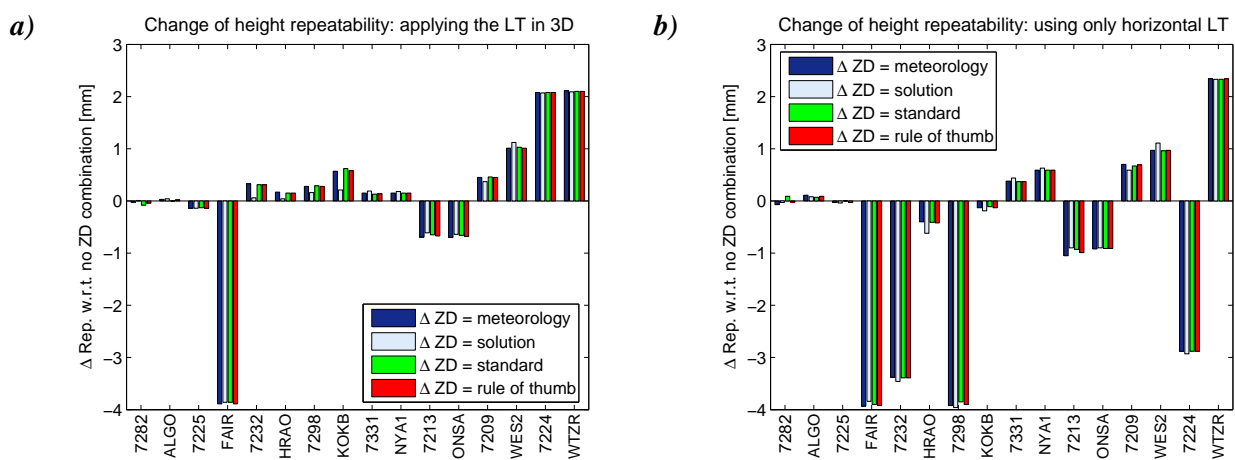


***Figure 6.28:*** *Change of the height repeatability due to the combination of the ZD for all sites using different values for the troposphere ties (negative values indicate an improvement): **a)** applying the LT in 3D, **b)** without applying the LT in height. For the reference solutions, only the TRF and EOP are combined.*

***Table 6.24:*** *Mean repeatability (height component) for a sub-set of sites (noted in the header) for different types of LT handling and combinations of the ZD. The LT for FAIR and WES2 are not applied in any case, and the GPS-SLR LT are always applied in 3D. The combination method "solution" for the ZD means that the weighted mean biases from Table 6.19 are introduced as nominal values. All other nominal values are listed in Table 5.2.*

| Application of GPS-VLBI LT | Combination of ZD | Mean repeatability for the height component [mm] | | | |
|---|---|---|---|---|---|
| | | All sites | GPS co-located with VLBI | VLBI co-located with GPS | All GPS-VLBI co-locations |
| *3D* | *-* | 7.85 | 6.30 | 5.81 | 6.06 |
| *3D* | *All sites; rule of thumb* | 7.84 | 5.94 | 6.07 | 6.01 |
| *3D* | *All sites; standard* | 7.84 | 5.95 | 6.08 | 6.02 |
| *3D* | *All sites; meteo* | 7.84 | 5.94 | 6.08 | 6.01 |
| *3D* | *All sites; solution* | 7.84 | 5.90 | 6.03 | 5.97 |
| *Horizontal* | *-* | 7.99 | 6.44 | 8.46 | 7.52 |
| *Horizontal* | *All sites; rule of thumb* | 7.89 | 5.97 | 7.04 | 6.53 |
| *Horizontal* | *All sites; standard* | 7.89 | 5.97 | 7.07 | 6.54 |
| *Horizontal* | *All sites; meteo* | 7.89 | 5.97 | 7.03 | 6.52 |
| *Horizontal* | *All sites; solution* | 7.89 | 5.97 | 7.03 | 6.52 |

*b) Combining troposphere gradients*

At first, the stacking of the troposphere gradients is analyzed site-by-site. For this purpose one solution for each co-location is computed by omitting the LT of the co-location in consideration, combining the ZD for the corresponding station (using the troposphere ties determined from meteorological data) and stacking the troposphere gradients of the corresponding co-location. In the site-specific reference solutions for evaluating the gradient stacking, only the ZD are combined and the corresponding LT is omitted. The repeatabilities of the horizontal station coordinates are considered as validation criteria. Figure 6.29a shows the change of repeatabilities for each site (negative values indicate an improvement). In general, the influence of the gradient stacking on the coordinate repeatabilities is clearly below 1 mm (a mean of -0.05 mm and -0.02 mm for the north and east component, respectively), thus the effect is smaller than for the combination of the ZD described in *Section a*. Unfortunately, it is not possible to find any systematic reason that can explain why the repeatability slightly improves for some sites whereas it degrades for other sites. At least the agreement or disagreement of the independently estimated time-series (see Fig. 6.15) is not correlated to an improvement or degradation of the repeatabilities, respectively. In order to give one example, the repeatabilities for Kokee Park degrade whereas they improve for Westford although in both cases a clear bias is present in the gradient time-series of the corresponding co-located sites (Fig. 6.15).

Finally, the stacking of the troposphere gradients in addition to the application of the LT is tested, but only for a fully combined solution, i.e., not separately for each co-location. Besides that all troposphere gradients are stacked in this solution, the ZD for all co-locations are combined using the troposphere ties derived from meteorological data, and the LT are introduced (except for Fairbanks and Westford). In Fig. 6.30 the combined time-series of gradients are shown together with the single-technique results for those co-locations already shown in Fig. 6.15 in the context of analyzing the single-technique solutions (see *Chapter 6.1.3*). The results demonstrate that the combined solution is not dominated by one technique as for some stations the combined time-series is closer to the GPS contribution whereas for other stations it rather follows the VLBI-derived estimates. This behavior can be interpreted as an indication that the relative weighting of the GPS and VLBI normal equation systems is well balanced. Regarding the coordinate repeatabilities, the combination of all troposphere gradients has only a small effect, as Fig. 6.29b nicely demonstrates, with a mean change for all co-locations of +0.08 mm and -0.02 mm for the north and east component, respectively.

**a)**

Change of repeatabilities due to site–specific gradient stacking

**b)**

Change of repeatabilities due to gradient stacking for all sites
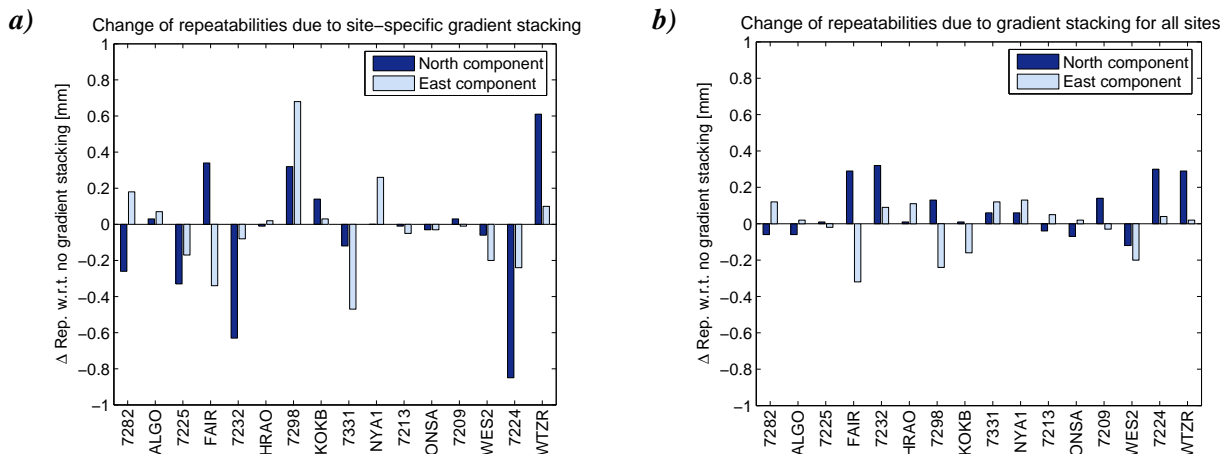
**Figure 6.29:** *Change of horizontal repeatabilities due to the stacking of troposphere gradients for co-located GPS and VLBI sites: **a)** site-specific solutions with omitting the corresponding LT, **b)** fully combined solution (LT, all troposphere ZD and gradients).*
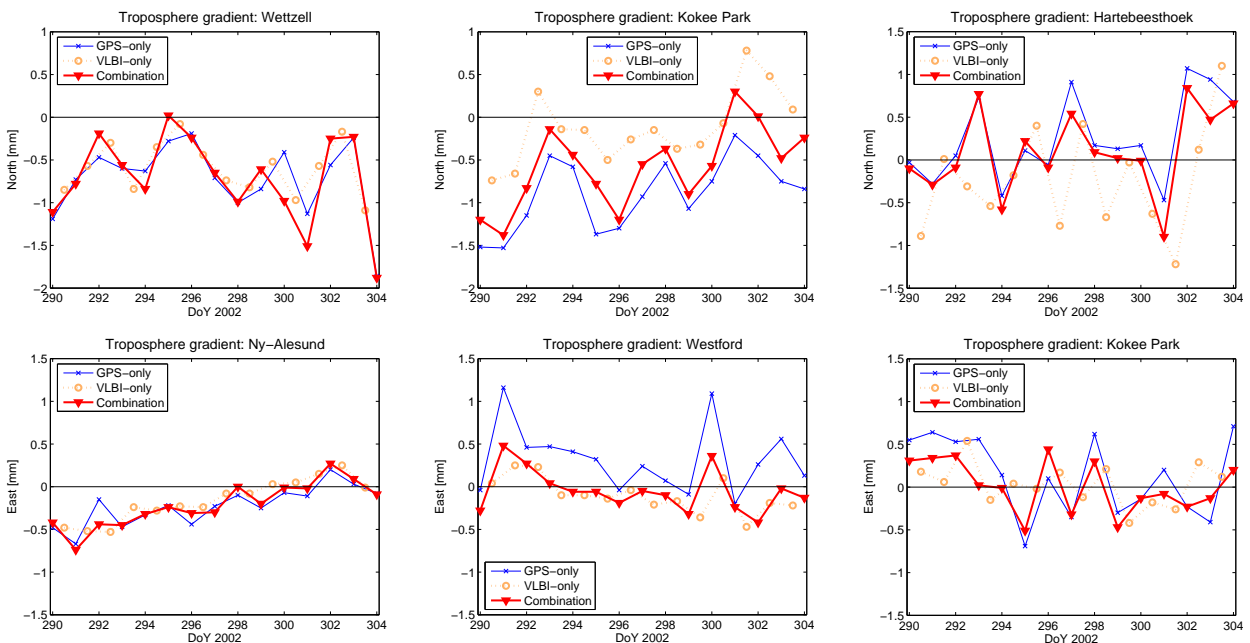
**Figure 6.30:** *Horizontal troposphere gradients for the single-technique solutions (see Fig. 6.15) and the combined estimates.*

# 6.3 Final combined solution

Considering the studies described in *Chapter 6.2*, a final combined solution was computed with the following characteristics:

– An NNR condition is applied on a sub-set of GPS sites.

– The GPS-VLBI LT for Fairbanks and Westford are omitted. The remaining LT (six GPS-VLBI, 14 GPS-SLR) are introduced in all three components.

– A scale parameter and three translations are estimated for GPS.

– All ERP are combined. The BLOCKRET constraint (constant and linear part) is applied on the 14-day NEQ.

– The nutation angles are combined using a 14-day linear representation.

- The troposphere ZD are combined at all eight GPS-VLBI co-locations using troposphere ties based on meteorological data.
- The troposphere gradients are stacked at all eight GPS-VLBI co-locations, resulting in a daily piece-wise linear parameterization.

### 6.3.1 Station coordinates

It can be stated from Table 6.25 that the goal of aligning the three techniques to the same level for the coordinate repeatabilities is reached for the final combined solution. Comparing with the single-technique solutions it is clear that mainly SLR benefits from the combination because it is the weakest single-technique solution. Figure 6.31 visualizes that the benefit is present for all SLR co-locations. The slightly worse north repeatability for the VLBI-only solution (compared to the east component) is balanced in the combination, due to the inclusion into a more homogeneous network. This is underlined by the fact, that mainly the isolated VLBI sites for Hartebeesthoek (7232) and Kokee Park (7298) contribute to this clear improvement (see Fig. 6.31). The horizontal repeatabilities for the GPS sites stay more or less at the same level, but this was not astonishing as they showed the best values for the single-technique solutions. All in all, the horizontal repeatabilities for the co-located sites are at the level of about 2 mm for all techniques. Taking into account all co-located sites for GPS, VLBI and SLR (except of the Shanghai co-location), the mean improvement is 2.32 mm and 2.13 mm for the north and east component, respectively.

Unfortunately, the original level of the GPS-only solution is not reached for the height repeatability in the combination (Table 6.25). Although the mean height repeatabilities for the VLBI and SLR co-locations clearly improve, the stability for the GPS sites is degraded, so that the averaged degradation for all co-locations is 0.23 mm. As mainly those GPS sites co-located with SLR degrade (see Fig. 6.31), the reason might be, again, that SLR on a daily basis is not stable enough to transfer the translational information to GPS.
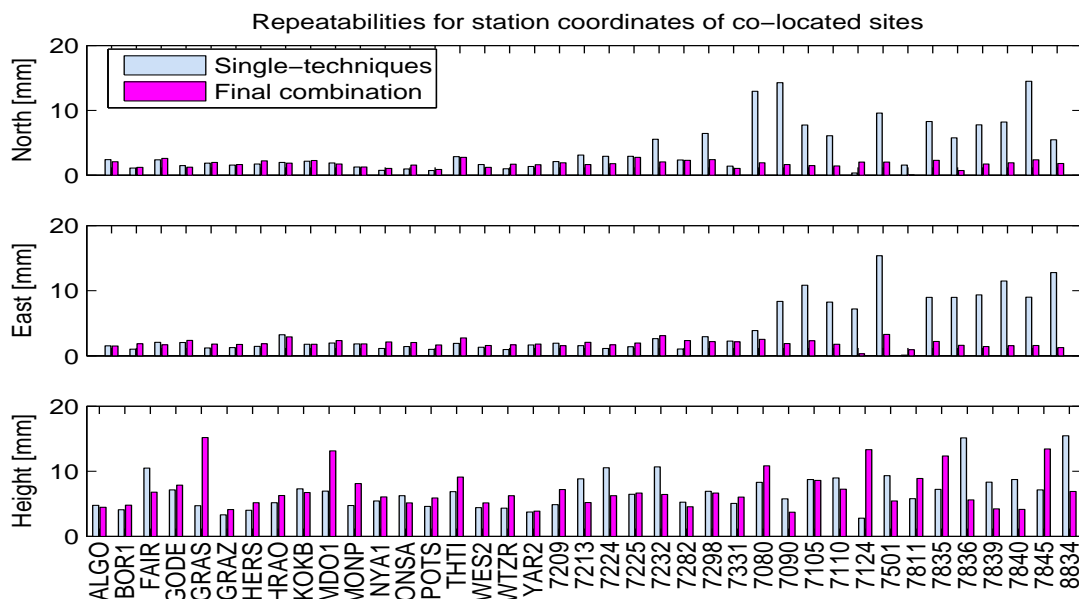


***Figure 6.31:*** *Site-specific repeatabilities for co-located sites: GPS co-locations (ALGO – YAR2), VLBI sites (7209 – 7331), SLR co-locations (7080 – 8834).*

One may ask, whether the method of computing the coordinate repeatabilities plays a role. As described in *Chapter 5.2.1*, a seven-parameter Helmert transformation is set up between every daily solution and the 14-day solution using all sites. This implies that GPS, VLBI and SLR sites together are used for the Helmert transformation for the combined solutions, which differs of course from the single-technique solutions. Therefore, another method was tested: The repeatabilities were directly computed from the time-series of daily coordinates without correcting for a Helmert transformation. The values for the repeatabilities resulting from this procedure are larger, of course, because the daily datum effects were not removed. However, the

relationship between the single-technique solutions and the final combined solution showed similar results, so that the results of this analysis can be omitted here.

***Table 6.25:*** *Mean daily repeatabilities for co-located sites (the co-location SHAO is omitted).*

| *Sub-set of sites* | *Single-technique solutions [mm]* | | | *Final combined solution [mm]* | | |
|---|---|---|---|---|---|---|
| | *North* | *East* | *Up* | *North* | *East* | *Up* |
| ***GPS co-locations (18)*** | 1.72 | 1.68 | 5.72 | 1.78 | 1.99 | 7.49 |
| ***VLBI co-locations (8)*** | 3.72 | 1.97 | 7.67 | 2.04 | 2.17 | 6.17 |
| ***SLR co-locations (13)*** | 9.43 | 9.98 | 9.21 | 1.77 | 2.02 | 7.82 |

## 6.3.2 Earth orientation parameters

The benefit of combining the contributions of GPS and VLBI to the sub-daily ERP has already been demonstrated in *Chapter 6.2.1*. Neither the inclusion of SLR, nor the combination of the troposphere parameters, nor the estimation of Helmert parameters has a significant impact on the ERP time-series. Thus, it is not astonishing that the comparison of the final solution with the IERS2003 model (Fig. 6.32) yields similar differences as for the comparison of the GPS-VLBI combined solution discussed in *Chapter 6.2.1* (Fig. 6.24). The RMS values of the unbiased differences are included in Table 6.16. The level of agreement is similar for all three components, i.e., about 0.15 mas for polar motion and 0.01 ms for universal time. It must be kept in mind that the IERS-C04 series as well has some deficiencies and cannot be considered to be the truth.

*a)*



*b)*



*c)*
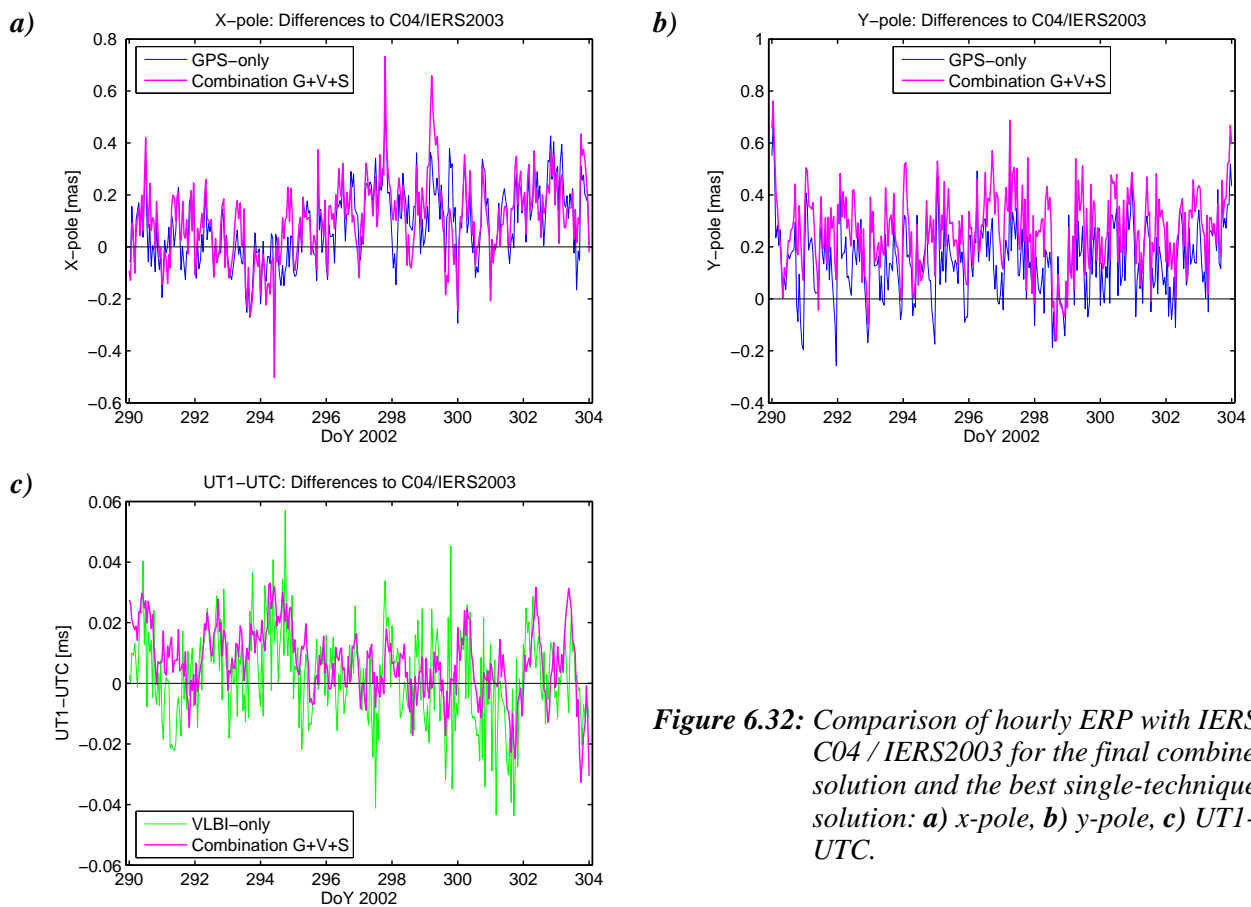


***Figure 6.32:*** *Comparison of hourly ERP with IERS C04 / IERS2003 for the final combined solution and the best single-technique solution:* ***a)*** *x-pole,* ***b)*** *y-pole,* ***c)*** *UT1-UTC.*

The nutation angles resulting from a combination with the satellite-techniques changes slightly compared to the VLBI-only solution (see Fig. 6.33). The contributions of GPS and SLR even force the nutation in obliquity to show a nutation rate with opposite sign, whereas the mean offset nearly remains the same as deter-

mined solely by VLBI (Fig. 6.33a). Concerning the nutation in longitude, it is striking that all combined solutions are shifted compared to the VLBI-only solution (Fig. 6.33b), although the satellite-techniques do not have access to the nutation in an absolute sense. As the combination of the troposphere parameters obviously reduce the shift (fourth solution vs. third solution), this behavior nicely demonstrates that all parameters in a combined solution are somehow correlated and, thus, can influence each other albeit a direct correlation between the troposphere parameters and the nutation angles is not known.
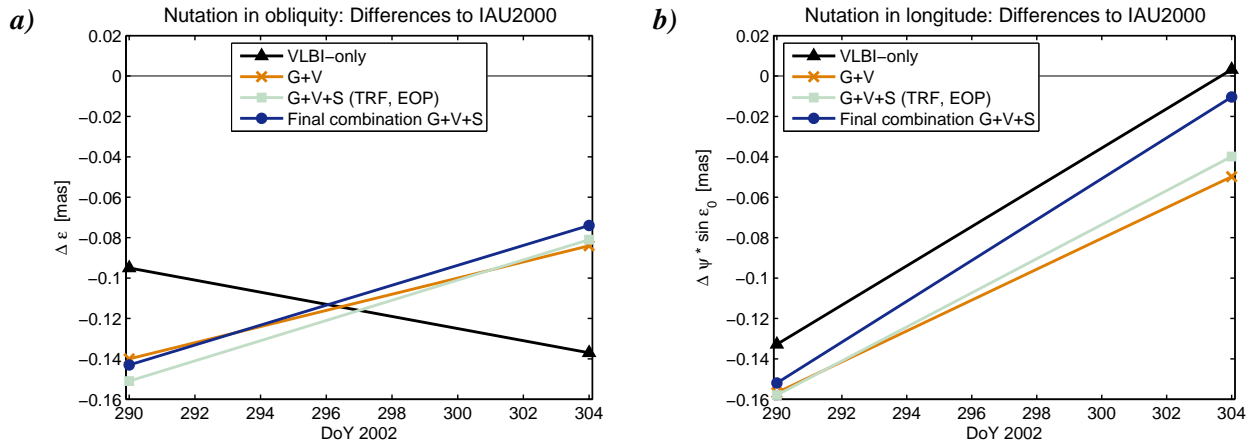


***Figure 6.33:*** *14-day nutation estimates for various combined solutions and the VLBI-only solution: **a)** nutation in obliquity, **b)** nutation in longitude.*

### 6.3.3 Troposphere parameters

The impact of combining the troposphere parameters on the remaining parameters has been discussed in *Chapter 6.2.3*, and Fig. 6.34c shows the impact on the GPS- and VLBI-derived ZD estimates themselves for the final solution, i.e., troposphere ties based on meteorological data are introduced. Depending on the site, the ZD are shifted by up to 2 mm (as a mean value for the whole time-series) compared to the solution with combined station coordinates and EOP only. The GPS-derived ZD as well as the VLBI-derived ZD change in the same order of magnitude. This behavior indicates that the relative weighting of the normal equation systems is done properly as, obviously, none of the techniques dominates the combined solution. The mean change for the ZD estimates due to their combination is at the same level as the changes seen for a solution with combined TRF compared to the single-technique solutions (see Table 6.17, Fig. 6.34a), although these biases are more pronounced and show smaller scatter from epoch to epoch (indicated by the error bars in Fig. 6.34a-c). Compared to the impact of a combined TRF on the ZD (Fig. 6.34a) or the changes due to combining the ZD (Fig. 6.34c), the impact of estimating a scale parameter for the GPS network is only half of the size, i.e., 1 mm at maximum (see Table 6.23, Fig. 6.34b). But the estimated scale for the GPS network was only 0.75 ppb (solution type A in Table 6.22) so that both values agree quite well.

Regarding the troposphere gradients, the results for the combination without estimating Helmert parameters for GPS has already been discussed in *Chapter 6.2.3*, and the combined time-series are shown in Fig. 6.30 for some selected sites. The only difference in the setup for the final solution is the estimation of a scale parameter and three translations for the GPS contribution. But as the troposphere gradients remain unaffected by the additional Helmert parameters it can be forgone to present further results here.
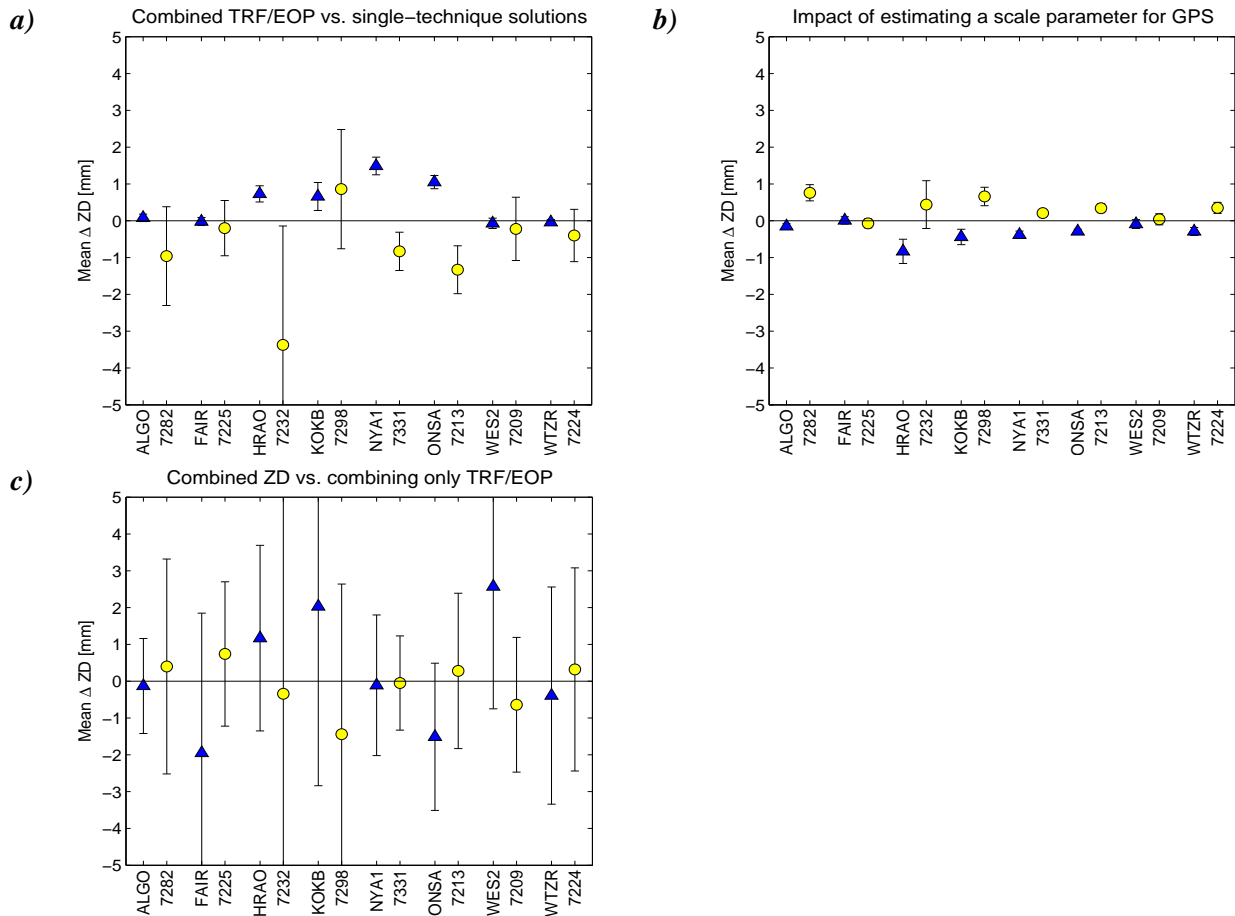
***Figure 6.34:*** *Changes in the ZD estimates due to different solution strategies. The error bars indicate the 1σ-level. **a)** Changes due to a combined TRF and EOP compared to the single-technique solutions, **b)** changes due to estimating a scale parameter for GPS, **c)** changes due to combining the GPS- and VLBI-derived ZD by introducing troposphere ties based on meteorological data.*

## 6.3.4 Datum parameters: translations and scale

The scale and translation parameters estimated for the final solution are listed in Table 6.22. Compared to the solution type C discussed in *Chapter 6.2.2*, the combination of the troposphere parameters in the final solution obviously does not change the values of the estimated Helmert parameters dramatically, but their formal errors are clearly smaller (especially for the translations). Thus, it can be concluded that the combination of the troposphere parameters improve the estimation of the Helmert parameters. The same conclusion can be drawn if the scatter of the daily transformation parameters listed in Table 6.20 are considered. Especially the daily scale of the combined network is stabilized due to combining the troposphere parameters. As the scale for the final solution is a weighted mean of the contributions by VLBI and SLR, and as the scale is correlated with the troposphere ZD, the stabilization of the VLBI-derived time-series of ZD achieved by the combination with the GPS-derived ZD in turn stabilizes the contribution of VLBI to the scale of the network. Comparing the weekly Helmert parameters of the final solution and the solution type C, i.e., without combining the troposphere parameters, there are nearly no differences visible (see Table 6.21). But, as already mentioned before, the suitability of weekly comparisons based on solely two weeks is limited, of course.

# 7 Conclusions and outlook

For the first time, homogeneous normal equation systems for GPS, VLBI and SLR were combined including station coordinates, EOP and troposphere parameters. Therefore, the studies presented in this thesis are a precursor with regard to three topics compared to the procedures that are actually applied within the IERS:

1) The detailed and careful homogenization concerning the a priori models used for generating the single-technique normal equation systems, the identical parameterization chosen for the common parameters, and the exchange of datum-free NEQs allow a rigorous combination, although the combination has been done on the normal equation level instead of the observation level.

2) Three major parameter types, i.e., station coordinates, EOP and troposphere parameters, have been included in the solution, so that all correlations are properly taken into account and the resulting parameters are fully consistent.

3) The troposphere parameters and all five components of the EOP have been combined.

The benefit of the combination could be shown for all parameter types. Concerning the station coordinates, it is clear that mainly the VLBI and SLR sites benefit as their single-technique solutions are weaker than a GPS-only solution. However, weakly determined GPS sites can be improved, too, if there is a strong contribution from a co-located VLBI or SLR site, as it has been seen for the site FAIR.

A general stabilization of the time-series due to the combination has been demonstrated for the sub-daily ERP as well. Thereby, GPS and VLBI are the major contributors because SLR cannot deliver ERP with such a high temporal resolution. But even the daily ERP time-series derived from SLR observations does not give a strong contribution. Regarding the sub-daily pole coordinates, the inclusion of VLBI allows that the necessary constraint for blocking a retrograde diurnal term in polar motion (BLOCKRET) can be applied to the full time span (i.e., 14 days), whereas it has to be applied to each daily interval if solely GPS is considered. Due to the mechanism of the BLOCKRET constraint, it is highly desirable to chose the time span as long as possible. To be more precise, a time span for that the nutation corrections can be represented by a linear parameterization (i.e., one offset and drift only), and, in the case of GPS, a time span for that the orbits can be represented by one arc only. Thus, it is clear that the latter condition is the major restriction for a GPS-only solution. Theoretical studies on the method of handling the singularity between a retrograde diurnal polar motion term and the nutation angles have been carried out.

One important outcome of the studies presented in this thesis is the successful combination for *UT* and *LOD* from contributions by VLBI and the satellite techniques into a piece-wise linear time-series of *UT1-UTC* values. It has been demonstrated that the high-quality short-term information delivered by the satellite techniques – especially by GPS – is stabilizing the VLBI-derived time-series of *UT1-UTC*. However, it must be admitted that for a combination with GPS using normal 24-hour VLBI sessions (mainly R1 and R4 sessions) the stabilization effect on a continuous time-series of *UT1-UTC*, as it was seen for the CONT02 sessions, will surely be less pronounced due to the gaps between the single VLBI sessions. An extrapolation of *UT1-UTC* with integrated *LOD* estimates from GPS for several days without an absolute value contributed by VLBI yields a systematic drift in the *UT* time-series. A possible strategy to overcome the problems with gaps between the 24-hour VLBI sessions might be the inclusion of the so-called VLBI Intensive sessions, as they deliver universal time nearly every day, at least for the past few years. A stabilization of the *UT* values derived from the VLBI Intensive sessions by combining the TRF, polar motion and the troposphere parameters with GPS has been shown by *Tesmer et al. (2006)*. But these studies were restricted to the Intensive sessions so that the benefit of a common treatment of regular 24-hour and Intensive sessions still has to be investigated.

Concerning the third parameter type included in the studies, the inclusion of the troposphere parameters into the solution yields time-series of ZD and horizontal gradients for the GPS and VLBI sites that are fully consistent with the common reference frame. The consistency is especially important as it has been shown that the time-series based on the independent single-technique solutions' reference frames differ from those time-series based on a common reference frame by up to 2 mm at mean. In the framework of the studies based on the homogeneous NEQs for CONT02, a combination for the troposphere parameters has been carried out for the first time. The results presented in this thesis base on a three-technique combination with SLR additionally included. The benefit of combining the troposphere ZD at co-located GPS-VLBI sites could be demonstrated. Due to the correlation of the ZD with the station height, a combination of the ZD can stabilize the de-

termination of the height coordinate, although this stabilization has not been seen for all co-locations. But it has been demonstrated that a stabilization of the height component by combining the ZD is achieved if the LT for the corresponding co-location is missing. It is clear that the combination of the ZD acts only indirectly on the stability of the station height, thus, the combination of the ZD cannot fully replace the information that is given by introducing the LT directly. However, as the problems concerning LT values are manifold, the combination of the troposphere parameters might be an alternative to the application of LT values that are questionable. Thereby, the method to derive the troposphere ties used for the combination plays a minor role, at least for the time span of CONT02. The analyses done by *Steigenberger et al. (2007)* for about eleven years of GPS- and VLBI-derived ZD indicate that the differential ZD does not show any large seasonal variations (in spite of a larger scatter of the differential ZD during summer) so that the usage of a mean value as troposphere tie should be sufficient for longer time spans as well.

A stabilization of the solution similar to the effect seen for the combination of the troposphere ZD could not be shown for the combination of the troposphere gradients, neither with horizontal LT additionally introduced nor without applying the LT. However, it could be demonstrated that the common treatment of troposphere gradients together with the TRF can give valuable information about the discrepancy between the LT and the coordinate differences derived from the space-geodetic techniques. This is especially desirable as this method allows testing the LT values nearly independently from the estimated station coordinates themselves.

For the same reason, it is important to see that the EOP can be employed for a careful selection of suitable LT for the combined solution.

As regards the TRF, there is an indication that the combination of the troposphere parameters stabilizes the scale of the network if the scale is re-opened (i.e. estimated) for the GPS contribution. However, as already mentioned several times before, all issues related to the terrestrial reference frame cannot be studied in a reasonable way on the basis of two weeks of data only. For these purposes the studies have to be extended to a longer time span, as it is already done within the Geotechnologien project named "GGOS-D" that started end of 2005[32]. First results out of this project are presented in *Thaller et al. (2006)* for a time span of one year of data. Besides the prolonged time span, the project "GGOS-D" represents the extension of the combination studies of this thesis regarding the parameters included in the combination, too: The low-degree spherical-harmonic coefficients derived from SLR and GPS are additionally included.

Another possible extension of the studies presented in this thesis is the inclusion of DORIS as a third microwave observation technique. Thus, an additional technique that can deliver troposphere parameters would be available. This is especially interesting because it has been seen that the suitability of the WVR data for comparisons is limited due to a clearly larger scatter in the time-series than the GPS- and VLBI-derived time-series of troposphere ZD. The good agreement of troposphere ZD derived from DORIS, GPS and VLBI has already been shown by *Snajdrova et al. (2005)*, although the analyses presented therein base on time-series of troposphere parameters that were derived independently for each technique without the adaption to common standards for the individual analyses.

Besides the extension of the parameter types considered in the combination and the inclusion of additional observation techniques, the combination studies can be improved and extended if the harmonization of the a priori models and parameterization were improved. Such an improvement could be, e.g., the switch to a more sophisticated modeling of the a priori hydrostatic troposphere delay by using better mapping functions, e.g., the "Vienna Mapping Function" (VMF) developed by *Böhm and Schuh (2004)* or the "Global Mapping Function" (GMF) developed by *Böhm et al. (2006)*. According to *Tesmer et al. (2007)*, the influence of different mapping functions on the time-series of station positions, the height repeatability and the scale variations is not negligible, so that it is highly desirable to use the best model that is actually available for mapping the troposphere delay to the direction of the observation. Furthermore, using an a priori ZD referring to the height of the VLBI reference point instead of the GPS reference height should improve the VLBI-derived troposphere parameters as the wet and hydrostatic part of the ZD are correctly mapped by their appropriate mapping functions. In that case, only the differential troposphere delay caused by the wet part has to be considered for the troposphere tie if the a priori hydrostatic ZD for the GPS and VLBI estimates refer already to the reference height of the GPS and VLBI antenna, respectively.

Regarding the relative weighting of the individual contributions (i.e., observation techniques), it has already been mentioned that a rather simple method was applied within the studies for this thesis instead of a variance component estimation (see, e.g., *Koch, 1988*). However, several results and outcomes of the studies indicate that the relative weights used here yield reasonable results in such a way that the strengths of each

---

32 *http://www.ggos-d.de*

technique can be exploited. The alignment of the coordinate repeatabilities to those of the GPS-only solution indicates that the weight of the GPS contribution is properly chosen. The fact that the time-series of *UT1-UTC* is not degraded by the contributions of the satellite techniques (but quite the contrary, it is even stabilized) shows that the NEQs for VLBI have a relative weight that is strong enough to deliver the absolute value of *UT1-UTC* with high stability. Furthermore, as most of the combined troposphere parameters (ZD as well as gradients) represent a mean value of the non-combined GPS- and VLBI-derived time-series, the relative weighting of the contributions by GPS and VLBI seems to be reasonable. The only question mark is behind the relative weight of the SLR contribution because the stabilization of the translational datum and the scale was not strongly visible. However, as already mentioned before, datum-related studies must base on a longer time span of data, and weekly solutions are clearly more stable than daily solutions for SLR, independent of the relative weighting. Thus, it is assumed that the demonstration of the capabilities of SLR did not fail due to the weighting method applied but due to the short time span considered and the analysis of daily instead of weekly solutions.

As continuous VLBI observations are highly desirable, especially for comparison and combination studies with other techniques, the continuation with CONT campaigns marks a positive development within the IVS. One further campaign - named CONT05 - took already place in October 2005 (see *Chapter 4.1*), and the next campaign is planned for mid of 2008 (*D. Behrend, personal communication*).

In order to conclude the outlook on further studies, it should not be forgotten to mention that the combination studies considering the space-geodetic techniques GPS, VLBI and SLR contribute to the "Global Geodetic Observing System" (GGOS) that has been established in 2003 as a project of the International Association of Geodesy (IAG). Within GGOS, the three fundamental pillars of geodesy, i.e., the geometry including deformations of the Earth's surface, the Earth rotation, and the gravity field, will be integrated into one common reference frame (*Rummel et al., 2005*). The necessity of a highly accurate reference frame becomes more and more important as studies devoted to, e.g., sea level rise or post-glacial rebound are of special interest. As the effects that should be detected are small, the requirements for the reference frame are very high (*Drewes, 2007*). The combination studies presented in this thesis cover two of the three pillars and demonstrate the potential of a rigorous combination.

# Bibliography

*Andersen, P.-H. (2000): Multi-level arc combination with stochastic parameters. Journal of Geodesy, Vol. 74(7-8), pp. 531-551, doi: 10.1007/s001900000115.*

*Altamimi, Z., P. Sillard, C. Boucher (2002): ITRF2000: A new release of the International Terrestrial Reference Frame for earth science applications. Journal of Geophysical Research, Vol. 107, B10, 2214.*

*Angermann, D., D. Thaller, M. Rothacher (2003): IERS SINEX Combination Campaign. In: Proceedings of the IERS Workshop on Combination Research and Global Geophysical Fluids, IERS Technical Note No. 30, edited by B. Richter, W. Schwegmann and W.R. Dick, pp. 94-101, Verlag des Bundesamts für Kartographie und Geodäsie, Frankfurt am Main, 2002. ISBN 3-89888-877-0.*

*Angermann, D. H. Drewes, M. Krügel, B. Meisel, M. GErstl, R. Kelm, H. Müller, W. Seemüller, V. Tesmer (2004): ITRS Combination Center at DGFI: A terrestrial reference frame realization 2003. Deutsche Geodätische Kommission, Reihe B, Heft 313, Bayerische Akademie der Wissenschaften, München, ISBN 3-7696-8593-8.*

*Angermann, D., R. Kelm, M. Krügel, B. Meisel, H. Müller, V. Tesmer, D. Thaller, R. Dill (2006): Towards a Rigorous Combination of Space Geodetic Observations for IERS Product Generation. In: Observation of the Earth System from Space, edited by J. Flury, R. Rummel, C. Reigber, M. Rothacher, G. Boedecker, U. Schreiber, pp. 373-387. Springer Verlag, Berlin Heidelberg, ISBN 978-3-540-29520-4.*

*Ashby, N. (2003): Relativity in the Global Positioning System. Living Reviews in Relativity, Vol. 6, published by the Max Planck Institute for Gravitational Physics, Albert Einstein Institute, Germany. Available at: http://www.linvingreviews.org/Articles/Volume6/2003-1ashby/*

*Berg, H. (1948): Allgemeine Meteorologie. Dümmler Verlag, Bonn, Germany.*

*Beutler, G. (1998): The Role of GPS in Space Geodesy. In: GPS for Geodesy, 2nd edition, edited by P.J.G. Teunissen and A. Kleusberg, Springer Verlag, Berlin Heidelberg New York.*

*Bizouard, C., D. Gambis (2007): The combined solution C04 for Earth Orientation Parameters consistent with International Reference Frame 2005. Available at: http://hpiers.obspm.fr/eop-pc/products/combined/C04_05.guide.pdf*

*Blewitt, G., Y. Bock, J. Kouba (1994): Constraining the IGS polyhedron by distributed processing. Workshop proceedings: Densification of ITRF through regional GPS networks, held at JPL, Nov 30 – Dec 2, 1994, pp. 21-37.*

*Böhm, J., H. Schuh (2004): Vienna mapping functions in VLBI analyses. Geophysical Research Letters, Vol. 31, L01603, doi: 10.1029/2003GL018984.*

*Böhm, J., A. Niell, P. Tregoning, H. Schuh (2006): Global Mapping Function (GMF): A new empirical mapping function based on numerical weather model data. Geophysical Research Letters, Vol. 33, L07304, doi: 10.1029/2005GL025546.*

*Boucher, C., Z. Altamimi, P. Sillard, M. Feissel-Vernier (2004): The ITRF2000. IERS Technical Note No. 31. Verlag des Bundesamts für Kartographie und Geodäsie, Frankfurt am Main, ISBN 3-89888-881-9.*

*Brockmann, E. (1997): Combination of Solutions for Geodetic and Geodynamic Applications of the Global Positioning System (GPS). Geodätisch Geophysikalische Arbeiten in der Schweiz, Schweizerische Geodätische Kommission, Vol. 55.*

*Brunner, F. (2004): personal communication*

*Campbell, J. (1979): Die Radiointerferometrie auf langen Basen als geodätisches Meßprinzip hoher Genauigkeit. Deutsche Geodätische Kommission, Reihe C, Nr. 254, München.*

*Campbell, J., A. Nothnagel, H. Schuh (1992): VLBI-Messungen für geodynamische Fragestellungen. Zeitschrift für Vermessungswesen, Vol. 117(4), pp. 214-227.*

*Cannon, W. (1999): Overview of VLBI. In: International VLBI Service for Geodesy and Astrometry 1999 Annual Report, edited by N.R. Vandenberg, NASA/TP-1999-209243, Greenbelt, MD.*

*Cohen, S.C., D.E. Smith (1985): LAGEOS Scientific Results: Introduction to the Special Issue. Journal of Geophysical Research, Vol. 90, No. B11, pp. 9217-9220.*

Coulot, D., P. Berio, R. Biancale, S. Loyer, L. Soudarin, A.-M. Gontier (2007): *Toward a direct combination of space-geodetic techniques at the measurement level: Methodology and main issues. Journal of Geophysical Research, Vol. 112, B05410, doi: 10.1029/2006JB004336.*

Dach, R., U. Hugentobler, P. Fridez, M. Meindl (eds.) (2007): *Bernese GPS Software Version 5.0. Astronomical Institute, University of Berne, Switzerland.*

Davis, J.L., T.A. Herring, I.I. Shapiro, A.E.E. Rogers, G. Elgered (1985): *Geodesy by Radio Interferometry: Effects of Atmospheric Modeling Errors on Estimates of Baseline Length. Radio Science, Vol. 20, pp. 1593-1607.*

Dawson, J. (2005): *Working Group on Site Survey and Co-location. In: IERS Annual Report 2004, edited by W. Dick and B. Richter, International Earth Rotation and Reference Systems Service, Central Bureau. Verlag des Bundesamts für Kartographie und Geodäsie, Frankfurt am Main.*

Degnan, J.J. (1993): *Millimeter Accuracy Satellite Laser Ranging: A Review. In: Contributions of Space Geodesy to Geodynamics: Technology, edited by D.E. Smith and D.L. Turcotte, Geodynamics Series, Vol. 25, American Geophysical Union, Washington, D.C., ISBN: 0-87590-526-9.*

Dill, R., M. Rothacher (2003): *IERS Analysis Campaign to Align EOPs to ITRF2000/ICRF. In: Observation of the System Earth from Space, Status Seminar at the Bavarian State Mapping Agency (BLVA), Munich, 12-13 June, 2003, Programme & Abstracts, GEOTECHNOLOGIEN Science Report No. 3, Koordinierungsbüro GEOTECHNOLOGIEN, Potsdam, ISSN 1619-7399.*

Drewes, H. (2006): *The Changing Objectives in Geodetic Research. Zeitschrift für Vermessungswesen (ZfV), Vol. 131, pp. 292-298.*

Drewes, H. (2007): *Science Rationale of the Global Geodetic Observing System (GGOS). In: Dynamic Planet, edited by P. Tregoning and C. Rizos, IAG Symposia, Vol. 130, Springer-Verlag, pp. 703-710.*

Drewes, H., D. Angermann (2002): *Remarks on Some Problems in the Combination of Station Coordinate and Velocity Solutions. In: Proceedings of the IERS Workshop on Combination Research and Global Geophysical Fluids, IERS Technical Note No. 30, edited by B. Richter, W. Schwegmann and W.R. Dick, Verlag des Bundesamts für Kartographie und Geodäsie, Frankfurt am Main, 2002. ISBN 3-89888-877-0.*

Ebner, H. (1997): *Ausgleichungsrechnung – Skriptum zur Vorlesung Ausgleichungsrechnung 1+2. Lehrstuhl für Photogrammetrie und Fernerkundung, Technische Universität München.*

Elgered, G. (1992): *Refraction in the Troposphere. In: Proceedings of the Symposium on Refraction of Transatmospheric Signals in Geodesy, Netherlands Geodetic Commission Series No. 36, edited by J.C. DeMunk and T.A. Spoelstra, pp. 13-19.*

Elgered, G., J.L. Davis, T.A. Herring, I.I. Shapiro (1991): *Geodesy by Radio Interferometry: Water Vapor Radiometry for Estimation of the Wet Delay. Journal of Geophysical Research, Vol. 96, No. B4, pp. 6541-6555.*

Elgered, G., R. Haas (2003): *The Geodetic VLBI Network Station at the Onsala Space Observatory – Activities During 2002. In: Proceedings of the 16th Working Meeting on European VLBI for Geodesy and Astrometry, edited by W. Schwegmann and V. Thorandt, Bundesamt für Kartographie und Geodäsie, Leipzig, Germany.*

Emardson, T.R. (1998): *Studies of Atmospheric Water Vapor Using the Global Positioning System. Technical Report No. 339, School of electrical and computer engineering, Chalmers University of Technology, Göteborg, Sweden.*

Eschelbach, C., R. Haas (2003): *The IVS Reference Point at Onsala (High-End Solution for a Real 3D-Determination). In: Proceedings of the 16th Working Meeting on European VLBI, held at Leipzig, May 09-10, 2003, edited by W. Schwegmann and V. Thorandt, Bundesamt für Kartographie und Geodäsie, Frankfurt/Leipzig, pp. 109-118.*

Essen, L., K.D. Froome (1951): *The refractive indices and dielectric constants of air and its principal constituents at 24000 MC/s. In: Proceedings of Physical Society, 64(B), pp. 862-875.*

Feltens, J. (2004): *2001 IGS Activities in the Area of the Ionosphere. In: 2001-2002 IGS Technical Reports, edited by K. Gowey, R. Neilan and A. Moore, IGS Central Bureau, Jet Propulsion Laboratory, California Institute of Technology, Pasadena, California, JPL Publication 02-012.*

Ferland, R., J. Kouba, D. Hutchison (2000): *Analysis methodology and recent results of the IGS network combination. Earth Planets Space, Vol. 52, pp. 953-957.*

*Fischer, D., A. Nothnagel, R. Kilger, W. Schlüter, S. Kurihara, K. Takashima (2003): The K4 Intensive project 2002 for UT1 determination. In: Proceedings of the16[th] Working Meeting on European VLBI for Geodesy and Astrometry, held at Leipzig, May 09-10, 2003, edited by W. Schwegmann and V. Thorandt, Bundesamt für Kartographie und Geodäsie, Frankfurt/Leipzig, pp.165-170.*

*Gambis, D. (ed.) (1999): 1998 IERS Annual Report. Observatoire de Paris.*

*Gambis, D. (2004): Monitoring Earth orientation using space-geodetic techniques: state-of-the-art and prospective. Journal of Geodesy, Vol. 78(4-5), pp. 295-303, doi: 10.1007/s00190-004-0394-1.*

*Gendt, G. (2001): Report of the Tropospheric Working Group. Available at: ftp://ftp.gfz-potsdam.de/pub/igstrop/Publications/wg_trop_report_01.pdf*

*Gowey, K., R. Neilan, A. Moore (eds.) (2004): IGS 2001-2002 Technical Reports. IGS Central Bureau, Jet Propulsion Laboratory, California Institute of Technology, Pasadena, California, JPL Publication 02-012.*

*Gradinarsky, L.P. (2002): Sensing Atmospheric Water Vapor Using Radio Waves. PhD Thesis. Chalmers University of Technology, Göteborg, Sweden.*

*Gross, R. (2000): Combinations of Earth-orientation measurements SPACE97, COMB97, and POLE97. Journal of Geodesy, Vol. 73(12), pp. 627-637, doi: 10.1007/s001900050001.*

*Hefty, J., M. Rothacher, T. Springer, R. Weber, G. Beutler (2000): Analysis of the first year of Earth rotation parameters with a sub-daily resolution gained at the CODE processing center of the IGS. Journal of Geodesy, Vol. 74(6), pp. 479-487, doi: 10.1007/s00190-00-00108.*

*Heinkelmann, R., J. Böhm, H. Schuh, S. Bolotin, G. Engelhardt, D. MacMillan, M. Negusini, E. Skurikhina, V. Tesmer, O. Titov (2007): Combination of long time series of troposphere zenith delays observed by VLBI. Journal of Geodesy, Vol. 81(6-8), pp. 483-501, doi: 10.1007/s00190-007-0147-z.*

*Helmert, F.R. (1872): Die Ausgleichungsrechnung nach der Methode der kleinsten Quadrate. Teubner, Leipzig.*

*Hofmann-Wellenhof, B., H. Lichtenegger, J. Collins (1994): GPS Theory and Practice. Third revised edition, Springer Verlag, Wien, ISBN 3-211-82591-6.*

*Hopfield, H.S. (1969): Two-quadratic tropospheric refractivity profile for correcting satellite data. Journal of Geophysical Research, Vol. 74, pp. 4487-4499.*

*Hulley, G., E.C. Pavlis, V.B. Mendes, D.E. Pavlis (2004): Multiwavelength refraction modeling improvements for SLR observations. Proceedings of the 14th International Workshop on Laser Ranging, held at San Fernando (Spain), June 7-11, 2004.*

*IGS Central Bureau (eds.) (2002): 2002 – 2007 IGS Strategic Plan. Jet Propulsion Laboratory, Pasadena, California.*

*IVS Analysis Coordinator (2005): The official list of VLBI antenna axis offsets. Available at: http://giub.geod.unibonn.de/vlbi/IVS-AC/data/axis-offsets.html*

*Johnston, G., J. Dawson (2004): The 2003 Yarragadee (Moblas 5) Local Tie Survey. Geoscience Australia, Record 2004/19, 27pp. ISBN 1-920871-18-7, Canberra, Australia.*

*Kaniuth, K., H. Müller, W. Seemüller (2002): Displacement of the space geodetic observatory Arequipa due to recent earthquakes. Zeitschrift für Vermessungswesen, Heft 4, pp. 238-243.*

*Koch, K.-R. (1988): Parameter Estimation and Hypothesis Testing in Linear Models. Springer, Berlin Heidelberg New York. ISBN 3-540-18840-1.*

*Krügel, M., D. Thaller, V. Tesmer, M. Rothacher, D. Angermann, R. Schmid (2006): Tropospheric parameters: Combination studies based on homogeneous VLBI and GPS data. Journal of Geodesy, Vol. 81(6-8), pp. 515-527, doi: 10.1007/s00190-006-0127-8.*

*Leick, A. (2004): GPS satellite surveying. Wiley Verlag, Hoboken. ISBN 0-471-05930-7.*

*Ma, C., E.F. Arias, T.M. Eubanks, A.L. Fey, A.-M. Gontier, C.S. Jacobs, O.J. Sovers, B.A. Archinal, P. Charlot (1998): The International Celestial Reference Frame Realized by Very Long Baseline Interferometry. Astronomical Journal, Vol. 116, pp. 516-546.*

*MacMillan, D.S. (1995): Atmospheric gradients from very long baseline interferometry observations. Geophysical Research Letters, Vol. 22, No. 9, pp. 1041-1044, doi: 10.1029/95GL-00997.*

*Marini, J.W., C.W. Murray (1973): Correction of laser range tracking data for atmospheric refraction at elevations above 10 degrees. NASA Report X-591-73-351, Goddard Space Flight Center, Greenbelt, Maryland.*

*Mathews, P.M., T.A. Herring, B.A. Buffet (2002): Modeling of nutation-precession: New nutation series for nonrigid Earth, and insights into the Earth's interior. Journal of Geophysical Research, Vol. 107(B4), doi: 10.1029/2001JB000390.*

*McCarthy, D.D., G. Petit (eds.) (2004): IERS Conventions (2003). IERS Technical Note No. 32. Verlag des Bundesamts für Kartographie und Geodäsie, Frankfurt am Main, ISBN 3-89888-884-3.*

*Mendes, V.B., G. Prates, E.C. Pavlis, D.E. Pavlis, R.B. Langley (2002): Improved mapping functions for atmospheric refraction correction in SLR. Geophysical Research Letters, Vol. 29, No. 10, 1414, doi: 10.1029/2001GL014394.*

*Mendes, V.B., E.C. Pavlis (2004): High-accuracy zenith delay prediction at optical wavelengths. Geophysical Research Letters, Vol. 31, L14602, doi: 10.1029/2004GL020308.*

*Mendes, V.B., E.C. Pavlis, S. Riepl (2003): Refraction Modeling. In: International Laser Ranging Service 2002 Annual Report, edited by M. Pearlman and C. Noll, Goddard Space Flight Center Greenbelt, Maryland, NASA/TP-2003-212239, pp. 43-45.*

*Menge, F., G. Seeber, C. Völksen, G. Wübbena, M. Schmitz (1998): Results of absolute field calibration of GPS antenna PCV. Porceedings of ION GPS-98, Nashville, Tennessee, pp. 31-38.*

*Mervart, L. (2000): Combining of Global Positioning System Solutions.*

*Moritz, H., I. Mueller (1987): Earth rotation: Theory and observation. Ungar Publishing Company, New York, ISBN 0-8044-4671-7.*

*Müller, J. (1991): Analyse von Lasermessungen zum Mond im Rahmen einer post-Newton'schen Theorie. Deutsche Geodätische Kommission, Reihe C, Nr. 383, München.*

*Niell, A.E. (1996): Global mapping functions for the atmosphere delay at radio wavelengths. Journal of Geophysical Research, Vol. 101(B2), pp. 3227-3246.*

*Niell, A.E., A.J. Coster, F.S. Solheim, V.B. Mendes, P.C. Toor, R.B. Langley, C.A. Upham (2001): Comparison of measurements of atmospheric wet delay by radiosonde, water vapor radiometer, GPS, and VLBI. Journal of Atmospheric and Oceanic Technology, Vol. 18(6), pp. 830-850.*

*Niell, A., A. Whitney, B. Petrachenko, W. Schlüter, N. Vandenberg, H. Hase, Y. Koyama, C. Ma, H. Schuh, G. Tuccari (2005): VLBI2010: Current and Future Requirements for Geodetic VLBI Systems. Report of Working Group 3 to the IVS Directing Board. Available at http://ivscc.gsfc.nasa.gov/about/wg/wg3/IVS_WG3_report_050916.pdf*

*Niemeier, W. (2002): Ausgleichungsrechnung. Verlag de Gruyter, Berlin New York, 2002, ISBN 3110140802.*

*Noomen, R., P. Shelus (2005): International Laser Ranging Service (ILRS). In: IERS Annual Report 2004, edited by W.R. Dick and B. Richter, International Earth Rotation and Reference Systems Central Bureau, Bundesamt für Kartographie und Geodäsie, Frankfurt am Main.*

*Nothnagel, A. (1991): Radiointerferometrische Beobachtungen zur Bestimmung der Polbewegung unter Benutzung langer Nord-Süd-Basislinien. Dissertation. DGK Reihe C, Nr. 368, Verlag des Instituts für Angewandte Geodäsie, Frankfurt am Main.*

*Nothnagel, A., D. Fischer, C. Steinforth, M. Vennebusch (2006): Combination of VLBI Analysis Results. In: Observation of the Earth System from Space, edited by J. Flury, R. Rummel, C. Reigber, M. Rothacher, G. Boedecker, U. Schreiber. Springer, Berlin Heidelberg, ISBN 3-540-29520-8.*

*Nothnagel, A., M. Pilhatsch, R. Haas (1995): Investigations of Thermal Height Changes of Geodetic VLBI Radio Telescopes. In: Proceedings of the 10th Working Meeting on European VLBI for Geodesy and Astrometry, Matera (Italy), 1995, May 24-26, edited by R. Lanotte and G. Bianco, Agenzia Spaziale Italiana, pp. 121-133.*

*Otsubo, T., G.M. Appleby (2003): System-dependent center-of-mass correction for spherical geodetic satellites. Journal of Geophysical Research, Vol. 108 (B4), 2201, doi: 10.1029/2002JB002209.*

*Pearlman, M.R., J.J. Degnan, J.M. Bosworth (2002): The International Laser Ranging Service. Advances in Space Research, Vol. 30, No. 2, pp. 135-143 .*

*Pottiaux, E., M. Becker, B. Bürki, R. Gyger, P. Häfele, C. Plötz, W. Schlüter, W. Schwarz, A. Somieski, R. Warnant (2003): The RadCalWet Observation Campaign. Geophysical Research Abstracts, Vol. 5, EGS-AGU-EUG Joint Assembly 2003, Nice, France.*

*Ray, J., Z. Altamimi (2005): Evaluation of co-location ties relating the VLBI and GPS reference frames. Journal of Geodesy, Vol. 79(4-5), pp. 189-195, doi: 10.1007/s00190-005-0456-z.*

*Ray, J., J. Kouba, Z. Altamimi (2005): Is there utility in rigorous combinations of VLBI and GPS Earth orientation parameters? Journal of Geodesy, Vol. 79(9), pp. 505-511, doi: 10.1007/s00190-005-0007-7.*

*Richter, B., W. Schwegmann, W. R. Dick (eds.) (2005): Proceedings of the IERS Workshop on site co-location, Matera, Italy, 23 - 24 October 2003 (IERS Technical Note No. 33). Verlag des Bundesamtes für Kartographie und Geodäsie, Frankfurt am Main. 148 pp., paperback, ISBN 3-89888-793-6 (print version) .*

*Riepl, S., W. Schlüter (2001): Normal point algorithm for reduction of two colour SLR observations. Surveys in Geophysics, Vol. 22, pp. 581-588, doi: 10.1023/A:1015696907252.*

*Rothacher, M. (1999): Analyse von GPS-Daten für hochpräzise Anwendungen – Vorlesungsskriptum Wintersemester 1999/2000. Institut für Astronomische und Physikalische Geodäsie, Technische Universität München, München.*

*Rothacher, M., G. Beutler, T.A. Herring, R. Weber (1999): Estimation of nutation using the Global Positioning System. Journal of Geophysical Research, Vol. 104(B3), pp. 4835-4859, doi: 10.1029/1998JB900078.*

*Rothacher, M. (2000): Ausgewählte Kapitel zur geodätischen Nutzung von GPS – Vorlesungsskriptum Sommersemester 2000. Institut für Astronomische und Physikalische Geodäsie, Technische Universität München, München.*

*Rothacher, M. (2002): Combination of Space Geodetic Techniques. In: International VLBI Service for Geodesy and Astrometry General Meeting Proceedings, Tsukuba, Japan, February 4-7, 2002, edited by N.R. Vandenberg and K. Baver, pp. 33-43, NASA/CP-2002-210002.*

*Rothacher, M., R. Dill, D. Thaller (2002): IERS Analysis Coordination. In: IERS Annual Report 2001, edited by Wolfgang R. Dick and Bernd Richter. International Earth Rotation and Reference Systems Service, Central Bureau. Verlag des Bundesamts für Kartographie und Geodäsie, Frankfurt am Main, 2002. ISBN 3-89888-868-1.*

*Rothacher, M., R. Dill, D. Thaller (2005): IERS Analysis Coordination. In: IERS Annual Report 2003, edited by Wolfgang R. Dick and Bernd Richter. International Earth Rotation and Reference Systems Service, Central Bureau. Verlag des Bundesamts für Kartographie und Geodäsie, Frankfurt am Main, 2002. ISBN 3-89888-914-9.*

*Rothacher, M. (2003): Erdmessung und Satellitengeodäsie 2 – Vorlesungsskriptum Sommersemester 2003. Institut für Astronomische und Physikalische Geodäsie, Technische Universität München.*

*Rothacher, M. (2003): Towards a Rigorous Combination of Space Geodetic Techniques. In: Proceedings of the IERS Workshop on Combination Research and Global Geophysical Fluids, held at the Bavarian Academy of Sciences, Munich, Germany, 18-21 November 2002, IERS Technical Note No. 30, edited by B. Richter, W. Schwegmann and W. R. Dick, Verlag des Bundesamts für Kartographie und Geodäsie, Frankfurt am Main, ISBN 3-89888-877-0.*

*Rummel, R., M. Rothacher, G. Beutler (2005): Integrated Global Geodetic Observing System (IGGOS) – science rationale. Journal of Geodynamics, Vol. 40, pp. 357-362, doi: 10.1016/j.jog.2005.06.003.*

*Saastamoinen, J. (1973): Contributions to the theory of atmospheric refraction. Bulletin Géodésique, Vol. 107, pp. 13-34.*

*Sarti, P., P. Sillard, L. Vittuari (2004): Surveying co-located space-geodetic instruments for ITRF computation. Journal of Geodesy, Vol. 78, pp. 210-222.*

*Schaer, S. (1999): Mapping and Predicting the Earth's Ionosphere Using the Global Positioning System. Geodätisch-geophysikalische Arbeiten in der Schweiz, Vol. 59, Schweizerische Geodätische Kommission, Institut für Geodäsie und Photogrammetrie, ETH Zürich.*

*Schillak, S. (2004a): Analysis of the process of the determination of station coordinates by the satellite laser ranging based on results of the Borowiec SLR station in 1993.5-2000.5. Part 1: Performance of the satellite laser ranging. Artificial Satellites, Vol. 39, No. 3.*

*Schillak, S. (2004b): Analysis of the process of the determination of station coordinates by the satellite laser ranging based on results of the Borowiec SLR station in 1993.5-2000.5. Part 2: Determination of the station coordinates. Artificial Satellites, Vol. 39, No. 3.*

*Schlüter, W., D. Behrend (2007): The International VLBI Service for Geodesy and Astrometry (IVS): current capabilities and future prospects. Journal of Geodesy, Vol. 81(6-8), pp. 379-387, doi: 10.1007/s00190-006-0131-z.*

*Schlüter, W., R. Zernecke, S. Becker, T. Klügel, D. Thaller (2005): Local Ties Between the Reference Points at the Fundamentalstation Wettzell. In: Proceedings of the IERS Workshop on site co-location, Matera, Italy, 23 - 24 October 2003 (IERS Technical Note No. 33), edited by B. Richter, W. Dick and W. Schwegmann. Verlag des Bundesamtes für Kartographie und Geodäsie, Frankfurt am Main. 148 pp., paperback, ISBN 3-89888-793-6 (print version).*

*Schmid, R., M. Rothacher (2003): Estimation of elevation-dependent satellite antenna phase center variations of GPS satellites. Journal of Geodesy, Vol. 77, pp. 440-446.*

*Schmid, R., M. Rothacher, D. Thaller, P. Steigenberger (2005): Absolute phase center corrections of satellite and receiver antennas. GPS Solutions, Vol. 9, Nr. 4, pp. 283-293, doi: 10.1007/s10291-005-0134-x.*

*Schmid, R., P. Steigenberger, G. Gendt, M. Ge, M. Rothacher (2007): Generation of a consistent absolute phase center correction model for GPS receiver and satellite antennas. Journal of Geodesy, online first, doi: 10.1007/s00190-007-0148-y.*

*Schüler, T. (2001): On Ground-Based GPS Tropospheric Delay Estimation. Dissertation. Schriftenreihe des Studiengangs Geodäsie und Geoinformation der Universität der Bundeswehr München, No. 73.*

*Schuh, H. (1987): Die Radiointerferometrie auf langen Basen zur Bestimmung von Punktverschiebungen und Erdrotationsparametern. Deutsche Geodätische Kommission, Reihe C, Nr. 328, München.*

*Schuh, H. (2000): Contributions of VLBI to Space Geodesy. In: Towards an Integrated Global Geodetic Observing System (IGGOS), edited by R. Rummel, H. Drewes, W. Bosch, H. Hornik. International Association of Geodesy Symposia, Vol. 120, Springer-Verlag, pp. 33-40.*

*Schuh, H., J. Böhm (2003): Determination of Tropospheric Parameters Within the new IVS Pilot Project. In: Proceedings of the 16th Working Meeting on European VLBI for Geodesy and Astrometry, held at Leipzig, May 09-10, 2003, edited by W. Schwegmann and V. Thorandt, Bundesamt für Kartographie und Geodäsie, Frankfurt/Leipzig, pp.257-264.*

*Schuh, H., P. Charlot, H. Hase, E. Himwich, K. Kingham, C. Klatt, C. Ma, Z. Malkin, A. Niell, A. Nothnagel, W. Schlüter, K. Takashima, N. Vandenberg (2002): IVS Working Group2 for Product Specification and Observing Programs – Final Report. In: IVS 2001 Annual Report, edited by N.R. Vandenberg and K.D. Baver, pp. 13-45, NASA/TP-2002-210001, Greenbelt, MD.*

*Seeber, G. (1993): Satellite Geodesy. Walter de Gruyter Verlag, Berlin, New York, ISBN 3-11-012753-9.*

*Snajdrova, K., J. Böhm, P. Willis, R. Haas, H. Schuh (2005): Mulit-technique comparison of tropospheric zenith delays derived suring the CONT02 campaign. Journal of Geodesy, Vol. 79(10-11), pp. 613-623, doi: 10.1007/s00190-005-0010-z.*

*Souchay, J., M. Feissel-Vernier (eds.) (2006): The International Celestial Reference System and Frame – ICRS Product Center Report for 2001-2004. IERS Technical Note No. 34. Verlag des Bundesamts für Kartographie und Geodäsie, Frankfurt am Main.*

*Sovers, O.J., J.L. Fanselow, C.S. Jacobs (1998): Astrometry and geodesy with radio interferometry: experiments, models, results. Reviews of Modern Physics, Vol. 70, No. 4, pp. 1393-1454.*

*Steigenberger, P., M. Rothacher, R. Dietrich, M. Fritsche, A. Rülke, S. Vey (2006): Reprocessing of a global GPS network. Journal of Geophysical Research, Vol. 111, B05402, doi: 10.1029/2005JB003747.*

*Steigenberger, P., V. Tesmer, M. Krügel, D. Thaller, R. Schmid, S. Vey, M. Rothacher (2007): Comparison of homogeneously reprocessed GPS and VLBI long time-series of troposphere zenith delays and gradients. Journal of Geodesy, Vol. 81(6-8), pp. 503-514, doi: 10.1007/s00190-006-0124-y.*

*Steinforth, Ch., R. Haas, M. Lidberg, A. Nothnagel (2003): Stability of Space Geodetic Reference Points at Ny-Alesund and Their Excentricity Vectors. In: Proceedings of the 16th Working Meeting on European VLBI, held at Leipzig, May 09-10, 2003, edited by W. Schwegmann and V. Thorandt, Bundesamt für Kartographie und Geodäsie, Frankfurt/Leipzig, pp. 83-89.*

*Tesmer, V. (2004): Das stochastische Modell bei der VLBI-Auswertung. Dissertation. DGK Reihe C, Nr. 573, Bayerische Akademie der Wissenschaften, München, ISBN 3-7696-5012-3.*

*Tesmer, V., D. Thaller, P. Steigenberger, M. Rothacher, M. Krügel (2006): Can low-latency UT1 estimates be improved combining VLBI Intensives and daily GPS sessions? Abstract EGU06-A-10138, presented at EGU General Assembly 2006, Vienna, 2-7 April 2006.*

*Tesmer, V., J. Böhm, R. Heinkelmann, H. Schuh (2007): Effect of different tropospheric mapping functions on the TRF, CRF and position time-series estimated from VLBI. Journal of Geodesy, Vol. 81(6-8), pp. 409-421, doi: 10.1007/s00190-006-0126-9.*

*Teunissen, P.J.G., A. Kleusberg (eds.) (1998): GPS for Geodesy. 2nd edition, Springer Verlag, Berlin Heidelberg New York, ISBN 3-540-63661-7.*

*Titov, O., V. Tesmer, J. Böhm (2001): OCCAM 5.0 users guide. AUSLIG Technical Report 7, AUSLIG, Canberra, Australia.*

*Thaller, D., M. Rothacher (2003): Comparison and Combination of GPS, VLBI and SLR Solution Series. In: Observation of the System Earth from Space, Statusseminar at the Bavarian State Mapping Agency (BLVA), Munich, 12-13 June 2003, Programme & Abstracts, GEOTECHNOLOGIEN Science Report No. 3, edited by A. Rudloff and L. Stroink, Koordinierungsbüro GEOTECHNOLOGIEN, GFZ Potsdam. ISSN 1619-7399.*

*Thaller, D., M. Krügel, M. Rothacher (2006): Combining one year of homogeneously processed GPS, VLBI and SLR data. Submitted to the Proceedings of the IAG GRF 2006 symposia, held in Munich, October 9-13, 2006.*

*Thaller, D., M. Krügel, M. Rothacher, V. Tesmer, R. Schmid, D. Angermann (2007): Combined Earth orientation parameters based on homogeneous and continuous VLBI and GPS data. Journal of Geodesy, Vol. 81(6-8), pp. 529-541, doi: 10.1007/s00190-006-0115-z.*

*Vennebusch, M., S. Böckmann, A. Nothnagel (2007): Contribution of Very Long Baseline Interferometry to ITRF2005. Journal of Geodesy, Vol. 81(6-8), pp. 553-564, doi: 10.1007/s00190-006-0117-x.*

*Wresnik, J., R. Haas, J. Böhm, H. Schuh (2007): Modeling thermal deformation of VLBI antennas with a new temperature model. Journal of Geodesy, Vol. 81(6-8), pp. 423-431, doi: 10.1007/s00190-006-0120-2.*

*Yaya, P. (2002): Apport des combinaisons de techniques astrométriques et géodésiques à l'estimation des paramètres d'orientation de la Terre. PhD Thesis, Observatoire de Paris.*

# Acknowledgements

# Abbreviations

| | |
|---|---|
| CHAMP | Challenging Minisatellite Payload |
| CRF | Celestial reference frame |
| DORIS | Doppler Orbitography and Radiopositioning Integrated by Satellite |
| EOP | Earth orientation parameters |
| ERP | Earth rotation parameters |
| GAST | Greenwich apparent sidereal time |
| GGOS | Global Geodetic Observing System |
| GMST | Greenwich Mean Sidereal Time |
| GNSS | Global Navigation Satellite Systems |
| GPS | Global Positioning System |
| GRACE | Gravity Recovery and Climate Experiment |
| IAG | International Association of Geodesy |
| ICRF | International Celestial Reference Frame |
| ICRS | International Celestial Reference System |
| IERS | International Earth Rotation and Reference Systems Service |
| IGS | International GNSS Service |
| ILRS | International Laser Ranging Service |
| ITRS | International Terrestrial Reference System |
| ITRF | International Terrestrial Reference Frame |
| ITRF2000 | International Terrestrial Reference Frame, realization 2000 |
| ITRF2005 | International Terrestrial Reference Frame, realization 2005 |
| IVS | International VLBI Service for Geodesy and Astrometry |
| LAGEOS | Laser Geodynamics Satellite |
| LLR | Lunar Laser Ranging |
| LOD | Length of day |
| LT | Local tie |
| NEQ | Normal equation system |
| NNR | No-net-rotation |
| NNSc | No-net-scale |
| NNT | No-net-translation |
| PCV | Phase center variations |
| RMS | Root mean square |
| SINEX | Solution Independent Exchange |
| SLR | Satellite Laser Ranging |
| TRF | Terrestrial reference frame |
| UT | Universal time |
| VLBI | Very Long Baseline Interferometry |
| WRMS | Weighted root mean square |
| WVR | Water vapor radiometer |
| ZD | Zenith delay |
| ZWD | Zenith wet delay |

# List of figures

# List of tables